Universidade de Aveiro Departamento de Ambiente e Ordenamento
2017

Sandra Isabel Moreira Rafael

Qualidade do ar e alterações climáticas à escala urbana: vulnerabilidade, resiliência e adaptação

Urban air quality and climate change: vulnerability, resilience and adaptation

Universidade de Aveiro
2017

Departamento de Ambiente e Ordenamento

Sandra Isabel Moreira Rafael

Qualidade do ar e alterações climáticas à escala urbana: vulnerabilidade, resiliência e adaptação

Urban air quality and climate change: vulnerability, resilience and adaptation

Tese apresentada à Universidade de Aveiro para cumprimento dos requisitos necessários à obtenção do grau de Doutor em Ciências e Engenharia do Ambiente, realizada sob a orientação científica da Doutora Myriam Lopes, Professora Auxiliar do Departamento de Ambiente e Ordenamento da Universidade de Aveiro.

Apoio Financeiro do FEDER através do Programa Operacional Fatores de Competitividade (COMPETE) e por Fundos Nacionais através da FCT do POCTI no âmbito dos Projetos CLICURB (EXCL/AAG MAA/0383/2012) e FUTURAR (PTDC/AAG-MAA/2569/2014).

Apoio Financeiro da Fundação para a Ciência e Tecnologia (FCT) e do Fundo Social Europeu (FSE) no âmbito do III Quadro Comunitário de Apoio pela Bolsa de Doutoramento com ref.ª SFRH/BD/103184/2014

o júri

presidente

Professor Doutor Nelson Fernando Pacheco da Rocha
Professor Catedrático, Universidade de Aveiro

vogal

Professora Doutora Myriam Alexandra dos Santos Batalha Dias Nunes Lopes (orientador)
Professora Auxiliar, Universidade de Aveiro

Professor Doutor José António Souto González
Professor Contratado, Universidade de Santiago de Compostela

Professor Doutor Manuel Joaquim Sabença Feliciano
Professor Adjunto, Instituto Politécnico de Bragança

Professora Doutora Oxana Anatolievna Tchepel
Professora Auxiliar, Universidade de Coimbra

Professora Doutora Ana Isabel Couto Neto da Silva Miranda
Professora Catedrática, Universidade de Aveiro

agradecimentos

Só agora ao escrever estas palavras percebi o seu signficado. É o términus de mais uma etapa. E de repente dou por mim a pensar de como todo este caminho, apesar de todos os desafios, passou tão depressa. Caminho esse que apenas foi possível percorrer por ter ao meu lado um conjunto de pessoas maravilhosas e que merecem o meu profundo agradecimento e reconhecimento.

Em primeiro lugar, à minha orientadora, a Professora Myriam Lopes, pelos conhecimentos que me transmitiu, pelas imprescindíveis sugestões e critícas ao longo da orientação deste trabalho, pela paciência e palavras de encorajamento nos momentos mais difíceis. Um agradecimento especial pela amizade e pelo cuidado ao longo de todo este tempo.

Ao Professor Carlos Borrego, pelas valiosas discussões científicas ao longo de todo o trabalho e pela revisão da tese nesta fase final. Um muito obrigado pela constante motivação, pelo carinho que sempre demonstrou e por estar sempre disponível. À Professora Ana Isabel pela presença e pelos ensinamentos científicos.

À Professora Sue Grimmond, que desde logo se disponibilizou por me receber na Universidade de Reading e pelos conhecimentos científicos que me transmitiu. Ao Professor Casimiro Pio, por ter disponibilizado o seu tempo no acompanhamento da campanha de monitorização e tratamento de dados, parte integrante do trabalho realizado.

A todos os Gemaquianos pela alegria, amizade e boa disposição que sempre manifestaram desde a minha entrada na "família Gemac" (e já lá vão 5 anos!). Aos "cotas", Anabela, Alexandra e Joana F. por todas as conversas mais ou menos científicas. Aos "caçulas", Sílvia e Vera pelo entusiasmo e alegria. Aos ex-gemaquianos, Helena, Joana V. e Elisa, pelos valiosos conhecimentos e amizade. Não posso deixar de fazer um agradecimento especial à Patricia, pela amizade, carinho e compreensão ao longo de todo este tempo. Por ter tornado o 312 uma "família" muito especial dentro desta grande "família". À Sara e ao Bruno por tornarem os meus dias mais sorridentes. À Sara pelo carinho e cuidado. Ao Bruno, pela alegria constante e contagiante, pela amizade e compreensão, mesmo quando de cinco em cinco minutos estou a questionar: "já escreveste o artigo?", "já enviaste o e-mail?", "desligaste o aquecimento? Está um frio aqui dentro".

Às "minhas meninas", Diana, Ana e Paula, por tudo. Pelos risos que levaram às lágrimas. Pelas lágrimas convertidas em risos. Por ouvirem os meus desabafos, stresses e aflições. Por estarem simplesmente ali. À Ana M. e ao Cris que mesmo longe estão tão perto.

À minha família um profundo e sincero obrigada por aquilo que sou, por aquilo que me permitiram ser e pelo apoio incondicional em todos os momentos, hoje e sempre. À minha "titi", estejas onde estiveres sei que não podes estar mais orgulhosa. É com um sentimento de dever cumprido que vos dedico este trabalho e todas as minhas conquistas.

A todos o meu muito obrigada!

palavras-chave

Alterações climáticas, fluxos urbanos de calor, medidas de resiliência, modelação numérica, qualidade do ar.

resumo

As cidades, áreas que albergam cerca de 70% da população europeia, enfrentam hoje um conjunto de desafios associados a alterações do metabolismo urbano, que num contexto de alteração climática (AC), afectam o microclima urbano e a qualidade do ar (QA). Compreender a interação entre as AC, qualidade do ar e fluxos urbanos de calor (FUC) é um tópico de investigação emergente, reconhecido como área de interesse para a definição e implementação de políticas locais.

O principal objetivo do presente trabalho é promover uma avaliação integrada das interações entre medidas de resiliência urbana e as AC, e respectiva influência no microclima urbano, QA e FUC, tendo como caso de estudo a cidade do Porto (Portugal). Pretende-se ainda impulsionar o desempenho dos modelos numéricos para que estes representem realisticamente os fenómenos físicos que ocorrem nas áreas urbanas. Para atingir este objetivo, o sistema de modelos WRF-SUEWS foi aplicado para a área de estudo para avaliar a influência de diferentes níveis de área urbanizada nas trocas de calor entre a superficie e a atmosfera. O modelo foi validado mediante a comparação dos seus resultados com dados medidos obtidos em campanhas de monitorização de fluxos. A influência das variáveis meteorológicas nos FUC, e a forma como estas, por sua vez, são influenciadas pela superfície urbana foi também avaliada. Para tal, o sistema WRF-SUEWS foi aplicado para 1-ano representativo de um período de clima presente (1986-2005) e de clima futuro de médio prazo (2046-2065). O cenário climático futuro foi projetado tendo por base o cenário RCP8.5. Esta análise permitiu quantificar e mapear os efeitos das AC nos FUC na cidade do Porto. Face à necessidade corrente de aumentar a resiliência urbana a futuros eventos meteorológicos extremos (e.g. ondas de calor), o sistema WRF-SUEWS foi ainda aplicado (com uma resolução espacial de 200 m) para avaliar a influência de medidas de resiliência nos FUC. Conhecendo a importância da morfologia urbana para as características do seu próprio clima, um conjunto de parameterizações urbanas (LSM, SUEWS e UCM) foram analisados para área de estudo, por forma a obter uma representação realista das características urbanas no modelo WRF e, consequentemente, obter um melhor desempenho na modelação da QA à escala local. Os resultados revelaram que o modelo UCM é a parameterização urbana que melhor representa os fluxos turbulentos de calor, a temperatura e velocidade do vento à superfície. Como resultado, o modelo CFD VADIS, inicializado pelo modelo WRF-UCM, foi aplicado com uma elevada resolução espacial (3 m) a um bairro típico da cidade do Porto. As simulações realizadas permitiram caracterizar o estado atual da QA na área de estudo, bem como avaliar a influência de diferentes medidas de resiliência nos padrões de velocidade do vento e na concentração de poluentes atmosféricos (PM10, NO_X, CO e CO_2).

Este trabalho constitui uma ferramenta científica inovadora no que diz respeito ao conhecimento dos processos físicos que ocorrem à escala urbana, proporcionando uma visão integradora entre AC, QA e FUC. Estes resultados são relevantes para o apoio à decisão política do que respeita à implementação de estratégias que permitam aumentar a resiliência urbana, nas suas diversas vertentes, a um clima em mudança.

keywords

Air quality, climate change, numerical modelling,resilience measures, urban surface energy balance.

abstract

Cities, home of about 70% of the European population, are facing important challenges related to changes in urban structure and its metabolism, and to pressures induced by climate change (CC) effects, which are affecting urban microclimate and air quality. The better understanding of the interactions between CC, air quality and urban surface energy balance (USEB) is an emerging priority for research and policy.

The main objective of the current study is to provide an integrated assessment of the interaction between resilience measures and CC effects, and its influence on the urban microclimate and air quality as well as on the USEB, having as case study the city of Porto (Portugal). The ultimate goal is to improve the accuracy of numerical modelling to better represent the physical processes occurring in urban areas. For this purpose, the relevant parameters to both USEB and air quality were analysed. The WRF-SUEWS modelling setup was applied to the study area to assess the influence of different levels of urbanization on the surface-atmosphere exchanges. To validate the modelling setup, the results were compared with measurements carried out on field campaigns. The way of how the meteorological variables affect the USEB and how, in turn, these variables are themselves affected by urban surface was also assessed. The modelling setup was applied for 1-year period statistically representative of a present (1986-2005) and medium-term future (2046-2065) climate. The climate projection was produced under the RCP8.5 scenario. This analysis gives insights of how the urban-surface exchanges will be affected by CC, allowing the mapping of the FUC over the study area. As result of the need of increase cities resilience to future extreme weather events (e.g. heat waves), the WRF-SUEWS model (with a spatial resolution of 200 m), was applied to Porto city to evaluate the influence of a set of resilience measures on the USEB. Knowing the importance of urban surfaces to its own microclimate, a set of urban parameterization schemes (LSM, SUEWS and UCM) were analysed for the study area, to achieve a more accurate representation of urban features in the WRF model and, in consequence, to improve the capability of air quality modelling at urban/local scale. The results point out that the UCM is the urban parameterization that provides a more realistic representation of the turbulent energy fluxes and the near-surface air temperatures and wind speed. As result, a CFD modelling (VADIS), forced by WRF-UCM, was used to provide a set of numerical simulations with a high spatial resolution (3 m) over a typical neighbourhood in the Porto city. These simulations allow the characterization of the current air quality status over the study area, as well as the assessment of the influence of different resilience measures in the wind flow and air pollutants dispersion (PM10, NO_X, CO and CO_2).

Overall, this research work is a step forward in understanding the physics of urban environments, providing also a linkage between CC, air quality and USEB. These findings are highly advantageous to support policy makers and stakeholders helping them to choose the best strategies to mitigate extreme weather events and air pollution episodes and so increase cities resilience to a future climate.

TABLE OF CONTENTS

LIST OF FIGURES

LIST OF TABLES

LIST OF ORIGINAL PUBLICATIONS

This thesis is based on the work contained in the following original publications:

I. **Rafael S**., Martins H., Borrego C., Lopes M. (2015). Urban vulnerability and resilience to climate change. WIT Transactions on Ecology and The Environment 198, 379-390. [doi: 10.2495/AIR150331].

II. **Rafael S**., Martins H., Sá E., Carvalho D., Borrego C., Lopes M. (2016). Influence of urban resilience measures in the magnitude and behaviour of energy fluxes in the city of Porto (Portugal) under a climate change scenario. Science Of The Total Environment 566, 1500-1510. [doi: doi.org/10.1016/j.scitotenv.2016.06.037]

III. **Rafael S.**, Martins H., Marta-Almeida M., Sá E., Coelho S., Rocha A., Borrego C., Lopes M. (2017). Quantification and mapping of urban fluxes under climate change: Application of WRF-SUEWS model to Greater Porto area (Portugal). Environmental Research 155, 321-334. [doi: doi.org/10.1016/j.envres.2017.02.033].

IV. Borrego C., **Rafael S**., Rodrigues V., Monteiro A., Sorte S., Coelho S., Lopes M. (2018). Air Quality, Urban Fluxes And Cities Resilience Under Climate Change – A Brief Overview. International Journal Of Environmental Impacts 1, 14-27. [doi: 10.2495/EI-V1-N1-14-27].

V. **Rafael S.**, Martins H., Matos M.J., Cerqueira M., Pio C., Lopes M., Borrego C. (Under review). Application of SUEWS model forced with WRF: energy fluxes validation in urban and suburban Portuguese areas. Boundary-Layer Meteorology.

VI. **Rafael S.**, Vicente B., Rodrigues V. Borrego C., Miranda A.I., Lopes M. (Under Review). Impacts of green infrastructures on aerodynamic flow and air quality in Porto's urban area. Environmental research.

VII. **Rafael S.**, Rodrigues V., Fernandes A.P., Borrego C., Lopes M. (submitted to publication). Evaluation of urban surface parameterizations in WRF model using energy fluxes measurements in Portugal. Urban Climate.

ABBREVIATIONS

ACASA	Advanced Canopy-Atmosphere-Soil Algorithm
ACC	Air and Climate Change
AMP	Área Metropolitana do Porto
ANN	Artificial Neural Networks
APA	Agência Portuguesa do Ambiente
AQ	Air Quality
AQEG	Air Quality Expert Group
AQGs	Air Quality Guidelines
AQMEII	Air Quality Model Evaluation International Initiative
BC	Black carbon
BCAO	International Bathymetric Chart of the Arctic Ocean
BEP	Building Effect Parameterization
CFD	Computational Fluid Dynamics
CH_4	Chemical formula for Methane
CHIMERE	A multi-scale chemistry-transport model for atmospheric composition analysis and forecast
CLACC	Capacity Strengthening in the Least Developed Countries for Adaptation to Climate Change
CLC	Corine Land Cover
CLMU	Community Land Model-Urban
CMIP5	Coupled Model Intercomparison Project Phase 5
CO	Chemical formula for Carbon monoxide
CO_2	Chemical formula for Carbon dioxide
DNS	Direct Numerical Simulation
EC	European Commission
EC	Eddy Covariance
ECMWF	European Centre for Medium-Range Weather Forecasts
ECO	Exposure Concentration Obligation
EEA	European Environmental Agency
EMEP	European Monitoring and Evaluation Programme
ETC	European Topic Centre
ETCCDI	Expert Team on Climate Change Detection and Indices
EU	European Union

FAC2	Fraction of predictions within a factor of two of observations
FAIRMODE	Forum for Air Quality Modelling in Europe
GCMs	General Circulation Models
GEBCO	General Bathymetric Chart of the Oceans
GHG	Greenhouse gases
GI	Green Infrastructures
GLOREAM	GLObal and Regional Atmospheric Modelling
H_2O	Chemical formula for water
IARC	International Agency for Research on Cancer
INE	Instituto Nacional de Estatística
IPCC	International Panel for Climate Change
IPMA	Instituto Português do Mar e da Atmosfera
IPPC	Integrated Pollution Prevention and Control
K↓	Incoming shortwave radiation
K↑	Outgoing shortwave radiation
LAD	Leaf Angle Distribution
LAI	Leaf Area Index
LES	Large-Eddy Simulation
LRTAP	Long-range Transboundary Air Pollution
LSM	Noah Land Surface Model
LUCY	Large scale Urban Consumption of energY model
LUMPS	Local-scale Urban Meteorological Parametrization Scheme
L↓	Incoming longwave radiation
L↑	Outgoing longwave radiation
MBE	Mean Bias Error
MPI-ESM	Max Planck Institute for Meteorology - Earth system model
MUCM	Multilayer Urban Canopy Model
NARP	Net All-wave Radiation Parameterisation
NE	North-east
NEC	National Emission Ceilings
NGA	National Geospatial Intelligence Agency
NH_3	Chemical formula for Ammonia
NMSE	Normalised mean square error
NMVOC	Non-methane volatile organic compounds
NO_2	Chemical formula for Nitrogen dioxide
NOAA	National Oceanic and Atmospheric Administration, United States Navy

NO_X	Chemical formula for Nitrogen oxides
NW	North-west
O_3	Chemical formula for ground-level Ozone
PBL	Planetary Boundary Layer scheme
PM	Particulate Matter
PM10	Particulate matter with an aerodynamic diameter less than or equal to a nominal 10 μm
PM2.5	Particulate matter with an aerodynamic diameter less than or equal to a nominal 2.5 μm
PT	Portugal
Q*	Net all-wave radiation
Q_E	Latent heat flux
Q_F	Anthropogenic heat flux
Q_H	Sensible heat flux
ΔQ_S	Net storage heat flux
r	Correlation factor
RANS	Reynolds-Averaged Navier-Stokes
RCMs	Regional Climate Models
RCPs	Representative Concentration Pathways
RF	Radiative Forcing
RMSE	Root Mean Square Error
RRTM	Rapid Radiative Transfer Model
RT	Rule of Thumb
SATURN	Studying Atmospheric Pollution in Urban Areas
SCI	Science Citation Index
SIO	Scripps Institution of Oceanography
SO_2	Chemical formula for Sulphur dioxide
SO_X	Chemical formula for Sulphur oxides
SPSS	Statistical Package for the Social Sciences
SRES	Special Report on Emissions Scenarios
SUEWS	Surface Urban Energy and Water Balance Scheme
SW	South-west
TAPM	The Air Pollution Model
TEB	Town Energy Balance
SLUCM/UCM	Single-layer Urban Canopy Model
UHI	Urban Heat Island
UN	United Nations

UNECE	United Nations Economic Commission for Europe
UNFCCC	United Nations Framework Convention on Climate Change
URL	Uniform Resource Locator
USEB	Urban Surface Energy Balance
USGS	United States Geological Survey
UTC	Universal Time Coordinated
VOC	Volatile Organic Compounds
VUCM	Vegetated Urban Canopy Model
WHO	World Health Organization
WRF	Weather Research and Forecasting Model
WRF-CHEM	Weather Research and Forecasting model coupled with Chemistry
WSM-5	WRF Single-Moment 5-Class Microphysics Scheme
YSU	Yonsei University Scheme

CHAPTER 1

This Chapter has been partially published as:

Rafael S., Martins H., Borrego C., Lopes M. (2015). *Urban vulnerability and resilience to climate change.* WIT Transactions on Ecology and the Environment 198, 379-390.

Borrego C., **Rafael, S**., Rodrigues V., Monteiro A., Sorte S., Coelho S., Lopes M. (2018). *Air Quality, urban fluxes and cities resilience under climate change – a brief overview*. International Journal Of Environmental Impacts 1, 14-27.

The author acknowledges the co-authors critical revision in both papers.

1. General Introduction

This chapter discusses the issues of air pollution and the urban surface energy balance as two key research challenges in a context of climate change in cities. These issues are linked as climate change will affect different sectors across the urban environment, namely urban microclimate and air quality, with implications for future urban planning and sustainability. It is also analysed the current state of air quality in European and Portuguese regions, and it is provided an overview of the current physical formulation of the urban energy balance. A revision of the available modelling tools in both research fields is also provided in this section, as well as an outline of the needs to improve the research knowledge in this field. Furthermore, the linkages between air quality and climate change are revised, as well as the way on how urban surface-atmosphere exchanges of heat are affected by climate change, based on previous research results. Such experiences have established the framework where the research objectives were outlined.

1.1. URBAN ENVIRONMENT

Europe is facing several challenges related to the economy, the climate, the environment and society. Most of these challenges have a strong urban dimension; they either manifest themselves mainly in around cities (EEA, 2014a). Cities play a vital role in the social and economic development of countries. Efficient and productive cities are essential for national economic growth. Strong urban economies are crucial for generating the resources needed for public and private investments in infrastructure, education and health, improved living conditions, and poverty alleviation. However, urban environmental problems (e.g., air pollution) are a serious threat to the full realisation of the socio-economic contribution that cities can make. Environmental degradation brings with it enormous costs, resulting in significant inefficiencies in the use of local natural resources.

Today, approximately 359 million people – 72% of the total European population – live in cities, towns and suburbs. Although the speed of urbanization has slowed down, the share of the urban population continues to grow, and it's likely to reach more than 80% by 2050 (EC, 2014). As result, the aspect of quality of life gains importance for planning strategies and is now the core of actions with the establishment of planning systems by city governments. The recognition of the fact that cities are a human product, contributes to understand the interactions between the flows of resources needed with

growth. Therefore, an urban transformation implies a city planning which integrate physical, social and cultural infrastructure, the economy and the environment of each individual city.
This section provides a review of the two main features of the urban environment: i) air quality, through a brief overview of the status of European and Portuguese regions (section 1.1.1); and ii) urban fluxes, through a revision of its physical formulation and a description of the most relevant research (section 1.1.2).

1.1.1. European and Portuguese Air Quality

Air pollution is a local, pan-European and hemispheric issue. Air pollution can be defined as "a situation in which substances are present in the atmosphere at concentration sufficiently high above their normal levels to produce a measurable effect on humans, animals, vegetation or materials" (Seinfeld and Pandis, 1998). The state of air pollution is often expressed as Air Quality (AQ). Therefore, AQ is a measure of the concentration of air pollutants and size or number of solid or liquid pollutants.

Relevant progress has been achieved in the past 20 years in the European Union (EU) by a dedicated and common policy. The main policy instruments within the EU include the ambient air quality directives (Directive 2008/50/EC on ambient air quality and cleaner air for Europe; Directive 2004/107/EC relating to arsenic, cadmium, mercury, nickel and polycyclic aromatic hydrocarbons in ambient air), and the National Emission Ceilings (NEC) Directive (Directive 2001/81/EC) (EU, 2001). The 2008 air quality directive merges most of the existing legislation into a single directive, establishing the standards on ambient air quality and cleaner air for Europe. In addition, the World Health Organization (WHO) recommends air quality standards to the human health protection, which are taken as a reference for the regulatory measures of large numbers of countries around the world, among then the European Countries. Table 1-1 and Table 1-2 summarize the air quality standards of the main pollutants taken as reference in Europe and Portugal for the protection of human health and vegetation, respectively. WHO guidance values are also included in Table 1-1. Source-specific legislation is focusing on industrial emissions, road and off-road vehicle emissions, fuel quality standards, etc. Emissions are also addressed internationally under the 1979 Long-range Transboundary Air Pollution (LRTAP) Convention, the Marine Pollution Convention and other conventions. In late 2013, the European Commission proposed a new Clean Air Policy Package for Europe, which aims to ensure compliance with existing legislation by 2020 and to further improve Europe's air quality by 2030 and thereafter. The package updates existing legislation that controls harmful emissions from industry, traffic, energy and agriculture, with a view to reduce their impact on human health and the environment

For that, in December 2013, the commission published the clean air programme for Europe, which updated the air policy objectives for 2020 and 2030. Under the scope of the clean air programme for Europe, a proposal for a new National Emission Ceilings (NEC) Directive (COM (2013) 920 final) for nitrogen oxides (NO_X), non-methane volatile organic compounds (NMVOC), sulphur dioxide (SO_2), ammonia (NH_3), particulate matter (PM) and methane (CH_4), and a ratification of the amended

Gothenburg Protocol (UNECE, 2012a; UNECE, 2012b) were considered. Additionally, every effort was made to ensure close coordination between the air quality proposals and those implementing the Union's greenhouse gas and energy objectives (e.g., reduce the greenhouse gas emissions by 20% and have 20% of renewable energy by 2020). A new NEC was adopted under the Directive 2016/2284/EU establishing more strict ceilings (for 2020 and 2030) of the main five pollutants NO_X, SO_2, NMVOC and NH_3, adding as well PM2.5 to what was previously defined (EU, 2016).

Table 1-1. Current European and Portuguese Air Quality standards and WHO guidelines for the protection of human health [Source: adapted from EEA, 2016].

	Reference[a]	Limit or target[b] value		Long-term objective		Information[c] and alert thresholds	
		Aver. Period	Value ($\mu g \cdot m^{-3}$)	Date	Value ($\mu g \cdot m^{-3}$)	Aver. Period	Value ($\mu g \cdot m^{-3}$)
SO_2	EU/ PT	Hour	350 (<24 $h \cdot y^{-1}$)			3h	500
		Day	125 (<3 $d \cdot y^{-1}$)				
	WHO	10 min	500				
		Day	20				
NO_2	EU/ PT	Hour	200 (<18 $h \cdot y^{-1}$)			3h	400
		Year	40				
	WHO	Hour	200				
		Year	40				
O_3	EU/ PT	8-h[d]	120[b] (<25 $d \cdot y^{-1}$ averaged over 3 years)		120	1h	180[c] 240
	WHO	8-h[d]	100				
PM10	EU/ PT	Day	50 (<35 $d \cdot y^{-1}$)				
		Year	40				
	WHO	Day	50				
		Year	20				
PM2.5	EU/ PT	Year	25[b] 20(ECO*)	2020	8.5 to 18		
	WHO	Day	25				
		Year	10				
CO	EU/ PT	8-h[d]	10 000				
	WHO	1h	30 000				
		8-h	10 000				

** ECO: The exposure concentration obligation for PM2.5, is fixed on the basis of the average exposure indication, with the aim of reduce harmful effects on human health. The range of long-term objective (between 8.5 and 18) indicated that the value depends on the initial concentrations in the Member states.

[a]Reference: EU, European Union, Directive 2008/50/EC (European Commission, 2008); PT, Portugal, DL n.º 102/2010 (DR, 2010); WHO, World Health Organization (WHO, 2006).

[b]Indicates that this is a target and not a legally binding limit value; see European Commission (2008) for definition of legal term.

[c]Indicates that this is an information threshold and not an alert threshold; see European Commission (2008) for definition of legal term.

[d]Maximum daily eight-hour mean concentration shall be selected by examining eight-hour running averages, calculated from hourly data and updated each hour.

Table 1-2. European and Portuguese air quality standards for the protection of vegetation [Source: adapted from EEA, 2016].

	Reference[a]	Critical level or target value		Long-term objective	
		Aver. Period	Value	Date	Value
SO_2	EU/ PT	Year and winter period (1 October to 31 March)	20 $\mu g \cdot m^{-3}$		
NO_X	EU/ PT	Year	30 $\mu g \cdot m^{-3}$		
O_3	EU/ PT	May to July	AOT40* 18000 ($\mu g \cdot m^{-3}$)·h averaged over five years	Not defined	AOT40* 6000($\mu g \cdot m^{-3}$)·h

**AOT40, accumulated O_3 exposure over a threshold of 40 ppb (expressed in ($\mu g \cdot m^{-3}$)·h), is the sum of the differences between hourly concentrations > 80 $\mu g \cdot m^{-3}$ (= 40 ppb) and 80 $\mu g \cdot m^{-3}$ accumulated over all hourly values measured between 8:00 and 20:00 Central European Time.

[a]Reference: EU, European Union, Directive 2008/50/EC (European Commission, 2008); PT, Portugal, DL n.º 102/2010 (DR, 2010).

Particulate matter, nitrogen dioxide (NO_2) and ground-level ozone (O_3), are now generally recognised as the three pollutants that most significantly affect human health. On the one hand, O_3 is a secondary pollutant produced in the atmosphere from air pollutants precursors such as NO_X and NMVOC, and the presence of solar radiation (Atkinson, 2000; Jacob, 2000). On the other hand, PM can be primary in the sense that they are emitted as particles from the source, or secondary if is produced by pollutants precursors (SO_2, NO_X, NH_3 and NMVOC). PM includes PM10 (particulate matter with an aerodynamic diameter less than or equal to a nominal 10 µm), PM2.5 (particulate matter with an aerodynamic diameter less than or equal to a nominal 2.5 µm), fine and ultrafine particles, which include a set of pollutants (metals, inorganic and organic compounds) in a complex multiphase system. Long-term and peak exposures to these pollutants range in severity of impact, from impairing the respiratory system to premature death.

Heart disease and stroke are the most common reasons for premature death attributable to air pollution and they are responsible for 80% of cases of premature death; lung diseases and lung cancer follow (WHO, 2014). In addition to cause premature death, air pollution increases the incidence of a wide range of diseases (i.e. respiratory and cardiovascular diseases and cancer), with both long- and short-term health effects. Emerging literature (WHO, 2005, 2013) also shows that air pollution has been associated with health impacts on fertility, pregnancy, and new-borns and children. The International Agency for Research on Cancer has classified air pollution in general, as well as PM as a separate component of air pollution mixtures, as carcinogenic (IARC, 2013). Estimates of the health impacts attributable to exposure to air pollution indicate that PM2.5 concentrations in 2013 were responsible for about 467 000 premature deaths originating from long-term exposure in Europe (over 41 countries), of which around 436 000 were in the EU-28. Additionally, PM2.5 in air has been estimated to reduce life expectancy in the EU by more than eight months. The estimated impacts on the population in the same 41 European countries of exposure to NO_2 and O_3 concentrations in 2013

were around 71 000 and 17 000 premature deaths per year, respectively, and in the EU-28 around 68 000 and 16 000 premature deaths per year, respectively (EEA, 2016).

The contribution of air pollution at different scales depends in the lifetime and properties of pollutants, emission sources, meteorological variables and transport patterns (Seinfeld and Pandis, 1998; EEA, 2016). In this section the emission sources feature is discussed. The links between meteorological variables and air quality are explored in section 1.3.2. Knowledge about the levels of air pollutants emitted by different sources and activities is crucial for understanding the origin of air pollution. Anthropogenic emissions of main pollutants occur as a result of almost all economic and societal activities. Emissions from natural sources are also important for certain pollutants, for example, PM from forest fires, sea spray, and dust episodes from Sahara.

Anthropogenic emissions of the main air pollutants (PM, NO_2) across Europe (EU-28) have decreased continuously between 2000 and 2014 (Figure 1-1, at left). The smallest reduction in the EU-28 was for NH_3 (8%) and the largest was for SO_X (69%), followed by NO_X and NMVOC (both with 39%). Emission of primary PM2.5 and PM10 have both decreased by 17% (between 2006 and 2014) and 23% (between 2000 and 2014), respectively (EEA, 2016). As for Europe, the main Portuguese emission reductions (Figure 1-1, at right) have been reported for SO_2 (89%), NMVOC (38%), NO_X (33%), NH_3 (27%) and PM2.5 (24%), between 1990 and 2014 (APA, 2016).

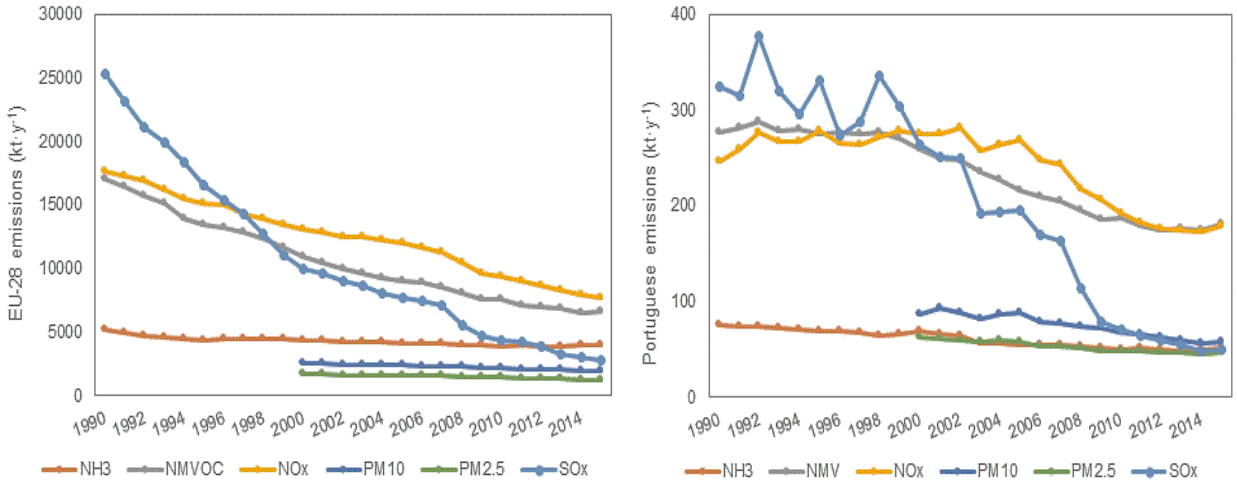

Figure 1-1. Air pollutants emission trends in Europe (EU-28, at left) and Portugal (at right) for the 1990-2015 period, in kilotons species per year ($kt \cdot y^{-1}$) [Source: adapted from URL1].

SO_X is mainly emitted by the combustion of fossil fuels containing sulphur, therefore power generation and industry combustion are the most important sources in Europe (58% and 24% of the total, respectively, in 2014) (EEA, 2016). High reductions in SO_X emissions result from the abatement policies through efficient measures like fuel desulphuration and switching to cleaner fuels (EEA, 2016). The main source of anthropogenic NMVOC is the solvent industry in Europe (51% for EU-28 in 2014) with contributions of industrial activities or domestic heating in urban areas. Reduction of NMVOC emission was due to the introduction of vehicle catalytic converters as well as the introduction of policy

measures limiting the use of solvents in non-combustion sector (EEA, 2016). Agriculture is another important contributor (11% of total NMVOC in EU-28).

NO_X emissions are originated by combustion at high temperatures. The transport sector is the largest contributor of NO_X emissions, accounting for 46% of total EU-28 emissions. NO_X emissions from road transport have not been reduced as much as expected with the introduction of the vehicle emissions standards (European standards), since emissions in real-life, driving conditions are often higher, especially for diesel vehicles, than those measured during the approval test. Power generation is the second most significant source of NO_X emissions (20% of total emissions in the EU-28 in 2014). NH_3 emissions have as main source the agriculture sector (94% in the EU-28). NH_3 has slight decreased in EU in part due to a reduction of the number of livestock, and to the improvements in agriculture practices, driven by EU Nitrates Directives (EEA, 2016). In Portugal, in 2014, the agriculture and road transport sectors, were the mainly sources of acidifying and eutrophying substances emissions (SO_X, NO_X, NH_3 and NMVOC), of 39.2% and 21.5%, respectively (APA, 2016).

Non-industrial combustion and road transport are the most important sources of PM10 and PM2.5 in Europe (EU-28) in 2014, counting 40% [PM10] and 56% [PM2.5] and; 13% [PM10] and 15% [PM2.5], respectively. At urban areas, the residential biomass combustion is also a main source of particulate matter emissions, especially in southern and eastern Europe, as is the case of Portugal. Emissions from residential combustion frequently occur in areas where air circulation is limited and during periods of higher atmospheric stability and thus poor dispersion (e.g., during cold periods or at night). Emission of primary PM10 and PM2.5 have been decreasing due to improvement of vehicle technologies and improvements of the levels and performance of particulate abatement equipment at industrial power plants (EEA, 2016).

A linear relationship between the reductions in anthropogenic emissions of primary PM and its precursor gases and the reductions in ambient air concentrations of PM is not observed. PM10 concentrations continued to be above the EU limit value in large parts of Europe in 2014 according to the data of the European air-quality database (Air Quality e-Reporting Database, EEA, 2016). Around 94% of the cases were observed in urban or suburban areas. A reduction in PM concentrations was also observed in Portugal; however, exceedances to the daily limit value were registered in 2015. The NO_2 concentration trends show an average downward trend at 70%, 61% and 55% of the urban, traffic and rural stations, respectively. This decrease was slower than the decrease in NO_X emissions, mostly due to the increase in the proportion of NO_2 in the NO_X emissions from diesel vehicles (Grice et al., 2009; ETC/ACC, 2010). Despite of that, in 2014, NO_2 concentrations above the annual limit were registered at 12% of the European stations. The highest concentrations, as well as 94% of all values above the annual limit value, were observed at traffic stations (EEA, 2016). Portugal shows a persistent exceedance of the NO_2 annual limit value, especially in urban areas (with a tendency to increase). Figure 1-2 shows the PM10 and NO_2 concentrations spatially distributed by Europe.

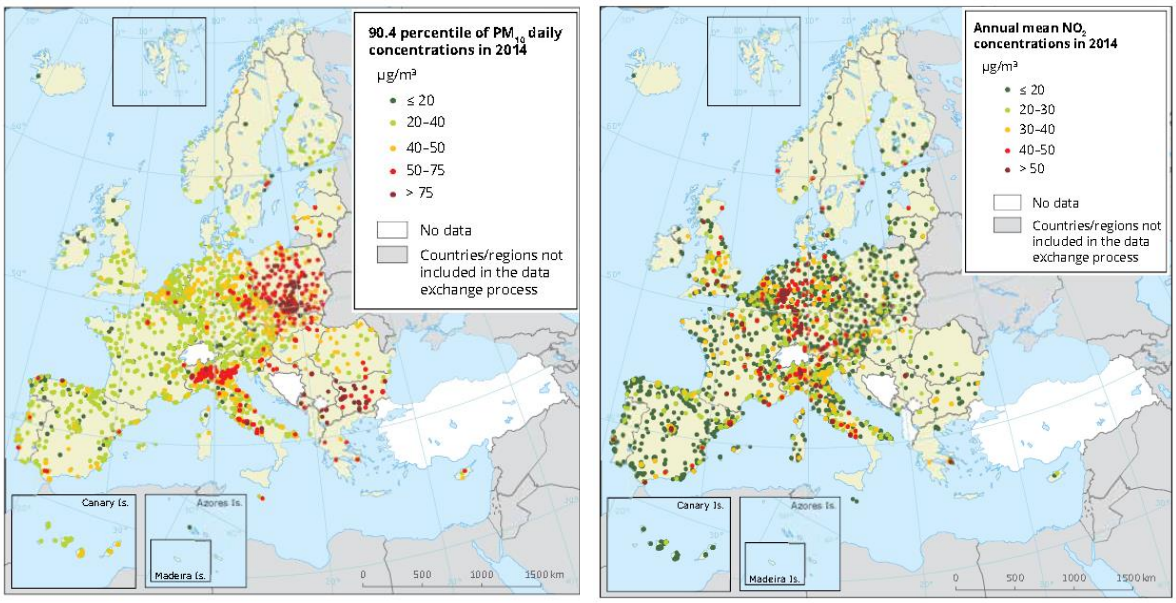

Figure 1-2. Observed concentrations of PM10 (at left) and NO_2 (at right) in 2014. The map shows the 90.4 percentile of the PM10 daily mean concentrations, representing the 36th highest value in a complete series; and the annual means NO_2 concentrations. The red and dark red dots indicate stations with concentrations above the PM10 daily limit and NO_2 annual limit values. Only stations with more than 75% of valid data have been included in the map [Source: EEA, 2016].

High concentrations of O_3 occurred at urban background stations, especially in the case of exceedance of the information threshold (also 11% of all stations showed concentrations above the target value for the protection of human health), mostly due to the O_3 formation that occurs at times in large urban areas during episodes of high solar radiation and temperatures. Therefore, reductions in anthropogenic O_3 precursor's emissions in Europe have not led to equivalent reductions in O_3 concentrations in Europe, as the relationship of O_3 concentration to the emitted precursors is not linear, meteorology plays a key role in ozone's chemistry, and hemispheric background concentrations are also important. In 2015, the exceedance of the information threshold was only registered in one day at one station. The tendency shows that the highest concentration levels typically occur in hot summers and in heat waves episodes. SO_2 concentrations are generally well below the limit value for the protection of human health; and CO concentrations decreased (by around 45%) in average for all stations types, in line with the decrease in total emissions.

To summarize, air-quality policies have delivered, and continue to deliver, many improvements on air quality across the region. Emissions of many air pollutants have decreased substantially over the past decades, and, for several pollutants, exceedances of European standards are rare (EEA, 2016). Despite of that, substantial challenges remain and considerable impacts on human health and on the environment, persist. A considerable proportion of European populations, especially cities dwellers, and ecosystems are still exposed to air pollution that exceeds European standards and, especially, World Health Organization (WHO) Air Quality Guidelines (AQGs). Although complying with the NEC Directive, with NO_X, NMVOC, SO_2 and NH_3 emissions 32%, 6%, 65% and 47% respectively below the ceiling (EEA, 2014b), Portugal is one of the European countries facing air quality problems with non–

compliance of the legislation (Monteiro et al., 2007; Monteiro et al., 2012). In 2014, exceedances to the annual limit value for NO_2 and to the daily limit value for PM10, as well as to the target value threshold for O_3 were registered (APA, 2016). Reducing air pollution therefore remains important.

1.1.2. Physical formulation of urban energy balance

Recent urban research has been interested in understanding how energy, in the form of radiation and heat, influences the urban climate and how this energy is transported, transformed and stored (e.g. in urban building structures). The effects of precipitation on cities, how storm water runoff is changed and how much water is emitted into the atmosphere through evapotranspiration was also an issue of interest. Knowing the distribution and flows of energy, water and carbon in typical urban systems, defined as urban metabolism, is a key factor to understand how much cities worldwide contribute to climate change and so, address the challenges of sustainable cities and urban planning. The urban metabolism of a city is strongly dependent on the prevailing regional and local climate and its built-up structure. Together these factors define the microclimate within the street canyons, on the roads, in the buildings, and at any other place in an urban area (Lietzke et al., 2015). In this context, a description of the urban energy balance concept (its physical formulation) and a summary of the most recent studies in this field are presented in this section.

The exchange of mass in the urban atmosphere is governed by several processes linked to the heterogeneity of the 3D urban structure. Following the volume balance approach, the energy balance of an urban system (Urban Surface Energy Balance - USEB) can be given by:

$$Q^* + Q_F = Q_H + Q_E + \Delta Q_S \tag{1.1}$$

where, Q* is the net all wave radiation, Q_F is the anthropogenic heat flux, Q_H is the turbulent sensible heat flux, Q_E is the turbulent latent heat flux, and ΔQ_S is the net storage heat flux. The advective flux (ΔQ_A) is not included in the energy balance at local scale, although it does not mean that advection does not exist. The micro-scale advection should be included within the sub-grid surface flux parameterizations. At the meso-scale, the inter-grid variations would be resolved by the overlying atmospheric model. All terms are usually expressed as energy flux density per horizontal, or vertical area (typically expressed by $W \cdot m^{-2}$).

Looking for each individual component of the urban energy balance, the net all wave radiation is the balance between the incoming (↓) and outgoing (↑) short- (K) and long-wave (L) radiation fluxes and represents the primary source of energy in the Urban Energy Balance. Mathematically can be expressed as:

$$Q^* = K\downarrow - K\uparrow + L\downarrow - L\uparrow \tag{1.2}$$

The sensible heat flux is a key term in the surface energy balance. Both the surface and the boundary layer temperature are determined, in part, by the sensible heat flux. In particular, the evolution and the depth of the boundary layer is intimately linked to the sensible heat flux and its relation to the latent

heat flux (Raupach, 2001). The vertical transport of energy by the sensible heat flux (in $W \cdot m^{-2}$) as measured by the Eddy Covariance method is expressed:

$$Q_H = \rho\, C_p \overline{w'T'} \tag{1.3}$$

where ρ is the air density ($kg \cdot m^{-3}$) Cp is the specific heat capacity of air ($J \cdot kg^{-1} \cdot K^{-1}$) and $\overline{w'T'}$ ($K \cdot m \cdot s^{-1}$) is the average of the product of the turbulent fluctuations of air temperature *T* and the vertical wind speed *w*. During daytime this term is primarily driven through energy input by the net all wave radiation, while at night storage release from the urban structure keeps sensible heat flux at a higher level compared to rural areas.

The turbulent latent heat flux (Q_E) transports moisture away from the surface because of a change of state (e.g. condensation, evaporation). This is widely dependent on the availability of water, particularly the presence of vegetated areas (transpiration) or wet surfaces (evaporation). Like the sensible heat flux, it can be written as (in $W \cdot m^{-2}$):

$$Q_E = L_v \overline{w'\rho_v'} \tag{1.4}$$

with Lv the latent heat of vaporization ($J \cdot kg^{-1}$) and ρ_v' the turbulent water vapor density ($kg \cdot m^{-3}$). Q_E can be directly measured using the Eddy Covariance method, however, this quantification can be complicated due to the extremely heterogeneous sources of moisture.

The rate of change of heat storage consists of the uptake or release of energy by the ground, buildings and vegetation in a volume. It includes the changes of latent and sensible heat content in the air of the considered control volume. The latter changes are often neglected as they are small compared to the heat storage changes in urban materials. It was early recognized on in urban climate studies that understanding the storage heat flux is crucial if the urban energy balance is to be correctly assessed (Barlow, 2014). A set of schemes have been emerged to capture the effect of urban heat storage (i.e. Objective Hysteresis Model [Grimmond et al., 1991]); however, since direct measurements in urban areas are practically unattainable due to the complexity of urban structures and materials, these schemes are hard to validate. A commonly used method is to consider the storage flux term as the residual of the energy balance (e.g. Roth and Oke, 1994; Grimmond and Oke, 1995; Grimmond and Oke, 1999a; Christen and Vogt, 2004; Spronken-Smith et al., 2006), considering the ΔQ_A and Q_F negligible:

$$\Delta Q_S = Q^* - Q_H - Q_E \tag{1.5}$$

The anthropogenic heat flux derives mainly of combustion exhausts by stationary and mobile sources (Grimmond, 1992; Sailor, 2011). Thus, its contribution to the Urban Energy Balance tends to be highest in the winter time when the energy input from human sources is larger (primarily due to domestic heating), as well as in summertime due to the use of high air conditioning usage for cooling purposes. Anthropogenic heat flux is difficult to determine because of its strongly varying patterns in space and time and because it cannot be measured directly. A set of different approaches can be

found in the literature to estimate this term. Sailor (2011) gave a comprehensive review of how these fluxes can be estimated and Martilli (2007) reviews the ways in which they are integrated in the mesoscale models. The different approaches can be synthetized in three methods: i) using inventories of existing socio-economic data (i.e. from energy use [Sailor, 2011]); ii) calculating as a residual term, if daily or yearly totals of the energy balance equation are considered and net storage heat flux can be assumed to be zero; iii) using micro-scale analysis of the eddy covariance data (Kotthaus and Grimmond, 2012) to determine the amount of energy released from buildings. The spatial and temporal patterns of anthropogenic heat flux, have large impacts on the urban climate and is impacted by many of the urban designs, therefore understanding the role and size of this term is crucial (Lietzke et al., 2015).

Theoretical knowledge of the processes forming the Urban Energy Balance and the resultant effects on the urban boundary layer is well characterised based on a set of large number of observational studies. Most have studied the energy balance of temperate “western” style cities (i.e. Nunez and Oke, 1977; Cleugh and Oke, 1986; Grimmond, 1992; Grimmond and Oke, 1995, 1999b), including a number of long term studies, comparison studies between urban, sub-urban and rural sites and in a range of synoptic conditions. Fewer observations have been taken in tropical (wet or dry) regions, but observations have been taken in Mexico (Oke et al., 1999; Garcia-Cueto et al., 2003), a number of locations in Asia (e.g. Yoshida et al., 1991) and in Africa (Offerle et al., 2003a).

For typical urban areas, the daytime energy balance is characterized by a significant storage heat flux term, a strong sensible heat flux away from the surface and weak evapotranspiration (latent heat flux). As a consequence of strong nocturnal release of stored heat, both turbulent heat fluxes remain directed upward on average at night, a notable difference to the rural environment. Compared with rural surface energy balances, urban areas shows as generally (Barlow, 2014): i) a higher sensible heat flux, due to the man-made materials and increased surface area; ii) a lower latent heat flux, due to the reduced fraction of vegetation land use cover; iii) a higher net storage heat flux, since the urban surfaces have higher thermal inertia due to high heat capacity of the man-made surfaces; iv) a similar net storage heat flux due to complex processes of shadowing and multiple reflections which affects short-wave radiation fluxes, and the wide range of materials which affects the emissivity and thus the long-wave radiation (Oke, 1987; Rotach et al., 2005); v) higher anthropogenic heat, due to a high population density and its related exhaust emissions, i.e. energy use for heating or cooling purposes.

More recently, due to the need of accurate weather forecasts and climate change information within cities, studies on urban energy balance have been developed following different approaches and goals. These studies can be classified in three main approaches:

- Studies that only consider the measurements of the energy fluxes through the eddy covariance method, mainly to understand how urban geometry, properties of urban materials, and presence/absence of vegetation influences the magnitude and behaviour of these fluxes (Oke and Cleugh, 1987; Christen and Vogt, 2004; Coutts et al., 2007; Sedlar and Hock, 2009). These types of studies usually compare different types of land use (e.g. urban/rural; different urban

typologies, among others) different geographical locations and different meteorological conditions; however, its main limitation is the spatial coverage of the study area, since the footprint of the flux observations is restricted to a neighbourhood/local scale (equal or less than 1 km) and the fact that the focus of the study is, in general, only based in the turbulent latent and sensible heat fluxes;

- Studies that combine flux measurements with model simulations, to help identifying knowledge gaps in the current understanding of flux processes and its physical formulation, to enhance the understanding and interpretation of the measured fluxes, and to evaluate the performance and the accuracy of the urban energy balance models results (Grimmond and Oke, 1999; Grimmond and Oke, 2002; Offerle et al., 2005; Flerchinger et al., 2012; Järvi et al., 2011; Järvi et al., 2014) the ultimate objective of these studies is to provide information to determine which approaches minimize the errors in the fluxes simulation;
- Studies that use models designed to simulate the key processes governing heat, moisture and momentum exchanges of the urban canopy for different applications (e.g. understanding of how energy in the form of radiation and heat influences the urban climate) and to provide a classification and comparison of urban energy balance models and their performance. More recently this type of studies also include climate change scenarios, specially linked to urban temperature analysis and Urban Heat Island (UHI) formation (Taha, 1997; Park et al. 2005; Oleson et al., 2010, Rafael et al., 2017) or to assess different urban planning alternatives (Rafael et al., 2016). Generally, these have been conducted with mesoscale meteorological models applied to individual cities using large-scale data (Oleson et al., 2010).

Additionally, recent research in this field has focused in combining imagery from Earth Observation satellites with conventional meteorological measurements at street level. The main goal of this approach, is to define a clear link between urban land-use patterns and energy consumption at local scale to estimate spatiotemporal patterns of anthropogenic heat flux (URL2). It is expected that the resulted satellite-based approach be easily transferable to any study area.

In summary, understanding the impact of urban surfaces (types and usages) on the urban local climate is a crucial research issue for studies of the near-surface urban air quality and the formulation of the sensible and latent heat fluxes in surface energy balance models of urban areas. Despite of the set of studies that have been developed, there are regions where few studies have been performed (i.e. Southern Europe countries, where Portugal is included). In this sense, and due to the importance of the urban energy balance to the understanding of the urban microclimate, studies in this research field remain required. This is particularly true for studies that provides a spatial analysis in the different approaches of the urban energy balance.

1.2. MODELLING TOOLS

Modelling setup have been emerging during the last decades as powerful tools for a set of research areas, namely in air quality and urban energy balance assessment. Due to the rapid development in computational hardware and numerical algorithms, substantial developments have been made in these tools, aiming at providing researchers, decision-makers, and the general population with more reliable information. Historically, most of the research studies in these fields have been based on measured data, as this was considered to be as close to reality as possible. Today, three major reasons to use numerical models are recognised, even though numerical tools are often seen as more inaccurate that measuring tools: i) the spatial coverage of the measured stations is usually limited; modelling can provide complete spatial coverage of air quality and urban fluxes; ii) modelling can be applied prognostically, for example, to predict the future air quality as result of changes in emissions or changing the meteorological conditions; this is also true for the energy balance through the prediction of its changes associated with land use changes or changes in meteorological conditions; iii) modelling allows an understanding of the sources, causes and processes (physical and chemical transformations) that influence the air quality (EEA, 2011a), as well as some guidance on the implementation of mitigation/adaptation/resilience measures.

In this sense, this section provides a brief overview of the state-of-the-art of urban energy balance models (section 1.2.1) and air quality models (section 1.2.2.).

1.2.1. Urban Energy Balance models

A large number of urban surface energy balance models (also called as land surface models parameterizations or urban surface parameterizations) now exist to model the distinct features of the urban surface and the associated energy exchange processes. These models have been developed to incorporate different assumptions related to the inclusion and representation of the relevant urban features for a range of purposes including global climate modelling (e.g., Oleson et al., 2008a,b); numerical weather prediction (e.g., Best, 2005; Best et al., 2006; Masson, 2000;Chen et al., 2004; Harman and Belcher, 2006; Liu et al., 2006); air quality forecasting (e.g., Martilli et al., 2003) and dispersion modelling (e.g., Hanna and Chang 1992, 1993); characterization of measurements (e.g., Krayenhoff and Voogt, 2007); and water balance modelling (e.g., Grimmond and Oke, 1986, 1991). Across these applications a wide range of urban features are incorporated; the models have varying levels of complexity, and different fluxes modelled. Despite of that, a fundamental aim of all of urban energy balance models is to accurately predict fluxes at the local scale. Table 1-3 exemplifies some of the existent urban energy balance models applied in the different fields of research.

Table 1-3. Examples of urban energy balance models [Source: adapted from Grimmond et al., 2010].

Abbreviation	Name	Reference
ACASA	Advanced Canopy-Atmosphere-Soil Algorithm	Pyles et al., 2003
BEP	Building Effect Parameterization	Martilli et al., 2002
CLMU	Community Land Model–Urban	Oleson et al., 2008a, b
LUCY	Large scale Urban Consumption of energY model	Allen et al., 2011; Lindberg et al., 2013
LUMPS	Local-scale Urban Meteorological Parameterization Scheme	Grimmond and Oke, 2002; Offerle et al., 2003b
MUCM	Multilayer Urban Canopy Model	Kondo and Liu,1998; Kondo et al., 2005
SLUCM/ UCM	Noah land surface model/Single-layer Urban Canopy Model	Kusaka et al., 2001; Chen et al., 2004
SUEWS	Surface Urban Energy and Water Balance Scheme	Järvi et al., 2011, 2014
TEB	Town Energy Balance	Masson, 2000; Masson et al.,2002; Lemonsu et al., 2004
VUCM	Vegetated Urban Canopy Model	Lee and Park, 2008

Urban energy balance models can be classified in a number of distinct ways (Grimmond et al., 2010); for example, they vary in terms of the fluxes they calculate. A set of features are used to classify the models, namely:

- Vegetation and latent heat flux. A key feature in an urban surface is whether or not latent heat flux is simulated. Three types of classification can be considered, where vegetation is not considered, modelled using a “tile” scheme, or “integrate” into the modelled urban surface. Not modelling the effect of vegetation (evapotranspiration) implies that there can be no latent heat except for periods immediately following rainfall (though evaporation). Even for densely urbanized areas, the assumption of no fraction of vegetated areas and so the absence of urban latent heat flux is unrealistic. The two types of models that incorporate vegetation differ in terms of interactions that occur between the built and vegetated areas. In the “tile” approach the built and vegetated fluxes are typically weighted by their respective plan area fractions to contribute to total fluxes (without interaction). The integrated case is the most physically realistic as it allows for direct interaction of built and vegetated surfaces. This additional complexity may require increased computing resources and parameter values.
- Anthropogenic heat fluxes. The magnitude of Q_F varies across cities, being its importance for the urban surface energy balance higher as higher was the level of urbanization. Four general approaches are considered: Q_F is assumed to be zero, negligible, or ignored; Q_F is assumed to be a fixed value that is required as an input of the model, or is directly coded into the program; Q_F is calculated based on assumed internal building temperature; Q_F is calculated and incorporates internal heat sources from buildings, and/or mobile sources associated with traffic, and/or metabolism. Anthropogenic heat flux varies both diurnally and seasonally, although only some models consider this. The inclusion of a diurnal and/or seasonal cycle is more significant for applications when the diurnal patterns are needed.

- Urban morphology. Urban morphology affects radiative and turbulent heat exchanges. A number of approaches are used to capture these features, including: slab or bulk surface, single-layer approaches, and multiple-layer approaches. Slab models represent the urban morphology as a flat horizontal surface with appropriate ‘‘bulk’’ radiative, aerodynamic, and thermal characteristics. Single-layer models simplify the urban form to an urban canyon with a roof, wall, and a road. Multilayer schemes divide the walls into a number of vertical and/or the roof and road into a number of horizontal patches; each with their own parameter values and energy exchanges modelled. The set of approaches have different levels of complexity (which implies different parameter requirements and different computational resource demand), where the multi-layer approach allows a more realistic representation of radiative trapping and turbulent exchange (Masson, 2000; Leen and Park, 2008). Models can also be subdivided by how urban canyon morphology, specifically the number of facets and orientations, are dealt with.
- Radiative fluxes. The modelled outgoing short and long-wave radiation (usually incoming short and long-wave radiation are given as input) are influence by both urban morphology and the number of reflections assumed: single, multiple or infinite. The single reflection model is the least computationally intensive and used in both slab and single-layer models. Models that simulate multiple reflections include both single-layer and multi-layer approaches. Infinite reflections may be accounted for by slab, single-layer and multi-layer approaches. Albedo and emissivity also plays a key role to determine the radiative fluxes. They may either be defined as a single value, as two facets, or may consist of combinations of a set of facets.
- Storage heat flux. Net storage heat flux, ΔQ_S, modelling is especially important in urban areas given the materials and morphology of the urban environments. In the surface energy balance models, it is determined in the following ways: i) difference or residual of the energy balance; ii) solution of the heat conduction equation by dividing the facets into a number of thickness layers; iii) function of Q* and surface characteristics. All three methods are used by slab or bulk models. For those models in which heat storage is calculated as the residual of the surface energy balance, assumptions as to which fluxes are included (specifically Q_F and Q_E) are important. The models that use the heat conduction equation requires a set of parameters for each (sub) facet, including: number of layers, layer thickness, thermal conductivity, and volumetric heat capacity of the various layer material. The third approach estimated ΔQ_S based on a fraction of Q*. Some models take into account the diurnal pattern of the flux through the objective hysteresis model, where the effects of surface morphology are incorporated into the statistically determined coefficients (e.g., SUEWS).

Three general types of inputs are required to model urban surface energy balance: i) site parameters to describe the surface morphology and materials (e.g., albedo, emissivity); ii) time series of atmospheric or forcing variables as boundary conditions (e.g., air temperature, mean wind speed, relative humidity, precipitation, air pressure and incoming short-wave radiation); iii) initial thermodynamic and moisture state conditions.

Due to different features used to classify the urban surface energy balance models, and despite there are preferred approaches, there is a notable diversity; models that have a similar approach for one aspect frequently use quite different approaches for other model components. The International Urban Energy Balance Comparison Project (Grimmond et al., 2010, 2011) was a collective effort to compare modelled fluxes using 32 different surface schemes with observations. According to this assessment, the urban surface energy models generally have best overall capability to model Q* and least capability to model Q_E (order Q*, ΔQ_S, Q_H, and Q_E). It seems to be difficult to minimize both Q* and Q_H errors. There is evidence that some classes of models perform better for individual fluxes but not overall. Typically, those that perform best during daytime do not perform best at night. The radiative fluxes are modelled better than the turbulent fluxes; where L↑ is not as well modelled as K↑.

Overall five main conclusions can been drawn based on the findings of Grimmond et al. (2010, 2011): i) no single model had the best performance across all fluxes; this finding has very significant implications for the application of any model highlighting the need of chose a model according to their "fitness for purpose"; ii) the importance of accurate representation of vegetation to the correct simulation of the turbulent fluxes partitioning; not including vegetation, even at a site with limited vegetation, yields the poorest performance for all fluxes during the day; iii) the results are highly dependent to the quality of the input (e.g., thermal characteristics of urban materials, morphology of buildings, meteorological conditions); iv) the use of an ensemble of models rather than one model is generally better than any individual model for an individual flux; v) the simplest and the most complex have similar results which were better than the medium complexity models; however, it is expected that more complex models may have more potential for future improvements as they are able to resolve more details without deteriorating their performance.

The assessment of urban surface energy balance model's capability and the potential for future improvements are directly dependent of the quality (and the amount) of urban flux (mostly turbulent latent and sensible heat fluxes) measurements. Throughout the last decades, the technological progress has improved the methodology of urban flux measurement. Consequently, a growing number of measurements have been performed. Some of these measurements are compiled in the Urban Flux Network that is maintained by the International Association for Urban Climate. Most of the measurements have been campaign-based, although data from long-term campaigns are emerging (Barlow, 2014). Another important issue related to flux measurements is the correct interpretation of the footprint area to guarantee that the measured data is in fact a representation of the local surface-atmosphere exchanges. For example, in highly heterogeneous districts (such as in densely urban areas) a local measurement of turbulent fluxes cannot be clearly interpreted without considering their spatial representativeness given by the footprint function. Additionally, as discussed in section 1.1.2., it has been observed that the magnitude of the urban fluxes is highly influenced by the multiple changes of surface types (e.g., the magnitude of sensible heat flux can vary by a factor of up to 4 between cities and its surroundings [Langford et al., 2010]); whereby measurements that characterize different land uses (e.g., different levels of urbanizations) will enhance the urban surface energy balance

development. As with all urban measurements, difficulty in obtaining permission to erect towers may lead to a compromise in sites selection.

In summary, much progress has been made in measurement and modelling of the urban surface energy balance: the effect of urban materials and morphology on Q* and Q_H is reasonably well explored; there is less accuracy in simulating latent heat flux when compared to measurements; there is some capability in modelling storage and anthropogenic fluxes, which cannot be directly measured. The potential for feedback between the surface energy balance and the boundary layer implies that a better understanding of the urban microclimate requires accurate measurement and numerical modelling of the exchanges between urban canopy and atmosphere, as well as their inclusion within numerical weather prediction models. The use of urban surface parameterizations should also be integrated in studies on climate change impacts, air quality and thermal comfort at city level, which in turn provide the basis to urban planning decision.

1.2.2. Air quality models

Air quality models can be defined as a numerical tool used to describe the causal relationship between emissions, meteorology, atmospheric concentrations, deposition, and other factors, through the application of physical and chemical laws translated into basic thermodynamics, fluid mechanic equations and chemical reactions. Since they are the only method that quantifies the relationship between emissions and concentrations/depositions, and allows the analysis of past and future scenarios, air quality models play an important role in science, in decision-making processes and in regulatory processes. The European legislation framework on air quality explicit recommends the use of modelling tools for different air quality applications, classified as follows (Denby et al., 2010):

- Air quality management. Air quality models allows to predict the impacts of pollutants, identify source contribution to air quality problems and help in the design of effective strategies to reduce the effect of pollutants. Air quality models are widely used in air quality forecast, providing next day and near real time information to the public and for the implementation of short term action plans. Air quality models are also useful to assist in the design and assessment of monitoring networks, since they predict pollutants spatial patterns;
- Air quality assessment. Air quality models can be used to supplement monitoring data where measurements do not provide enough information to fulfil the requirements of an air quality assessment;
- Air quality source apportionment. Air quality models are useful to assess the causes of exceedances of air quality thresholds, and to provide a speciation of the contribution of the different emission sectors for the air quality of a given study area, or the contribution of neighbouring countries (transport patterns).

An integrated system for air quality models should include three different modules, that take into account all the factors involved and closely related in the generation and dispersion of pollutants: i) meteorological model, which describes the state and evolution of the atmosphere; ii) emission model,

which describes the spatio-temporal distribution of both natural and anthropogenic emissions; iii) chemical transport model, which described the physical and chemical transformations that take place for emitted pollutant under specific meteorological conditions (Seinfield, 1988; Russel and Dennis, 2000; Menut and Bessagnet, 2010).

Emission models give information about quantity and kind of pollutants from different sources located in a determined geographical area in a period of time (Baldasano, 1998). Emission estimated are collected together into inventories which usually also contain data related to the source locations, emission measurements (when available), emission factors, activity rates, operating conditions, methods of emissions estimation, among other features. Atmospheric emission inventories are usually quantified using one of the two approaches: i) top-down, based on the disaggregation process of total emissions from a certain area to smaller administrative units or a regular grid with higher resolution (Ossés de Eicker et al., 2008); ii) bottom-up, based on emission estimation using detailed data of each emission source. The top-down approach is very useful when local detailed information about the emissions of different activity sectors are scarce (Palacios et al., 2001). Information on emission modelling can be found in a set of sources, e.g., the EMEP/EEA air pollutant emission inventory guidebook (EMEP, 2009).

Air quality models can be distinguished on many grounds: on the spatial scale (global, regional, mesoscale, urban, local); on the temporal scale; on the treatment of several processes (chemistry, wet and dry deposition); and on the complexity of the approach used for the physical process description (Borrego et al., 2001). The most commonly used air quality models can be classified as the following (Nguyen, 2014): i) dispersion model - typically used to estimate the concentration of air pollutants at specified ground level receptors surrounding emissions sources; ii) photochemical model - typically used to simulate the impacts from all sources by estimating pollutant concentrations and deposition of both inert and chemically reactive pollutants over large spatial scales; iii) source-receptor model - which are observational techniques which use the chemical and physical characteristics of gases and particles measured at source and receptor to both identify the presence of and to quantify source contributions to receptor concentrations.

Dispersion models use mathematical formulations to characterize the atmospheric processes that disperse a pollutant emitted by a source. Based on emissions and meteorological inputs, a dispersion model can be used to predict concentrations at selected downwind receptor location. The most commonly used air dispersion models can be categorised by their type (Gaussian, Lagrangian, Eulerian, and Computational Fluid Dynamics - CFD) and scales of application (Denby et al., 2011). Gaussian models assume that the concentrations from a continuously emitting source are proportional to the emission rate, inversely proportional to the wind speed, and that the time averaged pollutant concentrations horizontally and vertically are well described by Gaussian distributions (Boubel et al., 1994; Nieuwenhuijsen, 2003).

The Eulerian and Lagrangian approaches are more physically realistic, but numerically complex and computationally demanding (Seinfeld and Pandis, 2006). These models can provide realistic

simulations of the atmospheric transport and mixing of air pollutants at several scales (Thunis et al., 2016). In an Eulerian model, chemical species are transported in a fixed frame of reference, usually the surface of earth. This enables easy representation of the pollutant production and transformation processes. The space domain (geographical area or air volume) is divided into "small" squares (two-dimensional) or volumes (three-dimensional), e.g., grid cells. Most Eulerian models use a grid system to describe atmospheric dynamics (advection and diffusion), emission sources and chemical production, and generate four-dimensional (space and time) trace species concentrations fields for each of the species modelled (Seinfeld and Pandis, 2006). These models use numerical terms to solve the atmospheric diffusion equation (i.e. the equation for conservation of mass of the pollutant) (Seinfeld and Pandis, 2006). The numerical solution of the transport term in the Eulerian framework becomes more difficult and often requires substantial computational resources to be accurate enough compared to the Lagrangian approach. The main advantage of the Eulerian models is the well-defined three-dimensional formulations that are needed for the more complex regional scale air pollution problems.

In Lagrangian models, also called Lagrangian Particles or Random Walk model, the motion of air masses or particles following the flow is studied. In this approach, the concentration is computed by counting “fictions particles” (computer-particles) in a user defined volume (e.g. the cell of a regular grid). Each “particle” represents a particular mass of one or several pollutants emitted from a given source. Hence, transport caused by both the average wind and the turbulent terms due to wind fluctuations is taken into account. Time-dependent trajectories of particles are computed by stochastic differential equations (Langevin equations), which aim at describing turbulence properties (Degrazia, 2005). The computation time in Lagrangian models is directly linked to the number of particles within the model domain, which in turn is determined by the number of particles released, the size of the model domain and the wind speed. This type of models provides a better description of the dispersion and transport of pollutants than the simpler Gaussian models, particularly in complex terrain (Degrazia, 2005; Daly and Zannetti, 2007).

Numerical simulations with CFD have been used to characterize the atmospheric turbulent flow and the atmospheric pollutants dispersion in urban areas, using a high-resolution mesh. These numerical models require the definition of the morphological specificities of the urban environment, being able to reproduce the flow dynamics perturbations caused by the presence of the urban obstacles. CFD is a branch of fluid mechanics which aims at solving numerically a system of partial differential equations that describes the motion of fluids by Navier-Stokes equations. CFD models can be classified into three categories according to the technique to numerically solve the Navier–Stokes equations: i) Reynolds-averaged Navier-Stokes (RANS) approach; ii) Large-eddy Simulation (LES); iii) Direct numerical simulation (DNS) approach. The choice among these three methods is a balance between the cost and the goal. Recent reviews on numerical modelling of the flow dynamics and the pollutants dispersion in urban areas using CFD models are provided by Tominaga and Stathopoulos (2013) and Lateb et al. (2015).

Photochemical models have become widely recognized and routinely utilized tools for regulatory analysis and attainment demonstrations by assessing the effectiveness of air pollution control strategies. Photochemical models simulate the changes of pollutant concentrations in the atmosphere using a set of mathematical equations characterizing the chemical and physical processes in the atmosphere, and it are applied at multiple spatial scales (from local to global). According to Russell and Dennis (2000), photochemical models have been formulated in both the Lagrangian and Eulerian reference frames. The most commonly used air photochemical models are Eulerian type with multilayer which can be applied for urban scale (such as TAPM [Hurley, 2008]), regional scale (such as CHIMERE [Schmidt et al., 2001]), and multi-scale (such as CAMx [Morris et al., 2004]) and WRF-CHEM [Grell et al., 2005]).

With the increase of computational resources, the integration and coupling of numerical weather models and chemical transport models to study the feedback interactions between meteorological and chemical processes within the atmosphere became a research challenge. The way in which meteorological models can be coupled with chemistry models can be accomplished in one of two ways (Grell et al., 2005; Baklanov et al., 2014): i) off-line modelling system, also called one-way interactive model, which implies that the chemical transport model is run after the meteorological simulation is completed; ii) on-line modelling system, also called integrated or two-way interactive models, can be on-line access models, when meteorological data are available at each time step, or on-line integration of a chemical transport model into a meteorological model, where two-way feedbacks may be considered. Both off-line and on-line modelling system are widely used in current regional models (Zhang, 2008). Off-line systems are frequently used in ensembles and operational forecasting, adjoin modelling and sensitivity studies, whereas on-line models are increasingly used for applications in which air pollution feedbacks on meteorology processes and climate forcing become important and where higher computational cost is not a limiting factor.

Source-receptor models (also called as statistical models) are mathematical or statistical procedures for identifying and quantifying the sources of air pollutants at a receptor location. Unlike photochemical and dispersion air quality models, source-receptor models do not use pollutant emissions, meteorological data and chemical transformation mechanisms to estimate the contribution of sources to receptor concentrations. Instead, receptor models use the chemical and physical characteristics of gases and particles measured at source and receptor to both identify the presence of and to quantify source contributions to receptor concentrations. Different approaches are available in literature to define the source-receptor model structure, such as Artificial Neural Networks (ANN) (Carnevale et al., 2009; He et al., 2016). Artificial neural networks have been frequently used as a nonlinear tool in recent atmospheric and air quality forecasting studies. In addition, the low time (few minutes, or even seconds) required to estimate concentration levels as consequence of an emission variation, allows their application in integrated assessment models and in optimization processes (Carnevale et al., 2012).

The use of an air quality model without comparison with measurements is useless to an adequate air quality assessment. To instil confidence in the model's prediction for the future or model assessment of the air quality, should be assured that the model's process description and interactions are as accurate and realistic as possible (Russel and Dennis, 2000). In this sense, model quality assurance and scientific model evaluation are crucial elements to get this purpose. Model evaluation is in general a complex procedure (Thunis et al., 2012) involving different steps, namely:

- Verification is an internal process that determines the consistency, completeness and correctness of the fundamental equations, methods, hypotheses, computer codes and adequacy of the model design relative to the design model criteria.
- Validation is and external process that determines the veracity and legitimacy of the model with respect to a user's needs and requirements of the correctness of the model's representation of reality. This step is usually performed through the comparison of modelled and measured data, based on the estimation of statistical indicators and graphical analysis. Although validation cannot give a thorough insight into the properties of the model, it is seen as a good first step in the evaluation of model performance.
- Uncertainty analysis, refers to knowledge or information on the model's parameters, constants, input data and concepts. The total of model uncertainty may be defined by the sum of three components: i) model uncertainty which is associated with model formulation; ii) input data uncertainty which is related to emissions, measured data, meteorology, chemistry or model resolution; iii) inherent variability which refers to stochastic and anthropogenic processes that by nature are not known.
- Sensitivity analysis, which is the process to understand how a given model depends upon the information, fed into it. Sensitivity testing can be performed with respect to model's chemistry/physics parameters or with respect to input data (emissions and meteorology).
- Model inter-comparison, which is the process to assess a model performance by simultaneous comparison of modelling results provided by different models for the chosen situations. The differences in model results can reveal the strengths and weakness of particular modules or parameterizations schemes and can help to characterize conceptual uncertainties arising from the choice and implementation of the physical models applied.

Several studies have been developed to address the model quality assurance and evaluation of the model processes. In Europe, different model evaluation initiatives have been supported by the European Commission through projects and networks of excellence. There are several reports available to support modelling systems and best practices. The EUROTRAC-2 subproject SATURN (Studying Atmospheric Pollution in Urban areas) provided a review of air quality models for use in urban applications. Furthermore, within the subproject GLOREAM (GLObal and Regional Atmospheric Modelling) a set of activities were developed to provide regional-scale model inter-comparison for O_3 (Roemer et al., 2003) and inorganic aerosol compounds (Hass et al., 2003). In addition, the Air4EU project (Borrego et al., 2006, 2008) provided several reports recommending best practices for the use of models in air quality assessment and estimation of model uncertainty. Despite of that, the modelling

community is so broad and the applications of air quality modelling so varied that until recently there was not a clear and common understanding of the quality assurance requirements that should be applied in air quality modelling. To fulfil this gap of knowledge, the Forum for Air Quality Modelling in Europe (FAIRMODE), coordinated by the European Environmental Agency and the European Commission Joint Research Centre, aimed to bring together air quality modellers and users to promote and support the harmonised used of models by EU members. In this sense, FAIRMODE provided a dynamic document (with regular updates base on internal or external activities) which represents a consensual guidance on air quality modelling (Denby et al., 2010).

In parallel, in North America, the United States Environmental Protection Agency has published a guide on environmental modelling which presents recommendations and provides an overview of best practices for ensuring and evaluating the quality of environmental models. More recently, a joint initiative between North America and Europe has been established in terms of air quality evaluation, AQMEII (Air Quality Model Evaluation International Initiative), with the aim to bring together American and European regional scale modelling communities, for an effect and efficient exchanges of views and experiences through common activities.

In summary, until now there are not specific prerequisites for using air quality models. However, a general 'fit-for-purpose' criteria should be applied, namely, if the model has the appropriate spatial and temporal resolution for the intended application; if the model is adequately evaluated for the particular application; if the model contains the relevant physical and chemical processes needed for the type of application; if the relevant emission sources are well described and represented; and if the appropriate meteorological data are available. An increase of the accuracy of modelling tools is still a research challenge, especially in a context of climate change, where the need of realistic prediction of the impacts across the different sectors is vital to be able to adopt the appropriated strategies and policies. The need of increase the knowledge of how cities will be affected by climate change and the way of how them will be able to adapt, implies that the improvement of models' accuracy is mostly related to a better representation of the urban physical processes in mesoscale models (both weather and air quality models).

1.3. CLIMATE CHANGE IN CITIES

The last Intergovernmental Panel for Climate Change (IPCC) 2013 report (AR5) (IPCC, 2013), defined climate change as a change in the state of the climate that can be identified (e.g., by using statistical tests) through changes in the mean and/or the variability of its properties that persists for an extended period, typically decades or longer. Climate change may be due to natural internal processes or external forcing's such as the modulations of the solar cycles, volcanic eruptions, and persistent anthropogenic changes in the composition of the atmosphere or in land use.

Observations of climate variables have been made from measurements taken *in situ* (land and sea surface atmosphere and deep ocean), as well as remote measurements made by satellites since

1950s, providing sustained datasets available. The collected data of the global average annual land and ocean near-surface temperature in the decade 2006–2015 was 0.83 to 0.89°C higher than the pre-industrial average (mid- to the end of the 19th century). Globally, 2015 was the warmest year on record, namely about 1°C warmer than the pre-industrial temperature. Observations also show an increase of ocean heat content in the deeper ocean and increases in the sea level. Precipitation shows both positive (increase of precipitation levels) and negative (decrease of precipitation levels) trends. The AR5 concluded that human influence has been the dominant cause of the observed changes in climate variables (IPCC, 2013).

The period 2006-2015 was the warmest decade on record in Europe, with land temperatures around 1.5°C warmer than the pre‑industrial level (EEA, 2017). Europe has experienced several extreme summer heat waves since 2003, which have led to high mortality and economic impacts. Precipitation has increased in most of northern Europe, in particular in winter, and has decreased in most of southern Europe, in particular in summer. Heavy precipitation events have increased in several regions (northern and north-eastern Europe). In Portugal, similar trends have been observed. The mean temperature has risen in all regions of Portugal in the period 1976-2006, at a rate of approximately 0.52°C per decade, which more than double the rate of mean annual global temperature increase. The temperature increase was accompanied by a change in the frequency of very hot days and a decrease in the frequency of very cold ones. The heat waves of 2003, 2006, 2009, and 2010, becoming more frequent since the beginning of this century and were of particular relevance due to their duration and spatial extension (Ferreira et al., 2008; Carvalho et al., 2013).

Climate models (also called General Circulation Models - GCMs) are the most advanced tools for modelling the state of the climate system and simulating its response to changes in atmospheric concentrations of greenhouse gases and aerosols. GCMs simulate the climate system at the global scale (at a horizontal resolution between 50 and 250 km) based on the physical, chemical and biological properties of its components, their interactions and feedback processes, and accounting for its known properties (IPCC, 2013). For more detailed regional climate impact assessments, regional climate models (RCMs) have been used. RCMs are limited in area but can provide information on the climate in higher spatial resolution than GCMs. RCMs typically have a horizontal resolution of between 2 and 50 km, which allows for a better representation of topographic features (e.g. mountain ranges) and of regional-scale climate processes.

To be able to determine the impact of future climate change, a set of climate projections are needed to get a range of possible futures. The IPCC has been developed a set of emissions scenarios (greenhouse gas emissions scenarios), representative of a possible future, based on differing sets of assumptions about population changes, economic development and technological advances.

Until about 2010, most climate projections used the storylines and the associated emissions scenarios published by the IPCC in 2000 in the Special Report on Emissions Scenarios (SRES) (Nakicenovic et al., 2000). These SRES scenarios provide internally consistent socio-economic storylines and greenhouse gas emissions scenarios for four world regions. They are baseline scenarios, which

means that they do not take into account specific agreements or policy measures aimed to limiting the emission of greenhouse gases (e.g. the Kyoto Protocol to the UNFCCC). The SRES emissions scenarios are organised into families, which contain scenarios that are based on similar assumptions regarding demographic, economic and technological development. Based on their cumulative emissions throughout the 21st century, they can be broadly grouped into low (B1), medium–low (B2, A1T), medium–high (A1B) and high (A2, A1FI) scenarios.

The follow-up generation of scenarios to support climate change research are called representative concentration pathways (RCPs). The RCPs provide a consistent set of trajectories for future atmospheric composition and land-use change up to the year 2100, which is determined not only by direct anthropogenic greenhouse gas emissions, but also by the future development of the global carbon cycle and other processes (EEA, 2017). The four RCPs are named as RCP2.6, RCP4.5, RCP6.0 and RCP8.5 according to their radiative forcing level in the year 2100. The main characteristics of each RCPs are showed in Table 1-4.

Table 1-4. Main characteristics of RCPs scenarios (Source: adapted from EEA, 2017).

RCP	Radiative forcing	Concentration (ppm)	Pathway	Model providing RCP
RCP8.5	>8.5 $W \cdot m^{-2}$ in 2100	>1370 CO_{2eq} in 2100	Rising	MESSAGE
RCP6.0	≈6.0 $W \cdot m^{-2}$ at stabilization after 2100	≈850 CO_{2eq} (at stabilization after 2100)	Stabilization without overshoot	AIM
RCP4.5	≈4.5 $W \cdot m^{-2}$ at stabilization after 2100	≈650 CO_{2eq} (at stabilization after 2100)	Stabilization without overshoot	GCAM
RCP2.6	Peak at ≈3.0 $W \cdot m^{-2}$ before 2100 and then declines	Peak at ≈490 CO_{2eq} before 2100 and then declines	Peak and decline	IMAGE

Climate projections under the RCPs scenarios predict changes in the dynamics of the climate system, namely (IPCC, 2014a):

- An increase of the European annual average land temperature by the end of this century in the range of 1 to 4.5°C under RCP4.5 and 2.5 to 5.5°C under RCP8.5, which is more than the projected global average increase;
- An increase of the magnitude of very extreme heat waves, which are projected to occur as often as every two years in the second half of the 21st century (increase of frequency); the impacts will be particularly strong in southern Europe;
- An increase of the annual precipitation is generally projected in northern Europe, while a decrease is projected in southern Europe (especially in the summer). Heavy precipitation events are projected to become more frequent in most parts of Europe, in particular in winter;
- A decrease of the volume of European glaciers between 22 and 84% compared with the current situation by 2100 under a moderate greenhouse gas forcing scenario, and between 38 and 89% under a high forcing scenario; the melting of glaciers will contribute significantly to global sea level rise.

A recent study conducted over Portugal (Marta-Almeida et al., 2016) evaluated the future climate, for a short- and long-term period, using the RCP8.5. According to this projection, it is expected an increase of near-surface temperature, especially the maximum values, in a range of 2.8°C and 4.0°C by 2100, with a consequent increase of the frequency, magnitude and duration of heat waves (Carvalho et al., 2017). A decrease of the annual precipitation, between 5% to 20%, was predicted; the mean seasonal precipitation is expected to decrease substantially in all seasons, excluding winter. These results are in accordance with previous works (e.g., Soares et al., 2014) performed under the A1B emission scenario.

At the global scale, cities only cover a small fraction of the Earth (approximately 2% of the land surface). Despite of that, given the large and ever-increasing fraction of the world's population living in cities (the majority of the world now live in cities), and the disproportionate share of resources used by these urban residents, cities and their inhabitants are key drivers of global environmental change. Urban areas are the major sources of human generated carbon dioxide (CO_2) emissions - from the burning of fossil fuels for heating and cooling; from industrial processes; transportation of people and goods, and so forth. While the exact number is debated, overall 70% to 90% of carbon emissions are generated in cities (EEA, 2017).

While urban areas will generally experience the same exposures to climate as their surrounding region, the urban design can alter exposures as well as impacts at the local scale. For example, the impact of heat waves will be felt with particular intensely in cities, due to the urban heat island effect that will enhance the differences between the urban air temperatures compared with the air of rural surroundings. These patterns are a function of urban morphology, built materials, amounts of vegetation and human activity (IPCC, 2014b). The materials that make up cities (concrete, brick, and asphalt) have different thermal and hydrological properties than natural materials (soil, trees, grass), which affect how the surface absorbs and stores heat and water. This means that more energy from the sun is absorbed by the urban surface and stored, making the surface warmer. The morphology (shape) of the urban surface is also different from the natural landscape. The walls and roofs of buildings increase the surface area exposed at the surface which results in greater absorption of incoming radiation (energy) from the sun and affect the flow of air across the surface. Direct emissions by urban residents; whether heat (from traffic, industry, the heating of buildings) or gases (carbon dioxide from burning of fossil fuels) or particulates (from industrial processes or traffic) all affect the urban atmosphere and the absorption and transmission of energy, and thus the weather and climate of cities. In this sense, well-functioning and climate-cities resilience are key for a climate-resilient Europe (Grimmond, 2007; IPCC, 2014b).

In this section different features of climate change impacts in cities will be discussed. First will be reviewed the concepts of cities vulnerability and resilience applied to a context of climate change (section 1.3.1.). Then, an overview of the linkages between air quality and climate change (section 1.3.2) as well as the links between urban fluxes (section 1.3.3) will be provided.

1.3.1. Vulnerability and resilience

Studies on urban vulnerability tend to characterize this concept as the possibility to be harmed; that is, as the degree to which a system (e.g. city, population, infrastructure, economic sector) is susceptible to, and is unable to cope with, adverse effects of a single, or of several stressors (e.g. climate change) (Fussel, 2007). The IPCC defines vulnerability (to climate change) as a function of the character, magnitude and rate of climate change to which a system is exposed, its sensitivity and capacity to adapt (IPCC, 2007). According to this definition, is an integrated concept, expressed by the linkages of several dimensions: exposure, sensitivity, and adaptive capacity (Figure 1-3).

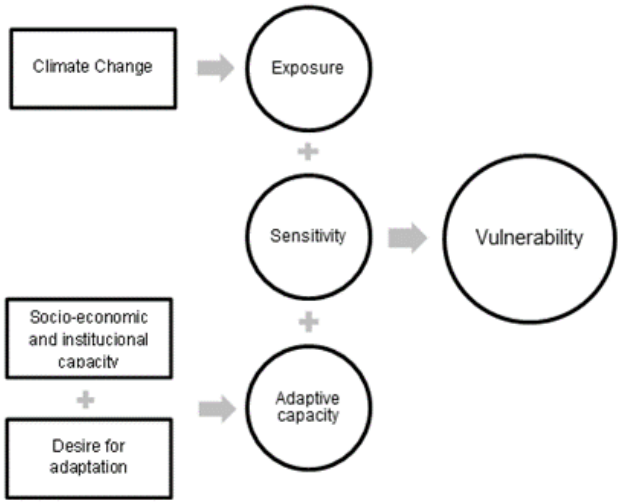

Figure 1-3. A conceptual framework of urban vulnerability to global climate and environmental change [Source: adapted from Romero-Lankao et al., 2011].

Exposure and sensitivity are related properties of a system and are dependent on the interaction between the characteristics of the system and on the attributes of the surrounding environment, namely climate stimulus. Exposure refers to the degree, duration, and/or extent to which the system is in contact with, or subject to, the perturbation (Kasperson et al., 2005; Adger, 2006). It is a property of the relationship between the system and its environment (specifically between the system and the perturbation), rather than a property of the system. The concept of sensitivity varies between authors. According to the IPCC (2007), sensitivity is “the degree to which a system is affected, either adversely or beneficially, by climate-related stimuli”. The effect may be direct (e.g., an increase of photochemical pollutants concentration in response to a change in the mean, range, or variability of temperature) or indirect (e.g., an increase of atmospheric pollutants concentrations caused by an increase in the energy consumption due to temperature rise). Conceptually, it can be described as the amount of transformation of the system per unit of the change in a given factor, but in the simplest case it only specifies if a system is or not responsive to a particular stressor (Gallopín et al., 2003). In this context, sensitivity is an attribute of the system, distinguished from its capacity of response.

The other central concept related to vulnerability is adaptive capacity, also referred to as “coping capacity” (Turner et al., 2003) or “capacity of response” (Gallopín et al., 2003). In general, adaptive

capacity is defined as “the ability of a system to adjust to climate change (including climate variability and extremes) to moderate potential damages, to take advantage of opportunities, or to cope with the consequences” (IPCC, 2007). “Adaptive capacity” can be assessed at different spatial scales, from national to local (EEA, 2012). However, as adaptation decisions are context-specific, and the adaptation decisions are often made at the local level, the local and regional scales are particularly relevant for assessment of adaptive capacity (Engle et al., 2010; Greiving et al., 2011). Six major elements are identified to support climate change policymaking at the local scale: (i) good governance; (ii) presence of national programmes facilitating local action; (iii) democratic and participatory nature of institutions; (iv) cities competences and authority to regulate climate-relevant issues; (v) the commitment of cities to take climate action; (vi) availability of economic resources, knowledge and information, for example through the involvement of cities in national and transnational networks which allows the exchange of experience (Martins and Ferreira, 2011). In sum, the adaptive capacity is directly related to the socio-economic and institutional capacity of a city, as well as, to the desire of adaptation of its citizens (Figure 1-3).

The main lineages of research on urban vulnerability to climate change are based on vulnerability in the general environmental change context: natural stressors, political economy (or ecology) and ecological resilience (O’Brien et al., 2009; Romero-Lankao et al., 2011). Figure 1-4 presents a schematic of the evolution of the main lineages of urban vulnerability research over time. The arrows represent the recent efforts within each lineage to converge with other traditions and develop a more integrated understanding of the different dimensions and determinants of urban vulnerability. Should be noted that the Figure 1-4 reflect the lineages well known and perfectly defined (as described by Romero-Lankao et al., 2011), as well as, the expected development on this area.

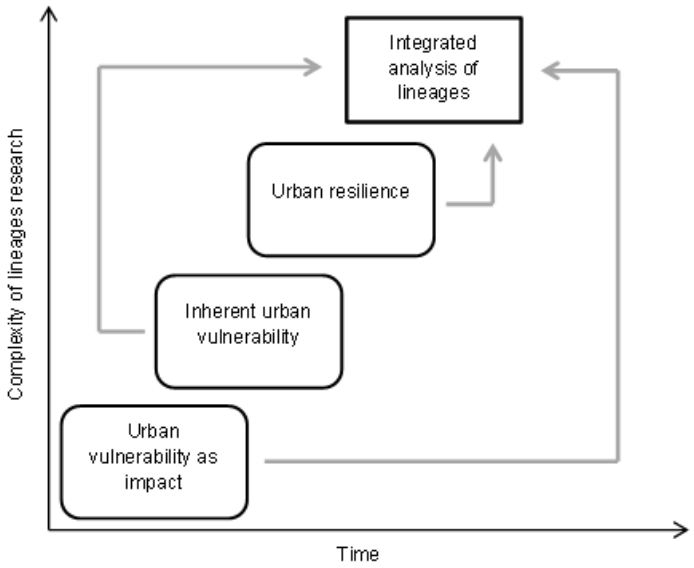

Figure 1-4. Lineages of urban vulnerability research [Source: adapted from Romero-Lankao et al., 2011].

The urban vulnerability as impact lineage addresses issues such as urban exposure or sensitivity to changes as a result of a stressor. There are two main types of research within this lineage. The first explores how changes in a variable or combination of variables (e.g. temperature, air pollution,

precipitation) impacts crops productivity, air pollution exposure or mortality. In addition, several studies investigate the geographical characteristics of urban settlements (e.g. low elevation coastal zones, water scarcity, and steep slopes) that make city residents vulnerable to the impacts of climate change (CLACC, 2009; Bhattari et al., 2010). The second group of studies applies a scaled-down version of global climate change scenarios to urban areas to estimate how parameters such as temperature and sea level rise will evolve in the future. Future climate impacts such as UHI effects, storms and heat waves, and its influence on atmospheric pollutants concentrations, are predicted under a climate change scenario (e.g., through the application of both meteorological and air quality models) (Chysoulakis et al., 2013). Some analysis also explore the implementation of adaptation measures, under realistic socioeconomic scenarios (considering future emissions, land use changes, evolution of population density), to evaluate how those impacts can be reduced (Romero-Lankao et al., 2011). According to Romero-Lankao et al. (2011), this approach not allows a complete understanding of a set of questions, namely: how and why specific urban areas, or populations and sectors within cities are differentially affected; whether local stakeholders and populations are receptive to adaptation options and motivated to make the necessary changes; whether they have the necessary skills, awareness and resources to be able to adapt; and how their potential adaptation measures are constrained by the social, economic, political, and environmental circumstances in which they live.

Due to the need of answer these questions, the urban inherent vulnerability lineage emerged with the goal of explore how and why particular cities or populations are more vulnerable or more able to adapt to climate stressors than others. Recent research has focused on urban areas, with limited socioeconomic power, which are expected to be more affected by the impacts of climate change, as a result of both development and management deficits. These studies want to answer the questions of which urban areas are vulnerable, who within a city is vulnerable, and how and why particular urban populations are vulnerable. This approach does not, for example, analyse how exposure to, and impacts from, changing stressors behave and evolve over time (Parnell et al., 2007; Satterthwaite et al., 2007). The most recent lineage of urban vulnerability is related to the emerging application of resilience science, which reflects a general change from vulnerability to response-capacity of cities in recent climate change research, with some attempts to explore vulnerability and resilience as two overlapping inherent properties of urban system (Leichenko, 2011.)

More recently efforts have been made to integrate relevant urban knowledge from the disaster-risk management, climate change and development communities (Figure 1-4), and by recent research applying a more integrated version of the stressors and a climate vulnerability framework in an urban context (Romero-Lankao et al., 2011). As result, it is expected that the urban vulnerability research evolves for an integration of the existing lineages and the development of a better integrated research approach to help fully understand the nature of and interactions between impacts, stressors and their precursors, adaptive capacities, and actual adaptations of urban environments to climate change. Ultimately, this lineage should be able to increase our ability to design and implement more effective response actions.

Understanding the factors that control the urban vulnerability to climate effects and to weather extreme events, and the scales at which they operate, provides a framework for considering resilience. The notion of resilience is gaining increasing prominence within the literature on cities and climate change, as result of a broad consensus that: i) cities must become resilient to a wider range of perturbations and stressors in order to be face climate change; ii) efforts to foster climate change resilience must be bundled with efforts to promote urban development and sustainability. Enhancement of resilience is widely cited as a fundamental goal for both adaptation and mitigation efforts in cities and urban regions (Cutter et al., 2008). Terms such as “climate resilient”, “climate-proofing”, and the “resilient city” are frequently used to emphasize the idea that cities, urban systems and urban communities need to be able to quickly recover from climate-related impacts and stressors. As result, a resilient city is characterized by its capacity to withstand or absorb the impact of a stressor through resistance or adaptation, which enable it to maintain certain basic functions and structures during an extreme event, and bounce back or recover from an event (Twigg, 2009).

Urban resilience studies are grounded in a diverse range of research lineages, which can be classified into four categories: i) urban ecological resilience; ii) urban hazards (stressors) and disaster risk reduction; iii) resilience of urban and regional economies; iv) promotion of resilience through urban governance and institutions. There is much overlap among these different sets of literature, each emphasizing different facets of urban resilience and each focused on different components of cities and urban systems:

- The urban ecological resilience literature, which is based on traditional notions of ecosystems resilience, defines urban resilience as the “ability of a city or urban system to absorb disturbance while retaining identity, structure and key processes” (Romero-Lankao et al., 2011). Within this literature, extreme climate events and gradual climatic changes are regarded as stressors that affect cities and urban systems (Coaffee, 2008; Maru, 2010).
- The urban hazards and disaster risk reduction literature, emphasis is placed on enhancing the capacity of cities, infrastructure systems, and urban populations, to quickly and effectively recover from both natural and anthropogenic stressors. The main outcome of this lineage is identify mechanisms and strategies to increase stressor resilience of urban communities (Romero-Lankao et al., 2011), and, ultimately, develop models of community resilience based on a wide range of quantitative indicators (Cutter et al., 2008) or measure variations in resilience of cities (Zhou et al., 2010).
- The resilience of urban and regional economies literature (Ernstson et al., 2010), analyses the evolution of urban and regional economic and industrial systems, through the use of the ideas and terminology from ecological resilience theory, emphasizing that climate change is one of many types of stressors that urban and regional economies face (Pendall et al., 2010; Pike et al., 2010). The emphasis on the relationship between resilience and geographical location raises important questions about the role of power and politics in influencing development paths and trajectories of urban areas (Pike et al., 2010).

- The promotion of resilience through urban governance and institutions literature is focused on questions of how different types of institutional mechanisms (e.g., financial instruments, insurance policies, and stakeholder involvement) affect the resilience of local environments (Ostrom, 2010) and how resilience thinking can influence the development of governance measures to promote adaptation to climate change (Swalheim and Dodman, 2008). The understanding, by the decision makers, that the successful of adaptation measures at local scales is strongly influenced by educational, cultural and social cohesion, will promote a dissemination of information and awareness of local communities regarding urban vulnerability to climate change (Tanner et al., 2009).

In the scope of urban ecological resilience literature, there is a growing recognition and awareness that nature can help to provide viable solutions that use and deploy the properties of natural ecosystems and the services that they provide in a smart, 'engineered' way. These solutions, knowing as nature-based solutions, provide sustainable, cost-effective, multi-purpose and flexible alternatives for various objectives. Working with nature, rather than against it, can further pave the way towards a more resource efficient, competitive and greener economy. It can also help to create new jobs and economic growth, through the manufacture and delivery of new products and services, which enhance the natural capital rather than deplete it (EC, 2015).

Example of nature-based solutions are the green (GI) (e.g., green roofs, green walls, urban parks) and blue infrastructures (e.g., ponds). In contrast to the most common ‘grey’ (man-made, constructed) infrastructure approaches that serve one single objective, GI promotes multifunctionality, which means that the same area of land is able to perform several functions and offer multiple benefits if its ecosystems are in a healthy state (EC, 2015). These functions could be environmental (such as conserving biodiversity or adapting to climate change), social (e.g. providing water drainage or green space) or economic (supplying jobs and raising property prices, for instance). A set of studies having been analysing the multiples benefits of urban GI, mostly related to: mitigation of urban heat island effect and heat waves impacts, based on the capabilities of GI to regulate the micro-climate by providing shade, thermal isolation and moisture and wind protection (e.g., Synnefa et al., 2008; Susca, 2012; Li et al., 2014; Carvalho et al., 2017), improvement of air quality (e.g., Makhelouf, 2009; Amorim et al., 2013; Nowak et al., 2014; Klingberg et al., 2017), and improvement of the synergistically physical, mental and social wellbeing and providing a habitat for a variety of species (Newton, 2007; Tzoulas et al., 2007). As such, GI has the potential to offer win-win, or 'no regrets' solutions by tackling several problems and unlocking the greatest number of benefits, within a financially viable framework. GI can therefore serve as a highly valuable policy tool for promoting sustainable development and smart growth, by meeting multiple objectives and addressing various demands and pressures (EEA, 2011b).

In summary, nature-based solutions comprise a wide range of environmental features that operate at different scales and form part of an interconnected ecological network. At the same time, these features must be multifunctional; they must be more than simply ‘a green space’. The implementation

of nature-based solutions is seen by EU as crucial measures to deal with the impacts of climate change (reduce the cities vulnerability) as well as to increase cities resilience to their current and future environmental problems. The implementation of such measures implies changes in the urban morphology and design, and so, changes in the surface energy balance and in the urban microclimate. It is known that each city has its own problems. In this sense, the same nature-based solution will have different effectiveness and effects according to the city characteristics where it is placed. Studies that analyse the benefits and effectiveness of nature-based solutions and that provide knowledge in how these measures will influence the urban microclimate prior to its implementation are then essential. Modelling tools, in a high spatial resolution, can have a key role in this assessment, since allow the study of different set of measures considering different scenarios, providing an approach to optimize the role of nature-based solutions on human comfort and health and create knowledge in urban planning.

1.3.2. Links between air quality and climate change

As have been mentioned, air pollution is a combination of emission sources (discussed in section 1.1.1.), meteorological variables and transport patterns. Meteorology plays an important role in air pollution formation, dispersion, transport and dilution. Changes in local meteorological conditions, e.g., wind speed and direction, temperature and relative humidity, can affect the temporal and spatial variations of air pollutants levels (Duenas et al., 2002; Satsangi et al., 2004; Elminir, 2005). The analysis of the physical processes that influences the variability of the air pollutant concentrations is based on statistical approaches, which may be aggregated into three groups: regression-based modelling, extreme value approaches and space-time models (Thompson et al., 1999).

Several studies have applied the Kolmogorov–Zurbenko filter method proposed by Rao and Zurbenko (Rao and Zurbenko, 1994) to assess the linkages between air quality and meteorological conditions. Most studies have concluded that ozone concentrations are strongly linked to meteorological conditions, being positively correlated with high temperatures, solar radiation and light winds. Higher temperature enhances biogenic emissions (VOC) as well as photochemical activity since most thermal atmospheric reactions show a positive temperature dependence. In Europe, the highest O_3 concentrations occur in summer under stable high-pressure systems with clear skies (Duenas et al., 2002). Contrariwise, PM10 is not as weather-dependent as O_3. However, wind speed, mixing height, and relative humidity are the meteorological variables believed to mostly influence PM10 concentrations. Stagnant conditions are thought to correlate with high PM10 concentrations because they allow particulates to accumulate near the earth's surface. Although high wind speeds can increase ventilation, they are normally correlated with high PM10 concentrations because they allow the resuspension of particles from the ground and long-range transport of particulates between regions. High PM10 concentrations are normally associated with dry conditions due to the increased potential for the resuspension of dust, soil, and other particles. In the Southwestern United States, the moisture level, namely the relative humidity, is the strongest predictor of PM10 concentrations (Wise and Comrie, 2005). Atmospheric stagnation affects both O_3 and PM10. Sá et al. (2015) assessed the

influence of meteorological conditions on O_3, NO_2 and PM10 over the two most critical agglomerations of Portugal: Lisbon and Porto. The analysis showed that NO_2 and PM10 were not as weather-dependent as O_3. For NO_2 and PM10, a meteorological variable with higher influence was not identified; while O_3 concentration showed a statistically significant relationship with temperature. Table 1-5 summarizes the dependence of O_3 and PM10 concentrations based on meteorological variables.

Table 1-5. Dependence of surface air quality on meteorological variables* [Source: Jacob and Winner, 2009].

Meteorological variables	O_3	PM10
Temperature	++	-
Wind speed	-	-
Humidity	=	+
Cloud Cover	-	-
Precipitation	=	--
Atmospheric stagnation	++	++

*Sensitivities of surface O_3 and PM10 concentrations. Results are summarized as consistently positive (++), generally positive (+), weak or variable (=), generally negative (-), and consistently negative (--).

Due to the linkages between meteorological conditions and air quality, and despite atmospheric pollution and climate change are distinct problems, they are linked in several key ways. Climate change will result in an impact on the general weather patterns, e.g., wind velocity and direction, temperature, sunshine hours and rainfall patterns. This may result in a change to the processes that govern chemical transformations in the atmosphere, which will cause air quality changes (AQEG, 2007). In turn, several air pollutants are climate drivers, having a potential impact on the planet's climate and global warming in the short term (e.g., decades). Tropospheric O_3 and black carbon (BC), a constituent of PM, are examples of air pollutants that are short-lived climate drivers and contribute directly to global warming. Other PM components such as organic carbon, ammonium, sulphate, and nitrate may have a cooling effect. Greenhouse gases (GHGs) and air pollutants impact the climate system through two main pathways: direct and indirect radiative forcing (RF). Direct RF refers to the change of fraction of radiant energy received from the sun being either absorbed (by the well-mixed GHGs, tropospheric O_3 and stratospheric water vapour) or scattered by sulphate aerosols, for example. Indirect RF refers primarily to aerosols changing cloud properties and precipitation patterns. Other indirect effects are the deposition of BC aerosol on ice and snow, resulting in less solar radiation being reflected by these surfaces, which promotes heat retention and an increase of net storage heat flux, with a consequent increase of the rate of melting of snow and ice masses (EEA, 2014a).

Evaluation of future air quality projections should account for changes in both future and climate conditions (Penrod et al., 2014). Sá et al. (2016) synthetize the studies of air quality under future climate based on air quality numerical tools in three main approaches, according to its characteristics:

- studies that only consider the effect of climate change, keeping anthropogenic emissions constant (Fiore et al., 2011; Carvalho et al., 2010; Tai et al., 2012; Manders et al., 2012);

- studies that maintain the meteorological conditions constant (same as the historical year) in future scenarios and only change the air pollutant emission scenarios (Dentener et al., 2005; Zhang et al., 2010); and
- studies that consider both effect of climate change along with the modification of the anthropogenic emissions in the future scenarios (Lei et al., 2012; Coleman et al., 2013; Doherty et al., 2013; Gao et al., 2013; Jiang et al., 2013; Colette et al., 2013; Penrod et al., 2014; Trail et al., 2014; Lacressonnière et al., 2014; Markakis et al., 2014).

Most of the studies assess the combined effects of climate change and future air pollutant emissions on O_3. Lacressonnière et al. (2014) simulated changes in European air quality for the 2030s and 2050s, under the RCP8.5 scenario. Results showed an increase of surface ozone in north-western Europe and a decrease in southern areas. Average O_3 levels steadily increased at a rate of approximately 3 $\mu g \cdot m^{-3}$ per decade in Summer time over the whole of Europe. Results also showed that the tropospheric ozone levels will be dominated by enhanced stratosphere–troposphere exchanges in future climate, while the chemical budget will be strongly reduced. The results also point out that a NOx-limited chemical regime will stretch over most of Europe, especially Western France in the future (Lacressonnière et al., 2014). Over Portugal, Carvalho et al. (2010) concluded that atmospheric O_3 monthly mean levels may increase almost 20 $\mu g \cdot m^{-3}$ in July when only climate change forcing was considered.

More recently, research has also been focused on the evaluation of the impacts on PM2.5 (Lam et al., 2011; Tai et al., 2012; Jiang et al., 2013; Colette et al., 2013; Penrod et al., 2014; Trail et al., 2014) and PM10 (Carvalho et al., 2010; Manders et al., 2012) levels. The impact of climate change on surface PM concentrations is not well known, with different conclusions being obtained, including the signal of the effect and the identification of the most important driver of PM sensitivity to climate change. Carvalho et al. (2010) found that, throughout Portugal, the maximum increases of PM levels are foreseen for the northern coastal region in September, reaching nearly 30 $\mu g \cdot m^{-3}$.

Despite the set of air quality studies performed under climate change conducted over the last year, the majority of these studies were focused on global or regional level, not reaching a higher detail (urban or city scale). Sá et al. (2016) evaluated air quality over mainland Portugal and over Porto urban area in 2050 under the RCP8.5 scenarios, using high spatial resolution modelling and emission scenarios at urban scale (1 km). The three critical pollutants in Portugal (O_3, PM10 and NO_2) were analysed. Results showed an increase in the occurrence, duration and intensity of extreme values of PM10 and O_3, surpassing the annual legislated values and registering a higher number of daily exceedances. Considering the climate change effects alone, results showed an increase of the NO_2 and PM10 annual means in both Portugal and Porto urban area. When projected anthropogenic emissions were combined with climate conditions, a decrease of NO_2 annual mean concentrations was obtained in Portugal and Porto urban area (around 50%), mostly due to the reduction of projected emissions. Overall, an air quality degradation is expected over Portugal for the medium-term climate future (2046-2065), related with the trends projected for this period, which implies warmer and dryer conditions and an increase of background concentrations of ozone and particulate matter.

In summary, the interaction between climate change, pollutant emissions and atmospheric concentrations is still of great debate and much has still to be explored in order to understand and accurately predict the changes in pollutant levels under future climatic conditions and at different spatial scales. In order to perform this kind of analysis it is important to understand that no single model is capable of reproduce a sufficiently wide range of spatial and temporal scales to address all issues related to air pollution and climate change. As Markakis et al. (2014) highlighted, the impact of climate change on air quality at the city scale is still a current research challenge. The analysis of the effect of climate change on air quality will require an increase in model simulations confidence for this purpose. For that, the inclusion of urban surface schemes and urban parameterizations in mesoscale models, especially in meteorological models, is crucial to realistic reproduce the physical processes that occurs at city level. In the case of Portugal, due to the current air quality problems and due to the projections of air quality degradation, research (based on numerical models' application) that assess the ability of different measures to increase cities resilience to both climate change effects and air quality issues is essential. Additionally, beyond the traditional and critical pollutants (PM and NO_2), studies that assess CO_2 levels are also needed, due to its importance as greenhouse gas and due to the most recent outcomes that show the harmful effects of CO_2 for human health.

1.3.3. Urban fluxes feedbacks

The Earth's climate system is powered by the incoming solar shortwave radiation that is nearly in balance with the outgoing longwave radiation. Of the incoming solar shortwave radiation, about half is absorbed by the Earth's surface; the rest is reflected back to space or absorbed in the atmosphere (Figure 1-5). The land surface on average is heated by net radiation balanced by exchanges with the atmosphere of sensible and latent heat fluxes; thereby a narrow linkage between urban fluxes and climate exists. Turbulent fluxes transport heat, mass and momentum from the surface to the atmosphere. As result, they influence weather conditions (e.g., atmospheric temperatures and humidity) and climate from the microscale (at street level) up to the synoptic scale. They also provide the lower boundary conditions (fluxes) to meso- and global-scale atmospheric models and are forced with meteorology from the overlying atmospheric model (EEA, 2017).

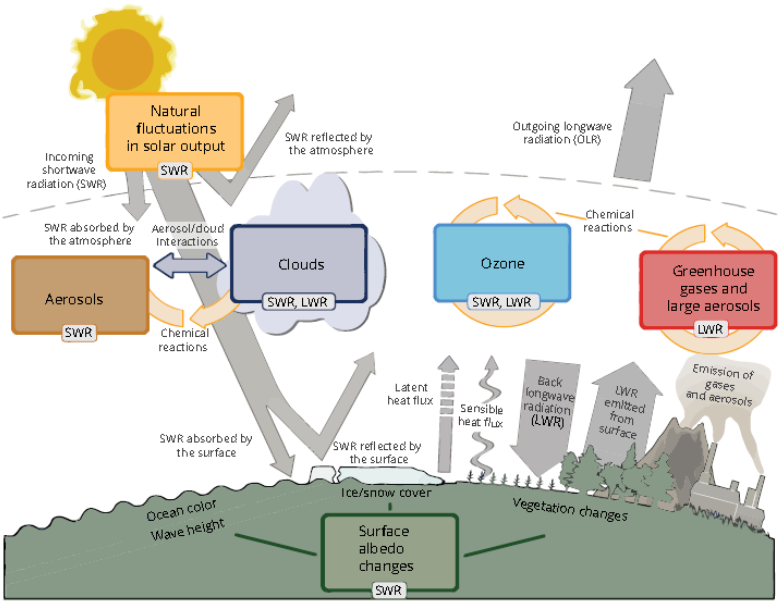

Figure 1-5. The Earth's energy balance and the drivers of climate change [Source: EEA, 2017].

The linkages between urban fluxes and urban microclimate occur in a set of different ways. Sensible heat is the energy carried by the atmosphere in its temperature and latent heat is the energy lost from the surface by evaporation of surface water. The latent heat of the water vapour is converted to sensible heat in the atmosphere through vapour condensation and this condensed water is returned to the surface through precipitation. For example, an increase of water vapour concentration with temperature promotes the relative amount of the latent heat flux as does low relative humidity. Vegetation can prolong the availability of soil water through the extent of its roots and so increase the latent heat flux but also can resist movement through its leaves, and so shift the surface energy fluxes to a larger fraction carried by the sensible heat flux. If a surface is too dry to exchange much water with the atmosphere, the water returned to the atmosphere should be on average not far below the incident precipitation, and radiative energy beyond that needed for evaporating this water will heat the surface. Under these circumstances, less precipitation and hence less latent heat flux will make the surface warmer. Reduction of cloudiness from the consequently warmer and drier atmosphere may act as a positive feedback to provide more solar radiation. A locally moist area (such as an oasis or pond), however, would still evaporate according to energy balance with no water limitation and thus should increase its evaporation under such warmer and drier conditions (IPCC, 2007). These linkages are established into a two-way, since urban fluxes to the atmosphere modify atmospheric variables and such changes feed back to the fluxes.

Due to the feedbacks between the surface and the atmosphere, if the properties of the land surface are changed locally and the meteorological variables are changed under a climate change context, the surface energy balance and the partitioning between latent and sensible heat fluxes may also change, with consequences for temperature and moisture storage of the surface and near-surface air. Due to the importance of the surface energy balance to the urban microclimate, some studies have been addressed the subject of the energy fluxes balance under future climate change conditions.

Wild et al. (1997) examined the flux changes in global climate model simulations with increased levels of greenhouse gases and related them to the systematic errors found in the simulation under a current climate. Georgescu et al. (2009) focused on the documentation of climatic effects of 30 years of landscape change over Greater Phoenix with a particular focus on the surface radiation and energy budgets. Two key findings were made: i) while a small difference in the net radiative flux between the 1973 and 2001 were obtained, changes in the repartitioning of surface-absorbed energy were found; these changes are critical for any modification of the near-surface climate; ii) the partitioning of surface absorbed energy into sensible and latent heating has been shown to be a significant driver of atmospheric circulations and convective activity. Sheng et al. (2010) identified regions with strong changes in climatic variables and surface energy fluxes through identification of their long-term trends and interannual variability from 1948 to 2000. A key finding of this work was related with the fact that sensible heat provides boundary layer heating and latent heat affects boundary layer moistening, therefore, regions with Q_H and Q_E hotspots (e.g., strong land–atmosphere feedbacks) could have more extreme weather activities (e.g. moisture convection precipitation events, summer heat waves) on shorter timescales and have more significant contributions to strong seasonal or interannual variability in climate on longer timescales (Sheng et al., 2010). Lindberg et al. (2013) used LUCY model to assess changes in anthropogenic heat flux over a 20-year period (1995–2015) across Europe. The results showed that the changing energy use and the variability of air temperatures can result in large changes in the Q_F magnitude. Considering the effect of only using changes in energy consumption over time, the impact is predicted to be a 10–12% increase in Q_F. Additionally, it was also highlighted that it is absolutely critical that for any application, whether global climate modelling or sources of energy from buildings, that the anthropogenic heat flux is calculated at the appropriate scale of the area of interest (Lindberg et al., 2013). Ma et al. (2014) estimate the heat flux changes caused by the projected land transformation over the next 40 years across China to improve the understanding of the impacts of land dynamics on regional climate. Hamdi et al. (2015) conducted a set of simulations of present and future urban climate over Brussels Capital Region and Grand Paris Region, based on the IPCC SRES A1B future scenario, disregarding however, the anthropogenic heat flux. For both locations, the latent heat flux is projected to decrease compared to present day. As such, urban air temperature will rise less than rural air temperature in the future. During the day, the downward shortwave radiation increases for the city centre of Brussels, which is in agreement with the increase in the number of cloud free days in the future.

In summary, while research focused on past-present-future climate is not new, still few urban studies assess the energy fluxes balance under future climate change conditions. A continuous knowledge of the state of the surface and the atmosphere, through the (quantitative) analysis of the behaviour and magnitude of the surface energy balance under climate change context (following the new IPCC climate scenarios), is required.

1.4. RESEARCH OBJECTIVES

The revision of the state-of-the-art of air quality in Europe and in Portugal and the comprehensive review of urban energy balance concept (section 1.1), linked to the available modelling tools in both research areas (section 1.2), and the implications of climate change in cities (section 1.3), allowed the definition of three main points of research needs: i) Increase the accuracy of the atmospheric processes at the urban/local scale in numerical weather and air quality models; ii) A full understand of the linkages between climate change, air quality and energy fluxes at city level; iii) Quantitatively assess the interaction between resilience measures (e.g., nature based solutions) and climate change effects (e.g., heat-waves), and its influence on the urban air quality and energy fluxes. All of this knowledge is crucial to achieve the urban sustainability which is directly dependent of cities resilience capacity and ability to adapt to climate change, responding at the same time to pressures induced by rapidly growing, air pollution and changes on urban metabolism (energy fluxes).

Following the identified research needs, the main objective of this thesis is to provide an integrated assessment of the interaction between resilience measures and climate change effects, and its influence on the urban air quality and on the urban surface energy balance, through the application of a modelling system tool. This research is complex and multidisciplinary; and is in accordance with the fifth societal challenge of the Horizon 2020. Four specific objectives were established to be accomplish along this thesis:

- Understand how urban areas influence the local climate, though the assessment of the urban surface energy balance in different typologies of cities (different levels of urbanization); this analysis was done to quantitatively assess the relative importance of each component of the urban energy fluxes considering different land uses;
- Understand how atmospheric variables (incoming solar and long-wave radiation, air temperature, atmospheric humidity, wind speed and precipitation) affect each component of the energy balance, and how, in turn, these atmospheric variables are themselves affected by urban fluxes; this analysis gives insights about how the urban surface-atmosphere exchanges of heat will be affected by climate change and the implications for urban planning and sustainability;
- Improve the numerical models and their accuracy to reproduce in a more realist way the physical processes occurring in urban areas, through the application of the Weather Forecast and Research model with an urban parameterization module, which take into account the urban surface energy balance; increase the accuracy of models (both meteorological and air quality models) will allow a better prediction of the current environmental issues and the future challenges related to climate change effects;
- Evaluate the influence of the application of a set of resilience measures in the energy balance components and in air quality (in terms of wind patterns and air pollutants dispersion); this analysis is crucial to define guidelines on adaptation and urban resilience to support urban planning, especially important in a changing climate.

The work was developed having as case study the city of Porto in Portugal. Porto is an interesting and challenging case study since is the second largest city in Portugal and it is one of the European urban areas that most growth in the last decades, stands out as the Portuguese urban area with the smallest amount of green and blue areas, and also due to its air quality problems (e.g., exceedances of PM10 limit values).

1.5. OUTLINE OF THE THESIS

This document presents the main results and the discussion of the PhD thesis entitled “Urban air quality and climate change: vulnerability, resilience and adaptation”, and it is structured as follows.

Chapter 1 has provided a characterization of urban environment, focused in nowadays air quality issues, with special emphasis on the European and Portugal domains, and on the urban surface energy balance research. The current modelling tools used to assess air quality and energy fluxes have been described. In addition, this Chapter has provided a state-of-the-art in climate change effects and its linkages to different research fields, as well as, a review on adaptation strategies and policies which increase resilience of urban areas. Concerning all this information, the objectives to be achieved within this thesis have been stated.

Chapter 2 evaluates the influence of different typologies of land use on the behaviour and magnitude of each component of the energy fluxes through the application of the modelling system Weather Research and Forecasting Model - Surface Urban Energy and Water Balance Scheme (WRF-SUEWS). Additionally, an evaluation of the modelling system performance is provided in this Chapter, using local-scale meteorological and flux data measured in two distinct areas: an urban and suburban areas. For that a specific methodology was developed and described, which encompasses: the use of urban flux measurements from a field campaign and the use of urban flux modelling, through a numerical modelling approach. This Chapter intends to accomplish the first objective of this thesis related to the understanding of how urban areas influence the local climate.

After the assessment of the modelling system performance and having confidence in the modelled results, Chapter 3 evaluates the influence of climate change on the magnitude and behaviour of each component of the energy fluxes, contributing to an increase of the knowledge of the surface energy balance research field. For that, two climatological scenarios were defined: present (1986-2005), to characterize the current climatological conditions of the study area, and medium-term future (2046-2065), based on the Representative Concentration Pathways RCP8.5 scenario. A 1-year simulation, statistically representative of each climatological scenario, were performed. A mapping of the spatial pattern of energy fluxes, at an urban scale (1 km of horizontal resolution) for both climatological scenarios is provided and discussed in this Chapter. Chapter 3 provides insights about how the urban surface-atmosphere exchanges of heat and water will be affected by climate change (accomplishing the objective number two of this thesis).

Knowing the spatial patterns of the energy fluxes in the study area and having insights of how this area is able to respond to the impacts of climate change, allows the identification of vulnerabilities (e.g., areas with a higher increase of temperatures) and the most appropriated measures to increase urban resilience. Chapter 4 investigates and quantify the influence of the application of a set of resilience measures, such as adaptation strategies to deal with heat waves impacts in the energy balance components for a future climate projection. For that, four scenarios were developed to consider different resilience measures, having been applied for a selected heat-wave in a future climate. Two types of results are discussed in Chapter 4: a complete spatial coverage of the energy fluxes, using a high spatial resolution modelling at urban scale (200 m); and the representation of the daily average profile of the energy fluxes. This Chapter provides guidelines on adaptation and urban resilience to support urban planning.

Having a full understand of the surface-atmosphere exchanges, namely through the knowledge of the linkage between each component of the energy balance and the climate change and resilience measures, an evaluation of a set of urban parameterizations with different complexity levels is described in Chapter 5. A performance of the selected urban parameterizations on the modelling of local energy fluxes is provided in this Chapter, as well as, an analysis of how these urban parameterizations influence the accuracy of meteorological modelling. In this sense, a selection of the most appropriate urban parameterization is made for the case study. This evaluation is a key factor since further progress in air quality modelling depends on the integration of urban representations into mesoscale models and, mainly, on the accuracy level of modelling the urban processes.

Chapter 6 provides a set of numerical simulations, with a high spatial resolution at neighbourhood scale (3 m), to assess the physical influence of different resilience measures in the flow (wind velocity) and dispersion (air pollutant concentrations) processes. A modelling system composed by the WRF-CFD models is used. An urban canopy parameterization scheme, based on the findings of Chapter 5, was used in WRF simulation to better simulate urban meteorological conditions. The resilience measures analysed were selected taking into account the main outcomes of Chapter 4. A multi-pollutant analysis is provided in this Chapter, namely focused on CO, CO_2, NO_X and PM10. Chapter 6 provides strategies to increase urban resilience to air pollution to support urban planners or policy makers (to accomplish the fourth objective purposed in section 1.4).

Finally, Chapter 7 summarizes the main outcomes achieved in this thesis, analysing the progresses made in the air quality and energy fluxes research fields and also some limitations attending to its state-of-the-science. In addition, this Chapter provides suggestions of possible tasks and future work to be developed in these research lines. The references used in this work are compiled in the end of each chapter.

This thesis contains modified versions of published peer-reviewed papers from Science Citation Index (SCI) journals or submitted works. The papers modifications concern the harmonization of i) literature references, since the papers were published in different journals, using different references styles, and ii) document formatting to make the text easier to read. In all the papers, the author was responsible

for the study conception and design, as well as for the results analysis and for the manuscript writing. The co-authors were responsible for the critical revision of the manuscript, and, when applicable, to perform measurement campaigns (e.g., Chapter 2) and provide initial climate data (e.g., Chapter 3 and 4). Professor Myriam Lopes, as co-author and main advisor of this work was responsible for the orientation of all the steps related to the successful development of the thesis.

1.6. REFERENCES

Adger W.N. (2006). Vulnerability. Global Environ Chang 16, 268–281.

Agência Portuguesa do Ambiente, APA. (2016). Relatório de Estado do Ambiente Portugal. Agência Portuguesa do Ambiente. Prime Graphics.

Air Quality Expert Group, AQEG (2007). Air Quality Expert Group from the Department for Environment, Food and Rural Affairs; Scottish Executive; Welsh Assembly Government; and Department of the Environment in Northern Ireland. ISBN 0-85521-172-5.

Allen L., Lindberg F., Grimmond C.S.B. (2011). Global to city scale model for anthropogenic heat flux. International Journal of Climatology 31, 1990 – 2005.

Amorim J.H., Rodrigues V., Tavares R., Valente C., Borrego C. (2013). CFD modelling of the aerodynamic effect of trees on urban air pollution dispersion. Science of the Total Environment 461-462, 541-551.

Atkinson R. (2000). Atmospheric chemistry of VOCs and NOX. Atmospheric Environment 34, 2063-2101.

Baklanov A., Schlunzen K., Suppan P., Baldasano J., Brunner D., Aksoyoglu S., et al. (2014). Online coupled regional meteorology chemistry models in Europe: current status and prospects. Atmospheric Chemistry and Physics 14, 317-398.

Baldasano J.M. (1998). Guidelines and formulation of an upgrade source emission model for atmospheric pollutants. In: Air Pollution Emissions Inventory, Volume 3, H. Power and J.M. Baldasano (Eds.), Computational Mechanics Publications, Southampton, UK and Boston, 238 pp.

Barlow J. (2014). Progress in observing and modelling the urban boundary layer. Urban Climate 10, 216-240.

Best M.J, Grimmond C.S.B., Villani M.G. (2006). Evaluation of the urban tile in MOSES using surface energy balance observations. Boundary-Layer Meteorology 118: 503–525.

Best MJ. 2005. Representing urban areas within operational numerical weather prediction models. Boundary-Layer Meteorology 114:91–109.

Bhattari K, Conway D. (2010). Urban vulnerabilities in the Kathmandu Valley, Nepal: visualizations of human/hazard interactions. International Journal of Geographical Information Science 2, 63-84.

Borrego C., Tchepel O., Carvalho A.C. (2001). Model Quality Assurance. EUROTRAC-2 Symposium 2000. 27-31 March Garmisch-Partenkirchen, Germany.

Borrego C., Miranda A.I., Costa A.M., Monteiro A., Martins H., Ferreira J., Tchepel O., Carvalho A.C. (2006). Uncertainties of models and monitoring. Final report. AMBQA-12/2006. Milestone Report M2 of Air4EU Project (SSPI-CT-2003- 503596). Aveiro, Portugal: Universidade de Aveiro; 2006.

Borrego C., Monteiro A., Ferreira J., Miranda A.I., Costa A.M., Carvalho A.C., Lopes M. (2008). Procedures for estimation of modelling uncertainty in air quality assessment. Environment International 34, 613-620.

Boubel R.W., Fox D.L., Turner D.B., Stern A.C. (1994). Fundamentals of air pollution. Academic Press, New York.

Capacity Strengthening in the Least Developed Countries for Adaptation to Climate Change, CLACC. (2009). Climate Change and the Urban Poor: Risk and Resilience in 15 of the World's Most Vulnerable Cities. International Institute for Environment and Development (IIED), London, United Kingdom.

Carnevale C., Finzi G., Pisoni E., Volta M., (2009). Neuro-fuzzy and neural network systems for air quality control. Atmospheric Environment 43, 4811-4821.

Carnevale C., Finzi G., Pisoni E., Volta M., Guariso G., Gianfreda R., Maffeis G., Thunis P., White L., Triacchini G. (2012). An integrated assessment tool to define effective air quality policies at regional scale. Environmental Modelling and Software 38, 306-315.

Carvalho A., Monteiro A., Solman S., Miranda A.I., Borrego C. (2010). Climate-driven changes in air quality over Europe by the end of the 21st century, with special reference to Portugal. Environmental Science and Policy 13, 445-458. doi:10/1016/j.envsci.2010.05.001.

Carvalho A., Schmidt L., Santos F.D., Delicado A. (2013). Climate change research and policy in Portugal. WIREs Climate Change 5, 199-217.

Carvalho D., Martins H., Marta-Almeida M., Rocha A., Borrego C. (2017). Urban resilience to future urban heat waves under a climate change scenario: A case study for Porto urban area (Portugal). Urban Climate 19, 1-27.

Chen F., Kusaka H., Tewari M., Bao J., Hirakuchi H. (2004). Utilizing the coupled WRF/LSM/Urban modeling system with detailed urban classification to simulate the urban heat island phenomena over the Greater Houston area. Fifth Symposium on the Urban Environment, CD-ROM. 9.11. Amer. Meteor. Soc., Vancouver, BC, Canada.

Chen F., Kusaka H., Tewari M., Bao J., Hirakuchi H. (2004). Utilizing the coupled WRF/LSM/Urban modeling system with detailed urban classification to simulate the urban heat island phenomena over the Greater Houston area. Proc. Fifth Conference on Urban Environment, Vancouver, BC, Canada. American Meteor Society, paper 9.11.

Christen A., Vogt R. (2004). Energy and radiation balance of a central European city. International Journal of Climatology 24, 1395 – 1421.

Chysoulakis N., Lopes M., San Jose R., Grimmong C.S.B., Jones M.B., Magliulo V., Klostermann J.E., Mitraka Z., Castro E.A., González A., Vogt R., Vesala T., Spano D., Pigeon G., Freer-Smith P., Staszewski T., Hodges N., Mills G., Cartalis C. (2013). Sustainable urban metabolism as a link between bio-physical sciences and urban planning: The BRIDGE project. Landscape And Urban Planning. 112, 100-117.

Cleugh H.A., Oke T.R. (1986). Suburban-rural energy balance comparisons in summer for Vancouver, B.C. Boundary-Layer Meteorology 36, 351–369.

Coaffee J. (2008). Risk, resilience, and environmentally sustainable cities. Energy Policy 36, 4633-4638.

Coleman L., Martin D., Varghese S., Jennings S.G., O´Dowd C.D. (2013). Assessment of changing meteorology and emissions on air quality using a regional climate model: Impact on ozone. Atmospheric Environment 69, 198-210. doi:10.1016/j.atmosenv.2012.11.048.

Colette A., Bessagnet B., Vautard R., Szopa S., Rao S., Schucht S., Klimont Z., Menut L., Clain G., Meleux F., Curci G., Rouïl L. (2013). European atmosphere in 2050, a regional air quality and climate perspective under CMIP5 scenarios. Atmospheric Chemistry and Physics 13, 7451-7471. doi:10.5194/acp-13-7451-2013.

Coutts A., Beringer J., Tapper N. (2007). Impact of Increasing Urban Density on Local Climate: Spatial and Temporal Variations in the Surface Energy Balance in Melbourne, Australia. Journal of Applied Meteorology and Climatology. 46, 477–493.

Cutter S.L., Barnes L., Berry M., Burton C., Evans E., Tate E., Webb J. (2008). A place-based model for understanding community resilience to natural disasters. Global Environ Chang 18, 598-605.

Daly A., Zannetti P. (2007). Air Pollution Modeling – An Overview. In: Ambient Air Pollution. P. Zannetti, D. Al-Ajmi, S. Al-Rashied (Eds). The EnviroComp Institute, Fremont, CA, pp.15-28.

Degrazia G.A. (2005). Lagrangian Particle Models. In: Air Quality Modeling: Theories, Methodologies, Computational Techniques and Available Databases and Software. P. Zannetti (Eds). EnviroComp.

Denby B., Larssen S., Guerreiro C., Li L., Douros J., Moussiopoulos N, et al. (2010). Guidance on the use of models for the European Air Quality Directive. A working document of the Forum for Air Quality Modelling in Europe, FAIRMODE. In: Denby B, editor. Technical Report Version 4.2ETC/ACC report.

Denby B.R., Douros I., Lia F. (2011). Modelling of Nitrogen Dioxide (NO_2) for air quality assessment and planning relevant to the European Air Quality Directive. FAIRMODE WG1, v. 3.3.

Dentener F., Stevenson D., Cofala J., Mechler R., Amann M., Bergamaschi P., Raes F., Derwent R. (2005). The impact of air pollutant and methane emission controls on tropospheric ozone and radiative forcing: CTM calculations for the period 1990–2030. Atmospheric Chemistry and Physics 5, 1731–1755.

Doherty R.M., Wild O., Shindell D.T., Zeng G., MacKenzie I.A., Collins W.J., Fiore A.M., Stevenson D.S., Dentener F.J., Schultz M.G., Hess P., Derwent R.G., Keating T.J. (2013). Impacts of climate change on surface ozone and intercontinental ozone pollution: a multi-model study. Journal of Geophysical Research 118, 3744-3763. doi:10.1002/jgrd.50266.

Duenas C., Fernandez M.C., Canete S., Carretero J., Liger E. (2002). Assessment of ozone variations and meteorological effects in an urban area in the Mediterranean Coast. The Science of the Total Environment 299, 97–113.

Elminir H.K. (2005). Dependence of urban air pollutants on meteorology. Science of the Total Environment 350, 225–237.

Engle N.L. and Lemos M.C. (2010). Unpacking governance: Building adaptive capacity to climate change of river basins in Brazil. Global Environ Chang 20, 4–13.

Ernstson H, Van der Leeuw S, Redman C, Meffert D, Davis G, Alfsen C, Elmqvist T. (2010). Urban transitions: on urban resilience and human-dominated ecosystems. AMBIO: A Journal of the Human Environment 39, 531-545. [DOI: 10.1007/s13280-010-0081-9].

European Commission, EC. (2014). Communication from the Commission to the European Parliament, the Council, the European Economic and Social Committee and the Committee of the Regions. The Urban Dimension of EU Policies – Key features of an EU urban agenda.

European Commission, EC. (2015). Towards an EU research and innovation policy agenda for nature-based solutions & re-naturing cities. Final report of the Horizon 2020 expert group on 'Nature-based solutions and re-naturing cities'. Luxembourg: Publications Office of the European Union. ISBN 978-92-79-46051-7.

European Union, EU. (2016). Directive (EU) 2016/2284 of the European parliament and of the council of 14 December 2016 on the reduction of national emissions of certain atmospheric pollutants, amending Directive 2003/35/EC and repealing Directive 2001/81/EC.

European Environmental Agency, EEA. (2011a). The application of models under the European Union's Air Quality Directive: A technical reference guide. EEA Report No.10/2011, Copenhagen. Luxembourg: Publications Office of the European Union. ISBN 978-92-9213-223-1.

European Environment Agency, EEA. (2011b). Green infrastructure and territorial cohesion: The concept of green infrastructure and its integration into policies using monitoring systems. Luxembourg: Publications Office of the European Union. ISBN 978-92-9213-242-2.

European Environmental Agency, EEA. (2012). Urban adaptation to climate change in Europe - challenges and opportunities for cities together with supportive national and European policies. EEA Report No. 2/2012, Copenhagen. Luxembourg: Publications Office of the European Union. ISBN 978-92-9213-308-5.

European Environment Agency, EEA. (2014a). Air quality in Europe – 2014 report. Luxembourg: Publications Office of the European Union. ISBN: 978-92-9213-490-7. DOI: 10.2800/22847.

European Environmental Agency, EEA. (2014b). NEC Directive Status Report 2013, Reporting by Member States under Directive 2001/81/EC of the European Parliament and of the Council of 23 October 2001 on National Emission Ceilings for Certain Atmospheric Pollutants, EEA Technical Report No 10/2014.

European Environment Agency, EEA. (2016). Air quality in Europe — 2016 report. EEA Report No 28/2016. Luxembourg: Publications Office of the European Union. ISBN 978-92-9213-847-9. DOI:10.2800/80982.

European Environment Agency, EEA. (2017). Climate change, impacts and vulnerability in Europe 2016. An indicator-based report. EEA Report No 1/2017. Luxembourg: Publications Office of the European Union. ISBN 978-92-9213-835-6.

European Monitoring and Evaluation Programme/European Environmental Agency, EMEP/EEA. (2009). EMEP/EEA air pollutant emission inventory guidebook – 2009. Technical report no. 9/2009.

European Topic Centre on Air and Climate Change, ETC/ACC. (2010). Status and trends of NO_2 ambient concentrations in Europe, Guerreiro, C., Horálek, J., de Leeuw, F., Hak, C., Nagl, C., Kurfürst, P. and Ostatnicka, J., Technical Paper 2010/19, European Topic Centre on Air and Climate Change.

Ferreira V.G., Pereira T.C., Seabra T., Torres P., Maciel H. (2008). Portuguese National Inventory Report on Greenhouse Gases 1990-2006, Submitted under the United Nations Framework Convention on Climate Change and The Kyoto Protocol, Portuguese Environmental Agency, April 15, Amadora.

Fiore A.M., Levy II H., Jaffe D.A. (2011). North American isoprene influence on inter Mainland ozone pollution. Atmospheric Chemistry Physics 11, 1697-1710. doi:10.5194/acp-11-1697-2011.

Flerchinger G., Reba M., Marks D. (2012). Measurement of Surface Energy Fluxes from Two Rangeland Sites and Comparison with a Multilayer Canopy Model. Journal of Hydrometeorology, 13, 1038-1051.

Fussel H. (2007). Vulnerability: a generally applicable conceptual framework for climate change research. Global Environ Chang 17, 155-167. [DOI: http://dx.doi.org/10.1016/j.gloenvcha.2006.05.002].

Gallopín G.C. (2003). Box 1. A systemic synthesis of the relations between vulnerability, hazard, exposure and impact, aimed at policy identification. In: Economic Commission for Latin American and the Caribbean (ECLAC). Handbook for Estimating the Socio-Economic and Environmental Effects of Disasters. ECLAC, LC/MEX/G.S., Mexico, D.F., pp. 2–5.

Gao Y., Fu J.S., Drake J.B., Lamarque J.F., Liu Y. (2013). The impact of emission and climate change on ozone in the United States under representative concentration pathways (RCPs). Atmospheric Chemistry and Physics 13, 9607-9621. http://dx.doi.org/10.5194/acp-13-9607-2013.

Garcia-Cueto R., Jáuregui E., Tejeda A. (2003). Urban / rural energy balance observations in a desert city in northern Mexico. In Proceedings of the Fifth International Conference on Urban Climate, Lódz, Poland.

Georgescu M., Miguez-Macho G., Steyaert L.T., Weaver C.P. (2009). Climatic effects of 30 years of landscape change over the Greater Phoenix, Arizona, region: 1. Surface energy budget changes. Journal of Geophysical Research: Atmospheres 114.

Greiving S., Fleischhauer M., Lindner C., Lückenkötter J., Peltonen L., Juhola S., et al. (2011), ESPON Climate - Climate change and territorial effects on regions and local economies. The ESPON 2013 Programme. Dortmund University.

Grell G., Peckham S., Schmitz R., McKeen S., Frost G., Skamarock W., Eder B. (2005). Fully coupled 'online' chemistry in the WRF model. Atmospheric Environment 39, 6957-6976.

Grice S., Stedman J., Kent A., Hobson M., Norris J., Abbott J., Cooke S. (2009). Recent trends and projections of primary NO2 emissions in Europe. Atmospheric Environment 2, 154–2 167.

Grimmmond C.S.B., Oke T.R. (1986). Urban water balance II: Results from a suburb of Vancouver, B.C. Water Resources Research 22, 1404–1412.

Grimmmond C.S.B., Oke T.R. (1991). An evaporation–interception model for urban areas. Water Resources Research 27, 1739–1755.

Grimmond C.S.B., Cleugh H.A., Oke T.R. (1991). An objective urban heat storage model and its comparison with other schemes. Atmospheric Environment Part B, 25, 311-326.

Grimmond C.S.B. (1992). The suburban energy balance: methodological considerations and results for a mid-latitude west coast city under winter and spring conditions. International Journal of Climatology 12, 481 - 497.

Grimmond C.S.B., Oke, T. (1995). Comparison of heat fluxes from summertime observations in the suburbs of four North American cities. Journal of Applied Meteorology 34, 873 - 889.

Grimmond C.S.B., Oke T. (1999a). Aerodynamic properties of urban areas derived from analysis of surface form. Journal of Applied Meteorology 38, 1262 - 1292.

Grimmond C.S.B., Oke T.R. (1999b). Heat storage in urban areas: Local-scale observations and evaluation of a simple model. Journal of Applied Meteorology 38, 922–940.

Grimmond C.S.B., Oke T.R. (2002). Turbulent Heat Fluxes in Urban Areas: Observations and a Local-Scale Urban Meteorological Parameterization Scheme (LUMPS). Journal of Applied Meteorology and Climatology, 41, 792–810.

Grimmond C.S.B. (2007). Urbanization and global environmental change: local effects of urban warming. Geographical Journal 173, 83-88.

Grimmond C.S.B., Blackett M., Best M.J., Barlow J., Baik J.J., Belcher S.E., Bohnenstengel S.I., Calmet I., Chen F., Dandou A., Fortuniak K., Gouvea M.L., Hamdi R., Hendry M., Kawai T., Kawamoto Y., Kondo H., Krayenhoff E.S., Lee S.H, Loridan T., Martilli A., Masson V., Miao S., Oleson K., Pigeon G., Porson A., Ryu Y.H, Salamanca F., Shashua-Bar L., Steeneveld G.J, Tombrou M., Voogt J.A., Young D.T., Zhang N. (2010). The International Urban Energy Balance Models Comparison Project: First Results from Phase 1. Journal of Applied Meteorology and Climatology, 40, 1268-1292.

Grimmond C.S.B, Blackett M., Best M.J., Baik J.J., Belcher S.E., Beringer J., Bohnenstengel S.I., Calmet I., Chen F., Coutts A., Dandou A., Fortuniak K., Gouvea M.L., Hamdi R., Hendry M., Kanda M., Kawai T., Kawamoto Y., Kondo H., Krayenhoff E.S., Lee S.H., Loridan T., Martilli A., Masson V., Miao S., Oleson K., Ooka R., Pigeon G., Porson A., Ryu Y.H., Salamanca F., Steeneveld G.J., Tombrou M., Voogt J.A., Young D.T., Zhang N. (2011). Initial results from Phase 2 of the international urban energy balance model comparison. International Journal of Climatology, 31, 244-272.

Hamdi R., Giot O., De Troch R., Deckmyn A., Termonia P. (2015). Future climate of Brussels and Paris for the 2050s under the A1B scenario. Urban Climate 12, 160-182.

Hanna S.R., Chang J. C. (1992). Boundary layer parameterizations for applied dispersion modeling over urban areas. Boundary-Layer Meteorology 58, 229-259.

Hanna S.R., Chang J. C. (1993). Hybrid Plume Dispersion Model (HPDM) improvements and testing at three field sites. Atmospheric Environment 27A, 1491-1508.

Harman I.N., Belcher S.E. (2006). The surface energy balance and boundary layer over urban street canyons. Quarterly Journal of the Royal Meteorological Society 132, 2749–2768.

Hass H., van Loon M., Kessler C., Stern R., Matthhijsen J., Sauter F., Zlatev Z., Langner J., Foltescu V., Schaap M. (2003). Aerosol modelling: results and intercomparison from European regional scale modelling systems. Special Report. EUROTRAC-2 ISS, Garmisch Partenkirschen.

He J., Yu Y., Xie Y., Mao H., Wu L., Liu N., Zhao S. (2016). Numerical Model-Based Artificial Neural Network Model and Its Application for Quantifying Impact Factors of Urban Air Quality. Water, Air and Soil Pollution 227, 1-16.

Hurley P. (2008). Development and Verification of TAPM. In: Borrego C., Miranda A.I. (eds) Air Pollution Modeling and Its Application XIX. NATO Science for Peace and Security Series Series C: Environmental Security. Springer, Dordrecht.

Intergovernmental Panel on Climate Change, IPCC. (2007). Climate change 2007: Synthesis report. Contribution of Working Groups I, II and III to the fourth assessment report of the Intergovernmental Panel on Climate Change, Cambridge University Press, Cambridge, United Kingdom.

Intergovernmental Panel on Climate Change, IPCC. (2013). Climate Change 2013: The Physical Science Basis. Contribution of Working Group I to the Fifth Assessment Report of the Intergovernmental Panel on Climate Change [Stocker, T.F., D. Qin, G.-K. Plattner, M. Tignor, S.K. Allen, J. Boschung, A. Nauels, Y. Xia, V. Bex and P.M. Midgley (eds.)]. Cambridge University Press, Cambridge, United Kingdom and New York, NY, USA, 1535 pp.

Intergovernmental Panel on Climate Change, IPCC. (2014a). Climate Change 2014: Impacts, Adaptation, and Vulnerability. Part B: Regional Aspects. Contribution of Working Group II to the Fifth Assessment Report of the Intergovernmental Panel on Climate Change. (Barros, V.R., C.B. Field, D.J. Dokken, M.D. Mastrandrea, K.J. Mach, T.E. Bilir, M. Chatterjee, K.L. Ebi, Y.O. Estrada, R.C. Genova, B. Girma, E.S. Kissel, A.N. Levy, S. MacCracken, P.R. Mastrandrea, and L.L. White (eds.)). Cambridge University Press, Cambridge, United Kingdom and New York, NY, USA, 688 pp.

Intergovernmental Panel on Climate Change, IPCC. (2014b). Climate Change 2014: Impacts, Adaptation, and Vulnerability. Part A: Global and Sectoral Aspects. Contribution of Working Group II to the Fifth Assessment Report of the Intergovernmental Panel on Climate Change. (Field, C.B., V.R. Barros, D.J. Dokken, K.J. Mach, M.D. Mastrandrea, T.E. Bilir, M. Chatterjee, K.L. Ebi, Y.O. Estrada, R.C. Genova, B. Girma, E.S. Kissel, A.N. Levy, S. MacCracken, P.R. Mastrandrea, and L.L. White (eds.)). Cambridge University Press, Cambridge, United Kingdom and New York, NY, USA, 1132 pp.

International Agency for Research on Cancer, IARC. (2013). Press Release No 221, (http://www.iarc.fr/en/mediacentre/iarcnews/pdf/pr221_E.pdf).

Jacob D.J. (2000). Heterogeneous chemistry and tropospheric ozone. Atmospheric Environment 34, 2131-2159.

Jacob D.J., Winner D.A. (2009). Effect of climate change on air quality. Atmospheric Environment 43, 51-63. doi:10.1016/j.atmosenv.2008.09.051.

Järvi L., Grimmond C.S.B., Christen A. (2011). The Surface Urban Energy and Water Balance Scheme (SUEWS): Evaluation in Los Angeles and Vancouver. Journal of Hydrology, 411 (3-4), 219-237. ISSN 0022-1694.

Järvi L., Grimmond C.S.B., Taka M., Nordbo A., Setala H., Strachan I.B. (2014). Development of the Surface Urban Energy and Water balance Scheme (SUEWS) for cold climate cities. Geoscientific Model Development, 7, 1691-1711. ISSN 991-959X.

Jiang H., Liao H., Pye H.O.T., Wu S., Mickley L.J., Seinfeld J.H., Zhang X.Y. (2013). Projected effect of 2000–2050 changes in climate and emissions on aerosol levels in China and associated transboundary transport. Atmospheric Chemistry and Physics 13, 7937–7960. doi:10.5194/acp-13-7937-2013.

Kasperson J.X, Kasperson R.E., Turner II., Schiller A., Hsiel W.H. (2005). Vulnerability to global environmental change. In: Kasperson, J.X., Kasperson, R.E. (Eds.), Social Contours of Risk, vol. II. Earthscan, London, pp. 245–285.

Klingberg J., Broberg M., Strandberg B., Thorsson P., Pleije H. (2017). Influence of urban vegetation on air pollution and noise exposure – A case study in Gothenburg, Sweden. Science of the Total Environment 599–600, 1728–1739.

Kondo H., Liu F.H. (1998). A study on the urban thermal environment obtained through a one-dimensional urban canopy model (in Japanese). Journal of Japan Society for Atmospheric Environment 33, 179–192.

Kondo H., Genchi Y., Kikegawa Y., Ohashi Y., Yoshikado H., Komiyama H. (2005). Development of a multi-layer urban canopy model for the analysis of energy consumption in a big city: Structure of the urban canopy model and its basic performance. Boundary Layer Meteorology 116, 395–421.

Kotthaus S., Grimmond C. (2012). Identification of micro-scale anthropogenic CO2, heat and moisture sources - processing eddy covariance fluxes for a dense urban environment. Atmospheric Environment 57, 301 - 316.

Krayenhoff E.S., Voogt J. A. (2007). A microscale three dimensional urban energy balance model for studying surface temperatures. Boundary-Layer Meteorology 123, 433-461.

Kusaka H., Kondo H., Kikegawa Y., Kimura F. (2001). A simple single-layer urban canopy model for atmospheric models: comparison with multi-layer and slab models. Boundary Layer Meteorology 101, 329–358.

Lacressonnière G., Peuch V. H., Vautard R., Arteta J., Déqué M., Joly M., Josse B., Marécal V., Saint-Martin D. (2014). European air quality in the 2030s and 2050s: Impacts of global and regional emission trends and of climate change. Atmospheric Environment 92, 348-358. doi:10.1016/j.atmosenv.2014.04.033.

Lam Y.F., Fu J.S., Wu S., Mickley L.J. (2011). Impacts of future climate change and effects of biogenic emissions on surface ozone and particulate matter concentrations in the United States. Atmospheric Chemistry and Physics 11, 4789-4806. http://dx.doi.org/10.5194/acp-11-4789-2011.

Langford B., Nemitz E., House E., Phillips G.J., Famulari D., Davison B., Road W.M. (2010). Fluxes and concentrations of volatile organic compounds above central London, UK. Atmospheric Chemistry and Physics 10, 627–645.

Lateb M., Meroney R., Yataghene M., Fellouah H., Saleh F., Boufadel. 2015. On the use of numerical modelling for near-field pollutant dispersion in urban environments - A review. Environmental Pollution,1–13.

Lee S.-H., Park S.-U. (2008). A vegetated urban canopy model for meteorological and environmental modelling. Boundary Layer Meteorology 126, 73–102.

Lei H., Wuebbles D.J., Liang X.-Z. (2012). Projected risk of high ozone episodes in 2050. Atmospheric Environment 59, 567-577. http://dx.doi.org/10.1016/j.atmosenv.2012.05.051.

Leichenko R. (2011). Climate change and urban resilience. Current opinion in Environmental Sustainability 3, 164-168.

Lemonsu A., Grimmond C.S.B., Masson V. (2004). Modelling the surface energy balance of an old Mediterranean city core. Journal of Applied Meteorology 43, 312–327.

Li D., Bou-Zeid E., Oppenheimer M. (2014). The effectiveness of cool and green roofs as urban heat island mitigation strategies. Environmental Research Letter. 9, 055002.

Lietzke B., Vogt R., Young D.T., Grimmond C.S.B. (2015). Physical fluxes in urban environment (Chapter 4). In: Chrysoulakis, N., de Castro, E. A. and Moors, E. J. (eds.) Understanding Urban Metabolism. Routledge, pp. 29-44. ISBN 9780415835114.

Lindberg F., Grimmond C.S.B., Yogeswaran N., Kotthaus S., Allen L. (2013). Impact of city changes and weather on anthropogenic heat flux in Europe 1995–2015. Urban Climate 4, 1-15.

Liu Y., Chen F., Warner T., Basara J. (2006). Verification of a mesoscale data-assimilation and forecasting system for the Oklahoma City area during the Joint Urban 2003 Field Project. Journal of Applied Meteorology and Climatolology 45, 912–929.

Ma E., Deng X., Zhang Q., Liu A. (2014). Spatial Variation of Surface Energy Fluxes Due to Land Use Changes across China. Energies 7, 2194-2206.

Makhelouf A. (2009). The effect of green spaces on urban climate and pollution. Journal of Environmental Health Science and Engineering 6, 35-40.

Manders A.M.M., van Meijgaard E., Mues A.C., Kranenburg R., van Ulft L.H., Schaap M. (2012). The impact of differences in large-scale circulation output from climate models on the regional modeling of ozone and PM. Atmospheric Chemistry and Physics 12, 9441-9458.

Manders A.M.M., van Meijgaard E., Mues A.C., Kranenburg R., van Ulft L.H., Schaap M. (2012). The impact of differences in large-scale circulation output from climate models on the regional modeling of ozone and PM. Atmospheric Chemistry and Physics 12, 9441-9458.

Markakis K., Valari Colette A., Sanchez O., Perrussel O., Honore C., Vautard R., Kilmont Z., Rao S. (2014). Air quality in the mid-21st century for the city of Paris under two climate scenarios; from the regional to local scale. Atmospheric Chemistry and Physics 14, 7323-7340. http://dx.doi.org/10.5194/acp-14-7323-2014.

Marta-Almeida M., Teixeira J.C., Carvalho M.J., Melo-Gonçalves P., Rocha A.M. (2016). High resolution WRF climatic simulations for the Iberian Peninsula: model validation. Physics and Chemistry of the Earth Parts A/B/C. 94,94-105.

Martilli A. (2007). Current research and future challenges in urban mesoscale modelling. International Journal of Climatology 27, 1909-1918.

Martilli A., Clappier A., Rotach M. W. (2002). An urban surface exchange parameterisation for mesoscale models. Boundary-Layer Meteorology 104, 261–304.

Martilli A., Roulet Y-A., Junier M., Kirchner F., Rotach M. W., Clappier A. (2003). On the impact of urban surface exchange parameterisations on air quality simulations: The Athens case. Atmospheric Environment 37, 4217–4231.

Martins R.D., Ferreira L.D.C. (2011). Opportunities and constraints for local and subnational climate change policy in urban areas: Insights from diverse contexts. International Journal of Global Environmental Issues 11, 37–53.

Maru Y. (2010). Resilient regions: clarity of concepts and challenges to systemic measurement systemic measurement. Socio-Economics and the Environment Discussion, CSIRO Working Paper Series. http://www.csiro.au/files/files/pw5h.pdf.

Masson V. (2000). A physically-based scheme for the urban energy budget in atmospheric models. Boundary-Layer Meteorology 41:1011–1026.

Masson V., Grimmond C.S.B., Oke T.R. (2002). Evaluation of the Town Energy Balance (TEB) scheme with direct measurements from dry districts in two cities. Journal of Applied Meteorology 41, 1011–1026.

Menut L., Bessagnet B. (2010). Atmospheric composition forecasting in Europe. Annales Geophysicae, European Geosciences Union 28, 61-74.

Monteiro A., Miranda A.I., Borrego C., Vautard R. (2007). Air quality assessment for Portugal. Science of the Total Environment 373, 22-31.

Monteiro A., Strunk A., Carvalho A. Tchepel O, Miranda A.I., Borrego C., Saavedra S., Rodriguez A., Souto J., Casares J., Friese E., Elbern H. (2012). Investigating a high ozone episode in a rural mountain site. Environmental Pollution 162, 176-189.

Morris E., Yarwood G., Emery C., Koo B. (2004). Development and Application of the CAMx Regional One-atmosphere Model to Treat Ozone, Particulate Matter, Visibility, Air Toxics and Mercury. Presented in 97th Annual Conference and Exhibition of the A&WMA, June 2004, Indianapolis.

Nakicenovic N., Davidson O., Davis G., Grubler A., Kram T., Rovere E.L.L., Metz B., Morita T., Pepper W., Pitcher H., Sankovski A., Shukla P., Swart R., Watson R., Dadi Z. (2000). Emissions Scenarios: A Special Report of Working Group III of the Intergovernmental Panel on Climate Change (Summary for Policy Makers), IPCC: 27.

Newton J. (2007). Wellbeing and the Natural Environment: A brief overview of the evidence. DEFRA discussion paper.
www.defra.gov.uk/sustainable/government/documents/Wellbeing_and_the_Natural_Environment_Report.doc (accessed 21 May 2014).

Nguyen D.L. (2014). A Brief Review of Air Quality Models and Their Applications. Open Journal of Atmospheric and Climate Change 1, 2374-3808.

Nieuwenhuijsen M.J. (2003) Exposure assessment in occupational and environmental epidemiology. Oxford University Press. Oxford, UK.

Nowak D.J., Hirabashi S., Bodina A., Hoehn R. (2014). Tree and forest effects on air quality and human health in the United States. Environmental Pollution 193, 119-129.

Nunez M. Oke T.R. (1977). The energy balance of an urban canyon. Journal of Applied Meteorology 16, 11–19.

O'Brien K., Hayward B., Berkes F. (2009). Rethinking social contracts: building resilience in a changing climate. Ecology and Society 14, Art 12.

Offerle B., Jonsson P., Eliasson I., Grimmond C.S.B. (2003a). Preliminary investigation of energy balance fluxes in Ouagadougou, Burkina Faso. In Proceedings of the Fifth International Conference on Urban Climate, Lódz, Poland.

Offerle B., Grimmond C.S.B., Oke T. R. (2003b). Parameterization of net all-wave radiation for urban areas. Journal of Applied Meteorology 42, 1157–1173.

Offerle B., Grimmond C.S.B., Fortuniak K. (2005). Heat storage and anthropogenic heat flux in relation to the energy balance of a central European city centre. International Journal of Climatology 25, 1405-1419.

Oke T.R. (1987). Boundary Layer Climates, chapter 8, pages 262–303. Routledge, 2nd edition.

Oke T.R., Cleugh H.A. (1987). Urban heat-storage derived as energy-balance residuals. Bound-Layer Meteorology, 39, 233-245.

Oke T.R., Sproken-Smith R.A., Jáuregui E., Grimmond C.S.B. (1999). The energy balance of central Mexico City during the dry season. Atmospheric Environment 33, 3919– 3930.

Oleson K.W., Bonan G.B., Feddema J. (2010). Effects of white roofs on urban temperature in a global climate model. Geophysical Research Letters, 37. [doi:10.1029/2009GL042194].

Oleson K.W., Bonan G.B., Feddema J., Vertenstein M., Grimmond C.S.B. (2008a). An urban parameterization for a global climate model:1. Formulation and evaluation for two cities. Journal of Applied Meteorology and Climatology 47, 1038–1060.

Oleson K.W., Bonan G.B., Feddema J., Vertenstein M. (2008b). An urban parameterization for a global climate model: 2. Sensitivity to input parameters and the simulated heat island in offline simulations. Journal of Applied Meteorology and Climatology 47, 1061–1076.

Ossés de Eicker M., Zah R., Triviño R., Hurni H. (2008). Spatial accuracy of a simplified disaggregation method for traffic emissions applied in seven mid-sized Chilean cities. Atmospheric Environment 42,1491-1502.

Ostrom E. (2010). Polycentric systems for coping with collective action and global environmental change. Global Environ Chang 20, 550–557. [DOI: http://dx.doi.org/10.1016/j.gloenvcha.2010.07.004].

Palacios M., Martín F., Cabral H. (2001). Methodologies for estimating disaggregated anthropogenic emissions—application to a coastal mediterranean region of Spain. Journal of Air Waste Management Association 51, 642–657.

Park S., Deser C., Alexander M. (2005). Estimation of the Surface Heat Flux Response to Sea Surface Temperature Anomalies over the Global Oceans. Journal of Climate, 18, 4582-4599.

Parnell S., Simon D., Vogel C. (2007). Global environmental change: conceptualising the growing challenge for cities in poor countries. Area, 39, 357-369.

Pendall R., Foster K., Cowell M. (2010). Resilience and regions: building understanding of the metaphor. Cambridge Journal of Regions, Economy and Society 3, 71-84.

Penrod A., Zhang Y., Wang K., Wu S.Y., Leung L.R. (2014). Impacts of future climate and emission changes on U.S. air quality. Atmospheric Environment 89, 533-547. http://dx.doi.org/10.1016/j.atmosenv.2014.01.001.

Pike A, Dawley S, Tomaney J. 2010. Resilience adaptation and adaptability. Cambridge Journal of Regions, Economy and Society 3, 59-70.

Pyles R. D., Weare B. C., Paw U. K. T., Gustafson W. (2003). Coupling between the University of California, Davis, Advanced Canopy-Atmosphere-Soil Algorithm (ACASA) and MM5: Preliminary Results for July 1998 for Western –North America. Journal of Applied Meteorology 42, 557 - 569.

Rao S.T., Zurbenko I.G. (1994). Detecting and tracking changes in ozone air quality. Journal of the Air and Waste Management Association 44, 1089–1092.

Raupach M., Antonia R. Rajagopalan, S. (1991). Roughwall turbulent boundary layers. Applied Mechanics Reviews 44, 1 - 25.

Roemer M., Beekmann M., Bergström R., Boersen G., Feldmann H., Flatoy F., et al. (2003). Ozone trends according to ten dispersion models. Special Report. EUROTRAC-2 ISS, Garmisch Partenkirschen.

Romero-Lankao P., Qin H. (2011). Conceptualizing urban vulnerability to global climate and environmental change. Current opinion in Environmental Sustainability.

Rotach M.W., Vogt R., Bernhofer C., Batchvarova E., Christen A., Clappier A., Voogt J.A. (2005). BUBBLE – an urban boundary layer meteorology project Theoret. Journal of Applied Climatology 81, 231-261.

Roth M., Oke, T. (1994). Comparison of modelled and measured heat storage in suburban terrain. Beitraege zur Physik der Atmosphaere 67, 149 - 156.

Russel A., Dennis R. (2000). NARSTO critical review of photochemical models and modelling. Atmospheric Environment 34, 2283-2324.

Sá E., Tchepel O., Carvalho A., Borrego C. (2015). Meteorological driven changes on air quality over Portugal: a KZ filter application. Atmospheric Pollution Research 6, 979-989.

Sá E., Martins H., Ferreira J., Marta-Almeida M., Rocha A., Carvalho A., Freitas S., Borrego C. (2016). Climate change and pollutant emissions impacts on air quality in 2050 over Portugal. Atmospheric Environment 131, 209-224.

Sailor D.J. (2011). A review of methods for estimating anthropogenic heat and moisture emissions in the urban environment. International Journal of Climatology 31, 189 - 199.

Satsangi G.S., Lakhani A., Kulshrestha P.R., Taneja A. (2004). Seasonal and diurnal variation of surface ozone and a preliminary analysis of exceedance of its critical levels at a semi-arid site in India. Journal of Atmospheric Chemistry 47, 271–286.

Satterthwaite D., Huq S., Pelling M., Reid H., Romero-Lankao P. (2007). Adapting to climate change in urban areas: The possibilities and constraints in low- and middle-income nations.

Schmidt H., Derognat C., Vautard R., Beekmann M. (2001). A comparison of simulated and observed O3 mixing ratios for the summer of 1998 in Western Europe. Atmospheric Environment 35, 6277–6297.

Sedlar J., Hock R. (2009). Testing longwave radiation parameterizations under clear and overcast skies at Storglaciären, Sweden. Cryosphere, 3, 75-84.

Seibert P., Fank A. (2004). Source-receptor matrix calculation with a Lagrangian particle dispersion model in backward mode. Atmospheric Chemistry and Physics 4, 51-63.

Seinfeld J.H. (1988). Ozone air quality models: a critical review. Journal of the Air & Waste Management Association 38, 616-647.

Seinfeld J.H., Pandis S.N. (1998), Armospheric chemistry and physics: from air pollution to climate change. John Wiley & Sons, Inc., 1326 pp.

Seinfeld J.H., Pandis S.N. (2006). Atmospheric Chemistry and Physics: From Air Pollution to Climate Change. 2nd. Hoboken: John Wiley & Sons. ISBN 978-0-471072019-8.

Sheng L., Liu S.H., Liu H.P. (2010). Influences of climate change and its interannual variability on the surface energy fluxes from 1948 to 2000. Advances in Atmospheric Sciences 27, 1438–1452.

Soares P.M.M., Cardoso R.M., Ferreira J.J., Miranda P.M.A. (2014). Climate change impact on Portuguese precipitation: ENSEMBLES regional climate model results. Climate Dynamics 45, 1771-1787.

Susca T. (2012). Enhancement of life cycle assessment (LCA) methodology to include the effect of surface albedo on climate change: comparing black and white roofs. Environmental Pollution 163, 48–54.

Swalheim S., Dodman D. (2008). Building Resilience: How the Urban Poor can Drive Climate Adaptation. Institute for Environment and Development (IIED), Sustainable Development Opinion. www.iied.org/pubs/pdfs/17043IIED.pdf.

Synnefa A., Dandou A., Santamouris M., Tombrou M., Soulakellis N. (2008). On the use of cool materials as a heat island mitigation strategy. Journal of Applied Meteorology and Climatolology 47, 2846–2856.

Taha H. (1997). Urban climates and heat islands: albedo, evapotranspiration and anthropogenic heat. Energy and Buildings, 25, 99-103.

Tai A.P.K., Mickley L.J., Jacob D.J. (2012). Impact of 2000-2050 climate change on fine particulate matter (PM2.5) air quality inferred from a multi-model analysis of meteorological modes. Atmospheric Chemistry and Physics 12, 11329-11337. doi:10.5194/acp-12-11329-2012.

Tanner T, Mitchell T, Polack E, Guenther B. (2009). Urban Governance for Adaptation: Assessing Climate Change Resilience in Ten Asian Cities. IDS Working Papers (p. 315). http://www.ntd.co.uk/idsbookshop/details.asp?id=1069.

Thompson M.L., Reynolds J., Cox L.H., Guttorp P. Sampson P.D. (1999). A Review of Statistical Methods for the Meteorological Adjustment of Tropospheric Ozone; Technical Report Series NRCSE-TRS No. 026; National Research Center for Statistics and the Environment: Seattle, WA.

Thunis P., Miranda A., Baldasano J.M., Blond N., Douros J., Graff A., Janssen S., Juda-Rezler K., Karvosenoja N., Maffeis G., Martilli A., Rasoloharimahefa M., Real E., Viaene P., Volta M., White L. (2016). Overview of current regional and local scale air quality modelling practices: Assessment and planning tools in the EU. Environmental Science & Policy. 65, 13-21.

Thunis P., Pederzoli A., Pernigotti D. (2012). Performance criteria to evaluate air quality modelling applications. Atmospheric Environment 59, 476-482.

Tominaga Y., StathopouloscT. (2013). CFD simulation of near-field pollutant dispersion in the urban environment: A review of current modeling techniques. Atmospheric Environment 79, 716–730.

Trail M., Tsimpidi A.P., Liu P., Tsigaridis K., Rudokas J., Miller P., Nenes A., Hu Y., Russel A.G. (2014). Sensitivity of air quality to potential future climate change and emissions in the United States and major cities. Atmospheric Environment 94, 552-563. http://dx.doi.org/10.1016/j.atmosenv.2014.05.079.

Turner II., Kasperson R.E., Matson P.A., McCarthy J.J., Corell R.W., Christensen L., et al. (2003). A framework for vulnerability analysis in sustainability science. Proceedings of the National Academy of Sciences of the United States of America 100, 8074–8079.

Twigg J. (2009). Characteristics of a Disaster-Resilient Community: A Guidance Note. DFID Disaster Risk Reduction Interagency Coordination Group.

Tzoulas K., Korpela K., Venn S., Yli-Pelkonen V., Kaźmierczak A., Niemela J., James P. (2007). Promoting ecosystem and human health in urban areas using Green Infrastructure: A literature review. Landscape and Urban Planning 81, 167–178.

United Nations Economic Commission for Europe, UNECE (2012b). Decision 2012/2 Amendment of the text of and annexes II to IX to the 1999 Protocol to Abate Acidification, Eutrophication and Ground–level Ozone and the Addition of New Annexes X and XI (ECE/EB.AIR/111/Add.l),

http://www.unece.org/fileadmin/DAM/env/documents/2013/air/ECE_EB.AIR_lll_Add.l_ENG_DECISION_2.pdf, accessed in July 2014.

United Nations Economic Commission for Europe, UNECE. (2012a). Decision 2012/1 Amendment of Annex I to the 1999 Protocol to Abate Acidification, Eutrophication and Ground–level Ozone, http://www.unece.org/fileadmin/DAM/env/lrtap/full%20text/ECE_EB. AIR_lll_Addl_l_E.pdf, accessed in July 2014.

URL1. National emissions reported to the Convention on Long-range Transboundary Air Pollution (LRTAP Convention). Available at: https://www.eea.europa.eu/data-and-maps/data/national-emissions-reported-to-the-convention-on-long-range-transboundary-air-pollution-lrtap-convention-11. [Last access: September 2017].

URL2. URBANFLUXES Newsletter. Urban Anthropogenic Heat Flux from Earth Observation Satellites. Issue 1. Editorial by Nektarios Chrysoulakis. Available at: http://urbanfluxes.eu/. [Last access: May 2017].

Wild M., Ohmura A., Cubasch U. (1997). GCM-Simulated Surface Energy Fluxes in Climate Change Experiments. Journal of Climate 10, 3093-3110.

Wise E.K., Comrie A.C. (2005). Meteorologically adjusted urban air quality trends in the Southwestern United States. Atmospheric Environment 39, 2969–2980.

World Health Organization, WHO. (2005). Effects of air pollution on children's health and development — a review of the evidence, World Health Organization, Regional Office for Europe, Copenhagen.

World Health Organization, WHO. (2013). Review of evidence on health aspects of air pollution — REVIHAAP Project, Technical Report, Regional Office for Europe, Copenhagen

World Health Organization, WHO. (2014). Burden of disease from Ambient Air Pollution for 2012 — Summary of results, World Health Organization (http://www.who.int/phe/health_topics/outdoorair/databases/AAP_BoD_results_March2014.pdf).

Yoshida A., Tominaga K., Watatani S. (1991). Field measurements on energy balance of an urban canyon in the summer season. Energy and Buildings 15, 417–423.

Zhang Y. (2008). Online-coupled meteorology and chemistry models: history, current status and outlook. Atmospheric Chemistry and Physics 8, 2895-2932.

Zhang Y., Liu X.-H., Olsen K., Wang W.-X., Do B., Bridgers G. (2010). Responses of future air quality to emission controls over North Carolina, part II: analyses of future-year predictions and their policy implications. Atmospheric Environment 44, 2767-2779.

Zhou H., Wang J., Wan J., Jia H. (2010). Resilience to natural hazards: a geographic perspective. Nat Hazards 53, 21-41.

CHAPTER 2

This Chapter has been submitted as:

Rafael S., Martins H., Matos M.J., Cerqueira M., Pio C., Lopes M., Borrego C. (Under review). *Application of SUEWS model forced with WRF: energy fluxes validation in urban and suburban Portuguese areas*. Boundary-Layer Meteorology.

The author acknowledges the co-authors critical revision. An acknowledgement to Professor Casimiro Pio and his team for providing the meteorological measured data used in this work.

2. Application of SUEWS model forced with WRF: energy fluxes validation in urban and suburban Portuguese areas

Abstract

Urban areas, home to over half of the world's population, are at the forefront of climate change impacts and adaptation's issues. Planning sustainable cities for the future requires not only a clear understanding of how climate change will influence urban areas but also how urban areas influence the local climate. Insights into surface fluxes of energy, water and carbon in typical urban systems are needed; urban land surface models are important tools to assess the urban surface-atmosphere exchanges and equally important is its evaluation.

This Chapter validates the Surface Urban Energy and Water Balance Scheme (SUEWS) model at an urban and a suburban site in Portugal, through five-months of simulations, with forcing data from the Weather Research and Forecasting Model (WRF). SUEWS was tested against direct flux measurements carried out at two study areas. The urban surface energy fluxes were also analysed in terms of the land cover characteristics of each study area, to understand the influence of the surface on the energy balance. At both sites SUEWS is able to simulate the turbulent sensible and latent heat fluxes and reproduces the diurnal cycle of the turbulent fluxes, but shows a consistent overestimation of the sensible heat flux. In terms of the latent heat flux, underestimation at the urban site and overestimation at the suburban site are evident. The behaviour of the energy balance fluxes, as well as their magnitude, is in accordance with typical behaviours and values at other urban similar studies. These results enable the use of WRF-SUEWS for emerging applications, such as urban planning and local/regional climate change mitigation and adaptation.

Keywords: Energy balance, Flux measurements, Flux modelling, Urban areas

2.1. INTRODUCTION

The fraction of the European population living in built-up areas (cities, towns and suburbs) is almost three quarters (72.4%) (EEA, 2012). By 2050 it is expected that urban areas will gain 2.6 billion people, while rural areas will lose 300 million people (EC, 2014). Rapid urbanization enhances the need for accurate weather forecasting at the urban scale, and longer-term studies of urban microclimate become more important for health and well-being as cities become larger, hotter and more polluted (EEA, 2012).

Given the atmospheric boundary layer is very sensitive to the surface energy balance, improved understanding of urban surface-atmosphere exchanges will allow a better assessment of the urban microclimate (Grimmond et al., 2009). The sustainable design and planning of cities is essential to address the challenges related to overcrowding, traffic and air pollution; on the other hand, a sound understanding of the microclimate is essential in planning for sustainability. Understanding urban energy fluxes, especially under extreme weather conditions (e.g., heat-waves, droughts etc.), can lead to the development of tools and strategies to minimize climate effects and improve the quality of life of the urban population, such as assessing the effectiveness of green urban infrastructures for mitigating climate extreme events (Susca et al., 2011; Li and Bou-Zeid, 2013; Li et al., 2014; Yang et al., 2015). As a result, this type of research is crucial for decision and policy makers operating at a range of spatial scales.

Much progress has been made in the measurement and modelling of the urban surface energy balance: the effect of urban materials and morphology on net all-wave radiation and sensible heat flux is reasonably well explored; there is less accuracy in modelling latent heat flux, when compared to measurements; there is some capability in modelling storage heat flux and anthropogenic heat, which cannot be directly measured. Due to the difficulty in performing measurements on urban areas, such as in this particular case related with the necessary permissions to install flux measuring towers in the top of buildings, the use of modelling tools can be essential to a full understanding of the atmosphere-biosphere system and the interaction of hydrological and dynamic processes, and therefore to the understanding of how urban structures affect the urban climate (Barlow, 2014). Additionally, and due to incomplete observations of land surface fluxes, simulations using comprehensive land surface models and historical atmospheric forcing data are useful tools for studying spatial patterns and temporal variations in land surface fluxes for local, regional and even global perspectives (Qian et al., 2007).

A large number of urban land surface models now exist that are able to simulate the urban surface-atmosphere exchanges [e.g., ACASA (Pyles et al., 2003; Marras et al. 2012), LUMPS (Grimmond and Oke, 2002; Loridan et al., 2011), SLUCM (Kusaka et al., 2001), SUEWS (Järvi et al., 2011), and TEB (Masson, 2000)]. However, there is no single ‘best’ urban land surface model (Grimmond et al., 2011) and when applying a model for the first time in a new area it is essential to guarantee good model performance and reliable predictions. Model evaluation involves different steps: scientific evaluation, code verification, model validation, sensitivity analysis, etc. (Thunis et al., 2012). The comparison of

modelled results with measurements through a statistical performance analysis has been used by the scientific community to determine the capability of a model to reproduce measured data. Although such a comparison between modelled and measured data cannot give a thorough insight into the properties of the model, it is a good first step in the evaluation of model performance (Derwent et al., 2010). In this sense, hereafter the term evaluation is referred to model validation.

Although the continuous growing interest in water and energy fluxes in urban areas, for some latitudes and locations these are scarcely studied. In this Chapter, the Surface Urban Energy and Water Balance Scheme model forced by Weather Research and Forecasting Model (WRF-SUEWS modelling system) is applied to estimate the surface energy fluxes in two distinct areas (urban and suburban) in Porto and Aveiro, Portugal (Section 2.2). The behaviour of SUEWS model was evaluated using local-scale meteorological and flux data measured in the distinct areas. Two different approaches were used to assess the surface energy fluxes: first using urban flux measurements from a field campaign (Section 2.3.1) and second using urban flux modelling, through a numerical modelling approach (Section 2.3.2). In addition, the influence of land cover on the behaviour of individual fluxes was analysed. The study of the surface energy fluxes is quite novel in the study region, both in terms of the application of measurement and modelling tools.

2.2. DATA AND METHODS

2.2.1. Measurement methodology

2.2.1.1. Field Campaign: Site Description

For this study, surface flux measurements using eddy covariance (EC) technique were undertaken for a five-month period (1 August to 31 to December 2014) at two sites with contrasting surface cover and anthropogenic activities, located in the north-west (NW) region of Portugal (Figure 2-1.).

The urban site is located approximately 3 km north (N) of the Porto city centre. The Porto urban area covers 41.4 km^2 with a population of 214,579 (INE 2015). It has warm, dry summers and mild, rainy winters. Unlike the south of Portugal, cool and rainy north Atlantic interludes interrupt the dry season and the season's average length is around three months. The annual precipitation is high and Porto is one of the wettest cities Europe. However, long periods with mild temperatures and sunny days are frequent even during the rainiest months (IPMA, 2013). The measurement site is surrounded by a dense residential and commercial area with a few sparse green areas; most of the area is covered by impervious surfaces (90%) (Table 2-1). In the vicinity of the site, both residential and commercial areas are characterized by high buildings (around 6 floors).

The suburban area is located in the outskirts of the city of Aveiro (population of 76,882; INE, 2015), approximately 75 km south of Porto. Aveiro has a humid temperate climate, with a dry season and summers which are not very warm but are long (IPMA, 2013). Due to the geographical features of this area, the frosts are rare and never severe. The suburban site is more vegetated than the urban site

and with sparse housing (1-2 storeys) and agriculture. With 30% of impervious surfaces, this site is typical of suburban areas in Porto. The very diverse vegetated area includes polyculture, grass crops, forage crops, fruit tree plantations, forest and unmanaged areas.

The climatology of both sites is influenced by the proximity of the coast (around 10 km in a straight line), through local circulations of land/sea breezes, which borders the region to the west and NW and moderates seasonal temperatures (Pinho and Manso, 2000).

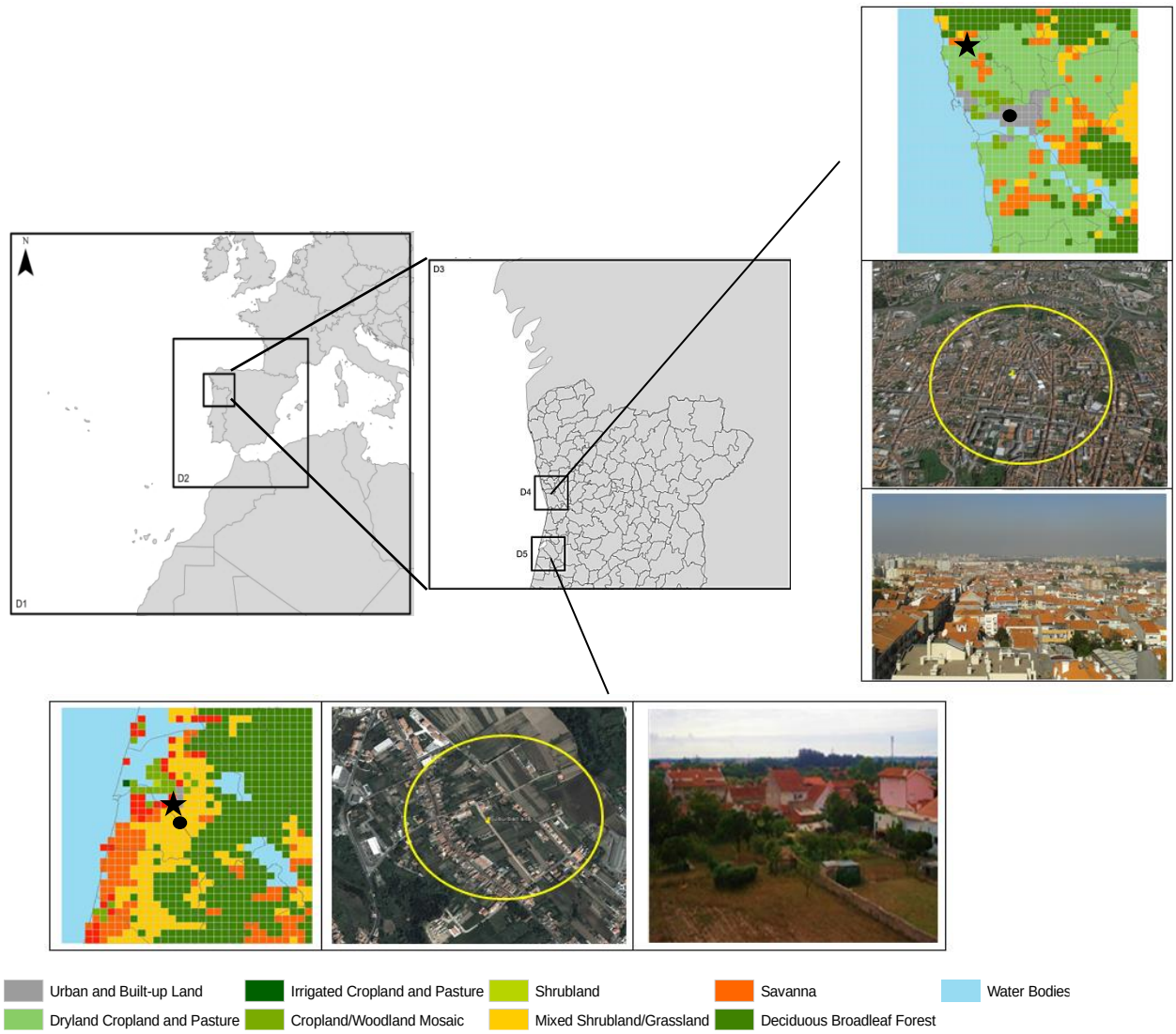

Figure 2-1. Location of the measurement sites in Portugal. Satellite images (Google Earth V10, Aveiro, Portugal, 40° 36' 51.07''N -8° 39' 05.90''W, and Porto, Portugal, 41° 09' 54.32''N, -8° 36' 50.91''W, SIO, NOAA, United States Navy, NGA, GEBCO, Image Landset, Image IBCAO, http://www.earth.google.com) of the measurement locations and the view from the towers (west). The yellow line is the 1 km radius circle that the surface cover fractions are calculated for (Table 2-1). The map shows the geographical location of the sites as well as the WRF model meteorological domains: D1: Europe and the north of Africa; D2: Iberian Peninsula; D3: north-west region of Portugal; D4: Porto urban area (urban site); D5: Aveiro suburban area (suburban site). The spatial distribution of dominant land-use types in the inner domains (D4 and D5) is also showed. The geographical locations of meteorological network stations (solid star) and surface energy fluxes sites (solid circle) are shown.

A detailed characterization of land cover was accomplished through the analysis of satellite images (obtained in Google Earth V10, Aveiro, Portugal, 40º 36' 51.07''N -8º 39' 05.90''W, and Porto, Portugal, 41º 09' 54.32''N, -8º 36' 50.91''W, SIO - Scripps Institution of Oceanography, NOAA - National Oceanic and Atmospheric Administration, United States Navy, NGA - National Geospatial-Intelligence Agency, GEBCO - General Bathymetric Chart of the Oceans, Image Landset, Image IBCAO – International Bathymetric Chart of the Arctic Ocean, http://www.earth.google.com [February 18, 2015]) and field-based surveys. The images were exported in a KMZ file (stands for Keyhole Markup language Zipped) extension and analysed with the tools available in a Geographic Information System (ArcGis software, Esri ©, V10) to estimate the surface cover of the measurement sites. The field-based surveys were useful to analyse the water movement between canopy storages within the area, allowing impervious connectivity to be accounted for. The field-based surveys also allowed the collection of information to understand the irrigation behaviour; namely, to determine the period for which there is irrigation (starting in June and ending in September) and the frequency and pattern of irrigation (the process is allowed every day of the week). The most relevant characteristics of the measurement sites are presented in Table 2-1. These data were included in the SUEWS model as input data. For simplicity, the term *urban* is used when referring the Porto site and the term *suburban* for the Aveiro site.

Table 2-1. Characteristics of the measurement sites. Surface cover for the eddy covariance (EC) sites are calculated for 1 km radius circles, based on satellite image and field-based surveys.
A: Surface area of the study grid; DLT_{Start}: Start of the daylight savings time (Julian day number); DLT_{End}: End of the daylight savings time (Julian day number); λ_{bldg}: Surface fraction of buildings; λ_{everg}: Surface fraction of evergreens; λ_{dec}: Surface fraction of deciduous trees; λ_{igrass}: Surface fraction of irrigated grass; λ_{pav}: Surface fraction of paved areas; λ_{grass}: Surface fraction of non-irrigated grass; λ_{veg}: Surface fraction of vegetation; λ_{unman}: Surface fraction of unmanaged land; λ_{water}: Surface fraction of water; p: Population density inside the grid (population km^{-2}, INE, 2011); z_{om}: Roughness length of momentum (m); z_{0v}: Roughness length for heat and water vapour (m); z: Height of the meteorological forcing data – the most important height is that of the wind speed measurement (m); z_h: Mean building height (m); z_t: Mean tree height (m). For z_{om}, z_{ov}: RT, rule of thumb (Järvi et al., 2011).

	Urban area	**Suburban area**
Lat	41° 09' 54.32''N	40° 36′ 51.07''N
Lon	-8° 36' 50.91''W	- 8° 39' 05.90''W
z (m)	30	10
A (ha)	100	100
Start of daylight savings time	120	120
End of daylight savings time	299	299
λ_{bldg}	0.6	0.2
λ_{everg}	0.015	0.15
λ_{dec}	0.02	0.15
λ_{igrass}	0.05	0.3
λ_{pav}	0.3	0.1
λ_{grass}	0.015	0.1
λ_{veg}	0.1	0.7
λ_{unman}	0	0
λ_{water}	0	0
***p* (in km^{-2}) (INE, 2011)**	54 296	10 254

Table 2-1. (Continued).

	Urban area	Suburban area
z_{om}, z_{ov} (m)	RT	RT
z_h (m)	12	4
z_t (m)	4	4

2.2.1.2. Instrumentation

Eddy covariance (EC) flux towers were installed at the two sites to monitor the exchanges of momentum, heat, water and carbon dioxide fluxes.

At the urban centre, the EC system has started its operation in July 2014, in the top of a 12 m height tower; the tower is installed on the top of the firefighters' training building (at the Batalhão de Sapadores Bombeiros do Porto, with 20 m of height). This means that the instruments are mounted 32 m above the ground surface (Figure 2-2a.). At the suburban area, the EC system is installed on the top of a 12 m tall tower located on the ground which operated since April 2014 (Figure 2-2b.). In both towers the EC instrumentation is located at similar heights above surrounding canopies, approximately 10-15 meters above the roofs of surrounding buildings at the urban site, and above the vegetation at the suburban site.

Figure 2-2. The EC flux towers installed at: (a) urban site: top of a firefighters' training tower at the *Batalhão de Sapadores Bombeiros do Porto* (*Rua da Constituição*); (b) suburban site: installation of the tower at *Verdemilho*, Aveiro; (c) instruments installed on the flux measurement towers (see equipment description in the text).

Each flux tower has a three-dimensional sonic anemometer (Windmaster Pro, Gill Instruments, Lymington, UK) to directly measure the three components of wind speed and virtual temperature, and an open-path infrared gas analyser (IRGA, LI-7500A, LI-COR Biosciences, Lincoln, NE, USA) to measure fluctuations of water vapour (H_2O) and carbon dioxide (CO_2) concentrations. These instruments allow the calculation of momentum, sensible and latent heat, and CO_2 fluxes. The EC sensors were mounted, separated by 0.20 m, on a 1.5 m horizontal boom located on the top of the

towers. In order to minimize interferences by the predominant winds (NW), the boom has a south-west (SW)/north-east (NE) direction, with the sonic anemometer positioned on the SW side and the gases analyser located on the NE side of the boom. The raw flux data were logged at 10 Hz (Xlite 9210 data logger, Sutron Corporation, USA).

At the suburban site, ancillary measurements of incoming solar radiation (LI COR, pyranometer LI-200SL), photosynthetically active radiation (LI COR, quantum sensor LI 190SL) and longwave radiation (Kipp & Zonen, net pyrgemeter, CG3), precipitation (tipping bucket rain gauge, environmental measurements Ltd., ARG100), soil heat flux (Campbell Scientific Ltd., HFT-3), soil temperature (PRT) and soil moisture (Delta-T Devices, Type ML2x) were performed, with a temporal resolution of 1 second and integrated and recorded at 15 minute averages (with the exception of precipitation which was recorded at each 0.2 mm of accumulated rainfall).

2.2.1.3. Flux Processing

For this study, EC data were analysed for the five-month period for both sites. The vertical flux, *F,* was calculated as the covariance between the vertical velocity, *w*, and scalar, *s*, of interest according to the eddy covariance technique (Lee et al., 2004):

$$\mathrm{F} = \overline{\mathrm{w}'s'} \tag{2.1}$$

where *w´* and *s´* are instantaneous fluctuations (in relation to the average) of *w* and *s*, respectively.

Fluxes were calculated from block averages over 30 minute time periods (see Matese et al. 2009 and Velasco and Roth 2010 for rationale).

The data were processed using EddyPro Advanced (version 5.2.1, LI-COR) following standard procedures, including despiking of raw data, correction for angle of attack, time-lag compensation, double coordinate rotation, high and low frequency spectral corrections (Moncrieff et al., 1997), a modification of the Kaimal formulation (Kaimal, 1972) and the density corrections of Webb et al. (1980).

Data quality checks were based on the flagging policy of Mauder and Foken (2004) with three quality classes (“0” for best quality fluxes, “1” for fluxes suitable for general analysis such as annual budgets and “2” for fluxes that should be discarded from the results dataset). Quality flags are based on a combination of partial flags from two tests widely adopted in literature (Foken and Wichura, 1996; Foken et al., 2004). This method is described in the documentation of the EddyPro Eddy Covariance software. Data with flagship “2” were discarded; data with flagship “1” were inspected by comparison with results flagged “0” from nearby periods and only accepted if presenting a similar behaviour. Also, data during periods of CO_2/H_2O detector wetness were discarded. A spectral plots analysis, as a monthly ensemble, for *w'T'*, *w'*H_2O*'* and *w'*CO_2*'* co-spectra and for *u*, *w*, *T* spectra, as three half hours binned, were used to guarantee the good performance of EC methodology at the urban site (Appendix A, Figure A-1 to A-3). A total of approximately 75%, with a minimum of 40% in November, of the maximum possible samples, were validated and used in flux calculations.

The footprint model of Hsieh et al. (2000), based on a combination of Lagrangian stochastic dispersion model results and dimensional analysis, was used to determine the probable source area of the turbulent fluxes, with z0m=0.15 zh (mean building height) and zd (zero displacement height) = 0.67 zh, according to LI-COR, Inc. (2009). Flux measurements represent a variable footprint distance, depending from the moment of the day and from season, but usually lower than one kilometre, therefore within homogeneous terrain coverage conditions.

2.2.2. Modelling methodology

2.2.2.1. Flux Modelling – SUEWS Model

The SUEWS model (version V2014b) (a full description if provided by Järvi et al., 2011, 2014) was used to simulate the urban fluxes for both study areas for the observation period (August-December 2014). The model simulates the urban energy and water balance fluxes at the local or neighbourhood scale using hourly meteorological variables and information about the urban surface. SUEWS incorporates several sub-models. The Objective Hysteresis Model (OHM) (Grimmond et al., 1991) calculates the net storage heat flux; the Net All-wave Radiation Parameterisation (NARP) (Offerle et al., 2003) provides the net all-wave radiation; the urban evaporation-interception scheme of Grimmond and Oke (1991) calculates the latent heat flux; the sensible heat is estimated as the residual of the energy balance; a change version of the Sailor and Vasireddy (2006) approach is used to calculate the anthropogenic heat flux; and the Local-scale Urban Meteorological Parameterisation Scheme (LUMPS) (Grimmond and Oke, 2002) provides an initial estimation of the atmospheric stability.

The schemes and modules which compose SUEWS allow a relatively undemanding set of inputs, namely only common meteorological variables (mean wind speed, relative humidity, air temperature, station air pressure, precipitation and incoming shortwave radiation) and characterization of land cover (surface fractions) for each model grid, including: the plan area fraction of paved areas, roofs, evergreen trees and shrubs, deciduous trees and shrubs, irrigated grass, non-irrigated grass and water, along with albedo, emissivity, moisture storage capacity, population density and building and tree heights (Järvi et al., 2011).

The SUEWS model considers the complete energy balance at the interface between the urban surface layer and the atmosphere:

$$Q^* + Q_F = Q_E + Q_H + \Delta Q_S \quad [W \cdot m^{-2}] \tag{2.2}$$

where Q* is the net all-wave radiation (the net incoming and outgoing radiative fluxes), Q_F is the anthropogenic heat flux (the energy released by human activities), Q_E is the latent heat flux (the energy taken up/released with the phase change of water), Q_H is the turbulent sensible heat flux (the energy that heats the air), and ΔQ_S is the net storage heat flux (which includes soil heat flux and also the heating and cooling of the complete urban structure).

The local scale advection is not resolved in the model, but rather is included within the parameterizations of the individual terms. The inter-grid advection is assumed to be negligible (see Järvi et al., 2014 for further details). This is consistent with the eddy covariance fluxes measurements used to assess the model.

The net all-wave radiation consists of shortwave (K) and long-wave (L) components, with the arrows denoting the direction (incoming - ↓ or outgoing - ↑):

$$Q^* = K\downarrow - K\uparrow + L\downarrow - L\uparrow \quad [W \cdot m^{-2}] \tag{2.3}$$

In the absence of detailed information, the same soil properties were assumed for the soil stores beneath each surface: a soil layer depth of 350 mm, with a maximum moisture capacity of 150 mm (saturated soil moisture content of 0.43 $m^3 \cdot m^{-3}$). The initial soil moisture state was set to 80% of the saturation value. For the suburban area, 2% of water from paved surfaces was allowed to flow to other surfaces (grass) and 10% of water from roofs was allowed to flow to other surfaces (4% to grass and 6% to paved surfaces). The remaining proportions (98% for paved surfaces and 90% for buildings) become runoff into pipes. Water from pervious surfaces is allowed to infiltrate into the soil stores beneath. The same conditions were used in the urban area, except for the water from buildings that flows completely to paved surfaces (none to grass) and 10% of the water from evergreen trees and deciduous trees that is allowed to flow to paved surfaces. Irrigation occurs between June and September. During this period, the transpiration is not limited by water availability.

A model time-step of 5 min was specified. The input meteorological dataset has a resolution of 60 min, which is linearly interpolated to 5 min to run the model. The model output was averaged back to 60 min for comparison with measurements.

2.2.2.2. SUEWS Forcing Data

The meteorological data required for SUEWS was obtained through the application of the Weather Research and Forecasting Model (WRF – version 3.3.1) (Skamarock et al., 2008). The WRF model was selected to force SUEWS rather than measured data, for two main reasons. First, the need to evaluate SUEWS with modelled forcing data given that Portugal has relatively few meteorological stations. The availability of measured data is a limitation for applications of SUEWS, or comparable schemes, and comparisons with other sites with similar land cover. Second, for a future assessment of the spatial distribution of the energy fluxes in Portugal, a complete spatial coverage of meteorological data is needed, which is only possible if a meteorological model is used. The WRF model has been widely used for different applications and purposes in Portugal, and found to have a good performance regarding temperature, precipitation and incoming shortwave radiation (Soares et al., 2012; Carvalho et al., 2012; Monteiro et al., 2013, 2015; Borrego et al., 2015).

The WRF model was applied to five domains, using the two-way nesting technique, for the study period (August-December 2014), corresponding to the measurement period of the urban and suburban fluxes. Figure 2-1 shows the model domain setup: domain 1 (D1) at 27 km grid spacing

covering Europe and the north of Africa (with 173×142 horizontal grid cells); D2 at 9 km grid spacing covering the Iberian Peninsula (175×166 horizontal grid cells); D3 at 3 km grid spacing over NW Portugal (121×109 horizontal grid cells); and D4 and D5 at 1 km grid spacing over the Porto urban area and Aveiro suburban area, respectively (both with 34×34 horizontal grid cells). The outermost domain was designed to cover a relatively large ocean area (with a time step of 162 seconds), reducing spurious boundary effects in the inner region. All the domains present 38 vertical layers, with the lowest model sigma level at approximately 10 m of height and model top at 50 hPa. The initial and boundary conditions for the coarse domain (D1) were initialized with global meteorological fields from the European Centre for Medium-Range Weather Forecasts (ECMWF) Re-Analysis Interim (ERA-Interim) model data (http://www.ecmwf.int/en/research/climate-reanalysis/era-interim) with 1°×1° spatial resolution and temporal resolution of 6-h for surface and pressure levels. For the other domains, the initial and boundary conditions come from the respective parent domain. In all domains 5 grid points are used as lateral relaxation areas. Different physics parameterizations were used for the modelled domains. The WRF model configuration for the 3 km and 1 km grid spacing included: the Noah land surface model (Tewari et al., 2004), the Rapid Radiative Transfer Model (RRTM) longwave radiation scheme (Mlawer et al., 1997), the Mellor-Yamada-Janjic planetary boundary-layer scheme (Janjic, 2002). No cumulus parameterization scheme was used since at this scale the model is able to represent the effects of sub-grid scale convective processes (Gilliland and Rowe, 2007). The Corine Land Cover data (http://land.copernicus.eu/pan-european/corine-land-cover) was remapped to the United States Geological Survey (USGS) 24 land use categories, following Carvalho et al., (2017). The parameterizations selection was based on recommendations included in Wang et al. (2014), as well as on validation and sensitivity studies previously performed over Portugal (Aquilina et al., 2005; Carvalho et al., 2006; Monteiro et al., 2015) and over the Iberian Peninsula (Fernandez et al., 2007).

The SUEWS model was applied for the two individual model grid cells, both with a resolution of 1×1 km^2, covering the area where the measurement towers were located (urban and suburban).

2.2.3. Statistical Analysis

Since the WRF model is used to force the SUEWS model, and therefore a bias in WRF's results could influence the SUEWS performance, two types of analyses were required: i) a statistical analysis to explore the relation between each component of the energy balance and the meteorological variables; ii) the estimation of statistical metrics to conduct the models' evaluation. This methodology was adopted to investigate if the meteorological variables that contribute the most to the energy flux variability are satisfyingly simulated, and therefore, suitable to force SUEWS.

The stepwise regression method was implemented using SPSS predictive analytics software version 23, which produces a set of statistical models (combination of the meteorological variables regressed with the respective component of the energy balance). This method allows considering all meteorological variables used to force SUEWS (modelled data) the same time, consisting in a series of multiple regressions, in which each time the weakest correlated variable is removed. At the end the

variables that best explain the variability of each component of the energy fluxes are obtained (Sá et al., 2015). Only variables that met a 0.05 significance level were accepted in the statistical models.

The models' evaluation consisted on its validation, and was performed through the direct comparison of modelled results against measurements, in the form of statistical metrics. Quantitative analysis is considered an accurate and detailed method to assure quality and demonstrate that a model can provide reliable results for a desirable purpose. Data provided by the field campaign were used to evaluate SUEWS, while data from the Portuguese meteorological station network were used to evaluate the WRF model. The meteorological data from the field campaign were not used to force SUEWS nor for WRF model validation, since a large amount of gap filling would be required to obtain a complete set of data acceptable for both applications. Two meteorological stations were selected as representative of each study area (urban site and suburban site), based on two main criteria: the proximity to the study site (within a radius of 6 km) and the similarity of the land cover. The validation was performed for temperature and relative humidity (Vaisala HMP45, sensor) as well as for wind speed (Vaisala Wind Set WA15, anemometer). The analysis of the incoming shortwave radiation (Kipp & Zonen, pyranometer, CMP11) was only undertaken for the suburban site, since those data were not available, for the analysed period, for the urban area. The data is recorded at 10 minute averages and provided at an hourly scale. The precipitation and air pressure were not validated since no measured data were available. For the analysed variables there was a data acquisition efficiency of 100% at both stations.

The performance of WRF and SUEWS models was assessed by applying the BOOT (i.e., bootstrap resampling method) Statistical Model Evaluation Software Package, version 2.0, by Chang and Hanna (2005). This is widely used in model evaluation exercises (e.g., Mosca et al., 1998; Nappo and Essa, 2001; Ichikawa and Sada, 2002). Four main statistical parameters were considered: (i) the correlation coefficient (r) - to provide an indication of the correspondence of the timing and evolution of observed and simulated values; (ii) the mean bias error (MBE) - the average difference between simulated and observed values; (iii) the root mean square error (RMSE) - which gives important information about the skill in predicting the magnitude of a variable; and (iv) the normalised mean square error (NMSE) relative to the multiplication of observed and modelled mean values. Unlike BOOT, the MBE expresses the arithmetic difference between model predictions and observations (consequently, positive MBE indicates an overestimation). Both RMSE and MBE have the units of the variables being evaluated and depend on the magnitude of the mean variables. Time-series and scatter plots were generated to complement the quantitative statistical analysis.

2.3. RESULTS AND DISCUSSION

Considering the previously described methodology (section 2.2). The meteorological variables provided by the WRF model and used as input in SUEWS were compared against data from national meteorological stations (sections 2.3.1.1 and 2.3.1.2). The SUEWS performance was assessed for the turbulent energy fluxes (section 2.3.1.3). Attention was also directed to the modelled energy balance for the two study areas, to assess the influence of surface cover in on the behaviour of the individual fluxes (section 2.3.2).

2.3.1. Model Evaluation

2.3.1.1. Stepwise Regression analysis

Table 2-2 shows the statistical model suggested by the stepwise regression procedure and the corresponding explained variance (proportion of variance in each flux which can be explained by the meteorological variables), which gives insights of the importance of each meteorological variable in the variability of the energy fluxes.

Table 2-2. Regression model selected by the stepwise regression for the energy balance data based on the meteorological inputs (3667 values).

T: temperature; R: incoming shortwave radiation; P: pressure; pr: precipitation; RH: relative humidity; WS: wind speed.

		Regression model	Variance explained (%)	p-value
Urban site	Q_E	1095.6+13.179pr-11.12P+4.861WS+0.02R+0.248RH-0.38T	26.3	< 0.01
	Q_H	-1476.3+0.359R-11.73pr+3.004T+14.46P-4.13WS+0.199RH	83.3	< 0.01
	ΔQ_S	252.118+0.424R+0.597RH-1.642T-3.264P	89.0	< 0.01
	Q_F	-2.542+0.009R-0.290T-0.096RH+0.628pr+0.216P	24.9	< 0.01
	Q*	-152.38+0.797R+1.157RH+1.29T+0.116P+0.04WS+ 0.033pr	100	< 0.01
Suburban site	Q_E	844.89+0.312R-7.798P+12.257pr-0.545RH+1.792WS	84.9	< 0.01
	Q_H	-1096.4+0.207R+1.15RH-11.219pr+9.607P+1.83T-1.735WS	69.9	< 0.01
	ΔQ_S	147.5+0.253R+0.499RH-0.785T-2.085P	91.2	< 0.01
	Q_F	-4.04-0.027RH+0.001R+0.046T+0.126pr+0.082P+ 0.015WS	28.5	< 0.01
	Q*	-154.069+0.770R+1.177RH+1.353T+0.101P	100	< 0.01

The meteorological variable that has the greatest influence on the variability of Q_E is precipitation (pr) for the urban area and incoming shortwave radiation (R) for the suburban area (followed by pr), indicating that the water availability is a limiting factor for the development of the latent heat flux (Q_E). At the urban site the variability of Q_E is explained only 26% by the meteorological variables; while the meteorological data explains around 85% of the Q_E variance at the suburban area. The weak relation between the meteorological variables and the Q_E at the urban area can be explained by the fact that

the magnitude of this flux is directly dependent on the (none) existence of vegetation, with land cover data being particularly important in this area.

In both areas, the variability of Q_H can be explained by the meteorological variables, 83% and 70% respectively for the urban and suburban areas. In both cases the incoming shortwave radiation contributes most to the variability of Q_H. This finding is in accordance with the expected behaviour of Q_H, since this flux is directly dependent on the air temperature, and so, directly dependent of the incoming shortwave radiation that arrives to the surface (Grimmond and Oke, 2002). Similar results were obtained for ΔQ_S at both sites. Wind speed and precipitation are not statistically significant in explaining the variance of ΔQ_S (p-value is larger than 0.05) and for this reason these components are not displayed in the regression equation.

Q_F is the energy flux least dependent on the meteorological variables. The meteorological inputs only explain around 23% and 28% of the Q_F at the urban and suburban sites, respectively. This result it is expected given the approach for the Q_F calculation (Sailor and Vasireddy, 2006), as well as the assumptions made in the modelling, especially the fact that the same anthropogenic heat flux profile was used for both areas. In contrast, the Q* variance is 100% explained by the meteorological variables in both areas, mainly the incoming shortwave radiation, relative humidity and temperature. This dependence is consistent with the parameterization used by SUEWS to estimate Q*.

This analysis reveals that, in general, the most important meteorological variables for the energy fluxes modelling are the temperature and incoming shortwave radiation, and therefore a good accuracy of these data is crucial. Also, precipitation is a determinant variable for the estimation of Q_E.

2.3.1.2. Meteorological Variables

The modelled meteorological variables were compared against measurement data for the study period (August-December 2014) (hourly time scale). The statistical analysis (Table 2-3) for temperature exhibits a good relation between modelled and measured data with a correlation coefficient greater than 0.9, for the two study areas, and a NMSE of 0.01 and 0.02 (close to the ideal 0) for the urban and suburban sites, respectively. There is a consistent underestimation of the temperature values for both areas, evidenced by the negative MBE (-1.08 and -1.19°C for urban and suburban sites, respectively) (see Appendix B for a complement analysis, Figures B-1 and B-2). This underestimation could be attributed to the urban heat island that is developing in the urban areas, which is not appropriately described by the model (Papanastasiou et al., 2010). The time series shows that WRF is able to reproduce the hourly cycle of temperature. The model presents similar skill for the incoming shortwave radiation (in the case of suburban site), with r greater than 0.9, a NMSE of around 0.4, and a MBE of -2.9 $W \cdot m^{-2}$.

For relative humidity, the model also shows reasonable performance, with a correlation coefficient around 0.6 and a NMSE of 0.05 and 0.03, for the urban and suburban sites, respectively. Unlike temperature, the WRF model overestimates the relative humidity, with a positive MBE of around 14%

for the urban and 9% for the suburban site. This overestimation is constant for all the time series of the two areas.

The WRF model performance is not as reasonable for the wind speed (at 10 m) with a correlation factor of 0.3 for the urban and 0.4 for the suburban site. This variable exhibits the highest NMSE (0.66 and 0.71 for the urban and suburban sites, respectively). The WRF model underestimates the wind speed, demonstrated by the negative MBE (-0.97 and -0.15 $m \cdot s^{-1}$ for urban and suburban sites respectively), as well as by the time series and the scatter plots. These results were mostly due to the poor performance of the model during the night-time (7 p.m. to 6 a.m.). This means that the land-surface model overestimates the differences between sea and land temperatures during the night, a fact that results in inadequate surface parameterization.

The obtained statistics metrics, for both areas, are in accordance with the acceptance criteria (MBE within ± 30% of the mean and NMSE <1.5) proposed by Chang and Hanna (2005). These findings guarantee that the most important meteorological variables for the variability of the energy fluxes are well modelled by WRF model, which strengthens the robustness of the model setup and gives confidence in the obtained flux results.

Table 2-3. Evaluation of WRF model performance for 1 August - 31 December 2014 (3667 hours). The temperature (T) and relative humidity (RH) were obtained at 2 m above ground, for both urban and suburban sites; the incoming shortwave radiation (K↓) was obtained at 10 m above ground; and the wind speed (WS) was obtained at 30 m and 10 m above ground for the urban and suburban sites, respectively.

		Measured	**Modelled Statistics**			
		Mean	**Mean**	**R**	**NMSE**	**MBE**
Urban site	T (°C)	16.33	15.25	0.950	0.01	-1.08
	RH (%)	74.58	89.14	0.686	0.05	14.56
	WS ($m \cdot s^{-1}$)	3.34	2.38	0.312	0.66	-0.97
Suburban site	T (°C)	17.20	16.01	0.944	0.02	-1.19
	RH (%)	77.15	86.37	0.640	0.03	9.23
	WS ($m \cdot s^{-1}$)	2.37	2.21	0.360	0.71	-0.15
	K↓ ($W \cdot m^{-2}$)	160.5	157.68	0.912	0.45	-2.85

The full understanding of the behaviour of the energy fluxes requires knowledge of the local meteorological conditions for the study period. Based on WRF model results, a climatology-analysis was undertaken. During the evaluation period, at the urban site, the summer month (August) was characterized by clear, sunny skies with average daytime temperatures of around 21°C. Autumn and winter temperatures ranged between 9°C (average temperature in December) and 19°C (average temperature in October) rarely dropping below 0°C at night. Winter was characterized by prolonged sunny periods although some periods of low intensity precipitation occurred. The precipitation was below the average of the climate Normal 1981-2010; values above the 150 mm received are usual in this season. Given the proximity of the river and the ocean, the relative humidity was above 80%. The wind was predominantly weak (bellow 5 $m \cdot s^{-1}$) and from the NW direction.

At the suburban site, the maritime influence results in a narrow temperature range, with a summer daytime average around 22°C. Typical of Mediterranean climates, August was dry with a total precipitation of 17.2 mm. During the study period, September was the warmest month with an average temperature of 24°C. It was also one of the rainiest months (with a total amount of 146 mm). The temperatures of the autumn and winter months ranged, on average, between 10 and 15°C. November was a rainy month, with a total amount of precipitation of 248 mm, well above the Normal (128 mm), while December registered a precipitation below the Normal (134 mm), with only 32 mm.

The climatology-analysis shows that the two sites experience similar meteorological conditions. Temperatures in the suburban areas tend to be slightly warmer than in the urban area, whilst humidity and precipitation is slightly lower. Both areas have a moderate climate with dry and mild summers. The key differences between the sites are the level of urbanisation, evident in the proportions of vegetation, impervious surfaces, height of buildings and population density (Table 2-1).

2.3.1.3. Energy fluxes

The individual turbulent heat fluxes (Q_H and Q_E) were evaluated at hourly time scale for the study period (Figure 2-3, Table 2-4). For that, the mean diurnal behaviour of both measured (EC) and modelled (SUEWS) turbulent energy fluxes were analysed. The first (25^{th}) and third (75^{th}) quartiles of the data values are also shown, along with individual plots for each month in the study period (Figures 2-4 and 2-5).

Statistics for the modelling of Q_H are generally good, for both areas, exhibiting a good relation overall between measured and modelled data with correlation factors around 0.7 and a NMSE of 4. There is a consistent overestimation of the sensible heat flux with a MBE of 14.70 and 51.43 $W \cdot m^{-2}$ for the suburban and the urban area, respectively (Figure 2-3). RMSE values of 49.38 and 85.87 $W \cdot m^{-2}$ were obtained at the suburban and urban sites, respectively, similar to the values obtained in previous studies (Järvi et al., 2011, 2014). The overestimation of Q_H during daytime is probably a result of two factors: i) an underestimation of ΔQ_S during daytime due to SUEWS difficulty in reproducing the observed wintertime behaviour (in this case December) as a result of the bias towards summertime observation in the currently available OHM coefficients (further research is needed to develop parameterisations which better account for anthropogenic heat flux, building volume, construction materials and seasonality [Ward et al. 2016]); ii) an underestimation of the air temperature which enhances the difference in temperature between the surface and the air, which can imply an increase of the heat energy transferred as Q_H. The large RMSE is explained by the generally high values of Q_H in urban areas in comparison with more vegetated suburban sites.

For Q_E, different behaviours were observed for the urban and suburban areas. At the suburban site, the statistical parameters revealed a good performance of SUEWS, with a correlation of around 0.6, a NMSE of 2.5 and a MBE of 26.8 $W \cdot m^{-2}$. The overestimation of the latent heat flux it is also evident in the scatter plot (Figure 2-3) This overestimation is probably a result of the irrigation period considered in the simulation (June to September), which added additional moisture and enhanced the evaporation

rate in August and September (months with highest MBE). The tree roots may be able to access deeper reserves of soil moisture than allowed by the model therefore irrigation could have been overestimated. However, at the urban site the statistics are poorer, especially in terms of the correlation coefficient (around 0.1). In this area, SUEWS underestimates Q_E, which is evident in the scatter plot and by the negative MBE (-12 W·m^{-2}). RMSE values of 77.5 and 41.3 W·m^{-2} were obtained at the suburban and the urban area, respectively. The better performance of Q_E in suburban areas is broadly consistent with previous studies (Ward et al., 2016).

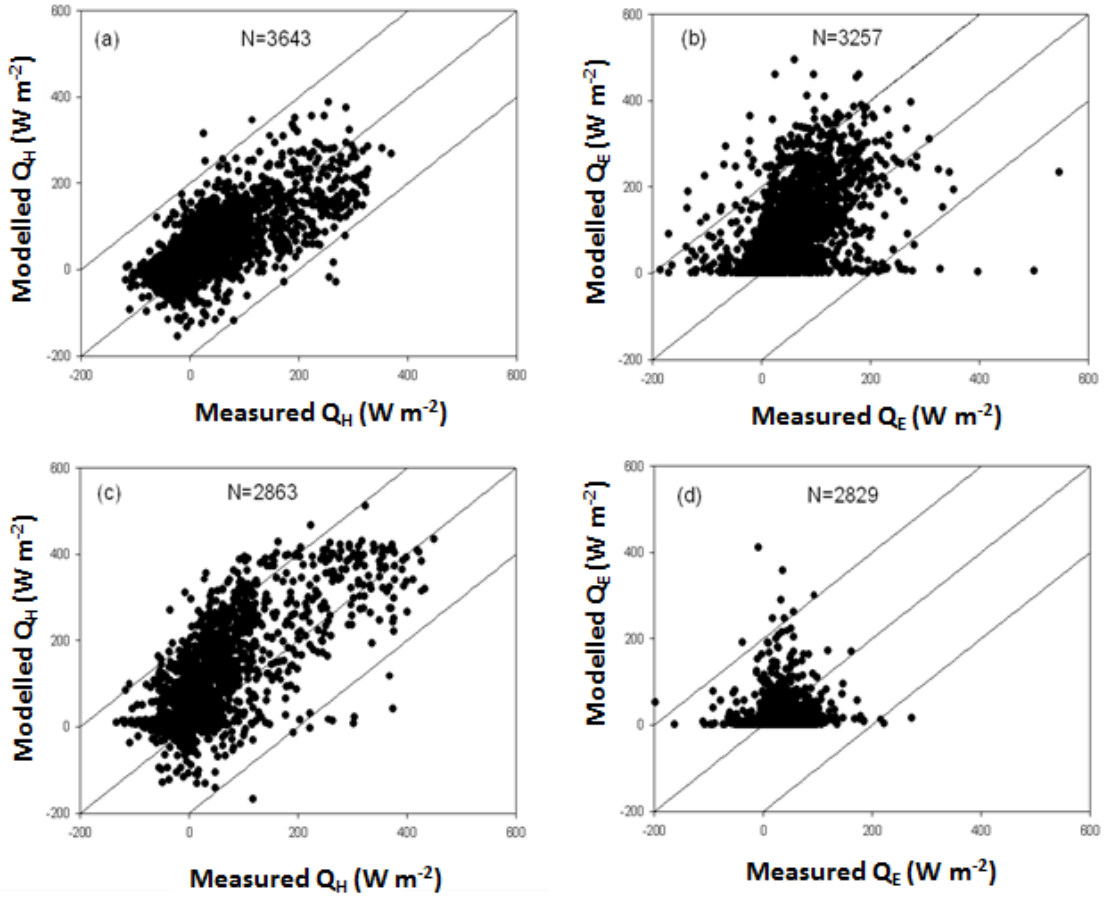

Figure 2-3. Measured (eddy covariance) and modelled (SUEWS) turbulent sensible and latent heat fluxes heat fluxes for the (a, b) suburban and (c, d) urban sites, for August-December 2014 (only hours when observations are available).

Table 2-4. Model evaluation statistics (Mod) based on SUEWS performance relative to observations (Obs) of sensible (Q_H) and latent (Q_E) heat fluxes, (*N* is the number of points in the linear fit for all the parameters).

			Mean (W·m^{-2})		R	NMSE	RMSE	MBE
		N	Obs	Mod			(W·m^{-2})	
Suburban	Q_H	3635	20.09	34.79	0.716	3.87	49.38	14.70
	Q_E	3256	37.53	64.35	0.607	2.50	77.48	26.82
Urban	Q_H	2859	26.81	78.25	0.744	3.54	85.87	51.43
	Q_E	2823	23.74	11.73	0.131	6.82	41.31	-12.01

At the suburban site during the analysed period (Figure 2-4), SUEWS reproduces well the diurnal cycle of the turbulent sensible and latent heat fluxes. The maximum monthly turbulent fluxes are in August for Q_H (220 $W \cdot m^{-2}$) and in September for Q_E (266 $W \cdot m^{-2}$). The high value of Q_E in September is related to high amounts of precipitation (total of 146 mm, higher than the value registered in December) combined with temperatures above 20°C, which promoted evapotranspiration. Additionally, evapotranspiration is dependent on the moisture content of the soil, which was on average around 12.7 $m^3 \cdot m^{-3}$ (modelled value). The highest soil moisture content was obtained in September and October. August had the second highest value of monthly Q_E (252 $W \cdot m^{-2}$), despite the small amount of precipitation (around 17 mm on the entire month). In this month, water was introduced to the system through irrigation, contributing to an increase of the soil moisture content. Both turbulent fluxes have their minima in November and December.

The measured data shows that Q_H is the dominant turbulent flux in summer (August), when drought conditions cause a low evaporative fraction. As the net all-wave radiation begins to decrease into the autumn months (September and October), and precipitation increases, Q_E becomes larger and Q_H decreases considerably. In the winter, as result of reduced Q* and reduced temperatures (around 9ºC-10ºC), the differences between Q_H and Q_E are not so evident.

Both model and measured results show that Q_E is more dominant during the day, because of greater moisture content, continuing as a positive flux at night. In an absolute sense there is not much variability in Q_H at night. Of particular interest, however, is the fact that measured data in the evening are negative, as a result of the reduced surface temperatures and turbulence. The model fails to simulate this phenomenon, in particular the frost formation at night during the autumn and winter months (October to December), characteristic of suburban sites of Portugal (IPMA, 2013).

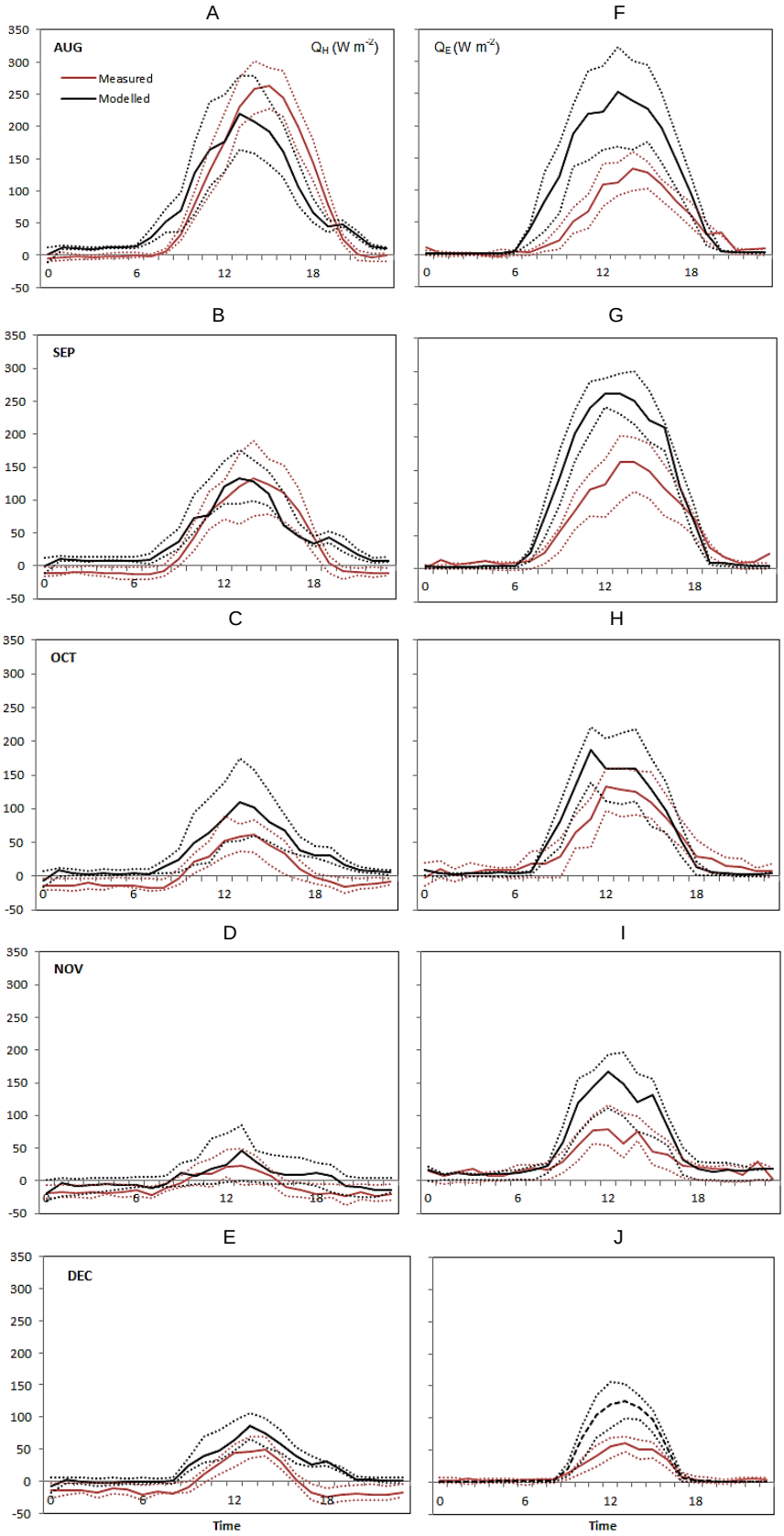

Figure 2-4. Mean monthly diurnal measured and modelled turbulent fluxes of sensible (Q_H) (A-E) and latent (Q_E) (F-J) heat at the suburban site. Dotted lines show the quartile deviations (25th and 75th percentiles).

Also at the urban site (Figure 2-5), the model is able to reproduce the behaviour of the diurnal average cycle of the turbulent heat fluxes. The measured data reveal that the role of vegetation in influencing Q_E in the Porto area is minimal given the small fraction of vegetation cover. Q_H dominance is mostly evident in August as a result of strong surface heating, an effect that decreases as winter approaches.

In general, SUEWS underestimates Q_E in the daytime when the fluxes are larger resulting in an overestimation of Q_H. This happens since the sensible heat flux is calculated as a residual from the hourly available energy minus the hourly latent heat flux (Järvi et al., 2011). The average daily maximum latent heat flux varied between 10 and 72 $W \cdot m^{-2}$ (respectively for the months of November and December), while the daily maximum sensible heat flux varied between 72 and 366 $W \cdot m^{-2}$ (respectively for the months of August and November). It is not a surprise that areas with little vegetation have extremely small latent heat flux values (Grimmond and Oke, 1999). The low values are partly due to the surface characteristics (high distribution of impermeable surface), combined with a low moisture content of the soil and an inability of water flowing through the surface.

Unlike the case of Q_E, there are no months with extremely small Q_H values. This is expected since heat is available everywhere at the surface, which is not the case for water. Comparing the magnitude of the Q_H and Q_E values, it is evident that the sensible heat flux is numerically the most important heat sink of the turbulent heat fluxes. This result compares well with the measured data behaviour.

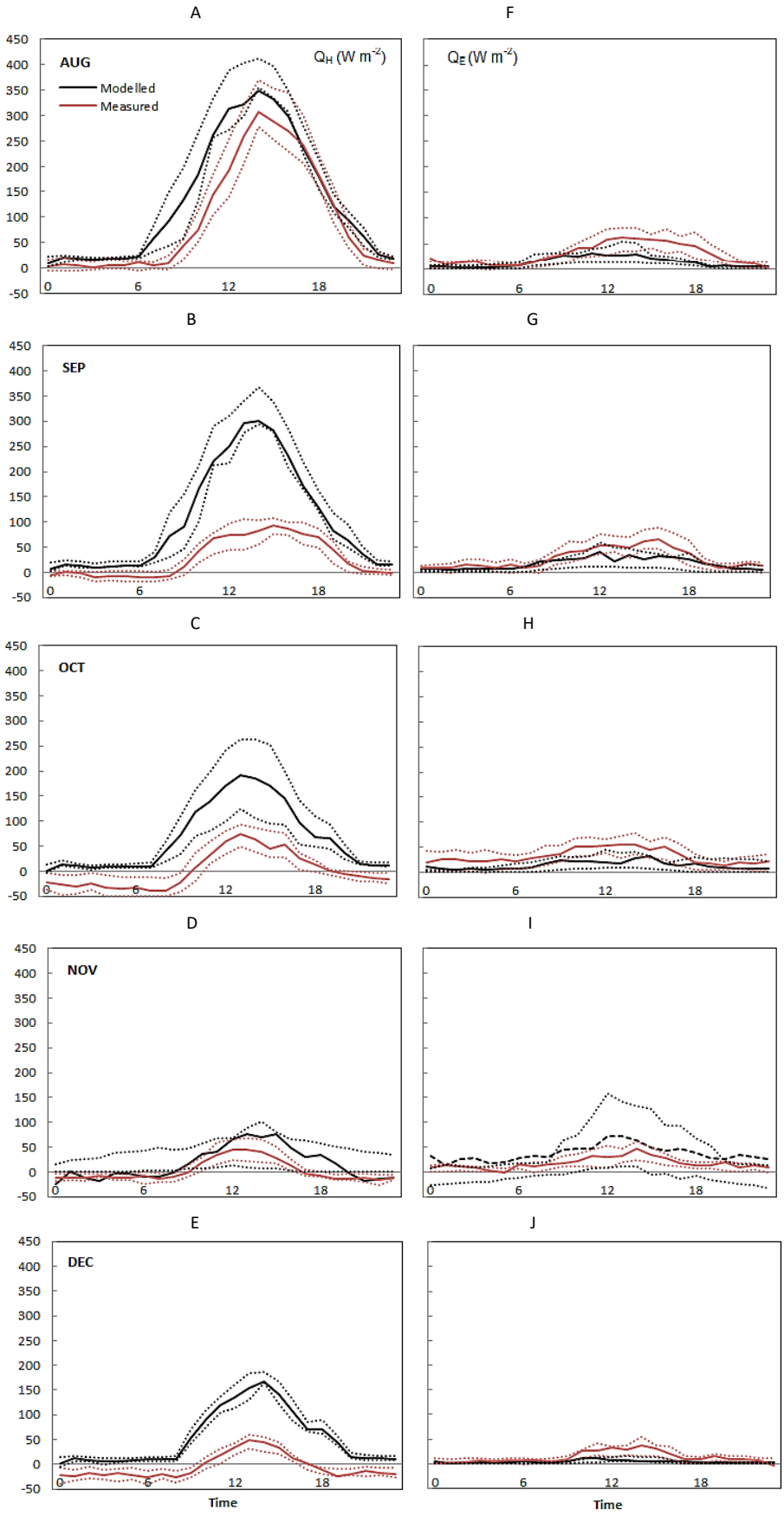

Figure 2-5. Mean monthly diurnal measured and modelled turbulent fluxes of sensible (Q_H) (A-E) and latent (Q_E) (F-J) heat at the urban site. Dotted lines show the quartile deviations (25th and 75th percentiles).

2.3.2. Energy Balance of Urban and Suburban Surfaces

Given that two study areas with different land cover characteristics were analysed, a comparison of the behaviour of the individual fluxes in the energy and radiation balances was performed using the SUEWS simulations. In addition to Q_H and Q_E previously shown, Q^*, Q_F and ΔQ_S, that were not measured but were modelled, are presented and discussed. Figure 2-6 shows the modelled average energy balance for the five-month simulation (August-December 2014).

At the suburban area, the average five-month daytime energy balance (10 a.m. – 3 p.m., time zone relative to UTC) is dominated by Q^* and Q_E, reaching 352 and 173 $W \cdot m^{-2}$. The majority of energy (Q^* and Q_F, the latter contributing only around to2 $W \cdot m^{-2}$), is partitioned to Q_E, accounting on average for 49% of the daytime available energy. The remaining energy is partitioned to turbulent sensible and storage heat fluxes (25.8 and 25.6 $W \cdot m^{-2}$, respectively, around 26%). As result, the daytime Bowen ratio (Q_H/Q_E) is 0.53, similar to the daytime evaporative fraction (Q_E/Q^*) 0.49. This is well within the expected relation at suburban areas (Coutts et al., 2007).

On the other hand, at the urban site the greatest share of energy (Q^* and Q_F, 352 and 12 $W \cdot m^{-2}$) is partitioned into Q_H (182 $W \cdot m^{-2}$, around 50%), followed by the storage heat flux (154 $W \cdot m^{-2}$, corresponding to 43%). The dominance of Q_H is consistent with the observations in more densely built areas (Coutts et al., 2007). Only 7.9% of ($Q^* + Q_F$) is dissipated by evaporation (29 $W \cdot m^{-2}$), due to the high impervious nature of the cover. The daytime evaporative fraction (0.08) is smaller than the value obtained at the suburban area, resulting in a high Bowen ratio (6.3). This value is in the range of values of the Bowen ratio observed in areas with sparsely vegetated fraction (Grimmond and Oke, 2002; Loridan and Grimmond, 2012).

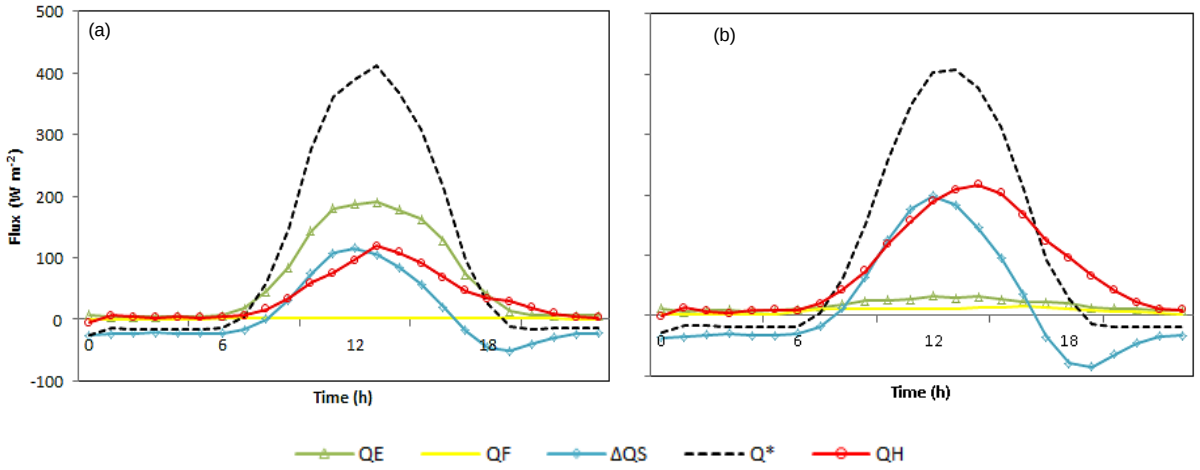

Figure 2-6. Modelled five-months (August-December 2014) averaged energy balance at the (a) suburban and (b) urban sites. Q^*: net all-wave radiation, Q_F: anthropogenic heat flux, Q_E: latent heat flux, Q_H: sensible heat flux, ΔQ_S: net storage heat flux.

The main contrast between the sites is the greater Q_E at the suburban site as a result of the greater vegetative cover and increased water storage in the soil. Additionally, the presence of the sea breeze aids the evaporation of water from the surface, since the moving air will increase the amount of Q_E. The more dense urban area is mainly characterized by extensive impervious surfaces, including buildings and pavements, where runoff water drains quickly leaving less surface water available for evapotranspiration.

Past studies conducted in autumn/ early winter (e.g. from October to December in the North Hemisphere) confirm the expectation of negative Q_H at rural areas (and also at the urban site) in the evening before sunset as the radiative inversion becomes established (Grimmond and Oke, 2002). The model, however, does not simulate well this phenomenon, with the exception of the month of November, characterized by rainfall and low temperatures (see section 2.3.1.2).

Important differences are also evident in the storage heat flux. A typical feature of the urban energy balance is an increased magnitude of ΔQ_S (Grimmond and Oke, 1995, 1999). Urban areas typically have surface materials, such as roofing and paving, which have a lower albedo than those in rural settings. In the case of the study areas, the urban and suburban areas present an albedo of 0.15 and 0.22 [estimated based on vegetation cover fraction (Skamarock et al., 2008)], respectively. The urban areas usually present a darker soil which allows a greater absorption of radiation, along with greater trapping by urban canyons and vertical areas. As result of these two aspects, values of ΔQ_S (during the daytime) are almost two times higher at the urban site. The storage heat flux density during the daytime is counterbalanced by a nocturnal release of ΔQ_S (especially at the urban area).

As expected, higher values of Q_F are obtained at the urban area, in accordance with other modelling studies (Hosler and Landsberg, 1977; Masson, 2000; Offerle at al., 2005). Q_F presents a fairly small magnitude when compared with the other components of the energy balance. This is the major reason why this flux is often omitted of the studies of energy balance (Oke and Cleugh, 1987; Grimmond and Oke, 2000). However, it is worth mentioning that Q_F is estimated taking into account the population density of each area and a diurnal profile. Due to the difficulty in the measurement of Q_F, a standard profile of the diurnal energy use for urban environments was used. Since Q_F is strongly dependent on-site characteristics and the behaviour of the people in that area (e.g., the response to cooling and heating degree day will change according to the socio-cultural-economic factors of the city), the daily profile used may not fully reproduce the reality of the study areas.

2.4. CONCLUSIONS

In this work the WRF-SUEWS modelling setup was applied to a central urban area (Porto) and a suburban area (Aveiro), for a period of five-months (August-December). The model's performance was assessed using directly observed data. The following can be concluded.

The application of stepwise regression method revealed that the meteorological variables that most influence the variability of each component of the energy balance were well modelled by the WRF

model, and therefore realistic meteorological data were used to force SUEWS. However, no model is perfect. This evaluation indicates that SUEWS does not fully replicate the observed fluxes at these sites. The turbulent sensible and latent heat fluxes are modelled relatively well, with a correlation factor of around 0.7 and a NMSE of 3. The model simulates the diurnal behaviour of the fluxes, but a consistent overestimation of the Q_H was observed (MBE of 14.7 and 51.4 $W \cdot m^{-2}$ for suburban and urban areas, respectively). The latent heat flux was underestimated in the urban area (negative MBE, -12 $W \cdot m^{-2}$) and overestimated (26.8 $W \cdot m^{-2}$) in the suburban area. A more detailed understanding of the model evaluation would be obtained if ΔQ_S were measured, since its underestimation increases the bias of Q_H and consequently the energy partitioning (Q_H/Q_E). Due to the current difficulty in directly measuring ΔQ_S, future developments of the measurement techniques are crucial. Additionally, a more accurate representation of the anthropogenic heat flux for the study sites could also improve the model performance. Inaccurate estimation of Q_F can result in poor simulation of the other heat fluxes, particularly in areas of high population density where a large Q_F is expected.

The surface cover fractions have a significant role on the surface energy balance, as shown in numerous previous studies. In the suburban site, most energy goes into Q_E (49% of the daytime available energy), with the remaining energy partitioned to Q_H and ΔQ_S fluxes (both around 26%). In the urban site, Q_H and ΔQ_S fluxes are the most important terms in the surface energy balance (50 and 43% of daytime Q*, respectively). A reduced Q_E was found due to the high impervious nature of the surface. The surface cover, notably the fraction of the vegetated surface, exerts an important control on Q_E. The energy behaviour as well as the magnitude of the fluxes obtained was in accordance with typical behaviours and values of previously modelled and observational studies. However, the model performance is site dependent and so more observations from Portuguese cities are needed to create more generalized conclusions.

We propose that the developed modelling system be used for emerging applications, in particularly at two types of studies: i) assessment of how climate change influences the behaviour and magnitude of the energy fluxes at the urban level and how the changes in the energy fluxes in turn impact the urban climate; ii) urban planning and local/regional climate change mitigation and adaptation. SUEWS can therefore be used to explore options for designing sustainable cities or to assess the merits of a set of planning scenarios, such as including green-space or water bodies to mitigate heat stress, or even assess the impact on surface energy exchanges of developing a suburban area into a dense urban region. Two key advantages of SUEWS regarding other urban energy balance schemes are its relatively undemanding input requirements and its simplicity, enabling simulations of several years and multiple model grids to be carried out without specialised computing facilities. For these reasons, the modelling system can be used as a decision-making tool to cater the needs of urban planners or policy makers.

2.5. REFERENCES

Aquilina N., Dudek A.V., Carvalho A., Borrego C., Nordeng T.E. (2005). MM5 high resolution simulations over Lisbon. Geophysical Research Abstracts 7, 08685.

Barlow J. (2014). Progress in observing and modelling the urban boundary layer. Urban Climate 10, 216–240. [DOI: 10.1016/j.uclim.2014.03.011].

Borrego C., Monteiro A., Martins H., Ferreira J., Fernandes A.P., Rafael S., Miranda A.I., Guevara M., Baldasano J.M. (2015). Air quality plan for ozone: an urgent need for North Portugal. Air Quality, Atmosphere and Health 1-14. [DOI: 10.1007/s11869-015-0352-5].

Carvalho AC, Carvalho A, Gelpi I, Barreiro M, Borrego C, Miranda AI, Perez–Munuzuri V (2006) Influence of topography and land use on pollutants dispersion in the Atlantic coast of Iberian Peninsula. Atmos Environ 40: 3969–3982.

Carvalho D., Rocha A., Gómez-Gesteira M., Santos C. (2012). A sensitivity study of the WRF model in wind simulation for an area of high wind energy. Environmental Modelling & Software 33, 23-34. [DOI:10.1016/j.envsoft.2012.01.019].

Carvalho D., Martins H., Marta-Almeida M., Rocha A., Borrego C. (2017). Urban resilience to future urban heat waves under a climate change scenario: A case study for Porto urban area (Portugal). Urban Climate 19, 1-27. [doi: http://dx.doi.org/10.1016/j.uclim.2016.11.005].

Chang J.C., Hanna S.R. (2005). Technical descriptions and user's guide for the BOOT statistical model evaluation software package, version 2.0.

Coutts A., Beringer J., Tapper N. (2007). Impact of Increasing Urban Density on Local Climate: Spatial and Temporal Variations in the Surface Energy Balance in Melbourne, Australia. Journal of Applied Meteorology and Climatology 46, 477–493.

Derwent D., Fraser A., Abbott J., Willis P., Murrells T. (2010). Evaluating the performance of air quality models (No. Issue 3). Department for Environment and Rural Affairs. United Kingdom. Available on: http://uk-air.defra.gov.uk/assets/documents/reports/cat05/1006241607_100608_MIP_Final_Version.pdf (last access: July 2015).

European Centre for Medium-Range Weather Forecasts, ECMWF. Climate reanalysis: ERA-Interim. Available on: http://www.ecmwf.int/en/research/climate-reanalysis/era-interim (last access: September 2015).

European Environment Agency, EEA. (2012). Urban adaptation to climate change in Europe - Challenges and opportunities for cities together with supportive national and European policies. Luxembourg: Office for Official Publications of the European Union. EEA Report No 2/2012. ISBN 978-92-9213-308-5.

European Commission, EC. (2014). The Urban Dimension of EU Policies – Key Features of an EU Urban Agenda. Communication from the Commission to the European Parliament, the Council, the European Economic and Social Committee and the Committee of the Regions. COM(2014) 490 final. Brussels, 18.7.2014.

Fernandez J., Montavez J.P., Saenz J., Gonzalez–Rouco J.F., Zorita E. (2007). Sensitivity of the MM5 mesoscale model to physical parameterizations for regional climate studies: Annual cycle. Journal of Geophysical Research: Atmospheres 112, 1-18.

Foken T., Wichura B. (1996). Tools for quality assessment of surface-based flux measurements. Agricultural and Forest Meteorology 78, 83-105.

Foken T., Gockede M., Mauder M., Mahrt L., Amiro B.D., Munger J.W. (2004). Post-field quality control. In: Lee, et al (eds) Handbook of micrometeorology: A guide for surface flux measurements. Dordrecht, Kluwer Academic, pp181-108.

Gilliland E. Rowe C. (2007). A comparison of cumulus parameterization schemes in the WRF model. 21st Conference on Hydrology, 15-18 January, 2007, San Antonio, USA.

Grimmond C.S.B., Oke T.R. (1991). An evapotranspiration-interception model for urban area. Water Resources Research 27, 1739–1755.

Grimmond C.S.B., Oke T.R. (1995). Comparison of heat fluxes from summertime observations in the suburbs of four north American cities. Journal of Applied Meteorology 34, 873–889.

Grimmond C.S.B., Oke T.R. (1999). Heat storage in urban areas: local-scale observations and evaluation of a simple model. Journal of Applied Meteorology 38, 922–940.

Grimmond C.S.B., Oke T.R. (2000). Urban-rural energy balance differences. In Surface Energy Balance in Urban Areas. Cost Action 715. Extended Abstracts of an Expert Meeting, Antwerp, Belgium, April 2000, EUR 19447, European Commission.

Grimmond C.S.B., Oke T.R. (2002). Turbulent Heat Fluxes in Urban Areas: Observations and a Local-Scale Urban Meteorological Parameterization Scheme (LUMPS). Journal of Applied Meteorology 41, 792-810.

Grimmond C.S.B., Cleugh H.A., Oke T.R. (1991). An objective urban heat storage model and its comparison with other schemes. Atmospheric Environment Part B 25, 311–326.

Grimmond C.S.B., Best M., Barlow J., Arnfield A.J., Baik J.J., Belcher S., Bruse M., Calmet I., Chen F., Clark P., Dandou A., Erell E., Fortuniak K., Hamdi R., Kanda M., Kawai T., Kondo H., Krayenhoff S., Lee S.H., Limor S.B., Martilli A., Masson V., Miao S., Mills G., Moriwaki R., Oleson K., Porson A., Sievers U., Tombrou M., Voogt J., Williamson T. (2009). Urban surface energy balance models: model characteristics & methodology for a comparison study. In: Baklanov A, Grimmond CSB, Mahura A (eds) Urbanization of Meteorological & Air Quality Models. Springer-Verlag, Athanassiadou, pp. 97– 123. [doi: 10.1007/978-3-642-00298-4_11].

Grimmond C.S.B, Blackett M., Best M.J., Baik J.J., Belcher S.E., Beringer J., Bohnenstengel S.I., Calmet I., Chen F., Coutts A., Dandou A., Fortuniak K., Gouvea M.L., Hamdi R., Hendry M., Kanda M., Kawai T., Kawamoto Y., Kondo H., Krayenhoff E.S., Lee S.H., Loridan T., Martilli A., Masson V., Miao S., Oleson K., Ooka R., Pigeon G., Porson A., Ryu Y.H., Salamanca F., Steeneveld G.J., Tombrou M., Voogt J.A., Young D.T., Zhang N. (2011). Initial results from Phase 2 of the international urban energy balance model comparison. International Journal of Climatology 31, 244-272.

Hsieh C.I., Katul G., Chi T. (2000). An approximate analytical model for footprint estimation of scalar fluxes in thermally stratified atmospheric flows. Advances in Water Resources 23, 765-772.

Hosler C.L., Landsberg H.E. (1977). The effect of localized man-made heat and moisture sources in mesoscale weather modification. Energy and Climate. National Academy of Sciences, Washington, DC.

Ichikawa Y., Sada K. (2002). An atmospheric dispersion model for the environmental impact assessment of thermal power plants in Japan – A method for evaluating topographical effects. Journal of the Air & Waste Management Association 52, 313-323.

Instituto Nacional de Estatística, INE (Statisical of Portugal). (2011). Censos 2011 Resultados Definitivos - Região Norte. Instituto Nacional de Estatística (in Portuguese), I.P. ISSN 0872- 6493. ISBN 978-989-25-0186-4. Available on: file:///C:/Users/sandra.rafael/Downloads/Censos2011_RDefinitivos_Norte_3.pdf (last access: July 2015).

Instituto Português do Mar e da Atmosfera, IPMA (meterology institute) Normais Climatológicas - 1981-2010 (provisórias) (in Portuguese). Retrieved 19 January 2013. Available on: http://www.ipma.pt/pt/oclima/normais.clima/1981-2010/014/ last access: September 2015).

Janjic Z. (2002). Nonsingular implementation of the Mellor-Yamada level 2.5 scheme in the NCEP meso model. NCEP Office Note No. 437, 60.

Järvi L., Grimmond C.S.B., Christen A. (2011). The Surface Urban Energy and Water Balance Scheme (SUEWS): Evaluation in Los Angeles and Vancouver. Journal of Hydrology 411, 219-237. [doi:10.1016/j.jhydrol.2011.10.001].

Järvi L., Grimmond C.S.B., Taka M., Nordbo A., Setälä H., Strachan I.B. (2014). Development of the Surface Urban Energy and Water Balance Scheme (SUEWS) for cold climate cities. Geoscientific Model Development 7, 1691-1711. [doi:10.5194/gmd-7-1691-2014].

Kaimal J.C., Wyngaard J.C., Izumi Y., Coté O.R. (1972). Spectral characteristics of surface-layer turbulence. Quarterly Journal of the Royal Meteorological Society 98, 563-589.

Kusaka H., Kondo H., Kikegawa Y., Kimura F. (2001). A simple single layer urban canopy model for atmospheric models: comparison with multi-layer and slab models. Bound-Layer Meteorology 101, 329-358.

Li D., Bou-Zeid E. (2013). Synergistic interactions between urban heat islands and heat waves: the impact in cities is larger than the sum of its parts. Journal of Applied Meteorology and Climatology 52, 2051-2064.

Li D., Bou-Zeid E., Oppenheimer M. (2014). The effectiveness of cool and green roofs as urban heat island mitigation strategies. Environmental Research Letter. 9, 055002.

LI-7500A Open Path CO_2/H_2O Analyzer Instruction Manual (2009) Publication No. 984-10563, LI-COR inc, USA, pp. 4-16.

Loridan T., Grimmond C.S.B., Offerle B.D., Young D.T., Smith T., Järvi L., Lindberg F. (2011). Local scale urban meteorological parameterization scheme (LUMPS): longwave radiation parameterization and seasonality-related developments. Journal of Applied Meteorology and Climatology 50, 185-202.

Loridan T., Grimmond C.S.B. (2012). Characterization of Energy Flux Partitioning in Urban Environments: Links with Surface Seasonal Properties. Journal of Applied Meteorology and Climatology 51, 219–241. [doi: http://dx.doi.org/10.1175/JAMC-D-11-038.1].

Marras S., Pyles R.D., Falk M., Casula M., Snyder R.L., Paw U K.T., Spano D. (2012). Urban fluxes estimation at local and regional scale by ACASA model. ICUC8 – 8th International Conference on Urban Climates, 6th-10th August, 2012, UCD, Dublin, Ireland.

Masson V. (2000). A physically-based scheme for the urban budget in atmospheric models. Boundary-Layer Meteorology 94, 357-397.

Matese A., Gioli B., Vaccari F.P., Zaldei A., Miglietta F. (2009). Carbon dioxide emissions of the city center of Firenze, Italy: measurement, evaluation, and source portioning. Journal of Applied Meteorology and Climatology 48, 1940-1947.

Mauder M., Foken T. (2004). Impact of post-field data processing on eddy covariance flux estimates and energy balance closure. Meteorologische Zeitschrift 15, 597-609.

Mlawer E.J., Taubman S.J., Brown P.D., Iacono M.J., Clough S.A. (1997). Radiative transfer for inhomogeneous atmospheres: RRTM, a validated correlated-k model for the longwave. Journal of Geophysical Research 102D, 16663-16682.

Moncrieff J.B., Massheder J.M., Bruin H., Ebers J., Friborg T., Heusinkveld B., Kabat P., Scott S., Soegaard H., Verhoef A. (1997). A system to measure surface fluxes of momentum, sensible heat, water vapor and carbon dioxide. Journal of Hydrology 188-189, 589-611.

Monteiro A., Ribeiro I., Tchepel O., Carvalho C., Martins H., Sá E., Ferreira J., Martins V., Galmarini S., Miranda A.I., Borrego C. (2013). Ensemble techniques to improve air quality assessment: focus on O_3 and PM. Environmental Modeling & Assessment 19, 249-257.

Monteiro A., Ferreira J., Ribeiro I., Fernandes A.I., Martins H., Gama C., Miranda A.I. (2015). Air quality over Portugal in 2020. Atmospheric Pollution Research 6, 788-796.

Mosca S., Graziani G., Klug W., Bellasio R., Bianconi R. (1998). A statistical methodology for the evaluation of long-range dispersion models: an application to the ETEX exercise. Atmospheric Environment 24, 4307-4324.

Nappo C.J., Essa K.S.M. (2001). Modeling dispersion from near-surface tracer releases at Cape Canaveral, Florida. Atmospheric Environment 35, 3999-4010.

Offerle B., Grimmond C.S.B., Fortuniak K. (2005). Heat storage and anthropogenic heat flux in relation to the energy balance of a central European city centre. International Journal of Climatology 25, 1405-1419.

Offerle B., Grimmond C.S.B., Oke T.R. (2003). Parameterization of net all-wave radiation for urban areas. Journal of Applied Meteorology 42, 1157–1173. [DOI:10.1175/1520-0450(2003)042].

Oke T.R. (1987). Boundary Layer Climates. Routledge, London, UK.

Oke T.R., Cleugh H.A. (1987). Urban heat-storage derived as energy-balance residuals. Boundary-Layer Meteorology 39, 233-245.

Papanastasiou D.K., Melas D., Lissaridis I. (2010). Study of wind field under sea breeze conditions; an application of WRF model. Atmospheric Environment 98, 102–117. [DOI: 10.1016/j.atmosres.2010.06.005].

Pinho O.S., Manso O. (2000). The urban heat island in a small city in coastal Portugal. International Journal of Biometeorology 441, 98-203.

Pyles R. D., Weare B. C., Paw U. K. T., Gustafson W. (2003). Coupling between the University of California, Davis, Advanced Canopy-Atmosphere-Soil Algorithm (ACASA) and MM5: Preliminary Results for July 1998 for Western –North America. Journal of Applied Meteorology 42, 557 - 569.

Qian T., Dai A., Trenberth K. (2007). Hydroclimatic Trends in the Mississippi River Basin from 1948 to 2004. American Meteorological Society 30, 4599-4614.

Sá E., Tchepel O., Carvalho A., Borrego C. (2015). Meteorological driven changes on air quality over Portugal: a KZ filter application. Atmospheric Pollution Research 6, 979-989.

Sailor D.J., Vasireddy C. (2006). Correcting aggregate energy consumption data account for variability in local weather. Environmental Modelling & Software 21, 733-738. [DOI:10.1016/j.envsoft.2005.08.001].

Skamarock W.C., Klemp J.B., Dudhia J., Gill D.O., Barker D.M., Huang X.Y., Wang W., Powers J.G. (2008). A Description of the Advanced Research WRF Version 3. NCAR/TN-475+STR, pp. 113.

Soares P., Cardoso R., Miranda P., Medeiros J., Belo-Pereira M., Espirito-Santo F. (2012). WRF high resolution dynamical downscaling of ERA-Interim for Portugal. Clim Dyn 26pp. [DOI: 10.1007/s00382-012-1315-2].

Susca T., Gaffin S.R., Dell'Osso G.R. (2011). Positive effects of vegetation: urban heat Island and green roofs. Environmental Pollution 159, 2119-2126.

Tewari M., Chen F., Wang W., Dudhia J., LeMone M., Mitchell K., Ek M., Gayno G., Wegiel J., Cuenca R. (2004). Implementation and verification of the unified NOAH land surface model in the WRF model. 20th conference on weather analysis and forecasting/16th conference on numerical weather prediction, 11–15.

Thunis P., Pederzoli A., Pernigotti D. (2012). Performance criteria to evaluate air quality modelling applications. Atmospheric Environment 59, 476-482.

Velasco E., Roth M. (2010). Cities as net sources of CO_2: Review of atmospheric CO_2 exchange in urban environments measured by eddy covariance technique. Geography Compass 4, 1238-1259.

Wang W., Bruyere C., Duda D., Dudhia J., Gill D., Kavulich M., Keene K., Chuan H–C., Michalakes J., Rizvi S., Zhang X. (2014). WRF–ARW Version 3 Modeling System User's Guide.

Ward H.C., Kotthaus S., Järvi L., Grimmond C.S.B. (2016). Surface Urban Energy and Water Balance Scheme (SUEWS): development and evaluation at two UK sites. Urban Climate 18, 1-32. [DOI: 10.1016/j.uclim.2016.05.001].

Webb E.K., Pearman G.I., Leuning R. (1980). Correction of flux measurements for density effects due to heat and water vapor transfer. Quarterly Journal of the Royal Meteorological Society 106, 85–100.

Yang J., Wang Z.-H., Chen F., Miao S., Tewari M., Voogt J.A., Myint S. (2015). Enhancing hydrologic modelling in the coupled weather research and forecasting - urban modelling system. Boundary-Layer Meteorology 155, 87-109.

CHAPTER 3

This Chapter has been published as:

Rafael S., Martins H., Marta-Almeida M., Sa E., Coelho S., Rocha A., Borrego C., Lopes M. (2017). *Quantification and mapping of urban fluxes under climate change: Application of WRF-SUEWS model to Greater Porto area (Portugal).* Environmental Research 155, 321-334.

The author acknowledges the co-authors critical revision. An acknowledgement to Professor Alfredo Rocha and Martinho Marta-Almeida for providing the climate data used in this work.

3. Quantification and mapping of urban fluxes under climate change: application of WRF-SUEWS model to Greater Porto area (Portugal)

Abstract

Climate change and the growth of urban populations are two of the main challenges facing Europe today. These issues are linked as climate change results in serious challenges for cities. Recent attention has focused on how urban surface-atmosphere exchanges of heat and water will be affected by climate change and the implications for urban planning and sustainability.

In this Chapter the energy fluxes for Greater Porto area, Portugal, were estimated and the influence of the projected climate change evaluated. To accomplish this goal, the Weather Research and Forecasting Model (WRF) and the Surface Urban Energy and Water Balance Scheme (SUEWS) were applied for two climatological scenarios: a present (or reference, 1986-2005) scenario and a future scenario (2046-2065), in this case the Representative Concentration Pathway RCP8.5, which reflects the worst set of expectations (with the most onerous impacts). The results show that for the future climate conditions, the incoming shortwave radiation will increase by around 10%, the sensible heat flux around 40% and the net storage heat flux around 35%. In contrast, the latent heat flux will decrease about 20%. The changes in the magnitude of the different fluxes result in an increase of the net all-wave radiation by 15%. The implications of the changes of the energy balance on the meteorological variables are discussed, particularly in terms of temperature and precipitation.

Keywords: Cities, Climate change, Energy balance, Flux modelling

3.1. INTRODUCTION

In Europe 72% of the population now lives in urban areas, even though these covers only 4% of the European area (EEA, 2015). By 2020, approximately 80% of Europeans will be living in urban areas (EEA, 2011). The effects of urbanization and climate change are converging in a critical way. Cities are major contributors to climate change, although covering less than 2% of earth's surface, cities consume 78% of the world's energy and produce more than 60% of all carbon dioxide and significant amounts of other greenhouse gas emissions (Lindberg et al., 2013). Georgescu et al. (2014) positions urban areas under a broader picture of global environmental change and shows that, on the one hand, the urban-induced warming is of the same order of magnitude as large-scale climate change, but on the other hand, that cities can act as agents of change through a variety of urban adaptation strategies. Related to the capacity of cities adaptation to climate change effects, studies such as Benson-Lira et al. (2016) highlight the need of promoting development of resilient and sustainable cities with capacity to deal with challenges from directly induced regional climate modification owing to the physical infrastructure of the built environments as well as impacts resulting from large-scale climate change. For this, a continuous knowledge of the state of the surface and the atmosphere is required.

As result of the anthropogenic activity in cities, the water and energy exchanges of urban areas are altered. Compared to naturally vegetated areas, urban land cover changes result in increases of surface runoff, reduction in evaporation and increased sensible heat emissions to the urban boundary layer (Mitchell et al., 2008; Flagg and Taylor, 2011). These have implications on flooding (Schiff et al., 2007), human comfort (McMichael et al., 2008), mixing in the boundary layer and pollutant dispersion (Järvi et al., 2011). Due to their importance, the evaluation of energy and water balance fluxes (urban fluxes) has been a key issue for urban research. The study of energy fluxes can be classified in three main approaches: i) studies that only consider the measurements of energy fluxes through the eddy covariance method; ii) studies that combine flux measurements with model simulations [e.g. Karsisto et al., 2016, that assess the performance of three urban land-surface models]; iii) studies that use urban energy balance models to assess the links between the urban climate and the surface energy balance behaviour [e.g., Li et al. (2015) contrast urban and rural energy budgets under heat wave conditions and show the synergistic behaviour between built and non-built environments in explaining urban heat island] or to assess the capability of different resilience measures for the mitigation of extreme climate events (Wouters et al., 2013).

Several atmospheric variables affect the energy balance and consequently the energy fluxes. Incoming solar and long-wave radiation determine net radiation. Air temperature and atmospheric humidity determine the diffusion gradients for sensible and latent heat, respectively. Precipitation determines soil moisture and through that the latent heat flux; as a result, water availability has a major role in controlling the energy partitioning into turbulent heat fluxes. Wind speed also affects sensible and latent heat. Finally, soil temperature affects the amount of heat flowing into the soil. In turn, these atmospheric variables are themselves affected by urban fluxes (Bonan, 2002). Besides that, the importance of the study of the energy fluxes is mainly related to the need of better resolving

the atmospheric processes at the urban scale in numerical weather and air quality models. This is especially important for modelling urban boundary layer (UBL) dynamics, since the growth rate and depth of the UBL is determined primarily by the sensible heat flux (Barlow, 2014).

While research focused on past-present-future climate is not new, still few urban studies have addressed the subject of the energy fluxes balance under future climate change conditions. Wild et al. (1997) examined the flux changes in global climate model simulations with increased levels of greenhouse gases and related them to the systematic errors found in the simulation under a current climate. Georgescu et al. (2009) focused on the documentation of climatic effects of 30 years of landscape change over Greater Phoenix with a particular focus on the surface radiation and energy budgets. Sheng et al. (2010) identified regions with strong changes in climatic variables and surface energy fluxes through identification of their long-term trends and interannual variability from 1948 to 2000. Lindberg et al. (2013) used LUCY to assess changes in anthropogenic heat flux over a 20-year period (1995–2015) across Europe. Ma et al. (2014) estimate the heat flux changes caused by the projected land transformation over the next 40 years across China to improve the understanding of the impacts of land dynamics on regional climate. Hamdi et al. (2015) conducted a set of simulations of present and future urban climate over Brussels Capital Region and Grand Paris Region, based on the IPCC SRES A1B future scenario, disregarding however, the anthropogenic heat flux.

This work attempts to investigate the energy fluxes on Greater Porto area, Portugal, and evaluate the influence of climate change on the magnitude and behaviour of these fluxes, contributing to an increase of the knowledge of the surface energy balance research field. To accomplish this, the Weather Research and Forecasting Model (WRF) and the Surface Urban Energy and Water Balance Scheme (SUEWS) have been applied for two climatological scenarios: present and future. The WRF model is used to estimate the meteorological variables needed to force SUEWS as well as to characterize the land cover and the related parameters; SUEWS is used to estimate each component of the energy balance. Both models are widely used, have been extensively tested and shown to produce robust and realistic results (Järvi et al., 2011, 2014; Borrego et al. 2015; Monteiro et al. 2015). Besides that, the SUEWS model was selected as urban energy balance model for three main reasons:

- it simulates the latent heat flux considering irrigation and runoff processes, and it has an integrated approach to the inclusion of urban vegetation, factors pointed as extremely important for energy fluxes modelling by the International Urban Surface Energy Balance Model Comparison Project (Grimmond et al., 2010, 2011);
- the surface resistance scheme is parameterized explicitly for urban areas rather than using schemes originally designed for non-urban areas (Järvi et al., 2011);
- the model has the ability to estimate the anthropogenic heat flux based on population density (Järvi et al., 2011).

The modelling system and the model setup, especially the fact that the Representative Concentration Pathways RCP8.5 scenario is used, as well as the fact that all the components of the energy balance are analysed (including the anthropogenic heat flux), are features that distinguish this work from

previous studies that analyse the urban energy fluxes exchanges. Additionally, the use of this modelling system allows the evaluation and visualization of the spatial patterns of the energy fluxes at different scales. The mapping of the spatial pattern of energy fluxes helps planners, developers and policy makers to understand how their cities are able to respond to the impacts of climate change, and thereby allows the identification the most critical vulnerabilities and the most appropriated measures to increase urban resilience. This Chapter is presented as follows, Section 3.2 describes the case study and the applied modelling system setup, including the characterization of the climate change modelling. The climate influence on the spatial pattern of energy fluxes are presented and discussed in Section 3.3. Summary and conclusions follow in Section 3.4.

3.2. DATA AND METHODS

3.2.1. Case study

Porto Greater Metropolitan area, located in Portugal's northern littoral region, is one example of urban expansion taking place at much faster rates than population (Martins, 2012). This sprawling 'effect' has major impacts that are evident in increased energy and water consumption, and soil use. These threaten both the natural and rural environments, with increased greenhouse gas emissions, and with atmospheric and noise pollution levels which often exceed the agreed human safety limits (EEA, 2006). Porto is the second largest city in Portugal and is the centre of a metropolitan area covering 1900 km^2 with more than 1.5 million inhabitants (INE, 2011). In the recently published EEA report *Urban adaptation to climate change in Europe*, Porto stands out as the Portuguese urban area with the smallest amount of green and blue areas. Additionally, according to the region's air quality reports, the Greater Porto area is an area of poor air quality, with ozone thresholds and PM10 limit values exceeded (Borrego et al., 2008). Greater Porto area is, therefore, an interesting and challenging case to be studied in the framework of the urban fluxes.

Greater Porto is a dense residential and commercial area with a few sparse green areas. The majority of the area has impervious surfaces (see Table 3-1, in section 3.2.2.2). A set of surfaces characterize the Greater Porto area: roads, pavements, hedges and small trees, buildings and the ocean. Both residential and commercial areas are characterised by tall buildings (around 6 floors). The surrounding suburban areas are more vegetated with sparse housing (low density urban fabric) and agricultural fields. The vegetated area is very diverse and includes areas of polyculture, grass crops, forage crops, fruit tree plantations and forest. Unmanaged vegetation is also present. The majority of the houses have one or two storeys (Figure 3-1).

Figure 3-1. Photos taken in the study area to exemplify the buildings typology that characterize the urban (left) and the suburban (right) areas.

The region selected for study is shown in Figure 3-2 (inner domain). The Porto municipality is the centre of the study region, around which there are two metropolitan rings, each of which has important connections to Porto, mainly in terms of mobility. These municipalities constitute the Greater Porto area, which covers 2.2% of the Portuguese territory (AMP, 2014). This region has a moderate Atlantic climate, with warm, dry summers and mild, rainy winters. Unlike the south of Portugal, cool and rainy North Atlantic periods interrupt the dry season and the season's average length is shorter, usually with three dry months. The annual precipitation is high (average of the last 10-years of around 826 mm); Porto is one of the wettest cities in Europe. However, long periods with mild temperatures and sunny days are frequent even during the rainiest months (IPMA, 2013).

3.2.2. Modelling system

3.2.2.1. Climate change modelling

The community model Weather Research and Forecasting Model, WRF version 3.5 (Skamarock et al., 2008) with the modifications performed by Fita et al. (2010) for regional climate simulations was applied in this work to perform climate simulations for the Porto city and surrounding areas through dynamical downscaling. The WRF model is a next-generation mesoscale numerical weather prediction system designed to serve both atmospheric research and operational forecasting needs. The WRF setup includes four domains online nested with increasing resolution at a downscaling ratio of three: domain 1 (D1) at 27 km resolution covering Europe and North Africa (with 173×142 horizontal grid cells); D2 at 9 km resolution over the Iberian Peninsula (153×138 horizontal grid cells); D3 at 3 km resolution over North West Portugal (121×109 horizontal grid cells); and D4 with 1 km resolution over the Greater Porto Area (75×66 horizontal grid cells). All the domains have 28 vertical layers. The domains are illustrated in Figure 3-2.

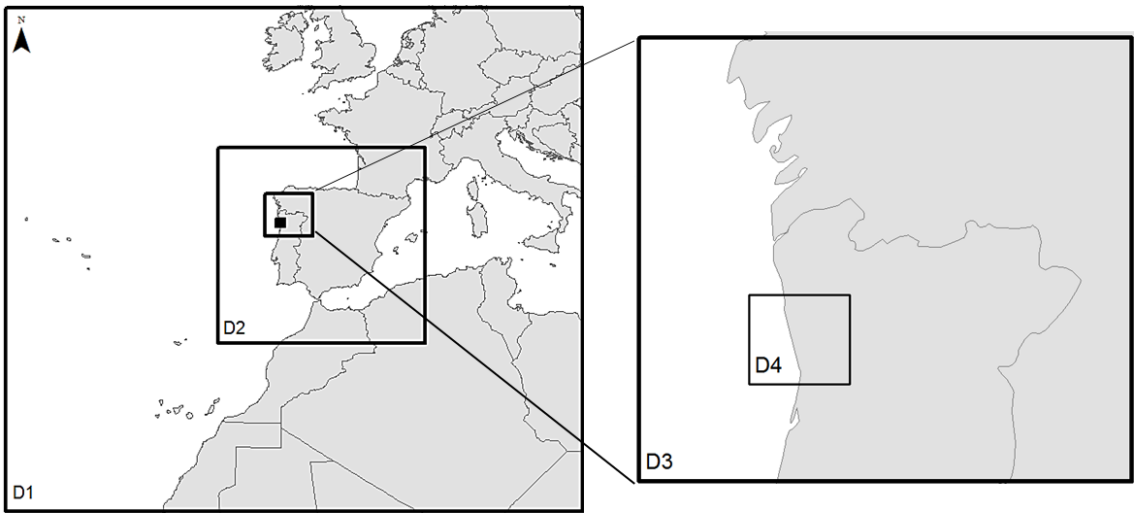

Figure 3-2. Meteorological modelling domains, D1: Europe and part of the North of Africa; D2: Iberian Peninsula; D3: North-western region of Portugal; D4: Greater Porto area (study area, including 17 municipalities).

All the domains, except the smallest one (D4), were used to simulate two sets of 20-year periods, including the past (1986-2005) which characterizes the present climate, and the medium-term future (2046-2065). For the future simulations, the Representative Concentration Pathway Scenario RCP8.5 has been adopted (Riahi et al., 2007). RCP8.5 was developed using the IIASA Integrated Assessment Modelling Framework, that encompasses detailed representations of the main emitting sectors of greenhouse gases (energy, industry, agriculture, and forestry), and the MESSAGE model. The greenhouse gas emissions and concentrations in this scenario increase considerably over time, leading to a radiative forcing (the change in the balance between incoming and outgoing radiation to the atmosphere caused primarily by changes in atmospheric composition) of 8.5 $W \cdot m^{-2}$ at the end of the century (2100) (IPCC, 2013). This scenario is considered by the scientific community to reflect the worst set of expectations with the most onerous impacts.

Two sets of atmospheric global simulation results, from different sources, were used to provide initial and boundary conditions to the urban configuration. Firstly, the WRF model was initialized with global meteorological fields from the European Centre for Medium-Range Weather Forecasts (ECMWF) Re-Analysis Interim (ERA-Interim) model data (http://www.ecmwf.int/en/research/climate-reanalysis/era-interim) with 1° spatial resolution and temporal resolution of 6-h for surface and pressure levels. Secondly, the MPI-ESM model (Max Planck Institute for Meteorology Earth System Model, Giorgetta et al., 2013), with 1.9º spatial resolution and 47 hybrid sigma-pressure levels, was used. This model participated in the Coupled Model Intercomparison Project Phase 5 (CMIP5). These two downscaling setups were used to simulate the present climate. The WRF-ERA-Interim results and its comparison with the observations were used as reference for the validation of the MPI-ESM model driven WRF results of the present climate simulations. With this approach, the confidence in the model configuration (MPI-ESM) for climate studies of future periods is guarantee. In this sense, for the future climate, the initial and boundary conditions were provided by the MPI-ESM model.

WRF simulations used a one-year spin-up period with a single initialization. This has been possible due to the usage of sea surface temperature update and spectral nudging for wave length larger than 1000 km (Marta-Almeida et al., 2016). Considering the findings of the previously studies performed over Portugal (Aquilina et al., 2005; Carvalho et al., 2012; Monteiro et al., 2015) the set of parameterizations used in the model physical configuration included: WRF Single-Moment 6-class Microphysical Scheme (Hong et al., 2006); Dudhia Shortwave radiation scheme (Dudhia, 1989); Rapid Radiative Transfer Model longwave radiation scheme (RRTM) (Mlawer et al., 1997); MM5 similarity surface layer scheme (Zhang and Anthes, 1982); Noah Land Surface Model (Tewari et al., 2004) with soil temperature and moisture in four layers, fractional snow cover and frozen soil physics; Yonsei University Planetary Boundary Layer scheme (Hong and Lim, 2006) and Grell-Freitas Ensemble Scheme for cumulus parametrization (Grell and Freitas, 2014) (this last, only for D1 and D2). For a more detailed description of the downscaling configuration including model validation over the Iberian Peninsula, see Marta-Almeida et al. (2016).

The Greater Porto area (D4) was used for the simulation of one reference year of the past period (reference scenario) and one future year of the medium-term future period (future scenario), statistically representative of each period of 20-years. This means that the simulated years represent the historical and future climate changes in daily temperature and precipitation extremes, detected through a set of indices proposed by the Expert Team on Climate Change Detection and Indices (ETCCDI). A more detailed description of these indices can be found in Bartolomeu et al. (2016) and Fonseca et al. (2016). The D4 results, at hourly resolution, were used in the current study.

Information regarding land use/land cover was taken from the Coordination of Information on the Environment Land Cover (CORINE land cover 2006, Bossard et al. (2000)) to initialize the WRF model. This has been re-categorized to be compatible with the model processes into the US Geological Survey (USGS) 24-category land use dataset. The remapping of the CORINE land cover to USGS 24 land use categories followed the methodology proposed by Carvalho et al. (2017). Teixeira et al. (2014) performed sensitivity tests for the usage of this dataset in WRF model simulations obtaining positive results. Figure 3-3 presents the land use classification for the study area. Nineteen categories characterize the study area, which can be grouped in seven main classes (Anderson et al., 2001):

i) Urban or Built-up Land which is comprised of areas of intensive use with the majority of the land covered by structures. Included in this category are cities, towns, strip developments along highways, transportation, power, and communications facilities, and areas such as those occupied by shopping centres, industrial and commercial complexes, and institutions that may, in some instances, be isolated from urban areas.
ii) Agricultural Land that is defined as land used primarily for production of food and fibre. This topic comprises three main categories: a) dry cropland and pasture; b) irrigated cropland and pasture; and c) mixed dryland/irrigated cropland and pasture;

iii) Rangeland is defined as land where the potential natural vegetation is predominantly grasses, grass like plants, forbs, or shrub. In this sense, the categories of grassland, shrubland and a mixed of the two vegetation types are comprised in this topic;

iv) Forest Lands concern areas that are stocked with trees capable of producing timber or other wood products, and exert an influence on the climate or water regime. Categories as deciduous or evergreen forest, as well as, mixed forest are included in this topic;

v) Wetland is the area where the water table is at, near, or above the land surface for a significant part of most years. This topic includes wetlands dominated by woody vegetation (wooden wetland) and herbaceous vegetation (herbaceous wetland);

vi) Water bodies integrates all areas that are persistently covered by water including the areas within the land mass that are covered by water, if linear, they are at least 200 m wide and, if extended, cover at least 16 hectares;

vii) Barren Land is the land with limited ability to support life and in which less than one-third of the area has vegetation or other cover. In general, it is an area of thin soil, sand, or rocks. Vegetation, if present, is more widely spaced than that in the Rangeland classification.

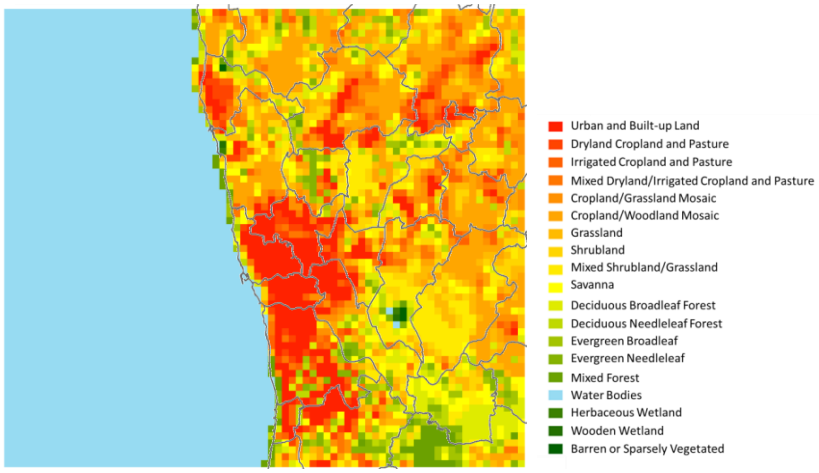

Figure 3-3. Land use categories for the study region (D4 domain) of the United States Geological Survey 24-category land use dataset, based on the Coordination of Information on the Environment Land Cover (CORINE land cover 2006) information.

The CORINE land cover information was combined in a complementary strategy with the land use/land cover high-resolution (10x10 m^2) data from the European Environment Agency Porto Urban Atlas (URL1) to produce the information required (inputs) by the SUEWS model (see more details in the next section).

3.2.2.2. Energy fluxes modelling

To simulate the urban energy fluxes for the Greater Porto area, the SUEWS (Surface Urban Energy and Water Balance Scheme) model was applied. The model simulates the urban energy and water balance components using common meteorological variables (wind speed, relative humidity, air temperature, pressure, precipitation and shortwave irradiance). In addition, information related to land cover, specifically the plan area fraction of each surface type, population density, and building and tree heights, for each individual model cell, is also required. SUEWS is a single-layer model which considers multiple surface types: paved, buildings, coniferous trees/shrubs, deciduous trees/shrubs, irrigated grass, non-irrigated grass and water, which allow its applicability for different land uses. Below each surface type, except water, there is also a single soil layer.

The SUEWS model has been developed from the urban water balance model of Grimmond et al. (1986) and the urban evaporation-interception scheme of Grimmond and Oke (1991), incorporating now several other sub-models.

The Objective Hysteresis Model (OHM) (Grimmond et al. 1991) calculates the net storage heat flux; the Net All-wave Radiation Parameterisation (NARP) (Offerle et al., 2003) provides the net all-wave radiation; and the Local-scale Urban Meteorological Parameterisation Scheme (LUMPS) (Grimmond and Oke 2002) provides an initial estimation of the atmospheric stability; and the Sailor and Vasireddy (2006) approach is used to calculate the anthropogenic heat flux. The Sailor and Vasireddy (2006) approach employs annual cooling and heating degree-days for each city using the standard base temperature of 18.2°C. A standard profile of the diurnal energy use for urban environments is included in the model and was used in the modelling, due to the difficulty in the measurement of Q_F. Besides of this factor, the magnitude of anthropogenic heating varies substantially as a function of the population density of the region under study (variable provided as input in the SUEWS model) (Sailor et al., 2015).

The SUEWS model, version 2014b, calculates the complete energy balance (radiative, convective and conductive fluxes) at the interface between the urban surface layer and the atmosphere, which is mathematically expressed by (Oke, 1987):

$$Q^* + Q_F = Q_E + Q_H + \Delta Q_S \quad [\mathrm{W \cdot m^{-2}}] \tag{3.1}$$

where Q* is the net all-wave radiation (the net incoming and outgoing radiative fluxes), Q_F is the anthropogenic heat flux (the energy released by human activities), Q_E is the latent heat flux (the energy taken up/released with the phase change of water), Q_H is the turbulent sensible heat flux (the energy that heats the air), and ΔQ_S is the net storage heat flux (which includes soil heat flux and also the heating and cooling of the complete urban structure).

The fundamental spatial scale of the model is the local or urban scale in the range of 0.1-10 km length. A more complete description of SUEWS can be found in Järvi et al. (2011, 2014). The meteorological data required for SUEWS was obtained from the application of WRF model. The

temperature and relative humidity were obtained at 2 m above ground; the shortwave irradiance, the pressure and the wind speed was obtained at 10 m above ground.

The SUEWS model was applied for each individual cell of the domain (each one with an area of 1000x1000 m^2). Therefore, individual inputs were required. A pre-processor was developed to create the SUEWS inputs automatically, such as meteorological information provided by WRF, the population density of the study domain (available from national statistics), as well as the land use characterization (based on the CORINE land use classification). Figure 3-4 summarises the modelling scheme. This modelling system (WRF-SUEWS) was previously applied to the study area and its comparability to measured data verified successfully (see Chapter 2).

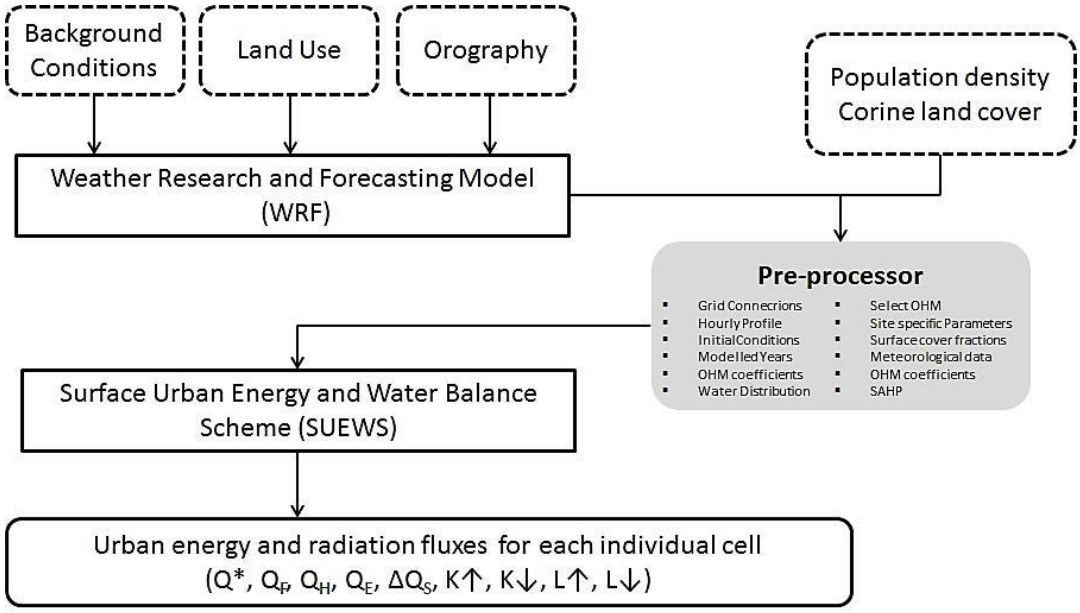

Figure 3-4. Modelling system. Q* is the net all-wave radiation, Q_F is the anthropogenic heat flux, Q_E is the latent heat flux, Q_H is the turbulent sensible heat flux, ΔQ_S is the net storage heat flux, K↓ is the incoming shortwave radiation, K↑ is the outgoing shortwave radiation, L↓ is the incoming long-wave radiation, and L↑ is the outgoing long-wave radiation.

To obtain the discrete land cover use information (surface cover fractions for the different surface types) needed for the application of SUEWS, and to enhance the detail of Porto's urban features, the CORINE land cover classification was combined with the Porto Urban Atlas information. The Porto Urban Atlas compiles thousands of images from European satellites to create reliable and comparable high-resolution maps of urban land cover in a cost-efficient manner. Its higher resolution provides an accurate picture of the urban area including relevant data to define the fraction of the plan area (in terms of percentage of buildings, pavements, vegetation, water and unmanaged land). In addition, satellite imagery and aerial photography (obtained in Google earth V10, Image Landsat, Image IBCAO, http://www.earth.google.com [January 26, 2016]) were analysed and field based surveys were carried out, to complement the characterization.

Given that the information in the Porto Urban Atlas is restricted to the Porto municipality, and the study domain is larger than that area, average land use fractions were determined based on the discretized information of the Porto Urban Atlas and the CORINE land use data for the same area (Table 3-1).

Table 3-1. Surface characteristics assigned to each land use cover (fraction of the plan area) based on Porto Urban Atlas information. For the land use classified as *urban and built-up land* was considered a mean building height of 12 m and a mean tree height of 4 m; for all other cases was considered a mean height of 4 m for both buildings and trees. The abbreviations are defined as follow.

Build: Surface fraction of buildings; paved: paved areas; unman: unmanaged land: ET_sh: evergreen trees; DT_sh: deciduous trees; UG: non-irrigated grass; IG: irrigated grass; wtr: water.

Land use classification based on CORINE land cover categories	build	paved	unman	ET_sh	DT_sh	Ug	IG	wtr
1 – Urban and built-up land	0.21	0.21	0.07	0.11	0.11	0.10	0.13	0.06
2 – Dryland cropland and pasture	0.14	0.17	0.07	0.15	0.15	0.13	0.12	0.07
3 – Irrigated cropland and pasture	0.15	0.17	0.07	0.15	0.15	0.10	0.14	0.07
4 – Mixed dryland/irrigated cropland and pasture	0.12	0.15	0.08	0.17	0.17	0.12	0.12	0.08
5 – Cropland/grassland mosaic	0.10	0.12	0.08	0.15	0.15	0.16	0.16	0.09
6 – Cropland/Woodland Mosaic	0.05	0.07	0.10	0.26	0.26	0.09	0.08	0.09
7 – Grassland	0.05	0.06	0.08	0.19	0.19	0.16	0.16	0.11
8 – Shrubland	0.07	0.09	0.13	0.27	0.27	0.07	0.06	0.04
9 – Mixed shrubland/grassland	0.03	0.05	0.09	0.26	0.26	0.12	0.12	0.07
10 – Savanna	0.04	0.07	0.13	0.27	0.27	0.06	0.05	0.11
11 – Deciduous broadleaf forest	0.07	0.09	0.12	0.17	0.35	0.07	0.07	0.06
12 – Deciduous needleleaf forest	0.08	0.10	0.10	0.17	0.29	0.10	0.09	0.07
13 – Evergreen broadleaf	0.08	0.10	0.10	0.27	0.19	0.10	0.10	0.07
14 – Evergreen needleleaf	0.06	0.08	0.10	0.31	0.15	0.09	0.09	0.12
15 – Mixed forest	0.17	0.20	0.05	0.11	0.11	0.16	0.14	0.06
16 – Water bodies	0.14	0.14	0.02	0.06	0.06	0.07	0.09	0.42
17 – Herbaceous wetland	0.0	0.0	0.0	0.0	0.0	0.3	0.3	0.4
18 – Wooden wetland	0.0	0.0	0.0	0.3	0.3	0.0	0.0	0.4
19 – Barren or sparsely vegetated	0.0	0.0	0.7	0.1	0.1	0.1	0.0	0.0

To enable the comparison between the two scenarios (reference and future) some parameters were kept constant for both scenarios, notably population density, land cover fractions and the related parameters (albedo, porosity, emissivity, the water movement between canopy storages and the external water use, and the Objective Hysteresis Model (OHM) coefficients). Also, information about irrigation behaviour was kept constant for both scenarios. The field-based surveys were particularly useful in determining the period in which there is irrigation (June to September) and to realize which external water use is allowed every day of the week. The meteorological conditions, however, vary between the scenarios. The daylight-saving times (impacts timing of anthropogenic heat flux) was specified and defined for each year. It starts on 31 March (91 day of year [doy]) ending on 27 October

(301 doy) for the reference scenario, and 28 March (88 doy) and 31 October (305 doy) for the future scenario. The roughness length for momentum (z_{0m}) and the zero-displacement height (z_{dm}) were calculated from mean building and three heights using the "Rule of Thumb" method (Grimmond and Oke, 1999; Grimmond and Oke, 2002) in both scenarios.

Since SUEWS outputs are created for each individual cell, a postprocessor was also developed to enable analysis of the spatial distribution of each energy flux and the average behaviour of the energy balance fluxes at three times scales (annually, monthly and daily).

3.3. RESULTS AND DISCUSSION

Given the methodology used (section 3.2), the monthly modelled energy balance for the two climate scenarios was analysed to assess the influence of the changing climate in the behaviour of the individual flux profiles (section 3.3.1). Then, the climate influence on the spatial distribution of energy fluxes (section 3.3.2) was considered.

3.3.1. Energy balance

Energy fluxes vary over the course of a day in response to the diurnal cycle of solar heating and urban activities, as well as over the year in response to the annual cycle. Figure 3-5 shows the modelled monthly energy balance for the reference and future scenarios. To provide a more detailed analysis, the absolute differences between scenarios, for each component of the energy balance, were also summarized in Table 3-2. The energy balance was estimated considering the different types of land use of the domain, and having been divided as follows:

- region as a whole, obtained through the weighted average of the energy fluxes, based on the land use proportions that exists in the domain, to assess the average behaviour of the study area, giving an idea of how climate change might influence the energy balance of this region;
- urban, obtained through the average of the energy fluxes for the grid cells classified as *Urban and Built-Up area*, to assess the urban feedback to the changing climate; and
- non-urbanised, obtained through the weighted average of the energy fluxes, excluding both grid cells classified as *Urban and Built-Up area* and *Water Bodies*, to assess how non-urbanized areas will respond to climate change.

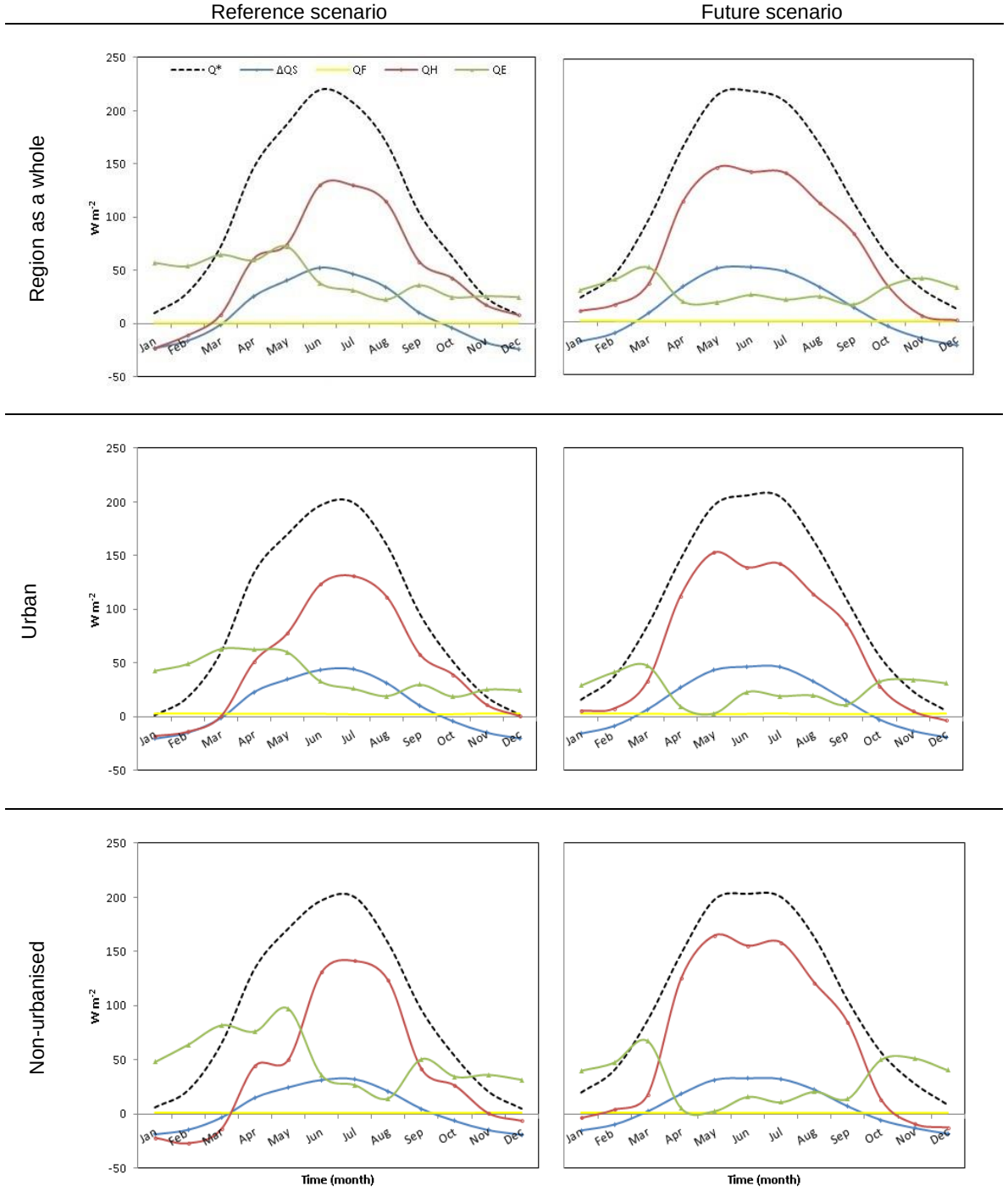

Figure 3-5. Modelled monthly averaged energy balance for the reference and future scenarios, for the different types of land use. Q*: net all-wave radiation, Q_F: anthropogenic heat flux, Q_E: latent heat flux, Q_H: sensible heat flux, ΔQ_S: net storage heat flux.

Table 3-2. Surface energy fluxes analysis in the climate scenarios. Monthly differences between the future and the reference scenarios, by type of land use (positive values indicate that the energy flux is higher in the future scenario; negative values indicate that the energy flux is higher in the reference scenario).

	Absolute differences of the surface energy fluxes (W·m $^{-2}$)											
	Jan	Fev	Mar	Apr	May	Jun	Jul	Agst	Sep	Oct	Nov	Dec
						Q*						
Region	13.2	16.1	25.7	20.3	29.0	0.15	2.11	-1.31	9.37	0.03	6.08	4.49
Urban	14.6	19.2	24.4	12.5	26.8	9.16	5.81	4.78	14.0	5.32	5.22	3.79
Non-urbanised	13.8	18.7	21.7	13.5	26.9	5.98	0.07	5.26	8.75	3.56	7.33	3.41
						Q_E						
Region	-26.9	-13.8	-12.8	-40.3	-53.9	-12.4	-10.1	1.57	-19.7	9.05	15.7	8.02
Urban	-13.8	-7.68	-15.4	-52.9	-57.3	-9.81	-6.78	0.54	-18.7	14.0	9.29	6.57
Non-urbanised	-8.01	-16.4	-14.7	-70.9	-94.8	-20.0	-15.9	6.01	-36.6	15.6	15.1	8.60
						Q_H						
Region	33.7	27.4	28.5	53.8	72.8	13.2	11.9	-1.72	25.7	-8.80	-12.0	-6.47
Urban	23.6	21.7	32.5	61.3	75.3	15.8	11.6	2.73	28.3	-10.4	-6.03	-4.09
Non-urbanised	18.2	31.0	31.8	81.0	115.0	24.6	17.1	-2.10	43.0	-13.0	-9.90	-6.20
						ΔQ_S						
Region	4.60	5.54	9.47	7.86	10.4	-0.59	0.99	-1.15	3.35	-0.38	1.99	1.69
Urban	4.81	6.30	7.99	4.05	8.70	2.99	2.21	1.61	4.77	1.72	1.56	1.19
Non-urbanised	3.63	4.90	5.72	3.54	7.04	1.55	0.14	1.36	2.34	0.92	1.87	0.89
						Q_F						
Region	0.02	0.02	-0.02	-0.05	-0.08	0.00	0.15	0.01	0.05	-0.01	-0.12	-0.03
Urban	0.03	0.03	-0.10	-0.16	-0.23	-0.06	0.69	0.10	0.35	-0.03	-0.42	-0.13
Non-urbanised	0.03	0.03	-0.02	-0.08	-0.12	0.01	0.22	0.01	0.07	-0.01	-0.18	-0.05

At the monthly time scale, the model produces the expected temporal variability in the energy balance results, as documented in past studies (Offerle et al., 2005; Coutts et al., 2007; Järvi et al., 2011), for both scenarios and for all land use types. As expected for both scenarios, the net all wave radiation (Q*) is highest in the summer months and lowest in the winter months. However, it is evident that the future scenario will have a slightly higher summer net radiation in comparison with the reference scenario (see Table 3-2). Despite this happens for all land use types, it is in the urban areas that the bigger differences between the scenarios for Q* are obtained, with maximum fluxes of around 197 and 206 W·m^{-2} registered in June, for the reference and future scenarios, respectively. The maximum difference between scenarios is obtained for the spring months (March, April and May) in all land use types (see Table 3-2).

In the region as a whole, for both scenarios, in the summer most of the net radiation is dissipated as sensible heat flux. In the reference scenario, two-time periods can be distinguished: March-June when the turbulent fluxes are nearly the same, and June-November where more energy is partitioned into Q_H than Q_E. The high importance of the sensible heat flux to the energy balance is expected given the types of surfaces in the study area. Beyond the highly-urbanised area, with little vegetation, an important part of domain even if non-urbanised is dryland cropland or grassland, with little water

availability. For the future scenario, the periods previously identified in the reference scenario do not apply. There are only short periods of transition when the prominence between the turbulent fluxes is changed. This fact is clearly a result of changes in the meteorological variables that affects the season's behaviour, namely, causing variations in season length. The most obvious change is the proximity between the summer and winter temperatures (in a yearly average base), which promotes a dwindled of the features that defines each season. Also, seasons are extremely important for the agriculture sector, and any changes in this equilibrium will require an adaptation of the type of vegetation (changes in the biodiversity); and of the agricultural crops (geographical distribution of crops, changes in planting dates and harvesting; increase of the intensity of pests and diseases).

The seasonal peaks in latent heat flux are also different for the two scenarios. Analysing the region as a whole, for the reference scenario, the Q_E peak is in May (72.6 $W \cdot m^{-2}$) and thereafter it declines, returning to exceed Q_H only in November. In contrast, in the future scenario, the peak latent heat flux is in March (two months earlier with a value of 52 $W \cdot m^{-2}$). This is a period (spring season) when there is higher precipitation to enable higher evapotranspiration. Additionally, despite a generalized decreasing of the latent heat in the future scenario, it is at the spring season that the highest reduction is obtained, ranging from -40 to -95 $W \cdot m^{-2}$ (see Table 3-2). Although these differences are consistent for all land use types, it is for non-urbanised areas that the bigger differences are obtained, which reinforces the strong dependence of the latent heat magnitude and the existence/absence of vegetation. The fraction of the net radiation that returns to the atmosphere as Q_E is clearly smaller in the future scenario. The increment of the sensible heat flux in the future scenario, as well as the change of its profile is also evident. The dominance of Q_H in the energy balance starts earlier and is prolonged during the year. During the winter months (particularly in January-February, for the reference scenario), Q_H is negative as a result of the reduced surface and air temperatures and turbulence and an increment of soil moisture (mostly related with the daytime duration and the amount of solar radiation that reaches to earth). This phenomenon, indicator of frost formation, is very common in Portugal, during the night-time periods of this season.

However, in the future scenario, this phenomenon is not evident, which is the result of high surface temperature and reduced relative humidity which increase the energy released by the surface, factors that minimize the frost formation. Therefore, the surface temperature doesn´t decreases enough (dew point) for this phenomenon to occur. This result clearly shows the strong urban feedback to the changing climate, promoted by the heat capacity of the man-made surfaces, since the frost formation will still occur in non-urbanised areas. In the urban areas, the nocturnal positive sensible heat flux has important effects in the boundary layer growth, since it delays the transition to stable conditions in the early evening (Kusaka and Kimura, 2004). A reduction in the stability of the boundary layer increases the turbulent mixing allowing the heat from the residual layer to be mixed downwards, reducing further the stability of the boundary layer by warming the lowest layers and deepening the stable boundary layer. The combined effects of surface morphology on the energy balance/boundary-layer system thus results in deeper, warmer, less stable nocturnal boundary layers when compared to a boundary layer over rural areas (Barlow et al., 2015). These boundary features imply that the urban boundary layer

remains near-neutral throughout the day, with consequences for the dispersion of air pollutants (a reduction of the dispersion and a degradation of air quality) as well as to the heat island effect, since it is during these conditions that the urban heat island is commonly observed. This change in the Q_H behaviour is also supported by changes in its magnitude, since an increase between 20-30 $W \cdot m^{-2}$ is obtained in the future scenario, during the months of frost formation (January and February, see Table 3-2).

Looking at all components of the energy balance, for the reference scenario and for the region as a whole, the annual balance is dominated by Q* and Q_H, reaching to 219.8 and 129.4 $W \cdot m^{-2}$, respectively. The majority of energy (Q* and Q_F, the latter contributing in average around 0.7 $W \cdot m^{-2}$), is partitioned to Q_H, accounting on average for 49% the available energy. The remaining energy is partitioned to turbulent latent heat flux and storage heat flux (41% and 10%, respectively). In contrast, for the future scenario, although the ordering of the energy partitioning is the same, the magnitude of the distribution is markedly different. The greatest share of energy goes to Q_H, representing more than 61% of the energy balance, followed by the latent heat flux (around 26%) and by the storage heat flux (around 12%). It should be noted that, although the latent heat flux is the second most important component of the energy balance in the future scenario, and as previously mentioned, its magnitude is reduced when compared with the reference scenario (an annual average difference of around 20%).

When comparing urban and non-urbanised areas, for the reference scenario, we find big differences in the energy balance. For the urban areas, sensible heat flux is higher due to the man-made materials and increased surface area, representing 51% of the available energy (against 42% obtained at non-urbanised areas); the turbulent latent heat flux is smaller due to a reduced fraction of vegetative land cover, accounting for 38% of the energy balance (against 54% at non-urbanised areas); and, the urban surfaces have higher heat capacity which leads to a non-negligible storage heat flux (11% and 4% of the available energy at the urban and non-urbanised areas, respectively). However, in the future scenario, these differences are smaller. The partitioning of the available energy is similar at the three levels of analysis, region as whole, urban and non-urbanised areas, which implies that the greatest difference between scenarios is obtained for non-urbanised areas. Since the land use was kept constant in both scenarios, these differences are linked to the changes in the meteorological variables (see section 3.3.2).

3.3.2. Fluxes spatial distribution

To understand the influence of the climate change scenarios on the energy fluxes a simple meteorological analysis was undertaken to determine how the meteorological variables evolved in the two scenarios. The meteorological variables were selected based on their importance and influence on urban fluxes modelling. The analysis consisted into three different approaches:

- estimation of the minimum, mean and maximum annual values (using a weighted average to consider the different types of land use previously defined) for the reference and future scenarios

and determination of the annual average differences between the two climate scenarios (Table 3-3);

- monthly average for both scenarios, for the different types of land use (Figure 3-6), to understand the impacts among the different seasons;
- mapping of the differences of the annual average between the future and the reference scenarios (Figure 3-7), to understand the spatial variability of the meteorological variables. The student's t test was applied, at each grid cell, to assess the results robustness. In this sense, Figure 3-7 also shows where in the domain the differences are not statistically significant at 5% level (noise showed as crosshatch).

In a future scenario, the 2 m air temperatures show increases between the 0.5 and 3ºC (Figure 3-7). The maximum difference is obtained inland (2.5ºC). The minimum difference (0.5ºC) is found along the coastline. A change on the seasonal behaviour is also evident, since for the future scenario temperatures higher than 15ºC are registered from April to October, while in the reference scenario this value is only reached two months later (June to October). This change is consistent in all land use types; however, it is at urban areas that the higher differences are achieved (maximum differences of 4.4ºC, in June). These results are in accordance with the values presented by the CMIP5 ensemble for this region (in terms of behaviour and magnitude) for the RCP scenario used. It should however be noted that the dynamic downscaling approach used in this work ensures the robustness of the results since, if a statistical downscaling in a very high resolution coastal region (as is the case) was used, the output variables wouldn't be consistent and probably the uncertainties would be well above the desirable.

An overall reduction of precipitation is predicted in the future scenario, generalized for all months. This implies a change in the annual cycle, most notably with an increase of drier summers and a reduction of wet winters (especially during January and February). The lowest precipitation (and highest reduction) is found on the eastern side of the domain (with a decrease of around 0.2 $mm \cdot h^{-1}$), which is mainly characterised by non-urbanised areas. Distinctive areas in the northern region of the domain are observed, with a maximum decrease of 0.15 $mm \cdot h^{-1}$. The changed precipitation rate in this specific case can be explained by the increase in number of days without rain (<1 $mm \cdot day^{-1}$) from 33.3% to 50.0%. The reduced precipitation and the increased number of clear-sky days in the future, directly influenced the surface energy balance.

Similar behaviour is evident in the relative humidity, with an average reduction of around 5%. The areas with a higher precipitation reduction correspond to those with maximum reduction in the relative humidity (around -9%). Analysing the relative humidity annual cycle, in the reference scenario, it is found that urban areas are drier in all months in comparison with the non-urbanised areas (around -6% in March and April, see Figure 3-6), which is in agreement with what was found for other cities (Lodz [Fortuniak et al., 2006] and Chicago [Ackerman, 1987]). The elevated city temperatures and lesser soil moisture availability in urban areas result in lower relative humidity. With a reduction of the relative humidity in the future scenario, this distinguished behaviour between built and non-built areas is masked. Overall the wind velocity is predicted to decrease, with an average value of around -0.3

$m \cdot s^{-1}$. Maximum decreases are along the coastline (around -1.2 $m \cdot s^{-1}$), while some areas in the inland domain do not reveal any changes between scenarios. During the summer (Figure 3-6), the changes between scenarios are small (less than 0.05 $m \cdot s^{-1}$) and similar over non-urbanised and urban areas. A decrease of wind speed (January-April) and a slight increase (particularly in October and November) is obtained, respectively during the winter/spring and autumn seasons.

Table 3-3. Meteorological analysis[1] of the climate scenarios: (a) annual minimum [Min], mean [Mean] and maximum values [Max] and (b) the spatial annual average of the differences between the future and the reference scenarios, by type of land use (positive values indicate that the meteorological variable is higher in the future scenario; negative values indicate that the meteorological variable is higher in the reference scenario).

Meteorological variables		**Reference scenario**			**Future scenario**			**Average differences (%)**
		Min	Mean	Max	Min	Mean	Max	
T2 (ºC)	Region	4.4	14.2	27.3	5.0	15.7	30.6	+10.9
	Urban	4.0	15.0	32.7	4.5	17.0	36.6	+13.3
	Non-urbanised	0.9	13.7	32.6	1.9	15.8	37.3	+15.8
P ($mm\ h^{-1}$)	Region	0.0	0.13	30.5	0.0	0.07	27.1	-23.8
	Urban	0.0	0.16	36.6	0.0	0.08	34.8	-46.3
	Non-urbanised	0.0	0.19	33.9	0.0	0.09	31.1	-49.9
WV ($m\ s^{-1}$)	Region	0.1	3.1	16.8	0.1	2.9	15.9	-7.8
	Urban	0.1	2.6	14.0	0.1	2.5	13.3	-4.1
	Non-urbanised	0.1	2.6	14.2	0.1	2.6	13.3	-2.6
RH (%)	Region	29.1	77.7	99.0	28.2	73.9	98.8	-5.0
	Urban	15.4	69.8	98.8	15.8	65.1	98.8	-6.7
	Non-urbanised	20.2	74.7	99.3	16.9	68.7	98.9	-7.9

[1] T2 is the air temperature at 2 m (ºC); P is the precipitation ($mm \cdot h^{-1}$); WV is the wind velocity at 10 m ($m \cdot s^{-1}$); and RH is relative humidity at 2 m (%).

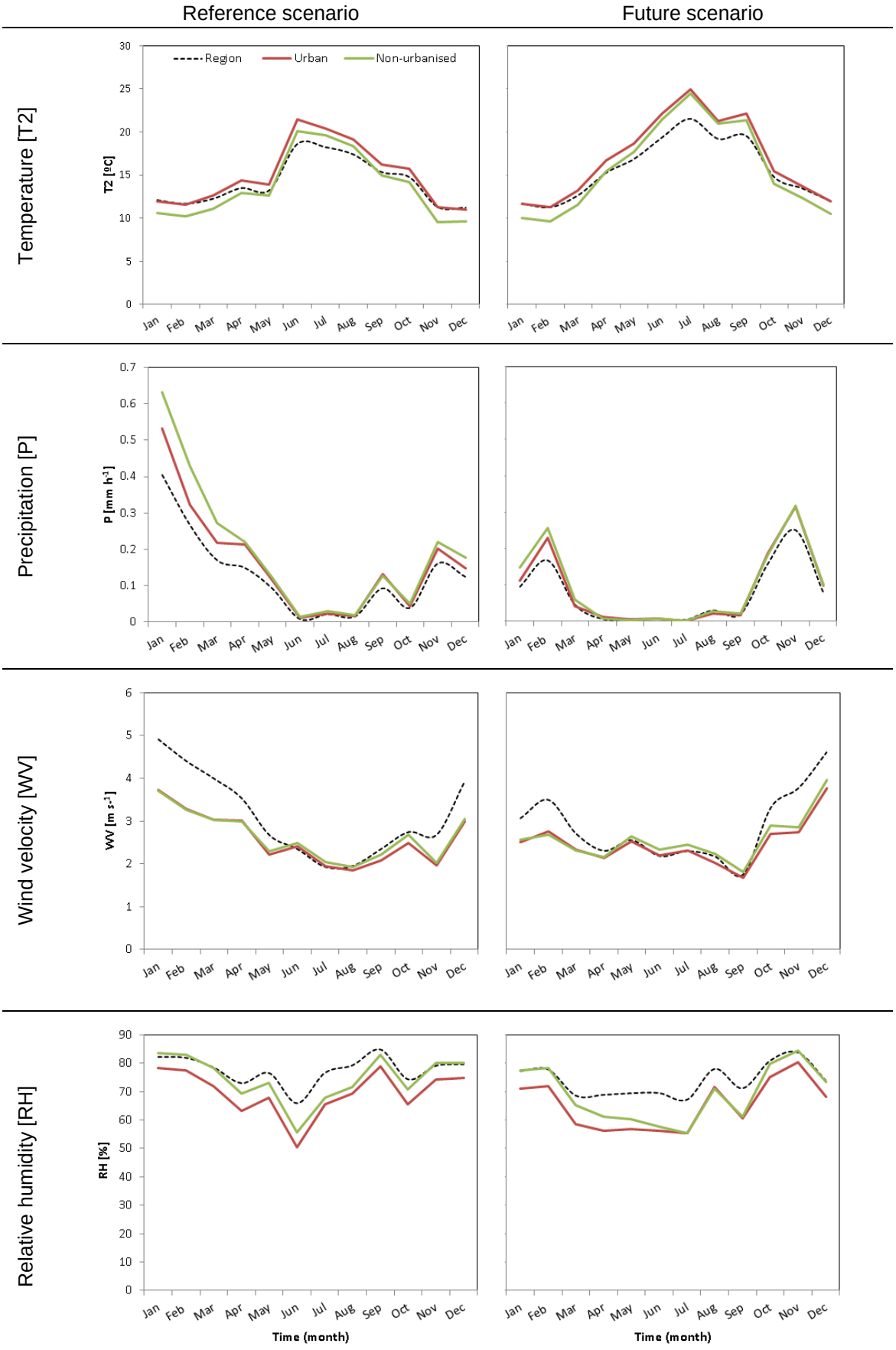

Figure 3-6. Monthly averaged meteorological variables, for the reference and future scenarios, for the different types of land use.

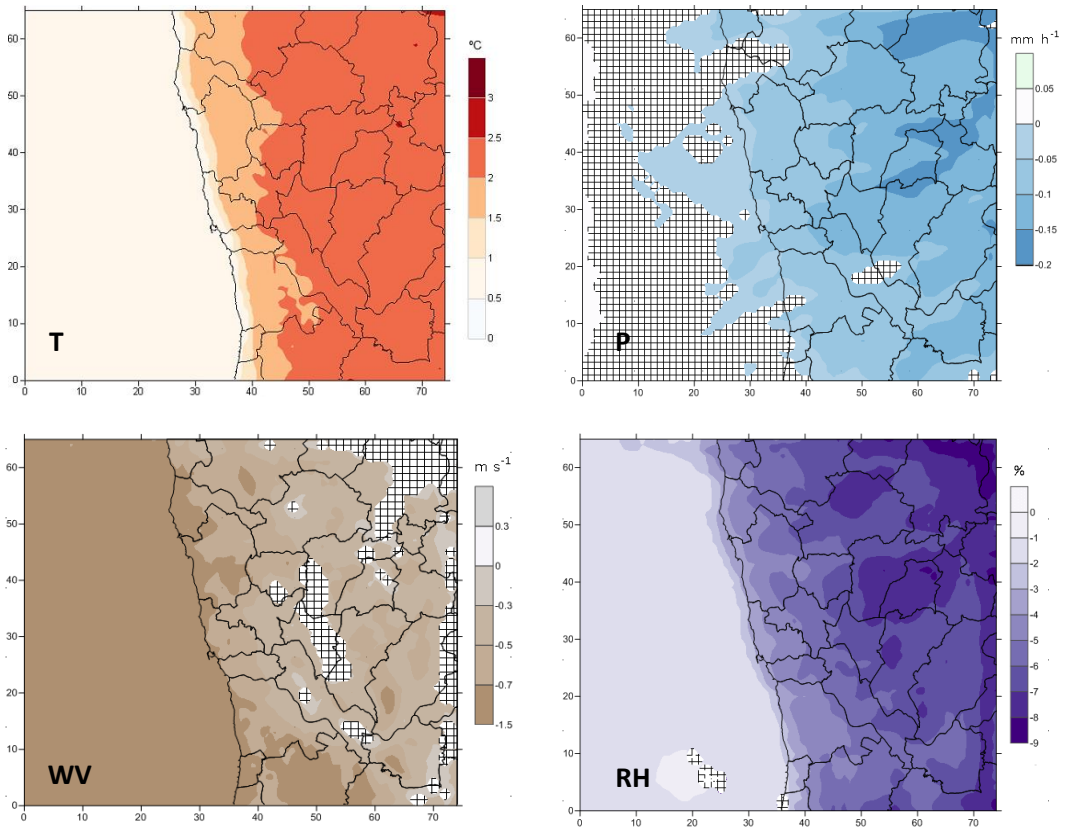

Figure 3-7. Annual average differences between the future and the reference scenario for air temperature at 2 m (T °C), precipitation (P mm·h^{-1}), 10 m wind velocity (WV m·s^{-1}), and 2 m relative humidity (RH %). The crosshatch shows the grid cells where the differences between scenarios are not statistically significant (noise).

Given these predicted changes in the climate variables, the spatial differences between the reference future scenarios for the sensible heat flux (Q_H), latent heat flux (Q_E), net storage heat flux (ΔQ_S), the incoming shortwave radiation ($K\downarrow$) and the net all-wave radiation (Q^*) were investigated (Figure 3-8). Similarity to what was done for the meteorological variables, the student's t test was applied, to assess the results robustness. The student's t test reveals that, for all the analysed variables, the differences between the future and reference scenarios are statistically significant, with a 95% probability (noise is showed as crosshatch in Figure 3-8).

The results suggest that the latent heat flux for the future scenario will decrease around 20% across the mainland study domain. Evaporation in most urban environments is water limited and so the decrease in precipitation rate (24%) impacts this. This causes a reduction in the [spatial average] daytime evaporative fraction (Q_E/Q^*) (10 a.m. – 3 p.m.) from 0.3 [reference] to 0.19 [future] scenarios. A reduction in latent heat flux can also contribute to a reduction in low cloud formation. It should be mentioned that the irrigation process does not influence these results since the conditions were kept constant at both climate scenarios.

It is well known that clouds reduce daytime heating by decreasing the amount of solar radiation that reaches the surface but warm night-time temperatures by enhancing downward long-wave radiation. Dry surfaces increase the diurnal temperature range by decreasing daytime evaporative cooling (Durre et al., 2000). As a result, the reduction of the latent heat flux, in a future scenario, imply a reduction of cloudiness (the number of days with cloudiness less than 40% increases from 8.3% to 25%), resulting in a consequently warmer and drier atmosphere, which may act as a positive feedback to provide more solar radiation (Ban-Weiss et al., 2011). With the ocean to the west, water is not limited and the air temperature is warm. Thus, the latent heat flux is projected to increase around 10%.

In contrast, the sensible heat flux will increase around 40% in the future scenario. This can be in part attributed to increases in K↓ (around 10%), possibly related to cloudiness reduction. This happens since clouds formation is linked to atmospheric motions (winds) that are produced by the radiative and latent heat (itself, in turn, affected by the presence of clouds), and a reduction of the wind speed is expected in a future climate (IPCC, 2013). Increasing the upward sensible heat flux from the surface to the atmosphere leads to an increment of the globally averaged surface temperature. The partitioning of net radiation into sensible and latent heat is also strongly influenced by soil moisture (Klink and Willmott, 1994). This means that if more (less) energy is used for latent heat flux, less (more) sensible heat is available within the near-surface environment. Given in a future scenario less water is available for evapotranspiration, and evaporation rates are predicted to drop significantly, the soil moisture will decrease and more energy will be dissipated as sensible heat flux. Because of this, the lower atmosphere is likely to be warm and dry. The Bowen ratio (defined as the ratio of sensible to latent heat flux (Q_H/Q_E)), an important indicator of the energy state of a system, is predicted to increase from 1.4 [reference] to 2.5 [future]. These values are typical of a suburban area in a temperate climate and of a semi–arid regions with extremely dry soils (values between 2 and 6) (Christen and Vogt, 2004; Loridan and Grimmond 2012).

An increase of ΔQ_S was also predicted of around 35% (Figure 3-8). Since the land use characteristics, namely albedo and the plan area surface cover fractions for the different surface types, were maintained constant in both simulations, the observed increase is mostly related to the increase of the greater solar radiation (an increase [spatial average] of around 10%) and available energy at the surface. Additionally, it is well known that water has a high specific heat capacity, which gives it the ability to absorb or lose a large amount of energy. Because of that, wet soils heat up more slowly and cool down more slowly than dry soils (Schaetzl and Thompson, 2005). Since precipitation is predicted to decrease in the future scenario, the soil moisture will also decrease. Therefore, the surface will warm rapidly and will lose energy rapidly to the atmosphere. This behaviour could increase surface air temperature at night and decrease the diurnal temperature variations (Zhou et al., 2007).

Heat energy in the soil can be used to i) evaporate water as latent heat flux; ii) warm the surface; or iii) radiate back to the atmosphere as outgoing long-wave radiation (Schaetzl and Thompson, 2005). The first point has already been discussed. Some of the heat resulting from the absorption of incoming shortwave radiation by the surface is emitted as long-wave radiation (L↑). The results showed a small variation in both components of the long-wave radiation (incoming and outgoing) [maps not showed] of

around 4% (maximum differences). This means that the majority of energy absorbed by the surface is used in its warming. However, outgoing long-wave radiation will account to the surface heat dissipation, which implies a heating of the lower atmosphere, which in turn warms the planet´s surface.

The anthropogenic heat flux (not shown) shows no significant differences (maximum differences of around 2%). This result is expected given the assumptions made in the modelling scenarios (the hourly profile of anthropogenic heat flux and the population density were kept constant in both climate scenarios) and since the magnitude of this flux is strongly dependent on-site characteristics and the behaviour of the people in that area (Allen et al., 2010). It should be mentioned that the modelled Q_F magnitude (a maximum Q_F summer of 8.1 $W \cdot m^{-2}$ and a maximum Q_F winter of 9.4 $W\ m^{-2}$) for the reference scenario, is in accordance with the values obtained for cities with similar characteristics (Sailor et al., 2015), considering the population density of the study area (850.5 pers km^{-2}). In this sense, there is not a direct relation between the Q_F behaviour and the changes in the meteorological variables. However, an indirect relation can be established, since the changes in the meteorological variables, particularly in terms of the temperature (either by its increase or decrease), will have impact on the energy consumption, either through heating or cooling (and therefore, changing the heating and cooling days), and consequently, will affect the behaviour and magnitude of Q_F. As investigated by Sailor et al. (2015), the magnitude of anthropogenic heating varies substantially as a function of underlying climate. This feedback is an important point, since the knowledge of Q_F patterns can lead to support climate change mitigation and adaptation planning, namely reducing winter and/or summer peak heat emissions, reducing carbon dioxide emissions, improving energy efficiency and also human comfort.

The overall changes in the energy fluxes (increase of Q_H and ΔQ_S; and reduction of Q_E) leads to an increase of the annual averaged surface temperature (average of domain) of 1.6°C (with a minimum and maximum difference of +0.8°C and +2.8°C, respectively). The changes in the magnitude of the different fluxes result in an increase of around 15% of the net all-wave radiation (see Figure 3-8). This type of results is needed for all cities to be able to document the magnitude of the effects of climate change on fluxes and thus to support sustainable planning strategies relevant to climate change mitigation and adaptation (e.g. green and blue infrastructures solutions which increase cities resilience to climate change impacts).

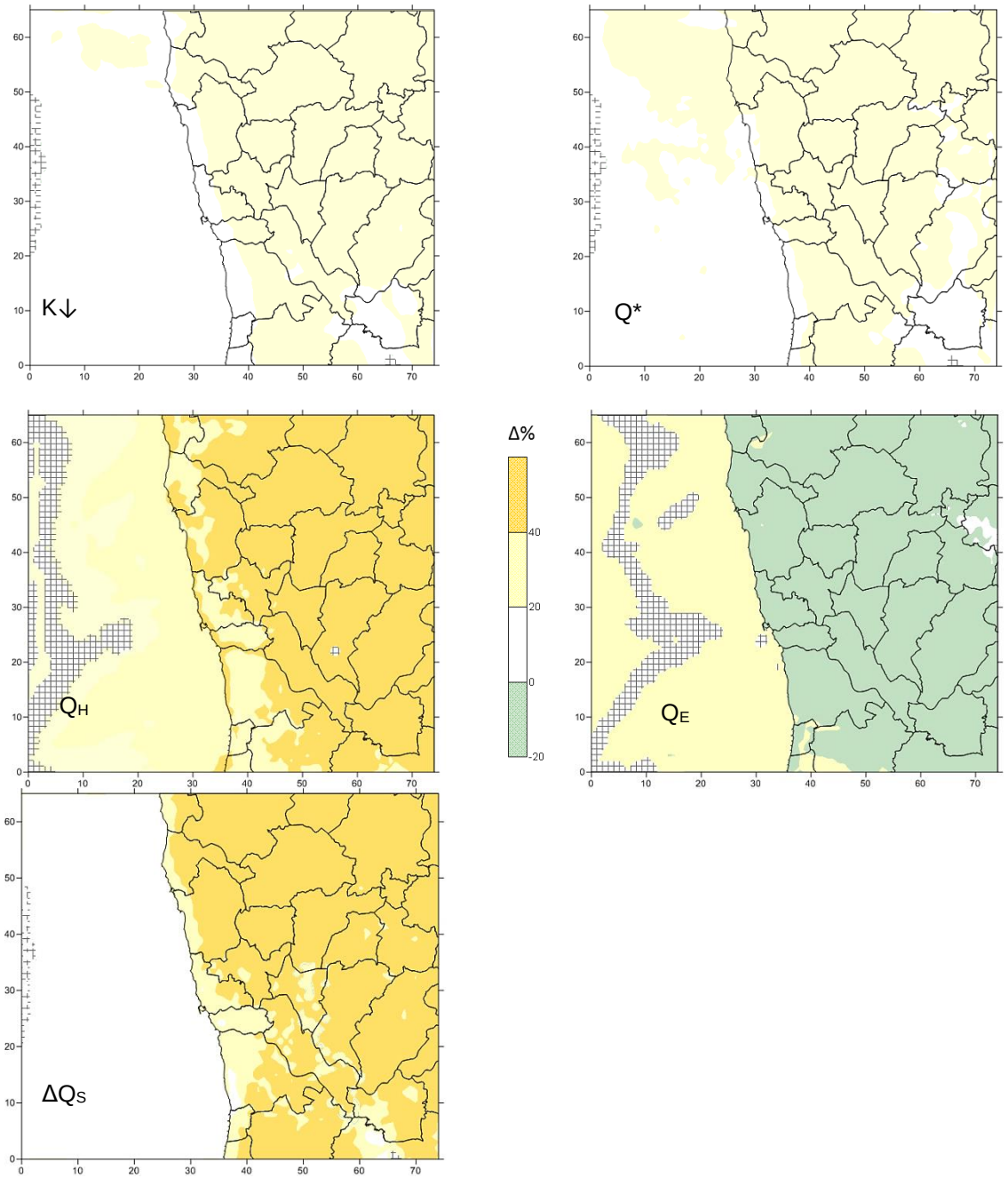

Figure 3-8. Spatial differences (%) between the future and the reference scenarios for the sensible heat flux (Q_H), latent heat flux (Q_E), net storage heat flux (ΔQ_S), the incoming shortwave radiation (K↓) and the net all-wave radiation (Q*). The crosshatch shows the grid cells where the differences between scenarios are not statistically significant (noise).

3.4. CONCLUSIONS

The impacts of climate change are likely to become more serious in the coming decades. Cities are locations where the effects and consequences will be most severe. Changes in regional meteorological variables, such as temperature and precipitation, can modify the urban energy balance fluxes, which in turn will feedback on the meteorological variables. In this work the SUEWS model was applied to assess the influence of climate change on the energy balance of the Greater Porto area.

The results reveal that the changes in the meteorological variables alter the partitioning of the energy fluxes. The future modelled scenario (compared with the reference scenario) predicts that global solar radiation, the sensible heat flux and the net storage heat flux will increase around 10%, 40% and 35% respectively. In contrast, the latent heat flux will decrease by around 20%. The changes in the magnitude of the different fluxes result in an increase of around 15% of the net all-wave radiation. Regarding the anthropogenic heat flux, the results revealed an indirect relation between its behaviour/magnitude and the changes in the meteorological variables.

Distinguished energy balance behaviours, due to land use type, are also investigated. For the reference scenario, urban areas (by comparison with non-urbanised areas) show higher values of sensible heat flux due to the man-made materials and increased surface area as well as due to a reduced fraction of vegetative land cover (which implies a smaller latent heat flux); the urban surfaces have also higher heat capacity which leads to a non-negligible storage heat flux. In the future scenario, the partitioning of the available energy is similar at the three levels of analysis, region as whole, urban and non-urbanised areas.

Due to the complexity of the atmosphere-biosphere system and of the continuous interaction of hydrological and dynamical processes, it is possible to predict the consequences of the changes in the energy balance in the meteorological variables actually experienced in the Greater Porto area. It is expected that an increase in the sensible heat flux and reduction of the latent heat flux, will result in higher surface temperature and a reduction of the precipitation. These results are particularly critical for the study area, since Porto is already dealing with problems from the urban heat island, and the changes in the energy fluxes obtained will increase the magnitude and the severity of this phenomenon in the future. These results highlight the need for investigating resilience measures (e.g., green and blue infrastructures solutions) and its effectiveness to mitigate the changes in the energy fluxes promoted by climate change.

3.5. REFERENCES

Ackerman B. (1987). Climatology of Chicago Area Urban-Rural Differences in Humidity. Journal of Climate and Applied Meteorology 26, 427-430.

Allen L., Lindberg F., Grimmond C.S.B. (2010). Global to city scale model for anthropogenic heat flux. International Journal of Climatology 31, 1990-2005. [doi: http://dx.doi.org/10.1002/joc.2210].

Área Metroplitana do Porto, AMP. (2014). AMP 2020 Estratégia de Base Territorial. Available at: http://portal.amp.pt/media/documents/2015/06/11/estrategia_amp_2020.pdf. [Last access: December 2015].

Anderson J., Hardy E., Roach J., Witmer E. (2001). A Land Use and Land Cover Classification System for use with Remote Sensor Data. A revision of the land use classification system as presented in U.S. Geological Survey. United States Government Printing Office, Washington.

Aquilina N., Dudek A.V., Carvalho A., Borrego C., Nordeng T.E. (2005). MM5 high resolution simulations over Lisbon. Geophysical Research Abstracts 7, 08685.

Barlow J. (2014). Progress in observing and modelling the urban boundary layer. Urban Climate 10, 216-240.

Barlow J., Halios C., Lane S., Wood C. (2015). Observations of urban boundary layer structure during a strong urban heat island event. Environmental Fluid Mechanics 15, 373–398.

Bartolomeu S., Carvalho M.J., Marta-Almeida M., Melo-Gonçalves P., Rocha A.M. (2016). Recent trends of extreme precipitation in the Iberian Peninsula using the high spatial resolution WRF model. Physics and Chemistry of the Earth 94 10-21.

Ban-Weiss G., Bala G., Cao L., Pongratz J., Caldeira K. (2011). Climate forcing and response to idealized changes in surface latent and sensible heat. Environmental Research Letters 6, 8 pp. [doi:10.1088/1748-9326/6/3/034032].

Benson-Lira V., Georgescu M., Kaplan S., Vivoni E.R. (2016). Loss of a lake system in a megacity: The impact of urban expansion on seasonal meteorology in Mexico City. Journal of Geophysical Research: Atmospheres 121, 3079-3099.

Bonan G. (2002). Ecological Climatology. Chapter 7: Surface Energy Fluxes. Cambridge University Press, 690 pages. ISBN: 0521800323.

Borrego C., Miranda A.I., Sousa S., Carvalho A., Sá E., Martins H., Valente J., Varum C., Jorge S. (2008). Planos e Programas para a Melhoria da Qualidade do Ar na Região Norte – Uma visão para o período 2001–2006. Departamento de Ambiente e Ordenamento da Universidade de Aveiro, Portugal.

Borrego C., Monteiro A., Martins H., Ferreira J., Fernandes A.P., Rafael S., Miranda A. I., Guevara M., Baldasano J.M. (2015). Air quality plan for ozone: an urgent need for North Portugal. Air Quality, Atmosphere & Health 9, 447-460. [doiI: 10.1007/s11869-015-0352-5].

Bossard M., Feranec J., Otahel J. (2000). CORINE land cover technical guide - Addendum 2000. Tech. Rep. 40, European Environmental Agency, Copenhagen.

Carvalho D., Rocha A., Gómez-Gesteira M., Santos C. (2012). A sensitivity study of the WRF model in wind simulation for an area of high wind energy. Environmental Modelling & Software 33, 23-34. [doi: 10.1016/j.envsoft.2012.01.019].

Carvalho, D., Martins, H., Marta-Almeida, M., Rocha, A. Borrego, C. (2017). Urban resilience to future urban heat waves under a climate change scenario: A case study for Porto urban area (Portugal). Urban Climate, 19 1-27. [doi: http://dx.doi.org/10.1016/j.uclim.2016.11.005].

Christen A., Vogt R. (2004). Energy and Radiation Balance of a Central European City. International Journal of Climatology 24, 1395-1421. [doi: 10.1002/joc.1074].

Coutts A., Beringer J., Tapper N. (2007). Impact of Increasing Urban Density on Local Climate: Spatial and Temporal Variations in the Surface Energy Balance in Melbourne, Australia. Journal of Applied Meteorology and Climatology 46, 477–493.

Dudhia J. (1989). Numerical study of convection observed during the winter monsoon experiment using a mesoscale two-dimensional model. Journal of the Atmospheric Sciences 46, 3077–3107.

Durre I., Wallace J.M., Lettenmaier D.P. (2000). Dependence of extreme daily maximum temperatures on antecedent soil moisture in the contiguous United States during summer. Journal of Climate 13, 2641-2651.

European Environment Agency, EEA. (2006). Urban Sprawl in Europe e the Ignored Challenge. Luxembourg: Office for Official Publications of the European Union. EEA Report No.10/2006. European Environment Agency, Copenhagen. ISBN 92-9167-887-2.

European Environment Agency, EEA. (2011). Analysing and managing urban growth. Available at: http://www.eea.europa.eu/articles/analysing-and-managing-urban-growth. [Last access: January 2016].

European Environment Agency, EEA. (2015). The European environment State and Outlook 2015: synthesis report. Luxembourg: Office for Official Publications of the European Union. European Environment Agency, Copenhagen. ISBN 978-92-9213-515-7.

Fita L., Fernández J., Garcıa-Dıez M. (2010). CLWRF: WRF modifications for regional climate simulation under future scenarios. In: 11th WRF Users's Workshop. NCAR Boulder CO.

Flagg D.D., Taylor P.A. (2011). Sensitivity of mesoscale model urban boundary layer meteorology to the scale of urban representation. Atmospheric Chemistry and Physics 11, 2951–2972. [doi:10.5194/acp-11-2951-2011].

Fonseca D., Carvalho M.J., Marta-Almeida M., Melo-Gonçalves P., Rocha A.M. (2016). Recent trends of extreme temperature indices for the Iberian Peninsula. Physics and Chemistry of the Earth 94, 66-76. [doi: /dx.doi.org/10.1016/j.pce.2015.12.005].

Fortuniak K., Klysik K., Wibig J. (2006). Urban–rural contrasts of meteorological parameters in Lódz. Theoretical and Applied Climatology 84, 91–101. [doi: 10.1007/s00704-005-0147-y].

Georgescu M., Miguez-Macho G., Steyaert L.T., Weaver C.P. (2009). Climatic effects of 30 years of landscape change over the Greater Phoenix, Arizona, region: 1. Surface energy budget changes. Journal of Geophysical Research: Atmospheres 114.

Georgescu M., Morefield P.E., Bierwagen B.G., Weaver,C.P. (2014). Urban adaptation can roll back warming of emerging megapolitan regions. Proceedings of the National Academy of Sciences 111, 2909-2914.

Grimmond C.S.B., Oke T.R. (1991). An evapotranspiration-interception model for urban area. Water Resources Research 27, 1739–1755.

Grimmond C.S.B., Oke T.R. (1999). Heat storage in urban areas: observations and evaluation of a simple model. Journal of Applied Meteorology and Climatology 38, 922–940.

Grimmond C.S.B., Oke T.R. (2002). Turbulent Heat Fluxes in Urban Areas: Observations and a Local-Scale Urban Meteorological Parameterization Scheme (LUMPS). Journal of Applied Meteorology and Climatology, 41, 792–810.

Grimmond C.S.B., Oke T.R., Steyn D.G. (1986). Urban water-balance 1. A model for daily totals. Water Resources Research 22, 1397–1403.

Grimmond C.S.B., Cleugh H.A., Oke T.R. (1991). An objective urban heat storage model and its comparison with other schemes. Atmospheric Environment Part B 25, 311–326.

Grimmond C.S.B., Blackett M., Best M.J., Barlow J., Baik J.J., Belcher S.E., Bohnenstengel S.I., Calmet I., Chen F., Dandou A., Fortuniak K., Gouvea M.L., Hamdi R., Hendry M., Kawai T., Kawamoto Y., Kondo H., Krayenhoff E.S., Lee S.H, Loridan T., Martilli A., Masson V., Miao S., Oleson K., Pigeon G., Porson A.,

Ryu Y.H, Salamanca F., Shashua-Bar L., Steeneveld G.J, Tombrou M., Voogt J.A., Young D.T., Zhang N. (2010). The International Urban Energy Balance Models Comparison Project: First Results from Phase 1. Journal of Applied Meteorology and Climatology 40, 1268-1292.

Grimmond C.S.B, Blackett M., Best M.J., Baik J.J., Belcher S.E., Beringer J., Bohnenstengel S.I., Calmet I., Chen F., Coutts A., Dandou A., Fortuniak K., Gouvea M.L., Hamdi R., Hendry M., Kanda M., Kawai T., Kawamoto Y., Kondo H., Krayenhoff E.S., Lee S.H., Loridan T., Martilli A., Masson V., Miao S., Oleson K., Ooka R., Pigeon G., Porson A., Ryu Y.H., Salamanca F., Steeneveld G.J., Tombrou M., Voogt J.A., Young D.T., Zhang N. (2011). Initial results from Phase 2 of the international urban energy balance model comparison. International Journal of Climatology 31, 244-272.

Giorgetta M.A., Jungclaus J., Reick C.H., Legutke S., Bader J., Böttinger M., Brovkin V., Crueger T., Esch M., Fieg K., et al. (2013). Climate and carbon cycle changes from 1850 to 2100 in MPI-ESM simulations for the Coupled Model Intercomparison Project phase 5. Journal of Advances in Modeling Earth Systems 5, 572–597.

Grell G.A., Freitas S.R. (2014). A scale and aerosol aware stochastic convective parameterization 346 for weather and air quality modeling. Atmospheric Chemistry and Physics 13, 845–23.

Hamdi R., Giot O., De Troch R., Deckmyn A., Termonia P. (2015). Future climate of Brussels and Paris for the 2050s under the A1B scenario. Urban Climate 12, 160-182.

Hong S.-Y., Lim J.-O. J. (2006). The WRF single-moment 6-class microphysics scheme (WSM6). Asia-Pacific Journal of Atmospheric Sciences 42, 129–151.

Hong S.-Y., Noh Y., Dudhia J. (2006). A new vertical diffusion package with an explicit treatment of entrainment processes. Monthly Weather Review 134, 2318–2341.

Instituto Nacional de Estatística, INE (Statisical of Portugal). (2011). Censos 2011 Resultados Definitivos - Região Norte. Instituto Nacional de Estatística (in Portuguese), I.P. ISSN 0872-6493. ISBN 978-989-25-0186-4

Instituto Português do Mar e da Atmosfera, IPMA (meterology institute). Normais Climatológicas - 1981-2010 (provisórias) (in Portuguese). Retrieved 19 January 2013. Available on: http://www.ipma.pt/pt/oclima/normais.clima/1981-2010/014/. [Last access: September 2015].

Intergovernmental Panel on Climate Change, IPCC. (2013). Summary for Policymakers. In: Climate Change 2013: The Physical Science Basis. Contribution of Working Group I to the Fifth Assessment Report of the Intergovernmental Panel on Climate Change [Stocker, T.F., D. Qin,G.-K. Plattner, M. Tignor, S.K. Allen, J. Boschung, A. Nauels, Y. Xia, V. Bex and P.M. Midgley (eds.)]. Cambridge University Press, Cambridge, United Kingdom and New York, NY, USA.

Järvi L., Grimmond C.S.B., Christen A. (2011). The Surface Urban Energy and Water Balance Scheme (SUEWS): Evaluation in Los Angeles and Vancouver. Journal of Hydrology 411, 219-237. [doi:10.1016/j.jhydrol.2011.10.001].

Järvi L, Grimmond CSB, Taka M, Nordbo A, Setälä H, and Strachan IB. (2014). Development of the Surface Urban Energy and Water balance Scheme (SUEWS) for cold climate cities, Geoscientific Model Development 7, 1691-1711. [doi:10.5194/gmd-7-1691-2014].

Karsisto P., Fortelius C., Demuzere M., Grimmond C.S.B. Oleson, K.W., Kouznetsov R., Masson V., Järvi L. (2016). Seasonal surface urban energy balance and wintertime stability simulated using three land-surface models in the high-latitude city Helsinki. Quarterly Journal of the Royal Meteorological Society 142, 401–417. [doi:10.1002/qj.2659].

Klink K., Willmott C.J. (1994). Influence of soil moisture and surface roughness heterogeneity on modeled climate. Climate Research 4, 105-118.

Kusaka H., Kimura F. (2004). Thermal Effects of Urban Canyon Structure on the Nocturnal Heat Island: Numerical Experiment Using a Mesoscale Model Coupled with an Urban Canopy Model. Journal of Applied Meteorology 23, 1889-1910.

Li D., Sun T., Liu M., Yang L., Wang L., Gao Z. (2015). Contrasting responses of urban and rural surface energy budgets to heat waves explain synergies between urban heat islands and heat waves. Environmental Research Letters 10, 054009.

Lindberg F., Grimmond C.S.B, Yogeswaran N., Kotthaus S., Allen L. (2013). Impact of city changes and weather on anthropogenic heat flux in Europe 1995-2015. Urban Climate 4, 1-15.

Loridan T. Grimmond C.S.B. (2012). Characterization of Energy Flux Partitioning in Urban Environments: Links with Surface Seasonal Properties. Journal of Applied Meteorology and Climatology 51, 219–241. [doi: http://dx.doi.org/10.1175/JAMC-D-11-038.1].

Ma E., Deng X., Zhang Q., Liu A. (2014). Spatial Variation of Surface Energy Fluxes Due to Land Use Changes across China. Energies 7, 2194-2206.

Marta-Almeida M., Teixeira J.M., Carvalho M.J., Melo-Gonçalves P. Rocha A. (2016). High resolution WRF climatic simulations for the Iberian Peninsula. Journal of Physics and Chemistry of the Earth 94, 94-105. [doi:10.1016/j.pce.2016.03.010].

Martins H. (2012) Urban compaction or dispersion? An air quality modelling study. Atmospheric Environment 54, 60-72. [doi: 10.1016/j.atmosenv.2012.02.075].

McMichael A.J., Wilkinson P., Kovats R.S., Pattenden S., Hajat S., Armstrong B., Vajanapoom N., Niciu E.M., Mahomed H., Kingkeow C., Kosnik M., O'Neill M.S., Romieu I., Ramirez-Aguilar M., Barreto M.L., Gouveia N., Nikiforov B. (2008). International study of temperature, heat and urban mortality: the 'ISOTHUM' project. International Journal of Epidemiology 37, 1121–1131. [doi: 10.1093/ije/dyn086].

Mitchell V.G., Cleugh H.A., Grimmond C.S.B., Xu J. (2008). Linking urban water balance and energy balance models to analyse urban design options. Hydrological Processes 22, 2891-2900. [doi: 10.1002/hyp.6868].

Mlawer E.J., Taubman S.J., Brown P.D., Iacono M.J., Clough S.A. (1997). Radiative transfer for inhomogeneous atmospheres: RRTM, a validated correlated-k model for the longwave. Journal of Geophysical Research 102D, 16663-16682.

Monteiro A., Ferreira J., Ribeiro I., Fernandes A.I., Martins H., Gama C., Miranda A.I. (2015). Air quality over Portugal in 2020. Atmospheric Pollution Research 6, 788-796.

Offerle B., Grimmond C.S.B., Oke T.R. (2003). Parameterization of net all-wave radiation for urban areas. Journal of Applied Meteorology and Climatology 42, 1157–1173. [doi: 10.1175/1520-0450(2003)042].

Offerle B., Grimmond C.S.B, Fortuniak K. (2005). Heat storage and anthropogenic heat flux in relation to the energy balance of a central European city centre. International Journal of Climatology 25, 1405-1419.

Oke T.R. (1987). Boundary Layer Climates. Routledge, London, UK.

Riahi K., Gruebler A. Nakicenovic N. (2007). Scenarios of long-term socio-economic and environmental development under climate stabilization. Technological Forecasting Social Change 74 887–935.

Sailor D.J., Vasireddy C. (2006). Correcting aggregate energy consumption data account for variability in local weather. Environmental Modelling Software, 21, 733-738. [doi:10.1016/j.envsoft.2005.08.001].

Sailor D.J., Georgescu M., Milne J.M., Hart M.A. (2015). Development of a national anthropogenic heating database with an extrapolation for international cities. Atmospheric Environment 118, 7-18.

Schaetzl R., Thompson M. (2005). Soils: Genesis and Geomorphology. Cambridge University Press.

Schiff K., Bax B., Markle P., Fleming T., Newman J. (2007). Wet and dry weather toxicity in the San Gabriel River. Bulletin, Southern California Academy of Sciences 106, 179-192. Available at: http://scholar.oxy.edu/scas/vol106/iss3/2. [Last access: November 2015].

Sheng L., Liu S.H., Liu H.P. (2010). Influences of climate change and its interannual variability on the surface energy fluxes from 1948 to 2000. Advances in Atmospheric Sciences 27, 1438–1452.

Skamarock, W.C., Klemp, J.B., Dudhia, J., Gill, D.O., Barker, D.M., Huang, X.Y., Wang, W., Powers, J.G. (2008). A Description of the Advanced Research WRF Version 3. NCAR/TN-475+STR, pp.113.

Teixeira J., Carvalho A., Carvalho M. J., Luna T., Rocha A.M. (2014). Sensitivity of the WRF model to the lower boundary in an extreme precipitation event–Madeira island case study. Natural Hazards and Earth System Science 14, 2009–2025.

Tewari M., Chen F., Wang W., Dudhia J., LeMone M., Mitchell K., Ek M., Gayno G., Wegiel J., Cuenca R. (2004). Implementation and verification of the unified NOAH land surface model in the WRF model. 20th conference on weather analysis and forecasting/16th conference on numerical weather prediction, 11–15.

URL1: European Environment Agency. Porto Urban Atlas. Available at: http://www.eea.europa.eu/data-and-maps/data/urban-atlas. [Last access: December 2015].

Wild M., Ohmura A., Cubasch U. (1997). GCM-Simulated Surface Energy Fluxes in Climate Change Experiments. Journal of Climate 10, 3093-3110.

Wouters H., Ridder K.D., Demuzere M., Lauwaet D., van Lipzig N.P.M. (2013). The diurnal evolution of the urban heat island of Paris: a model-based case study during Summer 2006. Atmospheric Chemistry and Physics 13, 8525-8541.

Zhang D., Anthes R.A. (1982). A high-resolution model of the planetary boundary layer-sensitivity tests and comparisons with SESAME-79 data. Journal of Applied Meteorology 21, 1594–1609.

Zhou L., Dickinson R., Tian Y., Vose R., Dai Y. (2007). Impact of vegetation removal and soil aridation on diurnal temperature range in a semiarid region: Application to the Sahel. Geophysics 104, 17937- 17942. [doi: 10.1073/pnas.0700290104].

CHAPTER 4

This Chapter has been published as:

Rafael S., Martins H., Sá E., Carvalho D., Borrego C., Lopes M. (2016). *Influence of urban resilience measures in the magnitude and behaviour of energy fluxes in the city of Porto (Portugal) under a climate change scenario*. Science Of The Total Environment 566, 1500-1510.

The author acknowledges the co-authors critical revision. An acknowledgement to David Carvalho for providing the climate data used in this work.

4. Influence of urban resilience measures in the magnitude and behaviour of energy fluxes in the city of Porto (Portugal) under a climate change scenario

Abstract

Different urban resilience measures, such as the increase of urban green areas and the application of white roofs, were evaluated with the WRF-SUEWS modelling system. The case study consists of five heat waves occurring in Porto (Portugal) urban area in a future climate scenario. Meteorological forcing and boundary data were downscaled for Porto urban area from the CMIP5 earth system model MPI-ESM, for the Representative Concentration Pathway RCP8.5 scenario.

In this Chapter was quantified and compared the influence of different resilience measures on the urban surface energy balance components. Results show that the inclusion of green urban areas increases the evaporation and the availability of surface moisture, redirecting the energy to the form of latent heat flux (maximum increase of +200 $W \cdot m^{-2}$) rather than to sensible heat. The application of white roofs increases the solar radiation reflection, due to the higher albedo of such surfaces, reducing both sensible and storage heat flux (maximum reductions of -62.8 and -35 $W \cdot m^{-2}$, respectively). The conjugations of the individual benefits related to each resilience measure shows that this measure is the most effective one in terms of improving the thermal comfort of the urban population, particularly due to the reduction of both sensible and storage heat flux. The obtained results contribute to the knowledge of the surface-atmosphere exchanges and can be of great importance for stakeholders and decision-makers.

Keywords: Energy fluxes, Future climate, Heat waves, Resilience measures, Urban areas

4.1. INTRODUCTION

Urban areas are home to over half of the world population and are at the forefront of the climate change issue. At the same time, urban areas are responsible for no less than 40% of global greenhouse gas emissions, and given current demographic trends, this level will likely increase over time (Rosenzweig et al., 2011). These challenges highlight the need for cities to rethink how climate will affect long-term growth and development plans, how infrastructure investments are prioritized, and how assets are deployed and people protected (EEA, 2010).

Despite the global effort to mitigate the negative impacts of climate change, its effects are already underway (Kharin and Zwiers, 2000; Santos and Corte-Real, 2006). Current observations of climate are in line with projections of the average climate change (van Engelen et al., 2008), which suggests, among others, that heat waves will become more frequent, intense and long-lasting under a warming climate; and will interact nonlinearly with Urban Heat Island (UHI), promoting extremely high heat stress events in urban environments (McCarthy et al., 2010; Li and Bou-zeid, 2013). The increase of the death rate associated with extreme meteorological episodes in Europe that has been reported it is extremely critical (Watkiss et al., 2009). This rate could double by 2040 and even increase up to ten times by the end of the current century, with southern Europe experiencing the highest increases in the summer (Watkiss et al., 2009).

Today it is well known that there is a link between the state of the atmosphere and the land. In urban areas, the surface morphology (i.e., urban form) and the presence of impervious building materials, the sparseness of vegetation, the presence/absence of blue areas, and atmospheric pollutants each have a significant role in the partitioning of the net radiation. The energy fluxes released to the atmosphere directly influences the climate of urban regions (e.g. boundary layer, air temperature, relative humidity and other climate system variables) (IPCC, 2013). In this sense, the need for studies on the energy fluxes as important determinants of the urban microclimate is clear.

Several studies in this area have been developed during the last decade with different approaches and goals. The study of energy fluxes can be classified in three main approaches:

- Studies that consider the measurements of the energy fluxes through the eddy covariance method, mainly to understand of how urban geometry, properties of urban materials, and presence/absence of vegetation influences the magnitude and behaviour of these fluxes (Oke and Cleugh, 1987; Christen and Vogt, 2004; Coutts et al., 2007; Sedlar and Hock, 2009). These types of studies usually compare different types of land use (e.g. urban/rural; different urban typologies, among others).
- Studies that combine flux measurements with model simulations, to help identifying knowledge gaps in the current understanding of flux processes, enhance our understanding and interpretation of the observed fluxes, and assisting in evaluating the reliability of measured and modelled fluxes (Grimmond and Oke, 1999; Grimmond and Oke, 2002; Offerle et al., 2005; Flerchinger et al., 2012; Järvi et al., 2011, 2014).

- Studies that use models designed to simulate the key processes governing heat, moisture and momentum exchanges of the urban canopy for different applications (e.g. understanding of how energy in the form of radiation and heat influences the urban climate). More recently this type of studies also includes climate change scenarios, specially linked to urban temperature analysis and UHI formation (Taha, 1997; Park et al. 2005; Oleson et al., 2010). The models have varying levels of complexity, and different fluxes modelled. (Grimmond et al., 2010). Generally, these have been conducted with mesoscale meteorological models applied to individual cities using large-scale data (Oleson et al., 2010).

Additionally, recent research in this field has focused in combining imagery from Earth Observation satellites with conventional meteorological measurements at street level. The main goal of this approach is define a clear link between urban land-use patterns and energy consumption at local scale to estimate spatiotemporal patterns of anthropogenic heat flux (URL1).

Although mesoscale observations of sensible heat flux modification by urban areas such as the UHI effect are widely documented (since Oke 1982), the urban meteorology is a relatively recent area of research. In this sense, the factors that influence the microscale variation of heat flux, or indeed the strength of this variation, still requires analysis. This type of knowledge is also vital to address the challenges of urban planning and sustainability, for example for managing resources, mitigation and adaptation to climate change or air pollution (Lietzke et al., 2015).

The main goal of this work is to investigate and quantify the influence of the application of resilience measures, such as adaptation strategies to deal with heat waves impacts in the energy balance components for a future climate projection downscaled to Porto urban area. This work is distinguishable from previous studies that analyse the urban energy fluxes exchanges, due to the high spatial resolution modelling at urban scale (200 m). It uses a modelling setup composed by the latest Weather Research and Forecasting (WRF) (version 3.7), which is one of the most widely used and recognized models employed in climate research and weather forecasting in the world, showing good performances when applied to Portugal (Borrego et al. 2015; Monteiro et al., 2013a, 2015); and the Surface Urban Energy and Water Balance Scheme (SUEWS) (version 2014b), an urban land surface model.

The modelling setup has two main features: i) it allows a complete spatial coverage of the energy fluxes and a prognostic analysis (e.g. different scenarios and different test runs) in a short time-consuming period (EEA, 2011); ii) it is able to simulate both energy and water fluxes for extended periods of time; this means that the irrigation and runoff processes are accounted for latent heat flux simulation, and thus, a more realistic simulation is obtained (Grimmond et al., 2010, 2011). Additionally, most of the studies are focused in the turbulent fluxes (sensible and latent heat) or in the storage heat flux, while, in this study, all the components of the energy balance are analysed. The study is conducted for the Representative Concentration Pathways RCP8.5 scenario (Taylor et al., 2012). Finally, although a set of the published research has been evaluating the effectiveness of resilience measures to mitigate urban temperatures (Rizwan et al., 2008; Synnefa et al., 2008;

Papangekis et al., 2012; Li et al., 2014; Lau et al., 2015), this type of studies is quite novel for Porto urban area, and to any Portuguese city or urban environment, especially in what is related to the analysis of the surface-atmosphere exchanges. This Chapter is presented as follows, Section 4.2 describes the methodology used to select the resilience measures to be analysed as well as the applied modelling setup. The effects of the resilience measures on the energy balance are presented in Section 4.3. Summary and conclusions follow in Section 4.4.

4.2. DATA AND METHODS

A specific methodology was followed to assess the influence of the application of resilience measures in the energy balance components on Porto Urban Area. Two main steps were performed: i) selection of resilience measures (section 4.2.2) and ii) modelling their application (section 4.2.3). A detailed description is presented in the following sub-sections.

4.2.1. Case study

The selected study region is Porto urban area (41° N and 8° W), the second largest city in Portugal (with an area of 41.4 km^2) and the centre of a metropolitan area with a population density of 5736 inhab km^{-2}, distributed in a disperse way in the territory (INE, 2011). Porto is located in the northwest of Portugal (Figure 4-1). The area is affected by various weather systems related to the complex atmospheric circulation in this zone, the nearby Azores Anticyclone and rapidly advancing depressions associated with Polar Front movements. The city is thus influenced by fluctuations of two distinctly different types of air masses, typically warm and humid from the subtropics, and colder and drier from the polar zone. This climatological context produces a changing daily sequence of contrasting, stressful and demanding thermal conditions, potentially affecting human health (Monteiro and Velho, 2014).

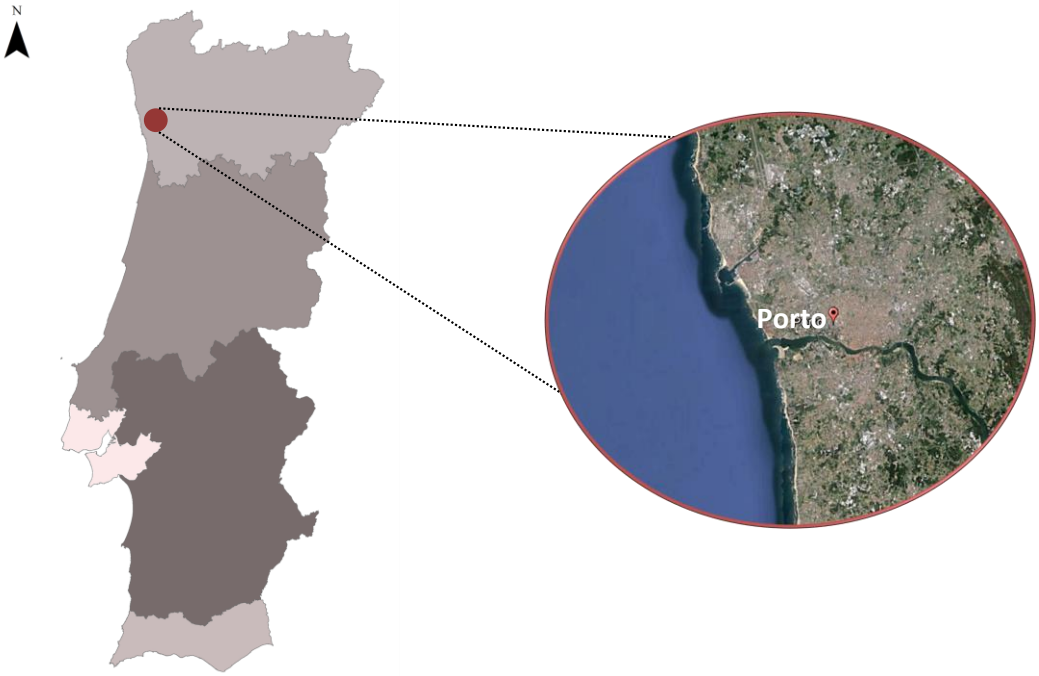

Figure 4-1. Geographic location of Porto urban area: Northwest region of Portugal. The territorial map of mainland Portugal (at right) it is divided accordingly the NUT II designations (represented by different grey scale). In the top of the map is located the North region, followed by the Centre region, the Metropolitan area of Lisbon, the Alentejo (including Lezíria do Tejo) and Algarve. Porto urban area is located in the North region of mainland Portugal at 41° 09' 54.32''N and 8° 36' 50.91''W (left image) (Google earth V10, SIO, NOAA, United States Navy, NGA, GEBCO, Image Landset, Image IBCAO, http://www.earth.google.com [February 18, 2016]).

Porto is located in a geographic region where most Representative Concentration Pathways (RCP) scenarios anticipate a considerable temperature increase during the 21st century, something which is already evident from Porto meteorological observations (Monteiro et al., 2012a). At the same time, an increased rate of mortality and morbidity was identified related to the occurrence of heat waves, namely in July 2006 and 2003 (Monteiro et al., 2012b; Monteiro et al., 2013b). In this context and with this climatic prediction it becomes paramount to investigate the influence of the application of urban heat resilience strategies under a future climate scenario, as well as its effectiveness.

In parallel, in recent years Porto urban area has experienced an urbanization process characterized by very fast growing, namely through a significant increase of roads and built-up area, with considerable pressure on sensitive areas. These changes in the land use, besides responding to the increased demand associated to the demographic rise, also act as a key inducer of the urbanization processes (AMP, 2008).

According to Marta-Almeida et al. (2016), anthropogenic climate change will likely increase the frequency, duration and magnitude of severe heat stress events mainly in highly populated urban areas. In this sense, Porto urban area will be one of the urban environments more exposed to the exacerbation of future heat waves (Carvalho et al., 2014; Fonseca et al., 2016) and thus, is an interesting case study.

4.2.2. Selection of the resilience measures

The notion of resilience is gaining increased prominence across a diverse set of literature on cities and climate change, as result of a wide consensus that: (i) cities must become resilient to a wider range of stresses in order to be prepared for climate change; and (ii) efforts to promote climate change resilience must be clustered with efforts to promote sustainable urban development (Leichenko, 2011). Terms such as “climate resilient”, “climate-proofing”, and “resilient city” are frequently used to emphasize the idea that cities, urban systems and urban communities need to be able to quickly recover from climate impacts. As a result, a resilient city is characterized by its capacity to tolerate or absorb the impact of a driver through resistance or adaptation, which enables it to maintain certain basic functions and structures during an extreme episode (Twigg, 2009).

The adoption of measures that improve cities resilience and offer a preparative support for dealing with the anticipated effects of climate change and extreme events is crucial. Green infrastructures (namely the use of trees and vegetation in the urban environment, as well as green roofs and green walls) are widely cited in the literature as having the potential to increase urban areas resilience to the effects of the UHI and heat waves (Bell et al., 2008). Additionally, the so-called cool roofs (mainly made of highly reflective and emissive materials) have also been identified by its capabilities to address the problem of the UHI (Chin et al., 2008; Jacobson and Hoeve, 2012).

Having in consideration studies which discuss the advantages of such measures in reducing temperature (Papangelis et al., 2012; Susca et al., 2012; Li et al., 2014; Yang et al., 2015; Carvalho et al., 2017), and the link between meteorological variables and the energy balance components (Lopes et al., 2015), three resilience measures were selected to be assessed in terms of its influence in each one of these components: latent and sensible heat flux, anthropogenic heat emission, net storage heat flux and net all-wave radiation. The main criteria underlying this selection include the consistently reported effectiveness and benefits of the measures in the mitigation of heat waves effects in built-up surfaces, its low-cost and its easy applicability in the study area. The selected measures comprised:

- the introduction of white roofs in areas with high residential density;
- the duplication of the existing green areas;
- the combination of the two previously measures (duplication of the existing green areas plus the introduction of white roofs in areas with high residential density).

It should be noted that according the criteria underlined for the selection of resilience measures, particularly for demonstrate to the stakeholders and policy makers the advantages of easily applicable strategies, the introduction of green roofs was not assessed. This is mainly due to some challenges related to its construction and maintenance that still need to be solved, namely ensure the waterproofing integrity, irrigation requirements, the appearance of wildlife, as well as the higher initial costs when compared with the most conventional or white roofs.

4.2.3. Modelling setup

To assess the influence of the selected resilience measures in the energy balance components, the WRF–SUEWS modelling system was applied. The WRF model, from the National Center for Atmospheric Research (NCAR) (Skamarock et al., 2008), version 3.7, is a next-generation mesoscale numerical weather prediction system designed to serve both operational forecasting and atmospheric research needs. SUEWS (Järvi et al., 2011, 2014), version 2014b, is an urban land surface model used to investigate both energy and water balances using hourly meteorological forcing data. The complete energy balance is mathematically expressed by (Oke, 1987):

$$Q^* + Q_F = Q_E + Q_H + \Delta Q_S \quad [W \cdot m^{-2}] \tag{4.1}$$

where Q* is the net all-wave radiation (the net incoming and outgoing radiative fluxes), Q_F is the anthropogenic heat flux (the energy released by human activities), Q_E is the latent heat flux (the energy taken up/released with the phase change of water), Q_H is the turbulent sensible heat flux (the energy that heats the air), and ΔQ_S is the net storage heat flux (which includes soil heat flux and also the heating and cooling of the complete urban structure).

The input meteorological data required for SUEWS (wind speed, relative humidity, air temperature, air pressure, rain, and incoming solar radiation) are supplied by the WRF model. The foundations of SUEWS include the urban evaporation-interception scheme of Grimmond and Oke (1991) and the urban water balance model of Grimmond and Oke (1986).

The WRF model was applied to a future climate change scenario to identify future heat waves in Porto urban area. Marta-Almeida et al. (2016) performed a dynamical downscaling of the MPI-ESM-LR global model future climate projection following the radiative forcing prescribed by RCP8.5 with the WRF model to the regional scale (Iberian Peninsula at 9 km of horizontal resolution) for past-present (1986-2005) and for a medium-term future period (2046-2065). The RCP8.5 emission scenario was selected since it corresponds to the pathway with the highest greenhouse gas emissions, and therefore it is the scenario that reflects more onerous impacts (Sá et al., 2016). Bartolomeu et al. (2015), Fonseca et al. (2016) and Marta-Almeida et al. (2016) provide a complete description and validation of the modelling system. Marta-Almeida et al. (2016) considered a set of variables to evaluate climate change (maximum daily temperature, minimum daily temperature, daily precipitation and daily wind speed and direction) and concluded that the annual number of consecutive dry days is projected to be higher in both future climates when compared with the reference climate. For the Porto region, results show an average temperature increase of 1.9˚C for the mid-term future and of 3.7˚C for the long-term future. They also concluded that between the recent past and the future, heat waves go from normal to moderate, to very extreme which suggests an increase in the number of heat waves frequency (around 2.2 times more than in the recent past) with higher magnitude (Marta-Almeida et al., 2016)

The climatic dataset for the future scenario were used to identify several heat waves occurring in Porto urban area. This selection was made following the methodology described in Russo et al. (2014). In

short, this methodology defines as a heat waves at least three consecutive days with daily maximum temperature above a daily threshold (90th percentile of daily maxima centred on a 31-day window) (Carvalho et al., 2014; Fonseca et al., 2016). Five heat waves were identified following this approach and considered as “heat wave episodes”.

After the selection of the heat waves, a two-way multiple nesting strategy was followed to downscale the original climatic dataset provided by Marta-Almeida et al. (2016), with a 9 km of spatial resolution, to Porto urban area with a 200 m of horizontal resolution. This simulation domain is shown in Figure 4-2A. The dynamical downscaling of the meteorological data from the high-resolution climatic dataset corresponding to the heat wave days to local-urban scale was performed by Carvalho et al. (2017) with the integrated WRF urban modelling system. This atmospheric modelling system provides a realistic prediction of meteorological conditions from regional scale to microscale, being this the reason why it has been widely applied to address future climate change impacts in urban environments and supporting the development of mitigation and adaptation strategies to deal with the extreme meteorological events (Chen et al., 2011). A detailed description of WRF urban modelling system can be found in Chen et al. (2011). The dynamical downscaling was also performed for the aforementioned resilience measures and a control run. The only difference between the control and the runs with resilience measures is the inclusion of a given resilient strategy. Further details of the simulations conditions can be found in Carvalho et al. (2017).

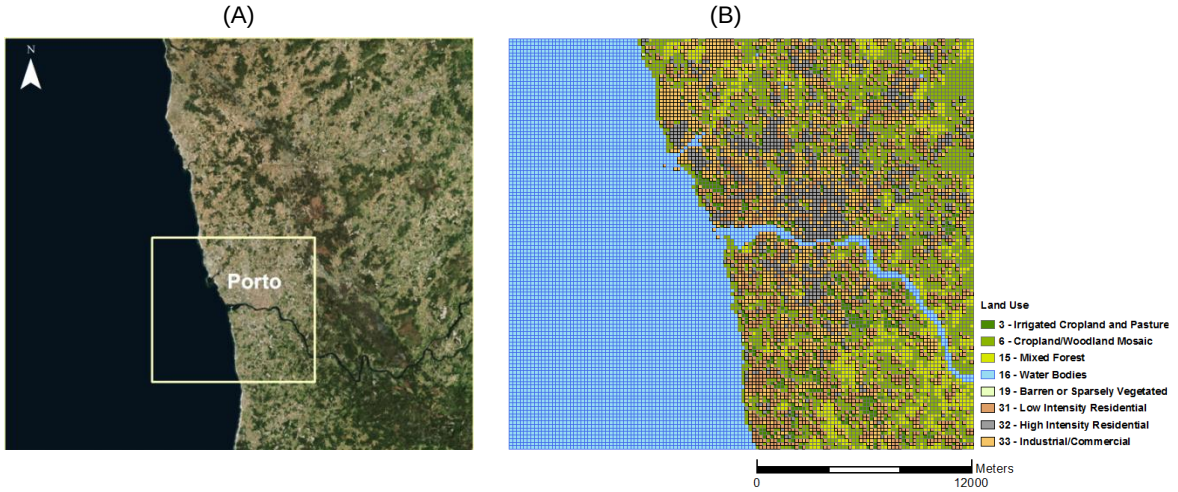

Figure 4-2. A. Innermost simulation domain - Porto urban area - with 200 m of horizontal resolution. B. Spatial distribution of the land use classification accordingly the United States Geological Survey 33-category land use dataset, obtained though the combination between the Corine Land Cover project 2006 version (CLC2006) and the European Environmental Agency Porto Urban Atlas data and subsequent remapping.

Information regarding the land use, needed for both WRF and SUEWS application, was obtained through a combination between the Corine Land Cover project 2006 version (CLC2006) and the European Environmental Agency Porto Urban Atlas, in a complementary strategy to better detail Porto Urban features. In this sense, the data from Porto Urban Atlas were used for the domain areas covered by this database, while CLC2006 was used for areas where such data were not available.

Both land use datasets were remapped to the United States Geological Survey (USGS) 33 land use categories (Figure 4-2B), which considers three different urban categories: i) High Intensity Residential, which includes highly developed areas where people reside in high numbers; ii) Low Intensity Residential, which includes areas with a mixture of built-up area and vegetation where population densities will be lower than in high intensity residential areas; and iii) Industrial/ Commercial, which includes infrastructures and all other built areas that do not fit into residential categories. The remapping of CLC2006 to UGS33 land use categories was made through an adaptation of the methodology proposed by Pineda et al. (2004), while the conversion of Porto Urban Atlas to USGS land use followed the proposed approach by Carvalho et al. (2017). Both methodologies are fully described in Carvalho et al. (2017). Besides the three different urban categories, five additional categories characterize the study area, namely: i) Irrigated Cropland and Pasture, which comprises permanently irrigated areas of crops (e.g. rice fields) or pasture (e.g. green urban areas); ii) Cropland/Woodland, characterized by a complex cultivation pattern which includes crops and forestry; iii) Mixed forest, which includes all forested areas with both evergreen and deciduous trees and neither of which predominates; iv) Water bodies, which includes areas covered by water; and v) Barren or Sparsely Vegetated, which includes areas where less than one-third of the area has vegetation or other cover.

The discretization of USGS33 land use categories in terms of paved areas, roofs, evergreen trees and shrubs, deciduous trees and shrubs, grass and water, needed for SUEWS application, was obtained through the available description of mapping categories for the Porto Urban Atlas. Additionally, satellite imagery and aerial photography (obtained in Google earth V10, Image Landset, Image IBCAO, http://www.earth.google.com [February 20, 2016]) were analysed and field based surveys were carried out, to complement the characterization. Table 4-1 summarises the surface characteristics included as input file for SUEWS application.

Table 4-1. Characteristics of the surface cover fractions for the different USGS 33 categories used as SUEWS inputs. For the land use classified as *High intensity residential* a mean building height of 12 m and a mean tree height of 4 m were considered; for the *Industrial or commercial* areas a mean building height of 6 m and a mean tree height of 4 m were considered; for all other cases a mean height of 4 m for both buildings and trees was considered. The abbreviations are defined as follow.

Build: Surface fraction of buildings; paved: paved areas; unman: unmanaged land: ET_sh: evergreen trees; DT_sh: deciduous trees; UG: non-irrigated grass; IG: irrigated grass; wtr: water.

USGS categories	**SUEWS surface characteristics**							
	build	paved	Unman	ET_sh	DT_sh	Ug	IG	Wtr
3 - Irrigated cropland and pasture	0.0	0.0	0.0	0.2	0.2	0.0	0.4	0.2
6 - Cropland/Woodland Mosaic	0.0	0.0	0.1	0.3	0.3	0.1	0.1	0.1
15 - Mixed forest	0.17	0.2	0.05	0.11	0.11	0.16	0.14	0.06
16 - Water bodies	0.02	0.02	0.02	0.02	0.02	0.0	0.0	0.9
19 - Barren or sparsely	0.0	0.0	0.6	0.1	0.1	0.1	0.1	0.0
31 - Low intensity residential	0.05	0.15	0.0	0.0	0.0	0.5	0.3	0.0
32 - High intensity residential	0.5	0.3	0.0	0.0	0.0	0.0	0.2	0.0
33 - Industrial or commercial	0.4	0.3	0.15	0.0	0.0	0.0	0.15	0.0

The meteorological conditions, land use (surface cover fractions) and its related parameters (albedo, porosity, emissivity, among others), variables related with the water movement between canopy storages and the external water use, were changed accordingly to the characteristics of the modelled scenario. The data of population density and the Objective Hysteresis Model (OHM) coefficients were kept constant. Also, information about irrigation behaviour was kept constant for all scenarios. This information was defined based in the current behaviour, through the field-based surveys, having been determined the period in which there is irrigation (starts at June and ends at September) and that this process is allowed every day of the week. Additionally, the daylight-saving times (needed for anthropogenic heat flux) were defined for the modelled future year. The daylight-saving times start at the 28th of March 2049 (88th day of year [doy]) ending at the 31st of October 2049 (305th doy). The roughness length for momentum (z_0 m) and the zero-displacement height (z_d m) were calculated from mean building and three heights with “Rule of Thumb” (Grimmond and Oke, 1999; Grimmond and Oke, 2002) in both scenarios.

Three different resilience scenarios were built using the two resilience factors previously selected (section 4.2.2). Scenario S1 comprises an increase of Porto green urban area (parks) to an area that duplicates its current dimension. For that, a new simulation domain was built, following a specific methodology. First, in the control simulation domain, the number of grid cells that had a land use category of “green urban area”, according the CLC2006 and Porto Urban Atlas data, were identified. After, the number of grid cells with this classification was duplicated and the land use category was changed to the USGS land use category 3 "Irrigated Cropland and Pasture". Scenario S2 simulates the application of white roofs in high-density residential areas (simulation domain grid cells classified as 32 with USGS land use category). For these areas, the roof surface albedo (a physical property defined as the ratio between the reflected radiation from the surface and the incident radiation) was defined as 80%, following the values defined in Susca (2012) as the albedo of a white-colour recently painted roof. Scenario S3 simulates the combination between S1 and S2 scenarios (increase urban green areas and application of white roofs).

The modelling setup was applied for all the selected heat wave episodes for the control and resilience scenarios. Since consistent results were obtained between all the heat wave episodes, the heat wave with highest extreme temperatures was selected as case study for the present work. This heat wave has a duration of 3 days and occurs from the 24th to the 26th of July 2049, reaching temperatures above 35ºC.

The confidence in the presented results is supported by the good performance of the modelling setup and the realistic results obtained in Chapter 2. As previously discussed, the modelling system was validated with measurements conducted during August-December 2014 in two different sites: an urban and a suburban area. The model setup simulates well the diurnal behaviour of the fluxes and the obtained statistics parameters are in accordance to the values achieved in past similar studies (Järvi et al., 2011, 2014). Statistics for the Q_H and Q_E modelling are generally good, for both areas, exhibiting a good relation between measured and modelled data with correlation factors around 0.7 and a NMSE of 3. There is a consistent overestimation of the sensible heat flux with a MBE of 14.7

and 51.4 $W \cdot m^{-2}$ for the suburban and the urban area, respectively. Q_E is underestimated in the urban area (negative MBE, -12 $W \cdot m^{-2}$) and overestimated (26.8 $W \cdot m^{-2}$) in the suburban area. Results showed better skills for the suburban area in comparison with the urban area.

These results are especially relevant due to the fact that modelled data are used to force SUEWS.

4.3. RESULTS AND DISCUSSION

The effects of the resilience measures on the energy balance for the selected heat wave in Porto urban area were investigated considering as reference the control run with no resilience measures. Differences in the mean energy balance components (calculated as the arithmetic mean of the hourly energy balance components for the duration of the heat wave) were analysed, considering as reference the control run.

Figures 4-3 to 4-5 show the results obtained for scenarios S1 to S3 in terms of the turbulent flux (sensible and latent heat flux, Q_H and Q_E, respectively) and the storage heat flux (ΔQ_S), respectively. The results of the anthropogenic heat flux (Q_F) - defined as the energy released by human activities - are not shown since no differences were obtained. This result was expected since the magnitude of this flux is strongly dependent on-site characteristics and the behaviour of the people in that area. In this sense, there is not a directly relation between the Q_F behaviour and the introduction of resilience measures. However, an indirect relation can be established. Changes in terms of the local temperature will have an impact on the energetic consumption, namely through the reduction of the use of air conditioning systems. Changes in the energetic consumption patterns and in its related atmospheric emissions will affect the behaviour and magnitude of Q_F.

Figure 4-3 shows the mean difference fields for S1 (duplication of the existent green urban areas).

The exchanges of sensible and latent heat between land and atmosphere occur due to air turbulent mixing and resultant heat and moisture transport (Bonan G., 2016). The behaviour and magnitude of the latent heat flux directly depends of the evaporation process (being by the definition the energy taken up/released with the phase change of water [Robinson and Henderson-Sellers, 1999]). This phenomenon is promoted by the existence of vegetation, water availability and appropriated temperatures. As a result, in this scenario, an increase of this flux is obtained (with a maximum value of around + 200 $W \cdot m^{-2}$ and an average increase in the domain of +3.3 $W \cdot m^{-2}$, when compared with the control run). This result implies that a higher proportion of solar radiation is used in the evaporative process. Thereby, two main conclusions can be drawn:

- due to the intrinsic link between the latent and sensible heat flux (mathematically expressed by the Bowen ratio - defined as the ratio of sensible and latent heat (Q_H/Q_E)) the increase of latent heat flux magnitude implies a reduction of the sensible heat flux (with a maximum reduction of up to -170 $W \cdot m^{-2}$ and an average reduction in the domain of -2.8 $W \cdot m^{-2}$), which contributes to a

reduction in the energy released into the atmosphere and consequently promotes the cooling of the surface;

- on the one hand, Q_E increment promotes a cooling effect of the air and an increase of the soil moisture, since heat from the air is being used to evaporate water. Because of that, the lower atmosphere is likely to be cold and wet. On the other hand, an increase of the evaporative rate means that more water is introduced in the system and stays available to precipitate, which in a climate change scenario where a reduction of precipitation is expected (Marta-Almeida et al., 2016), could be a key measure to mitigate the constraints related to the reduction of water availability. If more water is available for evapotranspiration, the surface moisture will increase, the canopy decreases, less energy will be dissipated as sensible heat flux, and a cooling effect of the lower atmosphere is expected.

A direct relation between the sensible heat reduction and the cooling effect of the lower atmosphere can be established since the sensible heat is energy that we can "sense", and temperature is a measure of the sensible heat content of the air. Thereby, as sensible heat in the air decreases, the temperature drops.

It should also be noted that the differences in the turbulent heat flux (latent and sensible heat flux) fields show a localized pattern, where the differences are located in the vicinity of the added green urban areas. However, the temperature decreases beneath the vegetation canopies, related with changes in the turbulent heat flux, promotes the so-called “park breeze effect”. This effect means that cool air advection will occur from the green area to the built-up surroundings, due to the pressure gradient resulting from the temperature differences between the green area (cooler) and its surroundings (warmer) (Oke et al., 1989; Carvalho et al., 2017). This fact is particularly relevant in the present case study, since in summer periods the formation and development of sea breezes is very common. The lower surface roughness of the green area will enhance the influence of the sea breeze (Papangelis et al., 2012), so that a larger built-up surrounding area will benefit from the cooler air masses.

Regarding the storage heat flux (which includes soil heat flux and also the heating and cooling of the complete urban structure), a localized decrease is obtained (with a maximum difference of -46 $W \cdot m^{-2}$). This is due to two main factors: firstly, vegetated areas have higher albedo when compared with urban areas (in the case of the study area, an average albedo of 0.13 and 0.05 is obtained for the vegetated and urban areas, respectively); secondly, the vegetated areas have a shading effect over the ground. The green areas, through the trees and shrubs, intercept and absorb solar radiation, allowing a reduction of the amount of heat that reaches the area below the tree canopy and creating shadow on the surface. Furthermore, a higher albedo means that less amount of solar radiation is absorbed by the surface, keeping it cooler (as compared with built-up areas) (Taha, 1997). As result of the reduced convective heat fluxes from cooler surfaces, the local and downwind ambient air temperatures will be lower (Taha, 1997). This cooler surface, in turn, reduces the heat transmitted between the surfaces and the atmosphere.

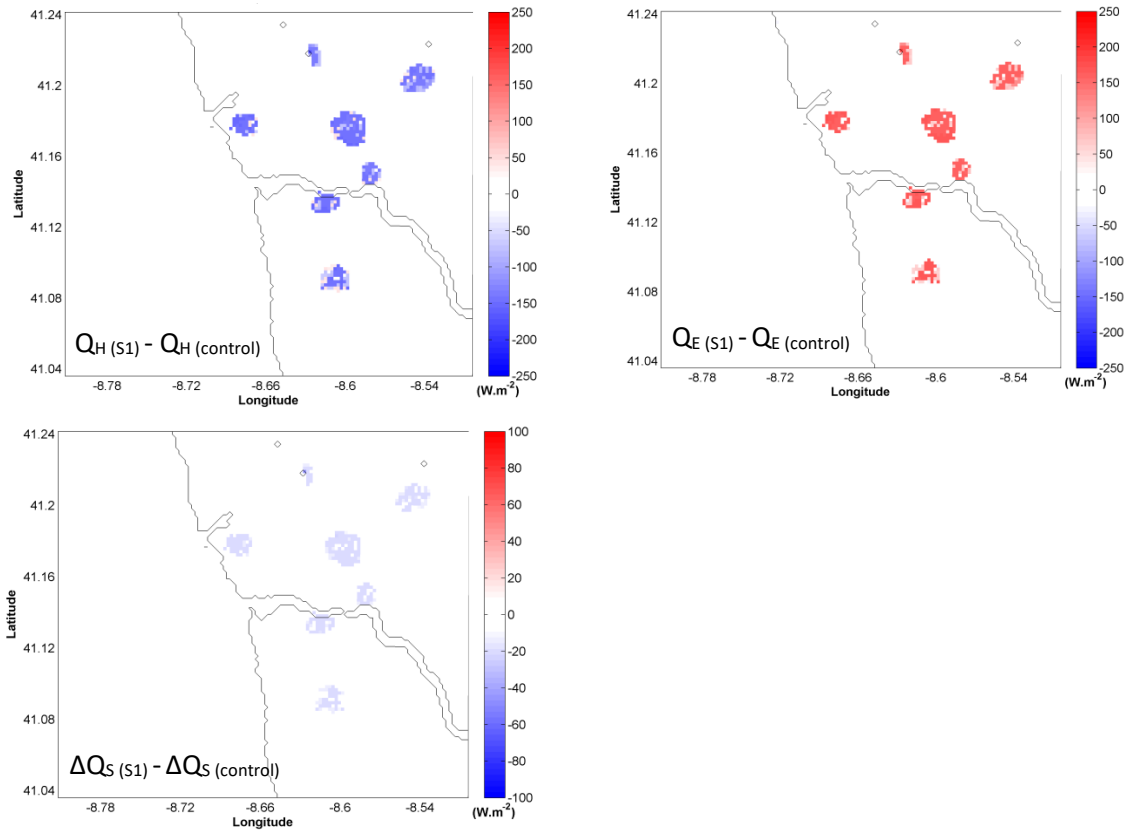

Figure 4-3. Mean difference fields for the selected heat-wave, for the turbulent fluxes of sensible (Q_H) and latent (Q_E) heat, and the storage heat flux (ΔQ_S). The difference is calculated between scenario S1 (duplication of the existent green urban areas) and the control run [S1-control run] through the arithmetic mean of the hourly energy balance components for the duration of the heat wave.

The behaviour of the energy balance components is completely different in S2 (application of white roofing) (see Figure 4-4). Since no vegetated areas were introduced, the effects of evapotranspiration and surface moisture availability are not reflected in the latent heat flux balance. Besides that, since the albedo is directly related with the amount of solar radiation absorbed by the surface, higher albedo means higher solar radiation reflectance and higher heat dispersion (Chin et al., 2008). This fact is visible in the reduction of the storage heat flux with a maximum magnitude of around -35 W·m^{-2}. Since less energy is absorbed by the surface, a reduction of the surface temperature is expected.

In urban areas, the ΔQ_S is the net uptake or release of energy by sensible heat changes in the urban canopy air layer, buildings, vegetation, and the ground (Grimmond and Oke, 1999). With a reduction of ΔQ_S, less energy will be exchanged in the form of sensible heat flux, promoting a temperature reduction. A maximum reduction of -62.8 W·m^{-2} (and an average reduction in the domain of -11.5 W·m^{-2}) is obtained for Q_H. Additionally, since less solar radiation is absorbed by the roof surface, less heat is transferred to the building bellow, so the building stays cooler and more comfortable. Such temperature reductions can bring substantial energy savings (Taha, 1997) because less energy is spent in cooling the buildings. To the extent that reduced energy demand leads to reduced burning of

fossil fuels, cool roofs contributes to fewer emissions of air pollutants (CO_2, NO_X and particulate matter) as well as, to an improvement of human health (Li et al., 2014).

Through the analysis of Figure 4-4, it is evident that the geographical distribution of both storage heat flux and sensible heat flux are coherent with the location of the high-density residential grid cells, where the albedo was increased to 80% to mimic the application of white roof coverage. It should also be noted that the white roof properties (thermal and others) are the same as the conventional roofs, with the exception of roof albedo.

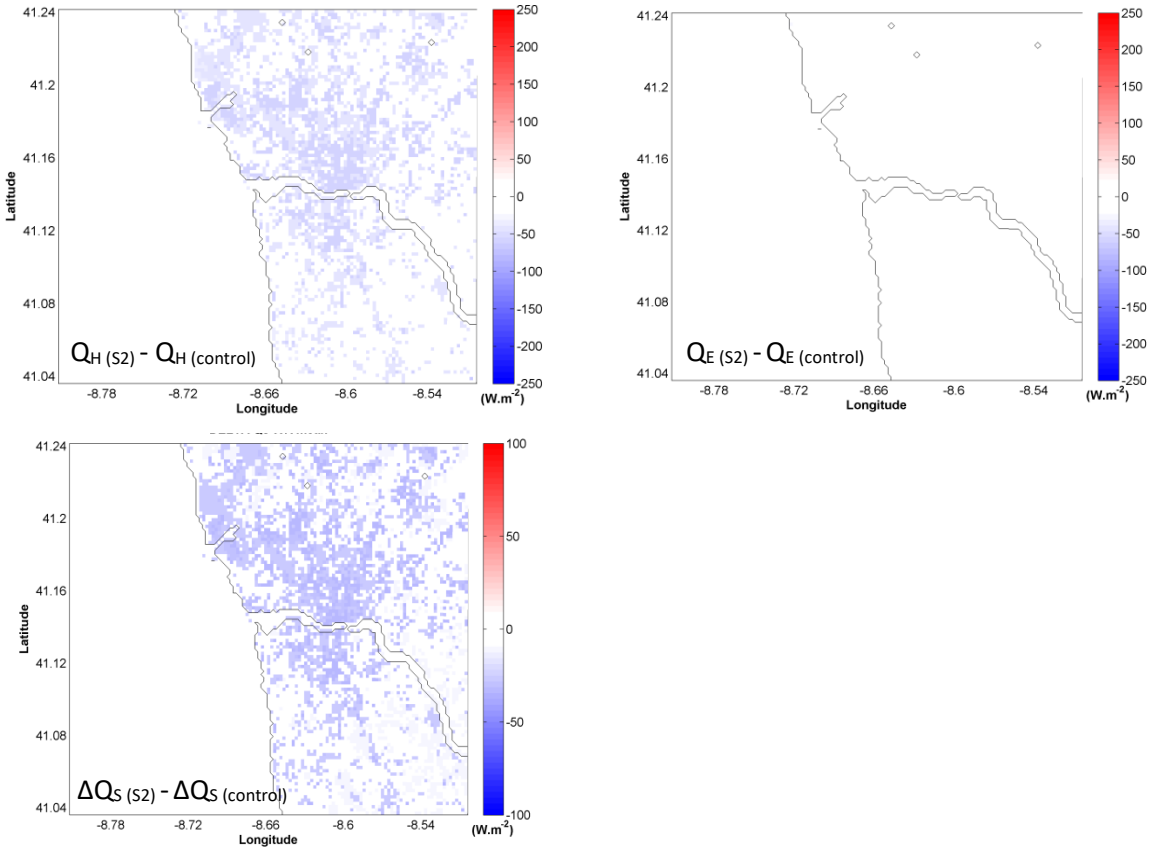

Figure 4-4. Mean difference fields for the selected heat-wave, for the turbulent fluxes of sensible (Q_H) and latent (Q_E) heat, and the storage heat flux (ΔQ_S). The difference is calculated between scenario S2 (application of white roofing) and the control run [S2-control run] through the arithmetic mean of the hourly energy balance components for the duration of the heat wave.

Figure 4-5 shows the combined effect of the resilience measures, which correspond almost linearly to the sum of the individual effects of each resilience scenarios application.

As result, the conjugation of the individual benefits related to each resilience scenario makes S3 the most effective resilience scenario, producing a clear reduction in the average Q_H and ΔQ_S field (-13.4 and -6.8 $W \cdot m^{-2}$, respectively) and an increase of Q_E (only related to the duplication of urban green areas, +2.3 $W \cdot m^{-2}$). As result, this scenario is of great effectiveness in improving the thermal comfort of the urban population, through the reduction of both mean and maximum temperature.

As highlighted by Li et al. (2014), in addition to the temperature reduction and consequent improvement of the urban population thermal comfort, the increase of green urban areas brings other advantages (not quantified in this study) such as improvements in air quality due to the photosynthesis process and to the reduction of photochemical activity (Li et al., 2010; Yang et a., 2008), as well as, a reduction in peak storm water runoff (Berndtsson, 2010), reduction of noise levels and increase of biodiversity (EEA, 2010). Additionally, the reduction of temperatures will mitigate the formation of urban smog, since its precursors are favoured by high temperatures. Also gains in the social, cultural and aesthetic issues are obtained, since vegetated areas provide a place to leisure and socialization (EC, 2015).

Moreover, the application of white roofs has the great advantage of being able to be used in dense built-up areas that may not have space for planting at the ground level. In this sense, this resilience measure is a much cheaper and simpler process than the increase of green urban areas. This fact, and the effectiveness in the Q_H and ΔQ_S reduction, shows that it is a viable, cost-effective and economically attractive approach for mitigation of urban heat waves effects.

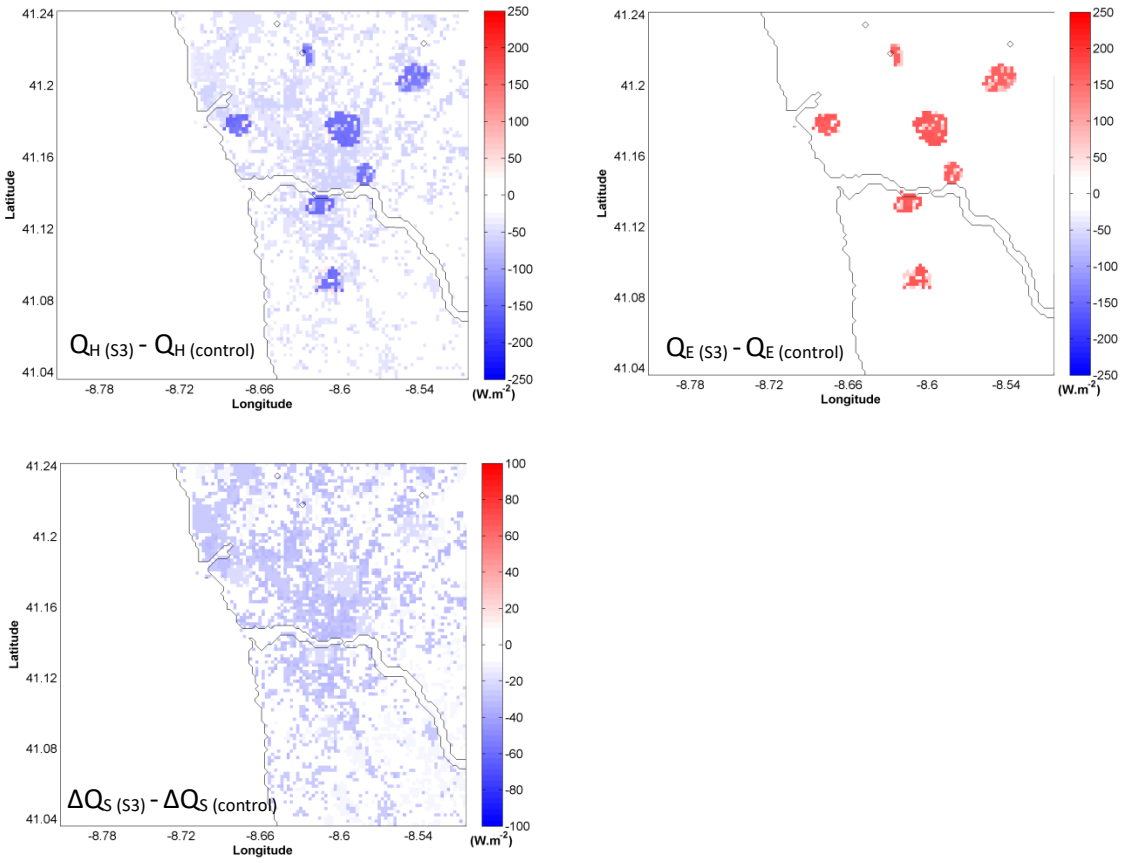

Figure 4-5. Mean difference fields for the selected heat-wave, for the turbulent fluxes of sensible (Q_H) and latent (Q_E) heat, and the storage heat flux (ΔQ_S). The difference is calculated between scenario S3 (duplication of the existent green urban areas plus the application of white roofing) and the control run [S3-control run] through the arithmetic mean of the hourly energy balance components for the duration of the heat wave.

For a more detailed analysis, the behaviour of the daily profile of Q_E, Q_H and Q_S (Figure 4-6) and its daytime energy balance was also investigated. This daily profile was obtained through the hourly average of the energy fluxes for the grid cells that are affected by the resilience measures (classified as *high intensity residential* and *green urban areas*). The results reinforce the conclusions previously discussed regarding the influence of each resilience measure in the energy fluxes (through a reduction or an increase). From the analysis of Figure 4-6 it is also evident that all the energy fluxes present the typical daily profile behaviour. For the control run, the daytime energy balance (10 a.m. – 3 p.m.) is dominated by Q* and Q_H, reaching 610 and 288 $W \cdot m^{-2}$. The majority of energy (Q* and Q_F, the latter contributing only around to 8 $W \cdot m^{-2}$), is partitioned to Q_H, accounting on average for 47% of the daytime available energy. The remaining energy is partitioned to turbulent latent and storage heat fluxes (18 and 35%, respectively).

For S2 the ordering of energy partitioning is the same; however, the magnitude of the distribution is markedly changed. Q* and Q_H reaches 382 and 156 $W \cdot m^{-2}$, respectively. Q_H, accounts on average for 40% of the daytime available energy, followed by ΔQ_S with 34% and Q_E with 26%. In contrast, for both S1 and S3 the greatest share of energy goes to Q_E, which represents more than 50% of the energy balance, followed by the storage heat flux (around 30%) and by the sensible heat flux (around 19 and 9%, respectively for S1 and S3). As result, the daytime Bowen ratio is 2.6 and 1.5 for the control run and for S2, respectively. The first value is well within the expected relation at urban areas with sparsely vegetated fraction (Grimmond and Oke 2002; Loridan and Grimmond 2012); the second is typically recorded in suburban environments (Christen and Vogt, 2004). For S1 and S3 the Bowen ratio is respectively 0.37 and 0.15, both common values over rural surfaces with vegetation canopy (Christen and Vogt, 2004). All these partitions of the daytime energy balance combine well with the surface-atmosphere exchanges arising from each of the resilience measures.

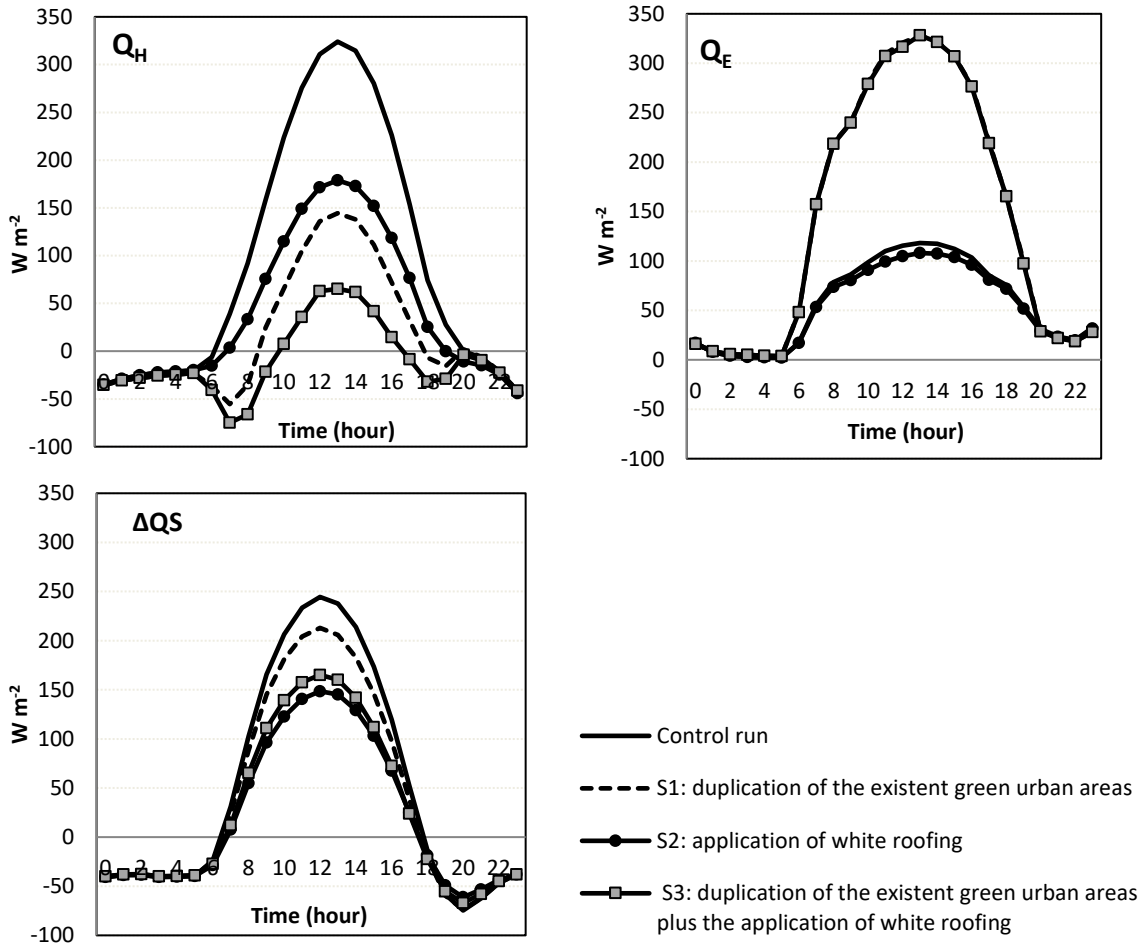

Figure 4-6. Daily average profile of the energy fluxes for the selected heat-wave and for the studied resilience measures. Q_E: latent heat flux, Q_H: sensible heat flux, ΔQ_S: net storage heat flux. S1: scenario considering the duplication of the existent green urban areas; S2: scenario considering the application of white roofing; S3: scenario considering the duplication of the existent green urban areas plus the application of white roofing.

For further clarification of the magnitude of the obtained results, a quantitatively summary of the data of all the studied resilience measures can be consulted in Table 4-2. Information regarding the minimum, mean and maximum values (estimated using a spatial average of the grid domain for the duration of the heat wave) for each energy flux is showed in Table 4-2. The values show the average behaviour of the study area, giving an idea of how the resilience measures might influence the energy fluxes of this region as a whole. In this sense, and despite of most of the changes being restricted to the area where the measures were applied, it is possible to conclude that the entire study area will benefit from the application of resilience measures. Additionally, to demonstrate the validity of the previously displayed conclusions and to show how these are strongly supported by the other four case studies, its results are also showed.

Table 4-2. Summary of the energy flux magnitude for each one of the resilience measures studied, including the control run, and for each heat waves episode. Min: minimum value obtained during the duration of each heat wave; Mean: average value obtained during the duration of heat wave; Max: maximum value obtained during the duration of each heat wave. E1, E2, E3, E4 and E5 represent the five identified heat wave episodes, being the latter, the heat wave selected to be displayed in this work.

		Resilience scenarios											
		Control Run			**S1**			**S2**			**S3**		
		Min	Mean	Max	Min	Mean	Max	Min	Mean	Max	Min	Mean	Max
E1	Q_H	-21.7	82.3	123.9	-156.7	28.9	96.6	-164.0	23.7	94.4	-159.8	22.2	94.9
	Q_E	11.3	45.4	155.3	31.4	95.6	256.5	30.3	91.1	261.4	30.6	93.6	253.6
	ΔQ_S	8.3	35.2	59.5	8.4	34.9	59.5	4.0	29.7	58.0	3.7	29.7	58.0
E2	Q_H	-5.6	68.8	113.6	-6.0	67.8	113.8	-7.3	58.7	111.8	-7.5	58.3	111.9
	Q_E	38.7	72.4	146.8	39.0	74.3	145.9	39.0	71.4	146.1	38.9	73.1	145.9
	ΔQ_S	12.4	44.7	75.9	12.4	44.8	76.0	7.4	38.5	74.1	7.3	38.7	74.2
E3	Q_H	-129.9	51.7	130.0	-129.8	49.0	129.6	-133.0	40.1	128.1	-132.5	39.2	128.6
	Q_E	34.5	112.4	293.2	34.6	115.5	292.9	33.3	109.4	292.1	34.4	113.4	292.3
	ΔQ_S	17.3	57.7	88.5	17.8	57.3	88.5	12.0	49.5	86.4	12.5	50.6	86.7
E4	Q_H	-59.2	78.7	137.5	-65.2	77.8	137.6	-63.5	68.8	135.6	-63.8	66.6	135.6
	Q_E	34.6	90.0	228.7	34.4	91.7	242.8	34.4	86.8	242.1	34.3	90.4	242.9
	ΔQ_S	21.4	56.1	96.4	21.0	60.4	96.5	15.9	53.1	94.4	15.8	53.3	94.4
E5	Q_H	-110.5	68.6	134.5	-110.2	65.8	134.0	-114.1	57.1	133.2	-114.0	55.2	132.4
	Q_E	28.3	91.7	263.8	28.7	95.0	258.6	28.9	90.7	256.2	28.7	94.0	265.6
	ΔQ_S	18.7	55.7	85.6	18.7	55.4	85.6	14.4	48.7	83.5	14.4	48.9	83.7

It is expected that the effects of the application of the tested resilience measures will vary with the synoptic/local scale weather conditions, geographical and topographical local characteristics, as well as with other characteristics of the urban areas under study (namely the properties of urban materials, the urban geometry, the anthropogenic heat, among others). Despite that, the results obtained in this study can serve as a sound and grounded case study concerning the investigation of the influence of resilient strategies in the energy balance components under climate change. Additionally, and knowing the direct relation between the heat flux and the meteorological variables, this study can also contribute to anticipate the effectiveness of these strategies to mitigate urban extreme temperatures. The described methodology can be replicated for any area in the world if the required input data (meteorological variables and land use characteristics) are available and are supplied to the modelling system.

4.4. CONCLUSIONS

The understanding of the behaviour of energy fluxes allows these to be used as a tool to evaluate the occurrence of extreme episodes. Porto (Portugal) is one of the urban areas potentially most exposed to a future increase of frequency, duration and intensity of heat waves, being an ideal case study to assess the influence of several resilience measures in the energy fluxes.

Results showed that the inclusion of green urban areas increases the evaporation and the available surface moisture, redirecting the energy to the form of latent heat flux rather than sensible heat (a maximum Q_E increase of +200 $W \cdot m^{-2}$ and a maximum Q_H decrease up to -170 $W \cdot m^{-2}$). The shading effect of vegetation and the absorption of solar radiation also promote a reduction of storage heat flux (a maximum reduction of -46 $W \cdot m^{-2}$). The application of white roofs (increases the solar radiation reflection, due to the higher albedo effect) reduces both sensible and storage heat flux (maximum reduction of -62.8 and -35 $W \cdot m^{-2}$, respectively). For all the analysed scenarios, the influence in the energy balance components is restricted to the area where the measures were applied.

The complexity of the atmosphere-biosphere system and the continuous interaction of hydrological and dynamic processes allow the prediction of the meteorological variables behaviour related to changes in the energy fluxes. As a result, it is expected that the introduction of these resilience measures will improve the urban population thermal comfort due to the reduction of both mean and maximum temperature. Additionally, other advantages such as the improvement of air quality, energy saving and reducing of peak storm water runoff have been linked to the studied resilience measures. In this sense, the most effective resilient strategy is obtained through the conjugation of the individual benefits related to each resilience scenario. Despite of that, the application of white roofs should be seen as a cost-effective and economically attractive alternative for reducing the sensible and storage heat flux, due to its low cost, simple application process and the ability to reduce the energy exchanges between the surface and the atmosphere.

This type of results shows that changes in the urban planning can influence the magnitude of the energy flux, which can directly affect the urban climate and urban sustainability. The main advantage of this approach is the study of a set of measures (through a quantification of its effectiveness) in a short period of time. Also, the approach can be applied to other cities. This is highly advantageous for policy makers and stakeholders' decision making. Such findings can be of great importance for Porto given the expected increase of extreme higher temperatures in future climate projections.

4.5. REFERENCES

Área Metroplitana do Porto, AMP.. (2008). Futuro Sustentável Plano de Acção – Síntese para consulta pública. Available on: http://www.futurosustentavel.org/fotos/gca/resumo_plano_de_accao.pdf (last access: January 2016).

Bartolomeu A.S.S., Carvalho M.J., Marta-Almeida M., Melo-Gonçalves P., Rocha A. (2015). Recent climate change trends of extreme precipitation in the Iberian Peninsula. Journal of Physics and Chemistry of the Earth.

Bell R., Cole D., Deangelo B., Desaultes L., Dickerhoff E., Estes M. Heisler G., Hitchcock D., Klunich K., Kollin C., Lewis M., Magee J., Mcpherson G., Nowak D., Rodbell P., Rosenthal J., Sarkovich M., Wolf K., Yarbrough J., Zalph B. (2008). Trees and vegetation - Reducing Urban Heat Islands: Compendium of Strategies In. US EPA. Chapter 2, 32 p.

Berndtsson J.C. (2010). Green roof performance towards management of runoff water quantity and quality: a review. Ecological Engineering 36, 351–360.

Bonan G. (2016). Turbulent fluxes. In: Ecological Climatology: Concepts and Applications (3rd edition). Cambridge University Press. ISBN: 978-1-107-04377-0.

Borrego C., Monteiro A., Martins H., Ferreira J., Fernandes A.P., Rafael S., Miranda A. I., Guevara M., Baldasano J.M. (2015). Air quality plan for ozone: an urgent need for North Portugal. Air Quality, Atmosphere & Health 9, 447-460. [doi: 10.1007/s11869-015-0352-5].

Carvalho D., Martins H., Marta-Almeida M., Rocha A., Borrego C. (2017). Urban resilience to future urban heat waves under a climate change scenario – a case study for Porto urban area (Portugal). Urban Climate 19, 1-27.

Carvalho M.J., Melo-Gonçalves P., Rocha A. (2014). CMIP5 – Performance and climate Change assessment of maximum and minimum temperatures in Europe. EMS Annual Meeting Abstracts.Vol. 11, EMS2014, 14th EMS Annual Meeting & 10th European Conference on Applied Climatology (ECAC).

Chen F., Kusaka H., Bornstein R., Ching J., Grimmond C.S.B., Grossman-Clarke S., Loridan T., Manning K.W., Martilli A., Miao S., Sailor D., Salamanca F.P., Taha H., Tewari M., Wang X., Wyszogrodzki A.A., Zhang C. (2011). The integrated WRF/urban modelling system: development evaluation and applications to urban environmental problems. International Journal of Climatology 31, 273–288,

Chin G., Desjarlais A., Estes M., HItchcock D., Lewis M., Parker D., Rosenthal J., Ross L., Ryan S., Schmeltz R., Turnbull P., ZalphB. (2008). Cool roofs. Reducing Urban Heat Islands: Compendium of Strategies In. US EPA. Chapter 4, 28 p.

Christen A., Vogt R. (2004). Energy and Radiation Balance of a Central European City. International Journal of Climatology 24, 1395-1421. [doi: 10.1002/joc.1074].

Coutts A., Beringer J., Tapper N. (2007). Impact of Increasing Urban Density on Local Climate: Spatial and Temporal Variations in the Surface Energy Balance in Melbourne, Australia. Journal of Applied Meteorology and Climatology 46, 477–493.

European Commission, EC. (2015). Towards an EU Research and Innovation policy agenda for Nature-Based Solutions & Re-Naturing Cities.Final Report of the Horizon 2020 Expert Group on 'Nature-Based Solutions and Re-Naturing Cities'.Luxembourg: Publications Office of the European Union. ISBN 978-92-79-46051-7.

European Environment Agency, EEA. (2010). The European Environment: State and Outlook 2010. Luxembourg: Publications Office of the European Union. ISBN 78-92-9213-151-7.

European Environment Agency, EEA. (2011). The application of models under the European Union's Air Quality Directive: A technical reference guide. Luxembourg: Publications Office of 579 the European Union. ISBN 978-92-9213-223-1.

Flerchinger G., Reba M., Marks D. (2012). Measurement of Surface Energy Fluxes from Two Rangeland Sites and Comparison with a Multilayer Canopy Model. Journal of Hydrometeorology 13, 1038-1051.

Fonseca D., Carvalho M.J., Marta-Almeida M., Melo-Gonçalves P., Rocha A. (2016). Recent trends of extreme temperature indices for the Iberian Peninsula. Physics and Chemistry of the Earth 94, 66-76. [doi: 10.1016/j.pce.2015.12.005].

Grimmond C.S.B., Oke T.R. (1986). Urban water balance 2: results from a suburb of Vancouver, British Columbia. Water Resources Research 22, 1404-1412.

Grimmond C.S.B., Oke T.R. (1991). An evaporation-interception model for urban areas. Water Resources Research 27, 1739-1755.

Grimmond C.S.B., Oke T.R. (1999). Heat storage in urban areas: local-scale observations and evaluation of a simple model. Journal of Applied Meteorology and Climatology 38, 922–940.

Grimmond C.S.B., Oke T.R. (2002). Turbulent Heat Fluxes in Urban Areas: Observations and a Local-Scale Urban Meteorological Parameterization Scheme (LUMPS). Journal of Applied Meteorology and Climatology 41, 792–810.

Grimmond C.S.B., Blackett M., Best M.J., Barlow J., Baik J.J., Belcher S.E., Bohnenstengel S.I., Calmet I., Chen F., Dandou A., Fortuniak K., Gouvea M.L., Hamdi R., Hendry M., Kawai T., Kawamoto Y., Kondo H., Krayenhoff E.S., Lee S.H, Loridan T., Martilli A., Masson V., Miao S., Oleson K., Pigeon G., Porson A., Ryu Y.H, Salamanca F., Shashua-Bar L., Steeneveld G.J, Tombrou M., Voogt J.A., Young D.T., Zhang N. (2010). The International Urban Energy Balance Models Comparison Project: First Results from Phase 1. Journal of Applied Meteorology and Climatology 40, 1268-1292.

Grimmond C.S.B, Blackett M., Best M.J., Baik J.J., Belcher S.E., Beringer J., Bohnenstengel S.I., Calmet I., Chen F., Coutts A., Dandou A., Fortuniak K., Gouvea M.L., Hamdi R., Hendry M., Kanda M., Kawai T., Kawamoto Y., Kondo H., Krayenhoff E.S., Lee S.H., Loridan T., Martilli A., Masson V., Miao S., Oleson K., Ooka R., Pigeon G., Porson A., Ryu Y.H., Salamanca F., Steeneveld G.J., Tombrou M., Voogt J.A., Young D.T., Zhang N. (2011). Initial results from Phase 2 of the international urban energy balance model comparison. International Journal of Climatology 31, 244-272.

Intergovernmental Panel on Climate Change, IPCC. (2013). Climate Change 2013: The Physical Science Basis. Contribution of Working Group I to the Fifth Assessment Report of the Intergovernmental Panel on Climate Change [Stocker, T.F., D. Qin, G.-K. Plattner, M. Tignor, S.K. Allen, J. Boschung, A. Nauels, Y. Xia, V. Bex and P.M. Midgley (eds.)]. Cambridge University Press, Cambridge, United Kingdom and New York, NY, USA, 1535 pp. [doi:10.1017/CBO9781107415324].

Instituto Nacional de Estatística, INE (Statisical of Portugal). (2011). Censos 2011 Resultados Definitivos - Região Norte. Instituto Nacional de Estatística (in Portuguese), I.P. ISSN 0872-6493. ISBN 978-989-25-0186-4. Available on: file:///C:/Users/sandra.rafael/Downloads/Censos2011_RDefinitivos_Norte_3.pdf (last access: January 2016).

Jacobson M., Hoeve J. (2012). Effects of Urban Surfaces and White Roofs on Global and Regional Climate. Journal of Climate 25, 1028-1044.

Järvi L., Grimmond C.S.B., Christen A. (2011). The Surface Urban Energy and Water Balance Scheme (SUEWS): Evaluation in Los Angeles and Vancouver. Journal of Hydrology 411, 219-237. ISSN 0022-1694.

Järvi L., Grimmond C.S.B., Taka M., Nordbo A., Setala H., Strachan I.B. (2014). Development of the Surface Urban Energy andWater balance Scheme (SUEWS) for cold climate cities. Geoscientific Model Development 7, 1691-1711. ISSN 991-959X.

Lau K.K., Lindberg F., Rayner D., Thorsson S. (2015). The effect of urban geometry on mean radiant temperature under future climate change: a study of three European cities. International Journal of Biometeorology 59, 799-814.

Leichenko R. (2011). Climate change and urban resilience.Current opinion in Environmental Sustainability 3 164-168.

Li D., Bou-Zeid E. (2013). Synergistic Interactions between Urban Heat Islands and Heat Waves: The Impact in Cities Is Larger than the Sum of Its Parts. Journal of Applied Meteorology and Climatology 52, 2051-2064. [doi: 10.1175/JAMC-D-13-02.1].

Li D., Bou-Zeid E., Oppenheimer M. (2014). The Effectiveness of Cool and Green Roofs as Urban Heat Island Mitigation Strategies. Environmental Research Letters 9. ISSN 17489326.055002.

Li J.F., Wai O.W.H., Li Y. S., Zhan J.M., Ho Y.A., Li J., Lam E. (2010). Effect of green roof on ambient CO_2 concentration. Building and Environment 45, 2644–51.

Litzke B., Vogt R., Young D.T., Grimmond C.S.B. (2015). Physical Fluxes in the Urban Environment. In: Understanding Urban Metabolism: A Tool for Urban Planning. Ed. Chrysoulakis, N., Castro, E. A. and Moors, E. J. Taylor & Francis: London. ISBN 978-0415835114.

Lopes M., Rafael S., Martins H., Borrego C. (2015). Quantificação e mapeamento de fluxos de calor na cidade do Porto: aplicação do modelo de balanço energético e hídrico. XVII Encontro da Rede de Estudos Ambientais de Países de Língua Portuguesa. 7-12 September 2015, Cabo Verde.

Loridan T., Grimmond C.S.B. (2012). Characterization of Energy Flux Partitioning in Urban Environments: Links with Surface Seasonal Properties. Journal of Applied Meteorology and Climatology 51, 219–241.

Kharin V., Zwiers F.W. (2000). Changes in the extremes in an ensemble of transient climate simulations with a coupled atmosphere-ocean GCM.Journal of Climate 13, 3760-3788.

Marta-Almeida M., Teixeira J., Carvalho M., Melo-Gonçalves P., Rocha A. (2016). High resolution climatic simulations for the Iberian Peninsula: Model validation. Physics and Chemistry of the Earth 94, 94-105.

McCarthy M., Best M., Betts R. (2010). Climate change in cities due to global warming and urban effects. Geophysical Research Letters 37, 5p.

Monteiro A., Carvalho V., Velho S.,Sousa C. (2012a). Assessing and monitoring urban resilience using COPD in Porto. Science of the Total Environment 414, 113-119.

Monteiro A., Fonseca L., Almeida M., Sousa M., Velho S., Carvalho V. (2012b). Atlas da saúde e da doença – Vulnerabilidades climáticas e socioeconómicas: Grande Área Metropolitana do Porto – Concelho do Porto (Atlas of health and sickness – climatic and socio-economic vulnerabilities in the Greater Metropolitan Area of Porto and Concelho of Porto – in Portuguese). – PROJECTO ONDAS (PTDC/SAUESA/73016/2006), FCT – COMPETE I and II.

Monteiro A., Ribeiro I., Tchepel O., Carvalho C., Martins H., Sá E., Ferreira J., Martins V., Galmarini S., Miranda A.I., Borrego C. (2013a). Ensemble techniques to improve air quality assessment: focus on O_3 and PM. Environmental Modelling & Assessment 19, 249-257.

Monteiro A., Carvalho V., Oliveira T., Sousa C. (2013b). Excessmortality and morbidity during the July 2006 heat wavein Porto, Portugal.International Journal of Biometeorology, 57 (1), 155-167.

Monteiro A., Velho S. (2014). Health heat stress in the PortoMetropolitan Area – a matter of temperature or inadequate adaptation? Journal of the Geographical Society of Berlin 145, 80-95. [doi: 10.12854/erde-145-7].

Monteiro A., Ferreira J., Ribeiro I., Fernandes A.I., Martins H., Gama C., Miranda A.I. (2015). Air quality over Portugal in 2020.Atmospheric Pollution Research 6, 788-796.

Offerle B., Grimmond C.S.B., Fortuniak K. (2005). Heat storage and anthropogenic heat flux in relation to the energy balance of a central European city centre. International Journal of Climatology 25, 1405-1419.

Oleson K.W., Bonan G.B., Feddema J. (2010). Effects of white roofs on urban temperature in a global climate model. Geophysical Research Letters 37. [doi:10.1029/2009GL042194].

Oke T.R. (1982). The energetic basis of the urban heat island. Quarterly Journal of the Royal Meteorological Society 108, 1-24.

Oke T.R. (1987). Boundary Layer Climates. Routledge, London, UK.

Oke T.R., Cleugh H.A. (1987). Urban heat-storage derived as energy-balance residuals. Bound-Layer Meteorology 39, 233-245.

Oke T.R., Crowther J.M., McNaughton K.G., Monteith J.L, Gardiner B. (1989). The micrometeorology of the urban forest [and discussion]. Philosophical Transactions of the Royal Society of London Series B Biological Sciences 324, 335-349.

Papangelis G., Tombrou M, Dandou A., Kontos T. (2012). An urban “green planning” approach utilizing the Weather Research and Forecasting (WRF) modeling system. A case study of Athens, Greece. Landscape and Urban Planning 105, 174-183.

Park S., Deser C., Alexander M. (2005). Estimation of the Surface Heat Flux Response to Sea Surface Temperature Anomalies over the Global Oceans. Journal of Climate 18, 4582-4599.

Pineda N., Jorba O., Jorge J., Baldasano J.M. (2004). Using NOAA AVHRR and SPOT VGT data to estimate surface parameters: application to a mesoscale meteorological model. International Journal of Remote Sensing 25, 129–143.

Rizwan A.M., Dennis L., Liu C. (2008). A review on the generation, determination and mitigation of Urban Heat Island. Journal of Environmental Sciences 20, 120-128.

Robinson P., Henderson-Sellers A. (1999). Contemporary Climatology (2nd Edition). Published by Prentice Hall.ISBN 0582276314.

Rosenzweig C., Solecki W., Hammer S., Mehrotra S. (2011). Climate Change and Cities - First Assessment Report of the Urban Climate Change Research Network. Published in the United States of America by Cambridge University Press, New York. ISBN 978-1-107-00420-7 Hardback.

Russo S., Dosio A., Graversen R.G., SillmannJ..Carrao H., Dunbar M.B., Singleton A., Montagna P., Barbola P., Vogt J.V. (2014). Magnitude of extreme heat waves in present climate and their projection in a warming world. Journal of Geophysical Research: Atmospheres 119, 500-512.

Sá E., Martins H., Ferreira J., Marta-Almeida M., Rocha A., Carvalho A., Freitas S., Borrego C. (2016). Climate change and pollutant emissions impacts on air quality in 2050 over Portugal. Atmospheric Environment. 131, 209-224.

Santos J., Corte-Real, J. (2006). Temperature extremes in Europe and wintertime large-scale atmospheric circulation: HadCM 3 future scenarios. Climate Research 3, 3-18.

Sedlar J., Hock R. (2009). Testing longwave radiation parameterizations under clear and overcast skies at Storglaciären, Sweden. Cryosphere 3, 75-84.

Skamarock W.C., Klemp J.B., Dudhia J., Gill D.O., Barker D.M., Huang X.Y. (2008). A description of the advanced research WRF Version 3. NCAR Technical Note, Mesoscale and Microscale Meteorology Division of NCAR.

Synnefa A., Dandou A., Santamouris M., Tombrou M., Soulakellis N. (2008). On the use of cool materials as a heat island mitigation strategy. Journal of. Applied Meteorology and Climatology 47, 2846-2856.

Susca T. (2012). Enhancement of life cycle assessment (LCA) methodology to include the effect of surface albedo on climate change: Comparing black and white roofs. Environmental Pollution 163, 48-54.

Taha H. (1997). Urban climates and heat islands: albedo, evapotranspiration and anthropogenic heat. Energy and Buildings 25, 99-103.

Taylor K.E., Stouffer R.J., Meehl G.A. (2012). An overview of CMIP5 and the experiment design. Bulletin of the American Meteorological Society 93, 485–498.

Twigg, J. (2009). Characteristics of a Disaster-Resilient Community: A Guidance Note. DFID Disaster Risk Reduction Interagency Coordination Group.

URL1. URBANFLUXES Newsletter. Urban Anthropogenic Heat Flux from Earth Observation Satellites. Issue 1. Editorial by Nektarios Chrysoulakis. Available at: http://urbanfluxes.eu/ [Last access: May 2016].

Van Engelen, A., Klein Tank, A., Van Der Schrier, G. and Klok, L. (2008). European Climate Assessment & Dataset (ECA&D). Report 2008 'Towards an operational system for assessing observed changes in climate extremes'.KNMI, De Bilt, Netherlands.

Watkiss P., Horrocks L., Pye S., Searl A., Hunt A. (2009). Impacts of climate change in human health in Europe. PESETA-Human health study.Office for Official Publications of the European Communities, Luxembourg.

Yang J., Wang Z-Hu, Chen F., Miao S., Tewari M., Voogt J.A., Myint S. (2015). Enhancing Hydrologic Modelling in the Coupled Weather Research and Forecasting - Urban Modelling System. Boundary-Layer Meteorology 155, 87-109

Yang J., Yu Q., Gong P. (2008). Quantifying air pollution removal by green roofs in Chicago. Atmospheric Environment 42, 7266–73.

CHAPTER 5

This Chapter has been submitted as:

Rafael S., Rodrigues V., Fernandes A.P., Borrego C., Lopes M. (submitted to publication). *Evaluation of urban surface parameterizations in WRF model using energy fluxes measurements in Portugal*. Urban Climate.

The author acknowledges the co-authors critical revision. An acknowledgement to Professor Casimiro Pio and his team for providing the meteorological measured data used in this work.

5. Evaluation of urban surface parameterizations in WRF model using energy fluxes measurements in Portugal

Abstract

The performance of WRF model was investigated for the simulation of urban microclimate, with particular focus on energy fluxes, using different urban surface parameterizations. The model performance was evaluated using measurements carried out between August and December 2014 in Portugal. Several simulations were performed over two different areas, Porto urban area and Aveiro suburban area in Northern Portugal, for the entire measurement period. Distinct simulations were performed using distinct urban parametrizations: i) the Noah Land Surface Model (original LSM); ii) a single-layer urban canopy model (UCM); and iii) a modelling system composed by WRF and SUEWS models (WRF-SUEWS).

The results show a good agreement between UCM simulation and the measurements over the low and high intensity residential areas, reducing the systematic model biases in the LSM simulation by 1–2°C in air temperature and by 0.5–1 $m \cdot s^{-1}$ in wind speeds at near surface layer, on average. UCM is able to reproduce the differences in the near surface air temperature, wind speeds and vertical wind profile related with distinct land use covers. The analysis performed show that a more accurate turbulent energy partitioning (sensible and latent heat) contributed to enhance the UCM simulation results. LSM results showed a significant underestimation of latent heat flux (-30 $W \cdot m^{-2}$, on average) and an overestimation of sensible heat flux (28 $W \cdot m^{-2}$, on average). SUEWS model show a good ability to represent energy fluxes at the low intensity residential area, while within the high intensity residential area the model presented some limitations. The overall results suggest that an appropriate land use surface representation (e.g. surface morphology, urban vegetation) followed by explicit parameterizations of the urban physical processes are crucial to improve numerical tools suited for the modelling of the urban atmospheric boundary layer.

Keywords: Energy fluxes, Meteorological variables, Numerical modelling, Urban areas

5.1. INTRODUCTION

Nowadays, worldwide about 54% of citizens live in cities, while cities only occupy less than 0.1% of the entire Earth's surface (UN, 2014). In addition, the levels of urbanization greatly vary across different regions – for instance in Europe the population living in urban areas was about 73% in 2014 (UN, 2014). The continuous urban growth of the last decades lead to a replacement of natural surfaces (e.g. grassland, forest) by impervious surfaces (e.g. buildings, roads) (Lee et al., 2011). These changes will likely continue, since it is expected that more than 60% of the global population will reside in urban areas by 2050 (UN, 2014). The changes in the land use alters the urban energy balance and the atmospheric boundary layer structure, which linked with anthropogenic emissions and anthropogenic heat released by human activities, significantly influence local microclimate (Lee et al., 2011). In turn, citizens are particularly vulnerable to the meteorological and environmental changes such as climate change and poor air quality.

As the urban growth proceeds and cities becomes larger, hotter and more polluted, the need for accurate weather and air quality at the urban scale becomes crucial (Barlow, 2014). Besides that, in the face of climate change impacts at urban scale, the need of consider sustainable designs (e.g. increasing green infrastructures) and planning of cities stands up, and so the choose of the most appropriate solution should consider the effects in the urban microclimate (as discussed in Chapter 4). In this sense, further progress in modelling thermal comfort, city ventilation, and air quality depends on the integration of urban representations into mesoscale models and, mainly, on the accuracy level of modelling the urban processes (Barlow, 2014).

Over the last decade, numerical modelling has progressed to reproduce in a more realistic way the physical process occurring in urban areas (Masson, 2000; Martilli et al., 2002, 2007; Baklanov et al., 2009). To achieve this progress, a set of urban parameterizations, with different levels of complexity, have been proposed (Li et al., 2016). Masson (2006) has classified urban parameterizations into three main categories:

- Empirical models that calculate fluxes based on statistical fitting to measurements (e.g., assuming the storage heat flux as a fixed fraction of the net radiation). The application of this type of models are usually limited to areas where the measurements were taken;
- Modified Land Surface Models (LSMs), originally designed for natural vegetated or bare soil surfaces, being then modified to represent urban landscapes (e.g., albedo, emissivity, heat capacity, thermal conductivity, and roughness length). Although these modifications, it has been shown that these models are still unable to capture urban fluxes (Grimmond et al., 2010, 2011) and the urban heat island effect (Lee et al., 2011; Zhang et al., 2011);
- Urban Canopy Models (UCMs) that in general, better represent the unique urban characteristics (e.g., multiple reflections of radiation among buildings). As result they are receiving more attention despite the usual large number of input data requirements.

The development of multiples urban parameterization schemes led to the first International Urban Energy Balance Comparison Project (Grimmond et al., 2010, 2011) which has represented a great

collective effort to compare modelled fluxes using 32 different urban parameterization schemes with high quality observations. The main outcomes of the project can be summarized in five main issues: i) no single model had the best performance across all turbulent fluxes, and the results were highly sensitive to the quality of input data (e.g., thermal characteristics of urban materials, morphology of buildings), which is often difficult to obtain; ii) the more complex schemes, such as UCMs, have more potential for improvements as compared to simple models whose performance is more dependent on parameters calibration; iii) all the models had its best performance in modelling net radiation, but they substantially overestimated the sensible heat flux and underestimated the latent heat flux; iv) the models had the poorest performance for the latent heat flux modelling, showing higher biases; and v) highlights the importance of accurate representation of vegetation in correctly modelling the partitioning of the turbulent fluxes; this is especially important for modelling urban boundary layer (UBL) dynamics, since the growth rate and depth of the UBL is determined primarily by the sensible heat flux.

The Weather Research and Forecasting (WRF) used in this study is a three dimensional, compressible and non-hydrostatic meteorological model (Skamarock et al., 2008). WRF model have being widely used around the world in a wide range of applications and research (e.g. numerical weather prediction, regional climate, air quality). Three urban parameterizations with different complexity level are implemented in the WRF model: the bulk urban parameterization (Liu et al., 2006); the single-layer urban canopy model (Kusaka et al., 2001) and the multi-layer urban canopy model (Martilli et al., 2002). This last one has the most complex parameterizations of urban physical processes but requires the most detailed information of urban morphology for input parameters. Despite the efforts of the last decade, further investigations are needed to accurate urban parameterization schemes, especially through the use of measured urban energy fluxes for validation (Mestayer et al., 2005; Rotach et al., 2005; Chen et al., 2011). In the case of WRF, one key requirement for urban applications is to accurately capture the influences of cities on local meteorology (Chen et al., 2011).

The main goal of this study is to assess the performance of three different urban parameterizations on the modelling of local energy fluxes. The bulk urban parameterization and the single-layer urban canopy model are evaluated as well as an individual/independent urban energy balance model, the Surface Urban Energy and Water Balance Scheme (SUEWS) (version 2014b). An analysis of how these urban parameterizations influence the accuracy of meteorological modelling is also made. This Chapter is presented as follows, Section 5.2 describes the WRF meteorological model, its configuration for the simulations, and the urban surface parameterizations evaluated. Also in Section 5.2 is addressed the measurements used for the model performance evaluation. Comparison between the measurements and the model simulations are present in Section 5.3. Summary and conclusions follow in Section 5.4.

5.2. DATA AND METHODS

5.2.1. Model description and configuration

5.2.1.1. WRF model and configuration

The WRF model, version 3.7.1, was set up with five domains (see Figure 5-1). The outer domain (D1), covering Europe and North of Africa, has 173x142 horizontal grid cells with horizontal resolution of 27 km; the nested domain D2 covers the Iberian Peninsula and has a 175×166 horizontal grid cells with a horizontal resolution of 9 km; and D3 covers the Northwest of Portugal and has 121×109 horizontal grid cells with a horizontal resolution of 3 km. The two inner domains (D4 and D5) have 34×34 horizontal grid cells with horizontal resolution of 1 km, covering the Porto urban area [high intensity residential area] and Aveiro suburban area [low intensity residential area], respectively (Figure 5-1). The vertical grid was composed by 30 vertical layers up to the top of the computational domain (50 hPa). The two-way nesting technique was applied for the simulations (Skamarock et al., 2008). The Dudhia shortwave radiation scheme (Dudhia, 1989) and the RRTM (Rapid Radiative Transfer Model) longwave radiation scheme (Mlawer et al., 1997) were also used. The Yonsei University (YSU) scheme (Hong et al., 2006) was used to calculate the vertical turbulent mixing of momentum and scalars. The YSU scheme has been widely applied to meteorological and environmental modelling due to its performance in a well-mixed atmospheric boundary layer and computational efficiency. Grid-scale clouds were resolved using the WRF single moment 5-class scheme (Hong et al., 2004), while subgrid-scale convective clouds (cumulus parameterization scheme) for higher resolution domains (D1, D2 and D3) were parameterized by the new Grell scheme (Grell, 1993; Grell and Devenyi, 2002). The modelling setup of the WRF model for the simulations is listed in Table 5-1.

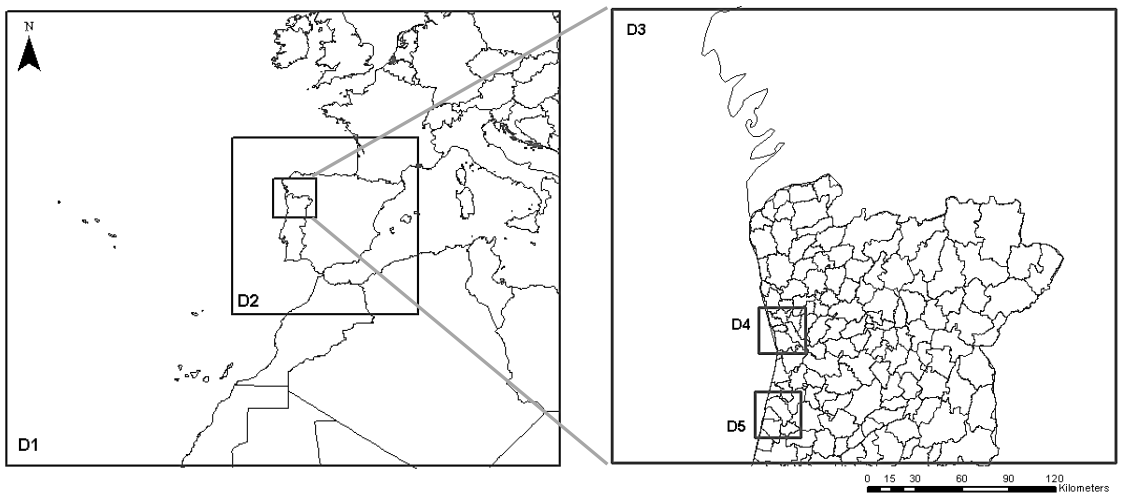

Figure 5-1. Configuration of the WRF model domains. Horizontal resolution of the coarse domain is 27 km with 173x142 horizontal grid cells (D1). The inner domains have a horizontal resolution of 1 km, both with 34x34 horizontal grid cells (D4 and D5).

Table 5-1. Modelling setup for the WRF simulations.

Category	Setup	Reference
Micro Physics Options	WSM 5-class scheme	Hong et al. (2004)
Shortwave radiation	Dudhia scheme	Dudhia (1989)
Longwave radiation	RRTM scheme	Mlawer et al. (1997)
Turbulence	YSU Planetary Boundary Layer scheme (YSU PBL)	Hong et al. (2006)
Land surface process	Noah Land Surface Model	Chen and Dudhia (2001)
Cumulus Parameterization Options	New Grell scheme (only for the D1, D2 and D3)	Grell (1993); Grell and Devenyi (2002)
Horizontal spacing	D1: Δx=Δy= 27 km (173x142) D2: Δx=Δy= 9 km (175x166) D3: Δx=Δy= 3 km (121x109) D4: Δx=Δy= 1 km (34x34) D5: Δx=Δy= 1 km (34x34)	-
Vertical spacing	30 vertical levels Lowest level: 10 m, model top level: 50hPa	-

The meteorological initial and boundary conditions was initialized with ERA-Interim data from the European Centre for Medium-Range Weather Forecasts (ECMWF) global analysis (horizontal resolution of 1° x 1º) with a temporal resolution of 6-h intervals. The sea surface temperatures and the soil moisture were also initialized using the ECMWF data. Information regarding the land use/land cover was taken from the Corine land cover project (Büttner et al., 2006) 2006 version (CLC2006), with a 3 arc-seconds horizontal resolution, remapped to the United States Geological Survey (USGS) 33 land use categories, following the methodology proposed by Pineda et al. (2004). The USGS 33 considers 3 different urban categories: High Intensity Residential, which includes highly developed areas where people reside in high numbers (apartment complexes, row houses, etc.); Low Intensity Residential, which includes areas with a mixture of constructed materials and vegetation where population densities will be lower than in high intensity residential areas (single-family housing units, etc); Industrial/Commercial, which includes infrastructures (roads, railroads, airports, harbours, etc.) and all other built areas that do not fit into residential categories. The analysis is focused on two Portuguese cities (D4 and D5) (Figure 5-2).

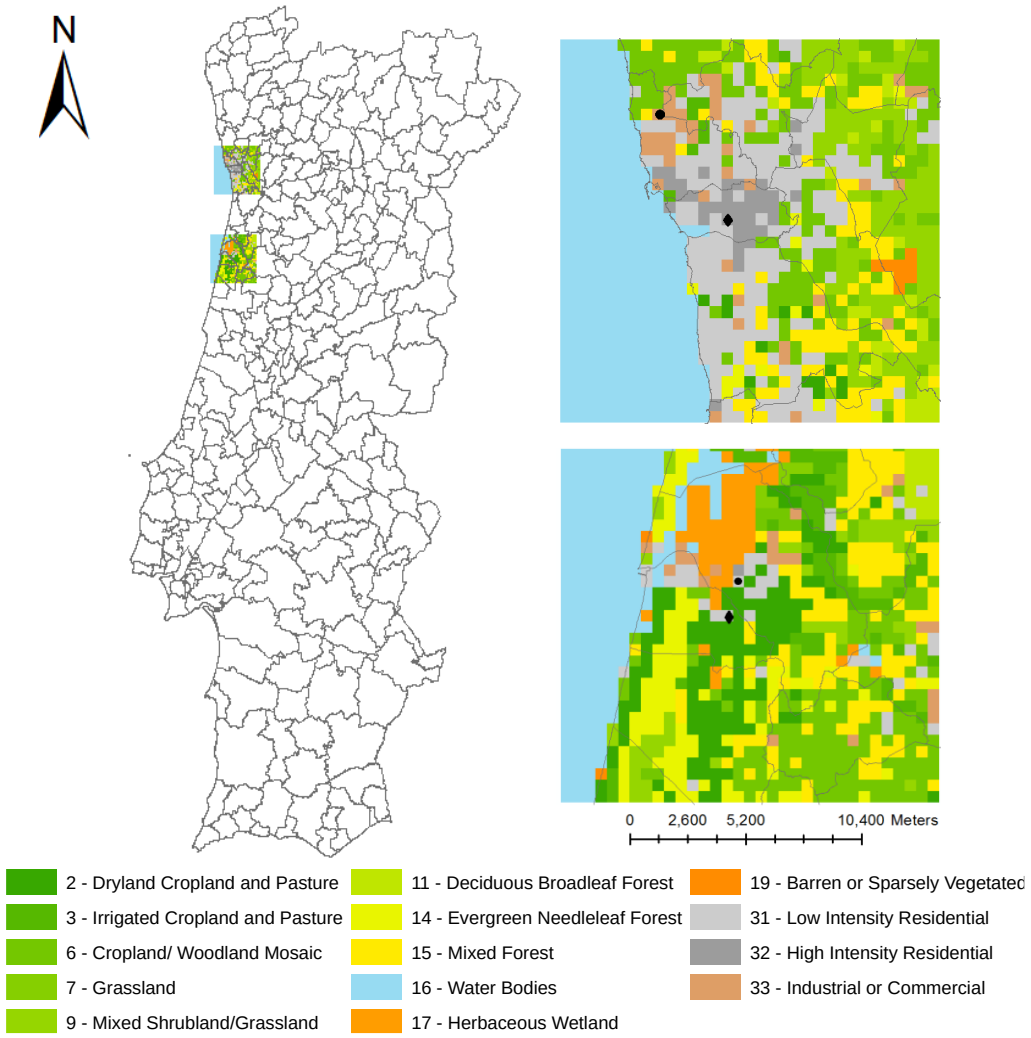

Figure 5-2. Spatial distribution of dominant land-use types in the inner domains (D4 [right top figure] and D5 [right bottom figure]). The geographical locations of meteorological sites (solid circle) and surface energy fluxes sites (solid diamond) are shown.

A set of simulations using different urban surface parameterizations were conducted for a five-month period (August-December of 2014), corresponding to the period of a flux measurement field campaign carried out in two Portuguese cities (see section 5.2.2).

5.2.1.2. Urban surface parameterizations

The different urban surface parameterizations analysed in this study comprises the Noah Land Surface Model (LSM) (Chen and Dudhia, 2001), the Single Layer Urban Canopy Model (SLUCM) (Chen et al., 2011), and the Surface Urban Energy and Water Balance Scheme (SUEWS) version 2014b (Järvi et al., 2011, 2014). The two first models are implemented as a WRF model module, whereas SUEWS is an individual model.

Noah Land Surface Model (LSM)

The Noah Land Surface Model (hereafter LSM for simplicity) provides physical boundary conditions to the WRF model, calculating, on the one hand, turbulence exchanges of momentum, mass and energy between the surface and the atmosphere for governing equations; and, on the other hand, surface temperature, albedo and emissivity for radiative transfer equations. The land surface at each grid cell is represented by land-use and soil, for which the LSM has 33 categorized land-use types and 16 soil categories. Each land use type is characterized by the physical and aerodynamic parameters such as surface roughness length and displacement height, albedo, emissivity, green vegetation fraction and leaf area index (LAI). Each soil categories are characterized in terms of soil heat conductivity and diffusivity, maximum soil moisture content and wilting point soil moisture. The LSM has one canopy layer and four soil layers (total soil depth of 2 m) from the ground surface down to the bottom (Sridhar, et al., 2002). The bulk urban parameterization is based on the approach described by Liu et al. (2006), namely that the physical parameterization for an urban area is identical to that for vegetation types. This means that the LSM does not parameterize urban physical processes explicitly, but it aims to reproduce urban effects by modifying the given values of vegetation and soil parameters for an urban area (Lee et al., 2011).

Single layer urban canopy model (UCM)

The single layer urban canopy model (hereafter UCM) was developed by Kusaka et al. (2001) and Kusaka and Kimura (2004), and it is available as a WRF model module, which coupling is made through the LSM. The UCM have being wide used to simulate meteorological conditions from regional to urban scales due to the realistic coupling between synoptic/mesoscale and urban/microscale meteorology. The UCM take into account the impacts of urban areas morphology, considering the following characteristics (Lee et al., 2011): i) two-dimensional street canyons are parameterized to represent the effects of urban geometry on urban canyon heat distribution; ii) shadow from buildings and reflection of radiation in the canopy layer; iii) canyon orientation and diurnal cycle of solar azimuth angle; iv) urban surfaces (roof, walls and roads) are resolved with different orientations; v) Inoue's model for canopy flows; vi) the multilayer heat equation for the roof, wall, and road interior temperatures; and vii) a very thin bucket model for evaporation and runoff from road surface. The UCM considers subgrid-scale inhomogeneous surface fluxes using a "tile" approach (Avissar and Pielke, 1989; Chen et al., 2004). This means that for a given grid cell the LSM calculates the surface fluxes for natural areas (trees, parks, etc.) whereas the UCM provides the surface fluxes for the artificial surface (Chen et al., 2011). This approach can be described as follow:

$$F = F_{urb} \times f_{urb} + F_N \times (1-f_{urb}) \quad (5.1)$$

where, F is the total surface flux; f_{urb} is the fractional coverage of impervious surfaces, such as buildings, roads and railways; F_N is the surface flux from the LSM (natural surfaces); and F_{urb} is the surface flux from SLUCM for artificial surfaces.

Since UCM considers about 20 parameters, each of them influencing the magnitude and behaviour of the surface flux, five numerical tests were conducted to obtain the best numerical modelling method (Table 5-2). The first was the control test, which considers the land use and building information, the oasis effect and the irrigation over urban green areas. These parameters are defined to guarantee that the latent heat flux from vegetation is accurately modelled. The oasis effect accounts for enhanced potential evapotranspiration rate of sparse vegetation in urban area due to the lack of obstacles to both radiation and wind. The irrigation option when activated is used to represent irrigation practice in urban areas, scheduled for 9 to 10 pm every day from May to September. During this period, urban vegetation soil moisture will reach critical volumetric soil water content where transpiration is not limited by water availability (Yang et al., 2015). The other tests were designed to estimate the contribution of the urban surfaces to the surface energy balance (Case 1-3).

In the case test 1 is assessed the contribution of the urban impervious surface to the latent heat flux from (IMP_scheme set to 2); this is, was quantified the average value of latent heat flux that is provided by the evaporation of the water (precipitation) stored in the urban impervious surface (buildings and roads) (Kawai and Kanda, 2010). Case test 2 and 3 were developed to assess the anthropogenic heat release related to the human activities, such as traffic and the use of air conditioners (ALHOPTION set to 1 and AHOPTION set to 1). Two different cases were considered to assess the percentage of the anthropogenic flux that is emitted as sensible and latent heat. In this paper the term anthropogenic sensible heat flux (AHOPTION set to 1) refers to the heat associated with the energy consumption (heat directly emitted through tailpipes, air-conditioning, heating equipment, chimneys, among others), while the anthropogenic latent heat flux (ALHOPTION set to 1) refers to heat exhausted from buildings through evaporative cooling equipment.

A case test 4 was also considered to take into account the anthropogenic sensible heat diurnal profile and anthropogenic latent heat diurnal profile that better represents the region of interest. These profiles were developed through the normalized mean diurnal profile of the differences between the measured and modelled, for both latent and sensible heat fluxes (case 4).

Table 5-2. Description of numerical tests.

Case number	Description
Control test	Using land use and buildings information, the oasis effect and the irrigation over urban green areas
Case test 1	Accounting for the latent heat flux from urban impervious surfaces
Case test 2	Accounting for the anthropogenic latent heat
Case test 3	Accounting for the anthropogenic sensible heat
Case test 4	Accounting for the anthropogenic latent and sensible diurnal profile

Surface Urban Energy and Water Balance Scheme (SUEWS)

The Surface Urban Energy and Water Balance Scheme (hereafter SUEWS), version 2014b, (Järvi et al., 2011) simulates the urban energy and water balance components on a local or neighbourhood scale using hourly meteorological forcing data. These data inputs are kept to a minimum to enhance the flexibility of the model and include: solar radiation, air temperature, relative humidity, surface air pressure, wind speed and precipitation. The required meteorological data were provided by WRF model, being the WRF-SUEWS modelling setup already validated (see Chapter 2). In addition, SUEWS model requires information about the characteristics of the area to be simulated, such as surface cover fractions of artificial surfaces (pavements and buildings), natural surfaces (evergreen trees/shrubs, deciduous trees/shrubs, irrigated and non-irrigated grass) and water. Information related to population density and building and tree heights are also needed.

Rates of evaporation/interception for a single layer for each of the surface types are calculated and below each surface type, except water, there is a single soil layer. At each time step (5 min to 1 h), the moisture state of each surface and soil type is calculated. Horizontal water movements at the surface and in the soil, are incorporated. Latent heat flux is calculated with a modified Penman–Monteith equation (Grimmond and Oke, 1991) and sensible heat flux as a residual from the available energy minus the latent heat. The model contains several sub-models, for example, for net all-wave radiation (Offerle et al., 2003; Loridan et al., 2011), storage heat fluxes (Grimmond et al., 1991), anthropogenic heat fluxes and external irrigation. The complete energy balance is mathematically expressed by (Oke, 1987):

$$Q^* + Q_F = Q_E + Q_H + \Delta Q_S \qquad [W \cdot m^{-2}] \tag{5.2}$$

where, Q^* is the net all-wave radiation, Q_F is the anthropogenic heat flux, Q_E is the latent heat flux, Q_H is the sensible heat flux and ΔQ_S is the net storage heat flux.

Table 5-3 lists the physical parameters of the UCM and SUEWS used for the three urban classes. The morphological parameters were estimated through the analysis of satellite images (obtained in Google Earth V10) and field-based surveys. The images were analysed with a geographic information system (ArcGis software, Esri ©, V10). The roughness length and displacement height for each urban class were calculated as a function of the morphological parameters according the “Rule of Thumb” (RT) (Järvi et al., 2011). The thermal and radiative parameters were taken from the literature (Oke, 1987; Järvi et al., 2011, 2014)

Table 5-3. Urban canopy parameters used in the UCM and SUEWS simulation for the three-urban land-use categories: low-intensity residential (U1), high-intensity residential (U2), and commercial/industrial area (U3).

Parameter	Unit	Specific Values for			UCM	SUEWS
		U1	U2	U3		
Artificial surface fraction (F_{urb})	Fraction	0.2	0.8	0.7	Yes	Yes
Natural surface fraction (F_N)	Fraction	0.8	0.2	0.3	Yes	Yes
Mean building height	M	4	12	6	Yes	Yes
Mean trees height	M	4	4	4	No	Yes
Roof width	M	6	8	10	Yes	No
Road width	M	6.0	8.75	10.0	Yes	No
Anthropogenic heat flux	W m^{-2}	15	50	90	Yes	No
Heat capacity of roof and wall	MJ m^{-3} K^{-1}	1.0	1.0	1.0	Yes	No
Heat capacity of road	MJ m^{-3} K^{-1}	1.4	1.4	1.4	Yes	No
Thermal conductivity of roof and wall	W m^{-1} K^{-1}	0.45	0.45	0.45	Yes	Yes
Thermal conductivity of road	W m^{-1} K^{-1}	0.45	0.45	0.45	Yes	Yes
Surface albedo of roof and wall	Fraction	0.15	0.15	0.15	Yes	Yes
Surface albedo of road	Fraction	0.09	0.09	0.09	Yes	Yes
Surface emissivity of roof and wall	-	0.90	0.90	0.90	Yes	Yes
Surface emissivity of road	-	0.95	0.95	0.95	Yes	Yes
Roughness length for momentum	m	RT	RT	RT	Yes	Yes

5.2.2. Measurements

Flux measurements were undertaken for a five-month period (August-31 December 2014) at two sites with contrasting morphology (such as artificial and vegetation fractions and building heights) and anthropogenic activities (such as building heating, traffic and human metabolism emissions). The flux measurement towers were located at the urban area of Porto (41º 09' 54.28'' N, 8º 36' 50.94'' W, high intensity residential area) and the suburban area of Aveiro (40º 38' 28'' N, 8º 39' 13'' W, low intensity residential area), in north-west region of Portugal. The geographical location of the measurements sites is showed in Figure 5-2 (shown as solid diamond).

The measurements were performed using an eddy covariance system, installed at 32 m within the urban area, and 12 m, within the suburban area, above ground level, measuring the energy fluxes (latent and sensible heat fluxes) every 30 min intervals. A detailed description of the instrumental system can be found in Chapter 2. The observed data were used for the evaluation of energy fluxes modelling performance. Two meteorological stations from the Portuguese monitoring network (shown as solid circle in Figure 5-2) with an hourly averaged data were also used for the evaluation of wind speed, air temperature and incoming shortwave solar radiation. These variables were analysed due to its importance for three main aspects: i) human comfort and human health (Moonen et al., 2012); ii) air quality modelling (Yang and Miller, 2002; Wise and Comrie, 2005; Sá et al., 2015); and iii) modelling of energy fluxes (as discussed in Chapter 3).

5.3. RESULTS AND DISCUSSION

A comparison between the modelled results and the measured data, for both UCM tests (section 5.3.1) and urban surface parameterizations (section 5.3.2), are displayed and discussed in this section. Two different approaches are considered: i) a quantitatively analysis, through the estimation of a set of statistic metrics; and ii) a qualitatively analysis, through the visual representation of diurnal profiles.

5.3.1. Urban canopy model (UCM) tests

Tables 5-4 and 5-5 shows the statistic metrics obtained for each case test considered, for the high and low intensity areas, respectively. Figure 5-3 shows the 5-month average diurnal profile associated with each case test. Both analysis is showed for the latent and sensible heat flux.

The comparison between the measured data and the control test shows that, for both areas, the model underestimates the latent heat flux, with a mean bias error (MBE) of -16.3 [high intensity residential area] and -32.5 $W \cdot m^{-2}$ [low intensity residential area]. The sensible heat flux exhibits different behaviour according the study area; the model underestimates this flux at the high-intensity residential area (with a MBE of -5.8 $W \cdot m^{-2}$) and overestimates the sensible heat flux at the low-intensity residential area (with a MBE of 22.2 $W \cdot m^{-2}$). High values of root mean square error (RMSE) (higher than 40 $W \cdot m^{-2}$) and normalized mean square error (NMSE) (higher than 9) are obtained for both turbulent fluxes and for both areas. A correlation factor (r) less than 0.2 is obtained between the measured and modelled latent heat flux, for both areas, which reveals a weak relation between the variables. For sensible heat flux a correlation higher than 0.7 is obtained in both areas. The model is able to represent the diurnal profile of both turbulent heat fluxes, at both areas. However, the modelled results and measured data present a higher bias. The overall results show that the relevant physical processes for the latent heat flux were not accurately represented by this urban parameterization. These results are in accordance with the conclusions reached by the International Urban Surface Energy Balance Model Comparison Project in which the modelling capability of the existing urban SEB models was the weakest for modelling surface latent heat flux (Grimmond et al., 2010, 2011).

When the evaporation scheme for impervious surface is changed (case 1) to take into account that these surfaces are able to partly store precipitation and supply evaporation over a given period, a slight improvement of the model results is obtained, especially, at the low-intensity residential area. This improvement is shown by an increase of the correlation factor and a slight decrease of bias and RMSE. No significant differences between the control test and case 1 are found for the sensible heat flux at both areas. Since the control test and case test 1 already take into account the irrigation over urban green areas, the oasis effect and the latent heat flux from urban impervious surfaces, the differences between the measured data and the modelled latent heat flux is mainly due to the anthropogenic latent heat flux. In the same sense, the differences between the measured and modelled sensible heat flux is mainly related to the anthropogenic sensible heat flux.

Case 2 and 3 take into account, respectively, the anthropogenic latent heat (case 2) and both anthropogenic latent and sensible heat flux (case 3), which means that the anthropogenic heating will be added to both latent and sensible heat flux terms. An improvement of the correlation factor is obtained for the latent heat flux, of around 40% and 11% at high and low intensity residential areas (compared to Control run), respectively. At the high intensity area, all the remaining parameters shows an improvement, with a reduction of the RMSE (around 87 and 39 $W \cdot m^{-2}$, respectively for the sensible and latent heat flux) and NMSE (4.8 and 4.7, respectively for the sensible and latent heat flux) (meaning a nearness of the ideal value [0]), for both latent and sensible heat. A change of MBE behaviour is found; when the anthropogenic heating is considered, the model overestimates both latent and sensible heat flux. Despite that, the results are still far from the measurements. At the low density residential area, slight differences are obtained. These results are in accordance with the expected, since the magnitude of the anthropogenic heat is most notorious as the level of urbanized area increases. A set of studies have been discussed the differences of the energy balance in urban, suburban and rural areas, showing that greater population density is related to a local land use of greater built-up environment, which results in substantially larger magnitudes of anthropogenic heat flux (Dong et al., 2017; Sailor et al., 2015; Kotthaus and Grimmond, 2014).

The differences between the modelled results of Case 3 and observation data is mainly due to the anthropogenic diurnal heat profile used in the simulations. As discussed by Sailor et al. (2015), the spatial location, as a function of underlying local climate, and socioeconomic data of the study areas is straight linked to the magnitude of the anthropogenic heating. Different locations imply, for example, different behaviours in terms of workdays and non-workdays, and in the electricity and heating fuel consumption. All of these factors directly influence the diurnal profiles specifications. In this sense, Case 4 take into account a developed city-specific diurnal profiles of anthropogenic heat for the region of interest. As shown in Tables 5-4 and 5-5, the average modelled latent and sensible heat flux in Case 4 are closer to the measurements. The bias and the NMSE significantly decrease comparative to all the previous case tests, for both turbulent fluxes and for both areas. A slight overestimation remains, of around 2 $W \cdot m^{-2}$, for both fluxes, at the high density residential area; and at the low density residential area, a bias of around 6 and 0.4 $W \cdot m^{-2}$ are obtained for the sensible and latent heat flux, respectively. For both areas, a NMSE of 4 is obtained for the sensible heat flux, while for the latent heat flux a value of 2 is found. Also, a decrease of RMSE is obtained, having a maximum value of around 53 $W \cdot m^{-2}$ at both areas. This improvement implies a reduction in the sensible heat flux by 19.7 and 55 $W \cdot m^{-2}$, respectively for the high and low density residential areas; for the latent heat flux a reduction by 5.9 and 19.2 $W \cdot m^{-2}$ is obtained at the high and low density residential areas, respectively. An increase of the correlation factor is obtained, especially in the latent heat flux, for both areas. Values of 0.4 and 0.6 are obtained at the high and low density residential areas, respectively.

The improvement of the statistics parameters is complemented by the good agreement between the modelled (Case 4) and measured 5-month average diurnal profile, as showed in Figure 5-3. Due to overall results, the UCM-case 4 simulation is further compared with two different urban surface

parameterizations, regarding its ability to modelled near-surface meteorological variables and the surface energy balance fluxes.

Table 5-4. Model statistic evaluation, based on measured data for the high intensity residential area, for all the components of the energy balance and for the different numerical simulations [a)]. The model performance is evaluated for August-December 2014, corresponding to a total of valid values (hours) of 2862 for the sensible heat flux and 2828 for the latent heat flux.

Case No.	Var	Mean		r	RMSE	NMSE	MBE	SD	
		Obs	Mod					Obs	Mod
Control	Q_H	26.84	21.05	0.760	72.31	9.25	- 5.79	81.30	110.88
	Q_E	23.78	7.51	0.066	40.74	9.29	-16.27	34.87	15.87
1	Q_H	26.84	21.13	0.755	72.95	9.38	- 5.71	81.30	110.87
	Q_E	23.78	7.50	0.063	40.72	9.30	-16.28	34.87	15.70
2	Q_H	26.84	19.95	-0.024	136.80	34.93	-6.89	81.30	107.82
	Q_E	23.78	13.83	0.068	39.15	4.66	-9.95	34.87	17.33
3	Q_H	26.84	59.40	0.762	87.34	4.78	32.56	81.30	123.56
	Q_E	23.78	16.96	0.092	38.72	4.65	10.24	34.87	16.96
4	Q_H	26.84	29.18	0.765	52.59	3.53	2.34	81.30	58.53
	Q_E	23.78	26.60	0.401	34.84	1.92	2.82	34.87	27.58

a) **Mean** indicates the average for the measured data (Obs) and for the modelled results (Mod); **r** is the correlation coefficient; **RMSE** is the Root Mean Square Error; **NMSE** is the Normalized Mean Square Error, relative to the multiplication of observed and modelled mean values; **MBE** is the Mean BIAS Error; and **SD** represents the standard deviation for the observed and modelled data.

Table 5-5. Model statistic evaluation, based on measured data for the low intensity residential area, for all the components of the energy balance and for the different numerical simulations [a)]. The model performance is evaluated for August-December 2014, corresponding to a total of valid values (hours) of 3641 for the sensible heat flux and 3257 for the latent heat flux.

Case No.	Var	Mean		r	RMSE	NMSE	MBE	SD	
		Obs	Mod					Obs	Mod
Control	Q_H	20.09	42.27	0.769	100.41	11.87	22.19	68.40	140.22
	Q_E	37.53	5.06	0.129	69.40	25.35	-32.47	59.82	23.30
1	Q_H	20.09	42.52	0.770	100.36	11.79	22.44	68.40	140.16
	Q_E	37.53	5.42	0.132	69.34	23.65	-32.11	59.82	24.07
2	Q_H	20.09	42.78	0.771	100.81	11.83	22.69	68.40	140.73
	Q_E	37.53	6.56	0.133	68.78	19.21	-30.97	59.82	23.94
3	Q_H	20.09	44.80	0.769	102.12	11.59	24.71	68.40	141.52
	Q_E	37.53	6.39	0.143	69.70	19.54	-31.14	59.82	23.15
4	Q_H	20.09	20.59	0.780	45.41	3.81	6.83	68.40	66.83
	Q_E	37.53	37.92	0.57	50.19	1.77	0.39	59.82	45.04

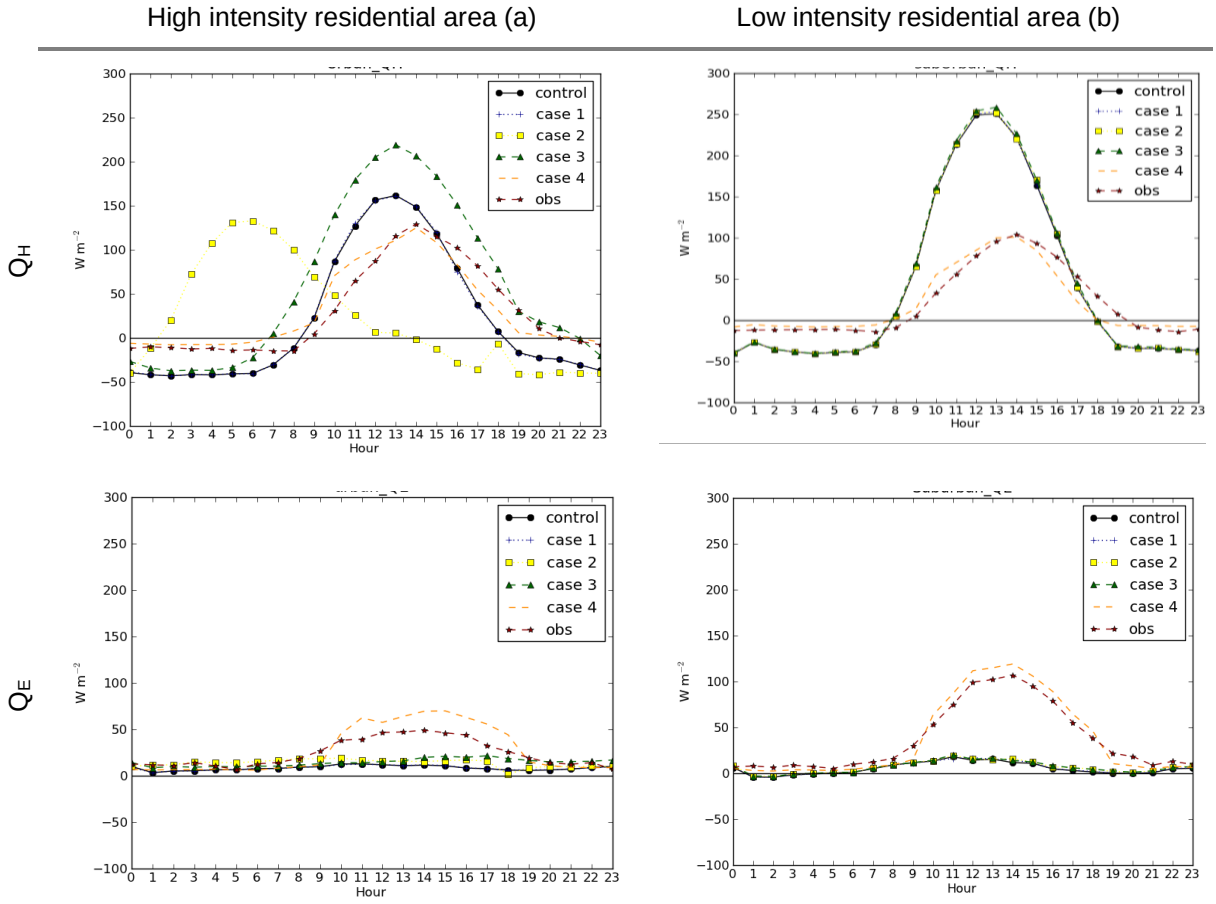

Figure 5-3. Comparison of 5-month average diurnal profile between the measured and modelled sensible and latent heat flux, for both high and low-intensity residential area. The modelled results obtained in each case test are displayed through different line styles.

5.3.2. Evaluation of urban surface parameterizations

5.3.2.1. Meteorological variables

The 2 m air temperature and wind direction at 10 m for each urban surface parameterization (only for LSM and UCM), for the three urban categories, were analysed to assess how the improvements in modelling surface energy balance components influence the accuracy of the meteorological variables simulation.

Figure 5-4 shows diurnal variations of the observed and modelled 2 m air temperatures, averaged for each urban land-use type of all the domain (D4 and D5), for the 5-month period. The UCM simulation compares better with the measurements than the LSM for both the residential areas, reproducing well the diurnal temperature profile, fact that is also shown by the statistic parameters. Both urban surface parameterizations show a correlation factor higher than 0.8; however, LSM overestimates the air temperature on both residential areas with a MBE of around 2°C in high intensity residential areas and 1°C in low intensity residential areas. For the commercial and industrial areas, when the diurnal temperature profile of UCM and LSM is compared, higher temperatures are simulated by LSM, which

is in accordance with the data obtained for both residential areas. The model performance is slightly improved in UCM simulation, for both areas, in terms of a reduction of the RMSE and NMSE (0.01 for both residential areas in UCM) (see Table 5-6). These results are in accordance with the findings made by Lee et al. (2011).

Additionally, the average 2 m air temperature (5-month average) is analysed for the three urban classes and natural surfaces in terms of daytime (8 a.m. – 6 p.m.) and nighttime periods (1 a.m. – 7 a.m. and 7 p.m. – 12 p.m.). The results revealed that when the UCM is used there is a more pronounced difference of the 2 m air temperature between the urban categories; when the LSM is used the 2 m air temperature shows differences less than 0.06 °C for both daytime and nighttime periods. The UCM simulations shows that the air temperature in commercial/industrial area are higher than those in the residential areas, having temperature differences of +0.5°C in daytime and +1.5°C in nighttime periods. The high intensity residential area shows higher temperatures then the low intensity residential area, especially during the nighttime period (around +1°C). These findings indicate that the UCM reproduces the urban heat island intensity better than the LSM. The natural surfaces present cooler air temperatures, at both daytime and nighttime periods, when compared with the urban classes of land use; higher differences are obtained between the commercial/industrial area and the natural surfaces, during the nighttime (difference around 2.3°C). These data reinforce the findings made in previously studies that indicates that the urban vegetation in residential areas have an important influence in the urban microclimate (Carvalho et al., 2017) and in the magnitude of energy fluxes (as discussed in Chapter 3 and 4). All of these findings are in accordance with similar studies (Lee et al., 2011).

Due to its linkage to the air temperature, Table 5-6 also shows the statistical parameters of incoming shortwave solar radiation, only for the low intensity residential area, since, for the period under study, no available data was found for the high intensity residential area. The results revealed that both urban surface parameterizations are able to represent the diurnal variations of the incoming shortwave solar radiation (results not shown). Overall the models' performance in predicting shortwave radiation is similar in terms of MBE (both underestimate this variable of around -20 $W \cdot m^{-2}$), RMSE (of around 100 $W \cdot m^{-2}$), NMSE (less than 0.6) and correlation factor (higher than 0.9), even though slight improvements are seen when the UCM is used.

Table 5-6. Model statistic evaluation a), based on measured data for the high and low intensity residential area, for 2 m air temperature (T2), incoming shortwave solar radiation (SWDOWN) and wind speed at 10 m (WS), and for the different numerical simulations (LSM and UCM). The model performance is evaluated for August-December 2014, corresponding to a total of valid values (hours) of 3667 for the low intensity residential area; for the high intensity residential area, 3650 and 3363 hours are used for the wind speed and temperature statistics, respectively.

Models		Var	Mean		r	RMSE	NMSE	MBE	SD	
			Obs	Mod					Obs	Mod
High intesnsity residential	**LSM**	T2	16.58	18.73	0.83	3.46	0.04	2.15	4.79	4.60
		WS	3.23	4.18	0.70	2.12	0.32	0.95	2.14	2.60
		SDOWN	-	-	-	-	-	-	-	-
	UCM	T2	16.58	16.90	0.92	1.90	0.01	0.32	4.79	4.33
		WS	3.23	3.42	0.69	1.62	0.24	0.19	2.14	1.94
		SDOWN	-	-	-	-	-	-	-	-
Low intemsity residential	**LSM**	T2	17.20	18.53	0.87	3.12	0.03	1.33	5.01	5.62
		WS	2.37	3.84	0.65	2.37	0.62	1.48	1.43	2.43
		SDOWN	160.5	140.7	0.91	111.1	0.55	-19.9	257.5	237.5
	UCM	T2	17.20	16.72	0.94	1.83	0.01	-0.48	5.01	4.93
		WS	2.37	3.42	0.69	1.71	0.36	1.05	1.43	1.85
		SDOWN	160.5	139.8	0.92	101.9	0.46	-20.7	257.5	238.6

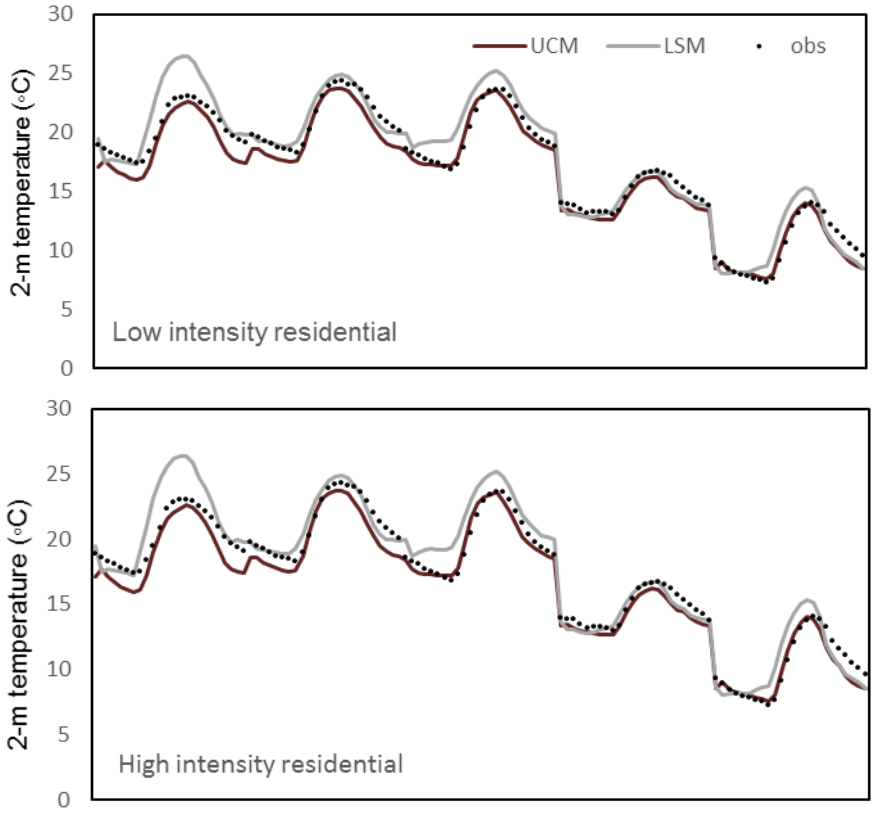

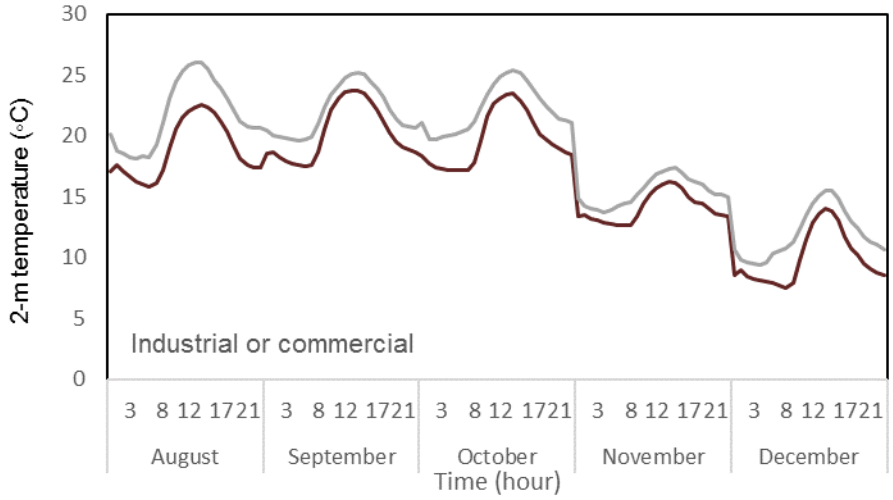

Figure 5-4. Diurnal profile of 2 m temperature (°C) from two simulations conducted with different urban surface parameterizations. The air temperatures are averaged in terms of the three urban categories considered in the USGS 33 land use classification.

Figure 5-5 compares the diurnal measured and modelled 10 m wind speed from the 5-month simulated period, averaged for each urban land-use type. The statistical performance in near-surface wind speed is shown in Table 5-6. Both UCM and LSM, for both study areas, shows some discrepancies in near-surface wind speed diurnal profile between modelled results and observed data. These discrepancies are more notable in LSM, as is also shown by the statistics metrics. Both urban surface parameterizations overestimate the near-surface wind speed. At the high-density residential area, values of 0.95 and 0.19 $m \cdot s^{-1}$ are found for LSM and UCM, respectively; at low-density residential area, bias is slight higher, with values of 1.5 and 1 $m \cdot s^{-1}$, respectively for LSM and UCM. This overestimation is mainly a result of an overestimation of nocturnal wind speeds (from later afternoon to early morning) in all simulations. At high intensity residential area, a correlation factor of 0.7 is found for both UCM and LSM; whereas, at low intensity residential area, a slight improvement is obtained, with an increase of the correlation factor from 0.65 (when LSM is used) to 0.7 (with UCM). Regarding the NMSE and RMSE, higher improvements are obtained at the low intensity residential area when the UCM is used, with a reduction of 38% of NMSE and a reduction of 0.7 $m \cdot s^{-1}$ of RMSE. At the high intensity residential area, slight differences between LSM and UCM is obtained. Overall the UCM simulation compares better with the observations than the LSM for both the residential areas.

Analysing the near-surface wind speed during day and nighttime, different behaviours are obtained with the different urban surface parameterizations. When the LSM is used, the magnitude of the near-surface wind speed is similar during the day and the night (less than 0.6 $m \cdot s^{-1}$ at all land use types), with higher magnitudes being obtained during the nighttime. When the UCM is used, a more pronounced difference of the near-surface wind speed between day and nighttime periods is obtained (around 1 $m \cdot s^{-1}$ at all surfaces), with higher magnitudes during the day. The results obtained with UCM are in accordance with the expected (and with the measured data), since during daytime the wind speeds near the surface are on average higher than at night. This fact is a result of the energy

exchanges between the surface and the atmosphere. During the night, the land surface cools the air from bellow, leading on average to a stable atmospheric stratification that is characterized by a low degree of vertical turbulent transport momentum. After sunrise, the situation changes as the land surface heats the air and vertical moment transport is enhanced due to buoyancy (Coceal and Belcher, 2004).

Also, when the UCM is used, differences of the near-surface wind speed between the three urban categories is obtained, as well as between the residential areas and the natural surfaces. Higher magnitudes of wind speed, both during day and nighttime, are obtained at natural surfaces (+0.5 $m \cdot s^{-1}$ on average). The wind flow through the urban categories is characterized by wind speeds that are 10 to 15% lower (during the day and nighttime periods, respectively) than those winds blowing across the natural surfaces. Comparing the three urban categories, the wind speed decreases with the increase of the urbanized level, this means that higher wind speeds are obtained at the low intensity residential areas than at the both high intensity residential areas and commercial/industrial areas. These results are also in accordance with the expected behaviour (also demonstrated by the measured data) of wind speeds under urban areas. The reduced wind speeds in built-up areas are well documented (Sharma et al., 2017). This difference occurs as a result of the increased frictional drag on air flowing over built-up urban surface, which is rougher than natural/rural areas. The roughness elements in a city are mainly buildings. As discussed since Munn (1970), they are not randomly distributed in space but are organized into city blocks, with streets forming canyons in where the wind flow. The airflow above and around the buildings reaches a lower overall air speed and a higher turbulence, due to the buildings friction. Thus, the urban wind field is characterized by a lower average speed but higher speed variations and turbulence, as compared with the wind flow over natural surfaces (Sharma et al., 2017).

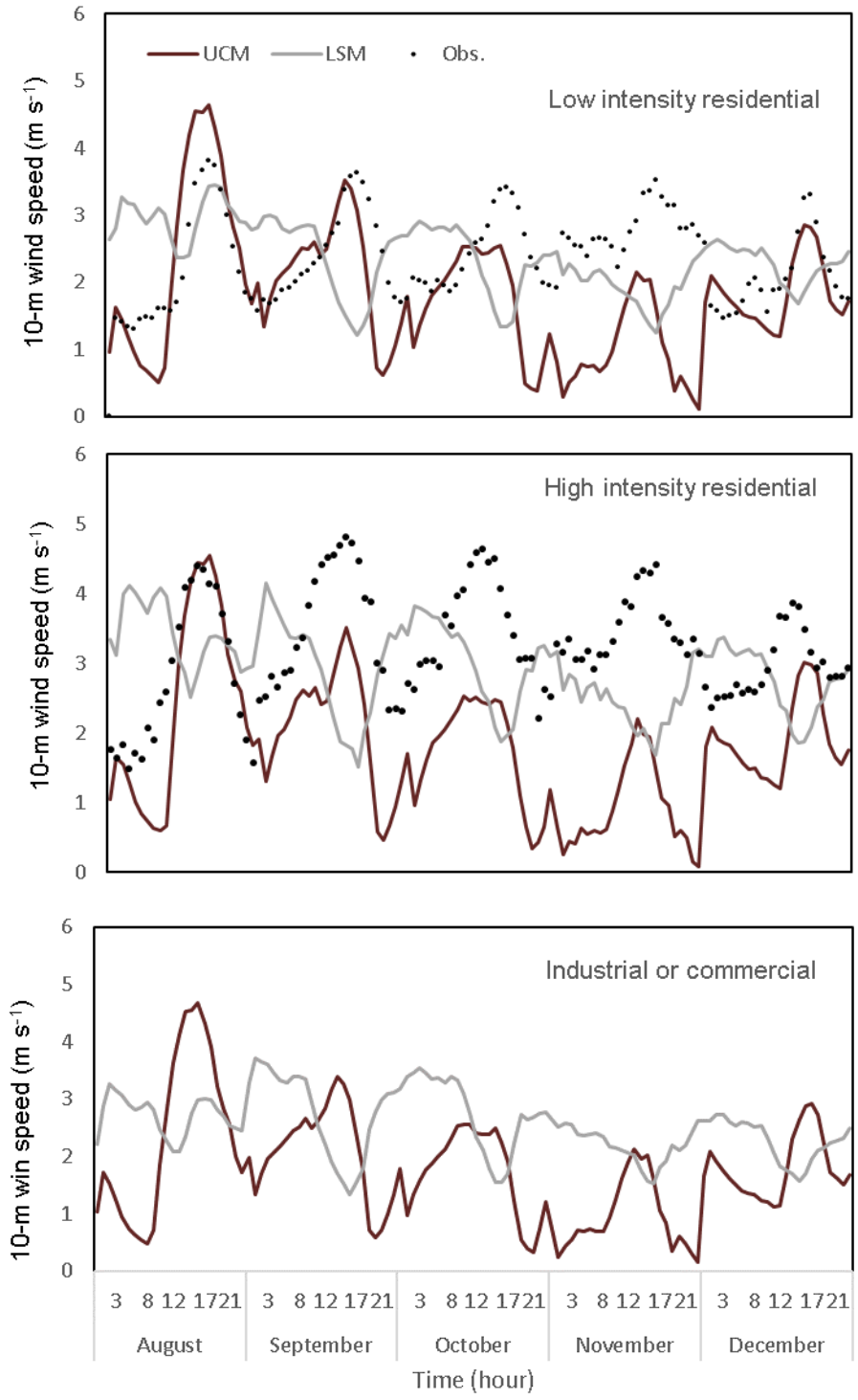

Figure 5-5. Diurnal profile of 10 m wind speed from two simulations conducted with different urban surface parameterizations. The wind speed is averaged in terms of the three urban categories considered in the USGS 33 land use classification.

To complement this analysis, the vertical profile of wind speed is also analysed, for each urban surface parameterization, for the three urban categories (see Figure 5-6). As previously discussed, urban roughness diminishes the air flux and so, urban wind profile is different from urban, suburban and natural areas (Oke, 1987). In particular, wind speed considerably increases with height for several hundreds of meters at these sites. Over the smooth rural areas this increase is confined to a lower layer. Figure 5-6 clearly shows a similar behaviour of wind profiles between the three urban categories when the LSM is used. The results also show that LSM is not able to reproduce the influence of built-up environments in wind profiles, since no differences are obtained between the wind profiles of urbanized areas and natural surfaces. When the UCM is used, the mean wind speed profiles in Figure 5-6 show large differences as the urbanized level change. The average wind profiles at high intensity residential area show the strongest increase in wind speed between 40 and 100 m above ground; this is in line with the knowledge reported in literature that, due to the increased surface roughness, wind speeds increase stronger with height than over rural surfaces. A maximum wind speed is found on average at 100 m height. This maximum is also observed in other urban areas; due to the increased vertical mixing above the urban area, the low-level air flow is perturbed and accelerated while crossing the warmer city areas (Emeis et al., 2007).

Additionally, and as previously discussed, LSM shows higher wind speeds than UCM. Higher differences are obtained as the height above ground increases and the level of urbanization decreases. A maximum difference is obtained at 2000 m for the natural surfaces, low intensity residential areas and industrial or commercial areas, with values of 3, 2.1 and 2.3 $m \cdot s^{-1}$, respectively. At high intensity residential areas, a maximum difference is obtained at 500 m with a value of 2.5 $m \cdot s^{-1}$.

Should also be noted that beyond the surface roughness, the wind speed vertical profile also depends on the nature of the terrain, the topography, and on the vertical temperature profile. The thermal stratification is particularly important to explain the way of how the wind profile develops, since the effect of the shear stresses due to friction of the ground is reduced with height, whereas the effect of buoyancy increases with height. Warm air has lower density than cold air and therefore tends to rise through the atmospheric surface layer; whereas cold air tends to sink in the atmospheric surface layer. Therefore, the way that the surface layer is heated up and cooled down over the 24-hour period affects the wind profile (Emeis et al., 2007).

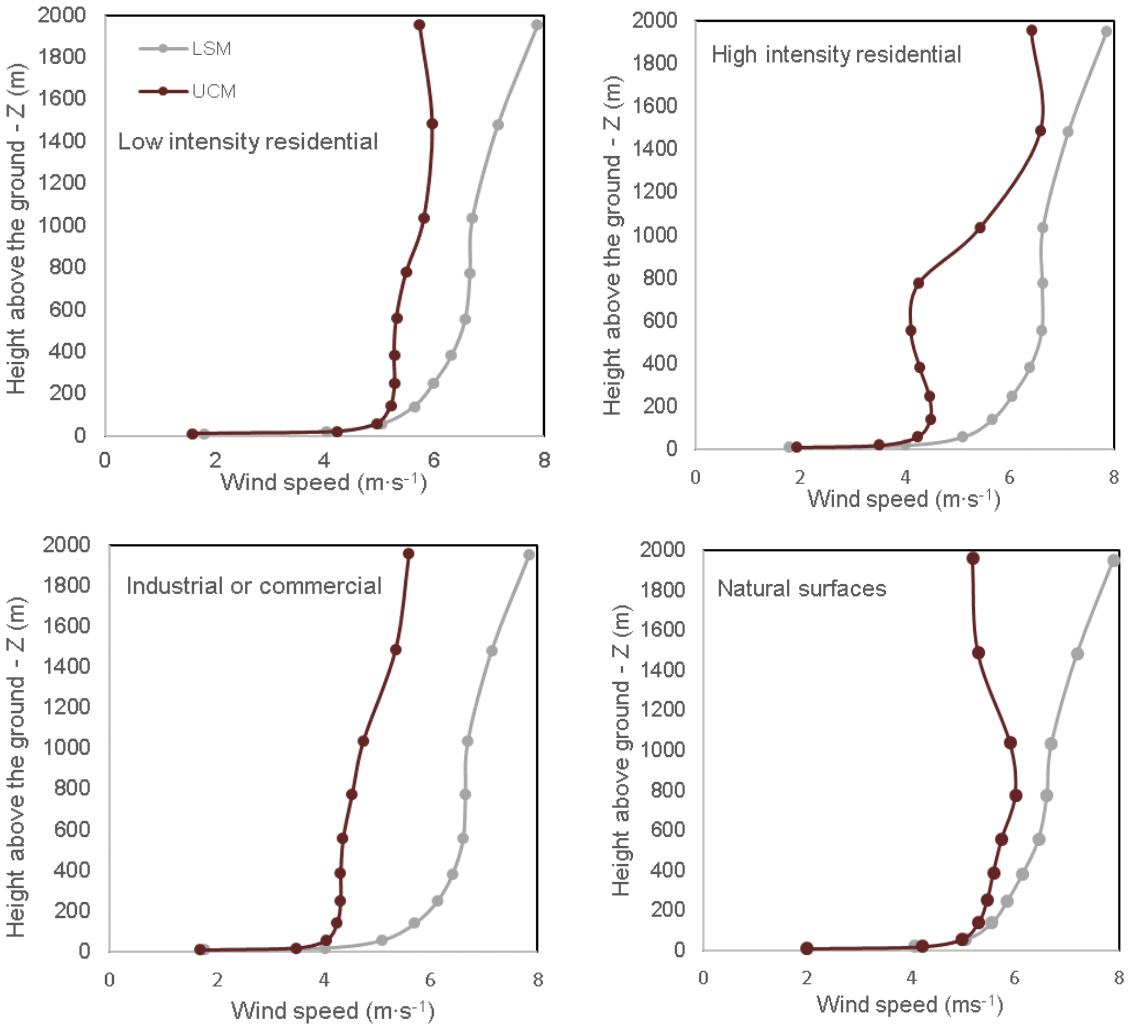

Figure 5-6. Comparison of 5-month average wind profile between the UCM and LSM models, for each one of the three urban categories. Z, in meters, is the height above the ground.

5.3.2.2. Surface energy balance fluxes

Evaluation of energy heat fluxes is of crucial importance to interpret the modelled near-surface meteorology. Figure 5-7 shows the measured and modelled 5-month average profile of sensible and latent heat flux, for both low and high intensity residential areas, for the three urban surface parameterizations under study (LSM, UCM and SUEWS). The observed and modelled 5-month average profile of net all-wave radiation (Q*) and net storage heat flux (ΔQ_S) is also showed for the low intensity residential area (no observed data is available for the high intensity residential area). Table 5-7 shows the quantitatively analysis for each urban surface parameterizations (statistics metrics).

The observed net all-wave radiation has peak values at 12 a.m., for the low intensity residential area, with a value of 349.8 W·m^{-2}. All simulations reproduce well the diurnal variations of the measurements, with a correlation factor higher than 0.9. Although, a consistent overestimation by LSM and SUEWS (MBE values of 39 and 42 W m·s^{-2}, respectively) and a slight underestimation by UCM (MBE value of

5 $W \cdot m^{-2}$) is obtained. The LSM and SUEWS models show similar values of NMSE and RMSE (around 0.8 and 88 $W \cdot m^{-2}$, respectively); UCM shows the lower value of RMSE (73.8 $W \cdot m^{-2}$). For the case of the net storage heat flux, the correlation factor ranges between 0.6 [UCM] to 0.8 [LSM]. All the urban surface parameterizations overestimate this flux, being UCM the model that shows a value closer to the ideal. LSM and SUEWS show a similar RMSE (of 14.5 and 16.5 $W \cdot m^{-2}$) and NMSE (-38 and -24). Also for this statistics metrics, the UCM shows a better performance.

Unlike the case of the net all-wave radiation and the net storage heat flux, the modelled sensible and latent heat fluxes using different urban surface parameterizations are significantly modified for both study areas. UCM and SUEWS show a better performance than LSM, being UCM the model that reproduces turbulent energy partitioning more accurately. The urban vegetation effects of suppressing latent heat flux are neglectable with LSM, at both areas. This underestimation is quantified by a high bias of around -23.6 and -37.2 $W \cdot m^{-2}$, respectively for the high and low intensity residential areas, and a poorer correlation between modelled and measured data. As result of this underestimation, LSM overestimates the sensible heat flux, for both areas (22 $W \cdot m^{-2}$ [high intensity residential area] and 34 $W \cdot m^{-2}$ [low intensity residential area]), showing however a good correlation between measured and modelled data. Higher values of NMSE and RMSE are also found for both areas. The daytime turbulent energy partitioning enhances the conductive heat flux into the soil layers during the daytime, which can result in an amplified nocturnal urban heat island (Lee et al., 2011). SUEWS model shows different behaviours for each of the study areas. As discussed in Chapter 2, at low density residential area SUEWS is able to well reproduce the latent heat flux profile, despite a clear overestimation (MBE of 27 $W \cdot m^{-2}$), whereas, at the high intensity residential area, a poorer correlation is obtained linked to an underestimation (-12 $W \cdot m^{-2}$). Higher RMSE is obtained for both areas, similar to LSM, showing however lower values of NMSE (6.5 and 2.5 for the high and low intensity residential areas). Regarding the sensible heat flux, a general good agreement, for both areas, is obtained with a correlation factor of 0.7 and a NMSE of 4. A consistent overestimation is found as well as higher values of RMSE; despite of that, the obtained values are in accordance with some of the studies conducted with this model (Ward et al., 2014, Järvi et al., 2014).

Overall, the UCM shows a better performance for both turbulent heat fluxes, for both areas. A consistent overestimation is obtained, with a MBE of around 3 $W \cdot m^{-2}$ at the high intensity residential area. At the low residential area, a MBE of 7 and 0.4 $W \cdot m^{-2}$ is obtained for the sensible and latent heat flux. Compared with the LSM and SUEWS, UCM shows the lowest RMSE, with values of 53 $W \cdot m^{-2}$ [high intensity residential area] and 45 $W \cdot m^{-2}$ [low intensity residential area] for the sensible heat flux; for the latent heat flux a RMSE of 35 and 50 $W \cdot m^{-2}$ is obtained for the high and low intensity residential areas. The NMSE is closer to the ideal, for both areas, with values of around 4 for the sensible heat flux and around 2 for the latent heat flux. Similar to this study, previous studies with the UCM have also showed the same performance (e.g., Lee et al., 2011).

Table 5-7. Model statistic evaluation [a)], based on measured data for the low intensity residential area, for all the components of the energy balance and for the different urban surface parameterizations (LSM, UCM and SUEWS).

Models		Var	Mean		R	RMSE	NMSE	MBE	SD	
			Obs	Mod					Obs	Mod
High intesnsity residential	LSM	Q*	-	95.8	-	-	-	-	-	176.1
		Q_H	26.84	48.74	0.814	65.15	3.24	21.9	81.30	105.29
		Q_E	23.78	0.20	0.132	41.98	369.2	-23.6	34.87	1.23
		ΔQ_S	-	5.40	-	-	-	-	-	88.1
	UCM	Q*	-	39.91	-	-	-	-	-	161.3
		Q_H	26.84	29.18	0.765	52.59	3.53	2.34	81.30	58.53
		Q_E	23.78	26.60	0.401	34.84	1.92	2.82	34.87	27.58
		ΔQ_S	-	8.40	-	-	-	-	-	60.4
	SUEWS	Q*	-	101.4	-	-	-	-	-	197.2
		Q_H	26.84	78.36	0.744	85.87	3.53	51.5	81.30	103.15
		Q_E	23.78	11.71	0.134	41.31	6.79	-12.1	34.87	28.11
		ΔQ_S	-	17.3	-	-	-	-	-	105.6
Low intensity residential	LSM	Q*	58.02	96.86	0.954	83.69	0.86	38.8	189.0	179.45
		Q_H	20.09	53.94	0.872	66.54	4.09	33.9	68.40	106.1
		Q_E	37.53	0.35	0.219	70.21	373.7	-37.2	59.82	1.28
		ΔQ_S	-1.44	3.79	0.805	14.54	-38.6	5.24	5.83	17.80
	UCM	Q*	58.02	52.97	0.943	73.79	1.46	-5.05	189.0	155.5
		Q_H	20.09	20.59	0.780	45.41	3.81	6.83	68.40	66.83
		Q_E	37.53	37.92	0.57	50.19	1.77	0.39	59.82	45.04
		ΔQ_S	-1.44	1.50	0.631	5.46	-13.8	2.94	5.83	4.52
	SUEWS	Q*	58.02	100.4	0.954	88.29	0.87	42.4	189.0	184.2
		Q_H	20.09	34.81	0.716	49.38	3.87	14.7	68.40	63.49
		Q_E	37.53	64.35	0.607	77.48	2.50	26.8	59.82	91.73
		ΔQ_S	-1.44	7.68	0.695	16.46	-24.4	9.12	5.83	17.10

The SUEWS and UCM simulations reproduce well the changes related to the different land cover characteristics in the individual fluxes of the energy balance. At the low intensity residential area, the daytime energy balance (10 a.m. - 3 p.m.) is dominated by Q* (average values of 249 and 350 W m^{-2} for UCM and SUEWS, respectively) and Q_E (average values of 101 and 174 W m^{-2} for UCM and SUEWS, respectively). The majority of energy (Q*) is partitioned to Q_E, accounting on average for 47 and 49% of the daytime available energy, for UCM and SUEWS, respectively. The remaining energy is partitioned to turbulent sensible and storage heat fluxes (around 39% [UCM] and 26% [SUEWS]; and 14% [UCM] and 26% [SUEWS], respectively). The modelled energy partitioning (of both models) is in accordance with the measured data (Q_E: 49%, Q_H: 42%, ΔQ_S: 9%), despite the UCM shows a greater similarity. The daytime Bowen ratio (Q_H/Q_E) is less than 1, with a value of 0.82 and 0.53, respectively for UCM and SUEWS. The daytime evaporative fraction (Q_E/Q^*) is 0.39 and 0.49 for UCM and SUEWS, respectively. These results are well within the expected relation at areas with low population density (Coutts et al., 2007), and are in accordance with the measured values (0.87 and 0.34, respectively for Bowen ratio and evaporative fraction).

At the high intensity residential area, the greatest share of energy goes to Q_H (42 and 50%, respectively for UCM and SUEWS), followed by the storage heat flux (corresponding to 33% and 43% for UCM and SUEWS). The energy dissipation in the latent heat form is of 24% and 8% for UCM and SUEWS. These results are in accordance with the expected energy distribution in more densely built up areas (Coutts et al., 2007). A smaller daytime evaporative fraction is obtained (0.26 [UCM] and 0.08 [SUEWS]), when compared with the low intensity residential area, resulting in a high Bowen ratio (1.6 [UCM] and 6.3 [SUEWS]). The observed Bowen ratio is of 2.0, which is consistent with the previous urban surface flux observations in European cities (with similar vegetation fraction in the measurement footprint) (Goldbach and Kuttler, 2012). The UCM model captures better the relation between the sensible and latent heat flux, despite both models are able to demonstrate that the Bowen ratio is persistently dominated by the sensible heat flux.

Compared with the measurements, UCM is able to reproduce better the nocturnal radiative cooling magnitude (negative Q*) than SUEWS, related to the energy lost by the surface volume during the night. Also, during the night, as the radiative inversion becomes established, a negative sensible heat flux is observed, which means an energy transport from the urban boundary layer into the surface (Kotthaus and Grimmond, 2014). This phenomenon is well capture by UCM, unlike happens with SUEWS model. This limitation of SUEWS model was already discussed in Chapter 2, which is probably related to the way as this flux is calculated in the model. The sensible heat flux is estimated as the residual of the energy balance and therefore accumulates the errors in all other terms (Ward et al., 2016). Should however be noted, that the magnitude of negative Q_H during the night is higher at the low intensity areas. This behaviour is in accordance with the findings of previously studies conducted for other dense urban environments, where was found that Q_H remains positive throughout the night, being almost exclusively responsible for the energy transport away from the surface (e.g. Mexico City [Velasco et al., 2005]). This suggests that strong anthropogenic energy sources are located in the study area. A combination of anthropogenic heat flux and a large heat storage capacity of the urban canopy could further explain the constant night-time upward transport of sensible heat (Kotthaus and Grimmond, 2014).

For both areas, and since LSM minimize the effects of urban vegetation, a completely different energy partitioning is obtained. The majority of energy is partitioned to Q_H and ΔQ_S (higher than 50% and 40%, respectively), almost suppressing the latent heat flux (only 0.3% of the daytime energy balance). As result, extremely higher Bowen ratio are obtained (higher than 10), consistent with vegetation-free sites, as well as, a reduced daytime evaporative fraction (0.03).

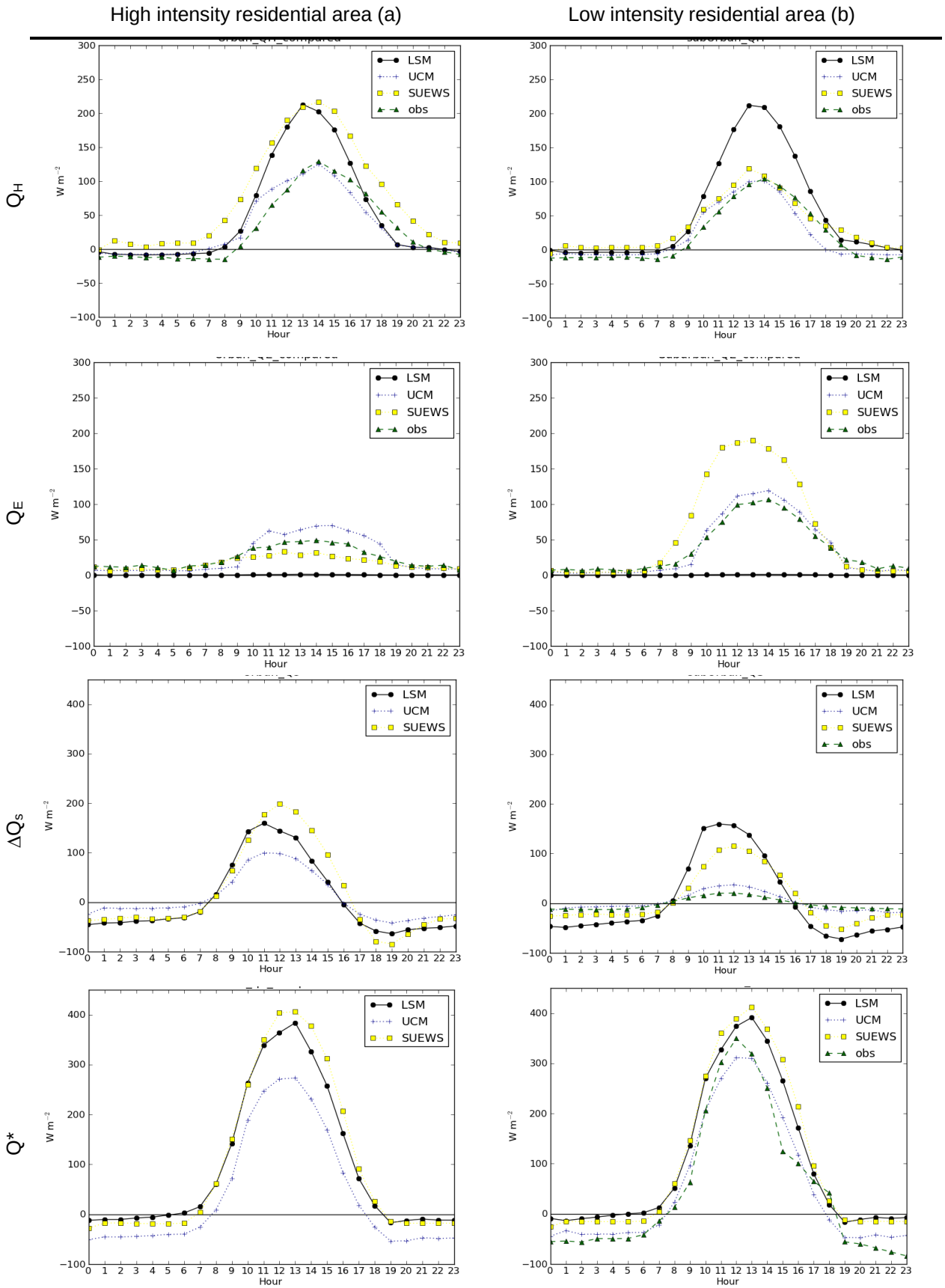

Figure 5-7. Modelled and measured (for the low intensity residential area) five-months averaged energy balance at the high and low intensity residential areas. Q*: net all-wave radiation, Q_E: latent heat flux, Q_H: sensible heat flux, ΔQ_S: net storage heat flux.

Due to the energy exchanges between the surface and the atmosphere, the obtained differences in the modelled surface energy balance fluxes, in particular the differences in the modelled turbulent energy partitioning, using different urban surface parameterizations, can explain the model performance in near-surface air temperatures, for the three urban land use categories. In turn, near surface temperature and wind speeds influence evaporation rates, thereby influencing the energy balance and the hydrological cycle. In addition, urban boundary layer flow characteristics arise in response to exchange of momentum and energy with the urban surface, which is clearly distinct from natural surfaces in form and material characteristics.

These linkages, encompassing the overall discussed results, demonstrate the relevance of the appropriated model physics definition, as well as the considered surface parameters, for an accurate simulation of the urban microclimate.

5.4. CONCLUSIONS

The performance of different urban surface parameterizations in the WRF model, two of them as a WRF module (LSM and UCM) and the other as an individual model (SUEWS), was quantitatively evaluated using measurements carried out in two distinct areas, high and low intensity residential, in Portugal. The study was focused in the ability of models to simulate the surface energy balance fluxes, as well as, to a realist representation of the urban microclimate (for this last, only UCM and LSM were evaluated). The international urban land surface model comparison concluded that no model had the best overall capability for modelling the surface energy balance fluxes within an urban area. The obtained results lead to similar conclusions.

Comparison between modelled and measured data showed that UCM simulation compares better with the near-surface air temperatures, being able to a more realist representation of the air temperatures differences related to different land covers (in particular, different levels of urbanization). Model performance for both UCM and LSM in modelling local wind speeds was similar in terms of statistic metrics. However, the results showed that the UCM has the potential to more accurately simulate the observed wind speeds in terms of the daytime profile related to the surface land use. This was also found for the vertical wind profile.

The UCM performance in modelling the urban microclimate was attributed to a good capability in simulate turbulent (sensible and latent heat fluxes) energy partitioning over urban covers. The higher suppression of urban vegetation effects in the LSM substantially overestimates the sensible heat and underestimates the latent heat fluxes, over both low and high intensity residential areas, resulting in systematic positive biases in near-surface air temperatures.

The UCM performance is also related to the different numerical tests conducted in this study to obtain the best numerical modelling procedure. The model runs demonstrate the importance of choose a suitable model according the study focus, not only regarding the model physics but also regarding the surface parameters used in the model runs. The need to ensure that these are considered as a whole

to understand their relative importance and their suitability for a given area, is critical. Considering four aspects (e.g., irrigation and oasis effect of urban green areas, evaporation of urban impervious surfaces, and anthropogenic latent and sensible heat release), improves the ability of the UCM to simulate latent and sensible heat flux. Additionally, it was also found as extremely important the use of city-specific diurnal profiles of anthropogenic heat for the region of interest, since this profile is highly dependent on the local climate (directly related with the geographical location), and socioeconomic data of the study areas.

Overall, this work is a step forward in understanding and modelling the physics of urban environments using different urban simulation schemes combined with urban parameters customized for individual urban areas. Guarantee the accuracy of urban microclimate modelling is essential to realistic predict the impacts of climate variability and climate change on cities and help develop appropriate adaptation/mitigation strategies to heat-related impacts. If the models are not capable to model current conditions and/or to respond appropriately to parameters changes, then simulations for future scenarios and different interventions could be very misleading.

5.5. REFERENCES

Avissar R. Pielke, R.A. (1989). A parameterization of heterogeneous land surfaces for atmospheric numerical models and its impact on regional meteorology. Monthly Weather Review 117, 2113–2136.

Baklanov A., Grimmond S., Mahura A., Athanassiadou M. (2009). Model Urbanization Strategy: Summaries, Recommendations and Requirements. In: Baklanov A., Grimmond S., Mahura A., Athanassiadou M. (Eds.). Meteorological and Air Quality Models for Urban Areas. Springer, Berlin, Heidelberg, p. 183. [doi: 10.1007/978-3-642-00298-4].

Barlow J. (2014). Progress in observing and modelling the urban boundary layer. Urban Climate 10, 216-240. [doi: 10.1016/j.uclim.2014.03.011].

Büttner G., Feranec G., Jaffrain G. (2006). Corine land cover nomenclature illustrated guide (Addendum 2006). http://eea.eionet.europa.eu/Members/irc/eionetcircle/spatial/library?l=/clc2005_update/clc2006_technical/draft/nomenclaturedoc/_EN_1.0_&a=d.

Carvalho D., Martins H., Marta-Almeida M., Rocha A. Borrego, C. (2017). Urban resilience to future urban heat waves under a climate change scenario: A case study for Porto urban area (Portugal). Urban Climate 19, 1-27. [doi: 10.1016/j.uclim.2016.11.005].

Coceal O., Belcher S.E. (2004). A canopy model of mean winds through urban areas. Quarterly Journal of the Royal Meteorological Society 130, 1349-1372. [doi: 10.1256/qj.03.40].

Coutts A., Beringer J., Tapper N. (2007). Impact of Increasing Urban Density on Local Climate: Spatial and Temporal Variations in the Surface Energy Balance in Melbourne, Australia. Journal of Applied Meteorology and Climatology 46, 477–493.

Chen F., Dudhia J. (2001). Coupling an advanced land-surface hydrology model with the Penn State-NCAR MM5 modeling system. Part I: Model description and implementation. Monthly Weather Review 129, 569–585.

Chen F., Kusaka H., Tewari M., Bao J.-W. Hirakuchi H. (2004). Utilizing the coupled WRF/LSM urban modeling system with detailed urban classification to simulate the urban heat island phenomena over the greater Houston area. Fifth Conference on Urban Environment, Vancouver, BC, Canada, American Meteorological Society, CD-ROM, 9.11.

Chen F., Kusak, H., Bornstein R., Ching J., Grimmond C.S.B., Grossman-Clarke S., Loridan T., Manning K.W., Martilli A., Miao S., Sailor D., Salamanca F.P., Taha H., Tewari M., Wang X., Wyszogrodzki A.A., Zhang C. (2011). The integrated WRF/urban modelling system: development, evaluation, and applications to urban environmental problems. International Journal of Climatology 31, 273–288.

Dong Y., Varquez A.C.G., Kanda M. (2017). Global anthropogenic heat flux database with high spatial resolution. Atmospheric Environment 150, 276-294. [doi: 10.1016/j.atmosenv.2016.11.040].

Dudhia J. (1989). Numerical study of convection observed during the winter monsoon experiment using a mesoscale two-dimensional model. Journal of the Atmospheric Sciences 46, 3077-3107.

Emeis S., Baumann-Stanzer K., Piringer M., Kallistratova M., Kouznetsov R., Yushkov V. (2007). Wind and turbulence in the urban boundary layer – analysis from acoustic remote sensing data and fit to analytical relations. Meteorologische Zeitschrift 16, 393-406. [doi: 10.1127/0941-2948/2007/0217].

Goldbach A., Kuttler W. (2012). Quantification of turbulent heat fluxes for adaptation strategies within urban planning. International Journal of Climatology 33, 143-159. [doi: 10.1002/joc.3437].

Grell G.A. (1993). Prognostic evaluation of assumptions used by cumulus parameterization. Monthly Weather Review 121, 764–787.

Grell G.A., Devenyi D. (2002). A generalized approach to parameterizing convection combining ensemble and data assimilation techniques. Geophysical Research Letters 29, 1693. [doi:10.1029/2002GL015311].

Grimmond C.S.B., Oke T.R. (1991). An evapotranspiration-interception model for urban area. Water Resources Research 27, 1739–1755.

Grimmond C.S.B., Cleugh H.A., Oke T.R. (1991). An objective urban heat storage model and its comparison with other schemes. Atmospheric Environment Part B 25, 311–326.

Grimmond C.S.B., Blackett M., Best M.J., Barlow J., Baik J.J., Belcher S.E., Bohnenstengel S.I., Calmet I., Chen F., Dandou A., Fortuniak K., Gouvea M.L., Hamdi R., Hendry M., Kawai T., Kawamoto Y., Kondo H., Krayenhoff E.S., Lee S.H, Loridan T., Martilli A., Masson V., Miao S., Oleson K., Pigeon G., Porson A., Ryu Y.H, Salamanca F., Shashua-Bar L., Steeneveld G.J, Tombrou M., Voogt J.A., Young D.T., Zhang N. (2010). The International Urban Energy Balance Models Comparison Project: First Results from Phase 1. Journal of Applied Meteorology and Climatology 40, 1268-1292.

Grimmond C.S.B, Blackett M., Best M.J., Baik J.J., Belcher S.E., Beringer J., Bohnenstengel S.I., Calmet I., Chen F., Coutts A., Dandou A., Fortuniak K., Gouvea M.L., Hamdi R., Hendry M., Kanda M., Kawai T., Kawamoto Y., Kondo H., Krayenhoff E.S., Lee S.H., Loridan T., Martilli A., Masson V., Miao S., Oleson K., Ooka R., Pigeon G., Porson A., Ryu Y.H., Salamanca F., Steeneveld G.J., Tombrou M., Voogt J.A., Young D.T., Zhang N. (2011). Initial results from Phase 2 of the international urban energy balance model comparison. International Journal of Climatology 31, 244-272.

Hong S.-Y., Dudhia J., Chen S.-H. (2004). A revised approach to ice microphysical processes for the bulk parameterization of clouds and precipitation. Monthly Weather Review 132 103–119.

Hong S.-Y., Noh Y., Dudhia J. (2006). A new vertical diffusion package with an explicit treatment of entrainment processes. Monthly Weather Review 134, 2318-2341.

Järvi L., Grimmond C.S.B., Christen A. (2011). The Surface Urban Energy and Water Balance Scheme (SUEWS): Evaluation in Los Angeles and Vancouver. Journal of Hydrology 411, 219-237. [doi: 10.1016/j.jhydrol.2011.10.001].

Järvi L., Grimmond C.S.B., Taka M., Nordbo A., Setälä H., Strachan I.B. (2014). Development of the Surface Urban Energy and Water balance Scheme (SUEWS) for cold climate cities. Geoscientific Model Development 7, 1691-1711. [doi: 10.5194/gmd-7-1691-2014].

Kawai T., Kanda M. (2010). Urban energy balance obtained from the comprehensive outdoor scale model experiment. Part i: Basic Features of the surface energy balance. Journal of Applied Meteorology and Climatology 49, 1341-1359.

Kotthaus S., Grimmond C.S.B. (2014). Energy exchange in a dense urban environment – Part I: Temporal variability of long-term observations in central London. Urban Climate 10, 261-280. [doi: 10.1016/j.uclim.2013.10.002].

Kusaka H., Kondo H., Kikegawa Y., Kimura F. (2001). A simple single layer urban canopy model for atmospheric models: comparison with multi-layer and slab models. Boundary Layer Meteorology 101, 329-358.

Kusaka H, Kimura F. (2004). Coupling a single-layer urban canopy model with a simple atmospheric model: impact on urban heat island simulation for an idealized case. Journal of the Meteorological Society of Japan 82, 67–80.

Lee S-H., Kim S-W., Angevine W.M., Bianco L., McKeen S.A., Senff C.J., Trainer M., Tucker S.C., Zamora R.J. (2011). Evaluation of urban surface parameterizations in the WRF model using measurements during the Texas Air Quality Study 2006 field campaign. Atmospheric Chemistry and Physics 11, 2127–2143.

Li D., Malyshev S., Shevliakova E. (2016). Exploring historical and future urban climate in the Earth System Modeling framework: 1.Model development and evaluation. Journal of Advances in Modeling Earth Systems 8, 917–935. [doi:10.1002/2015MS000578].

Liu Y., Chen F., Warner T., Basara J. (2006). Verification of a mesoscale data assimilation and forecasting system for the Oklahoma City area during the joint urban 2003 field project. Journal of Applied Meteorology and Climatology 45, 912–929, 2006.

Loridan T., Grimmond C.S.B., Offerle B.D., Young D.T., Smith T., Järvi L., Lindberg F. (2011). Local scale urban meteorological parameterization scheme (LUMPS): longwave radiation parameterization and seasonality-related developments. Journal of Applied Meteorology and Climatology 50, 185-202.

Martilli A., Clappier A., Rotach M.W. (2002). An urban surface exchange parameterization for mesoscale models. Boundary Layer Meteorology 104, 261–304. [doi: 10.1023/A:1016099921195].

Martilli, A. (2007). Current research and future challenges in urban mesoscale modelling. International Journal of Climatology 27, 1909–1918. [doi: 10.1002/joc.1620].

Masson V. (2000). A physically-based scheme for the urban energy budget. Boundary Layer Meteorology 94, 357–397.

Masson V. (2006). Urban surface modeling and the meso-scale impact of cities. Theoretical and Applied Climatology 84, 35–45. [doi:10.1007/S00704-005-0142-3].

Mestayer P.G., Durand P., Augustin P., Bastin S. (2005). The urban boundary-layer field campaign in Marseille (UBL/CLU–ESCOMPTE): set-up and first results. Boundary Layer Meteorology 114, 315–365. [doi: 10.1007/s10546-004-9241-4].

Mlawer E.J., Taubman S.J., Brown P.D., Iacono M.J., Clough S.A. (1997). Radiative transfer for inhomogeneous atmospheres: RRTM, a validated correlated-k model for the longwave. Journal of Geophysical Research 102D, 16663-16682.

Moonen P., Defraeyec T., Dorerb V., Blockend B., Carmeliet J. (2012). Urban Physics: Effect of the micro-climate on comfort, health and energy demand. Frontiers of Architectural Research 1, 197-228. [doi: 10.1016/j.foar.2012.05.002].

Munn R.E. (1970). Airflow in urban areas. WMO Tech. Note 108. WMO, Geneva, 15-39.

Offerle B., Grimmond C.S.B., Oke T.R. (2003). Parameterization of net all-wave radiation for urban areas. Journal of Applied Meteorology and Climatology 42, 1157–1173. [doi:10.1175/1520-0450(2003)042].

Oke T.R. (1987). Boundary Layer Climates. Routledge, London, UK.

Pineda N., Jorba O., Jorge J., Baldasano J.M. (2004). Using NOAA AVHRR and SPOT VGT data to estimate surface parameters: application to a mesocale meteorological model. International Journal of Remote Sensing 25, 129-143.

Rotach M.W., Vogt R., Bernhofer C., Batchvarova E., Christen A., Clappier A., Voogt J.A. (2005). BUBBLE – an urban boundary layer meteorology project. Theoretical and Applied Climatology 81, 231–261. [doi: 10.1007/s00704-004-0117-9].

Sá E., Tchepel O., Carvalho A., Borrego C. (2015). Meteorological driven changes on air quality over Portugal: a KZ filter application. Atmospheric Pollution Research 6, 979-989.

Sailor D., Georgescu M., Milne J., Hart M. (2015). Development of a national anthropogenic heating database with an extrapolation for international cities. Atmospheric Environment 118, 7-18. [doi: 10.1016/j.atmosenv.2015.07.016].

Sharma A., Fernando H., Hamlet A., Hellmann J., Barlage M., Chen F. (2017). Urban meteorological modeling using WRF: a sensitivity study. International Journal of Climatology 37, 1885-1900. [doi: 10.1002/joc.4819].

Skamarock W.C., Klemp J.B., Dudhia J., Gill D.O., Barker D.M., Huang X.Y., Wang W., Powers J.G. (2008). A Description of the Advanced Research WRF Version 3. NCAR/TN-475+STR, pp.113.

Sridhar V., Elliott R.L., Chen F., Brotzge J.A. (2002). Validation of the NOAH-OSU Land surface model using surface flux measurements in Oklahoma. Journal of Geophysical Research 107, 1-18. [doi:10.1029/2001JD001306].

United Nations, UN. (2014). Report on World urbanization prospects. Department of economic and social affairs. Available on: http://www.atmos-chem-phys.net/11/2127/2011/acp-11-2127-2011.pdf.

Velasco E., Pressley S., Allwine E., Westberg H., Lamb B. (2005) Measurements of CO_2 fluxes from the Mexico City urban landscape. Atmospheric Environment 39, 7433-7446.

Ward H.C., Kotthaus S., Järvi L., Grimmond C.S.B. (2016). Surface Urban Energy and Water Balance Scheme (SUEWS): development and evaluation at two UK sites. Urban Climate 18, 1-32. [doi: 10.1016/j.uclim.2016.05.001].

Wise E.K., Comrie A.C. (2005). Meteorologically adjusted urban air quality trends in the Southwestern United States. Atmospheric Environment 39, 2969-2980.

Yang J., Miller D.R. (2002). Trends and variability of ground-level O_3 in Connecticut over the period 1981-1997. Journal of the Air & Waste Management Association 52, 1354-1361.

Yang J., Wang Z-Hu, Chen F., Miao S., Tewari M., Voogt J. A., Myint S. (2015). Enhancing Hydrologic Modelling in the Coupled Weather Research and Forecasting-Urban Modelling System. Boundary-Layer Meteorology 155, 87-109. [doi: 10.1007/s10546-014-9991-6].

Zhang D.L., Shou Y.X., Dickerson R.R., Chen F. (2011). Impact of upstream urbanization on the urban h eat island effects along the Washington-Baltimore corridor. Journal of Applied Meteorology and Climatology 50, 2012–2029.

CHAPTER 6

This Chapter has been submitted as:

Rafael S., Vicente B., Rodrigues V., Borrego C., Miranda A.I., Lopes M. (Under review). *Impacts of green infrastructures on aerodynamic flow and air quality in Porto's urban area*. Environmental Research.

The author acknowledges the co-authors critical revision.

6. Assessing the effectiveness of resilience measures to improve air quality by using WRF-CFD setup model in a built-up area

Abstract

Air pollution is an environmental and social issue at different spatial scales, especially in a climate change context, with an expected decrease of air quality. Despite the technological evolution of the last decades in the transport sector, road traffic emissions are still one major source of air pollution at the city level.

The main goal of this study was to evaluate the influence of a set of resilience measures, based on nature-based solutions, in the wind flow and in the dispersion of air pollutants, in a built-up area in Portugal. For that, four pollutants were analysed (CO, CO_2, NO_X and PM10) and four scenarios were developed: i) a baseline scenario, ii) an urban green scenario, iii) a green roof scenario, iv) a "grey" scenario. Two models were used, namely the Weather Research and Forecasting model (WRF) and the CFD model VADIS (pollutant dispersion in the atmosphere under variable wind conditions). The WRF model was used to initialize the CFD model, while the last was used to perform the set of numerical simulations, in an hourly base. The implementation of a green urban area promotes a reduction of air pollutants concentrations, 16% on average; while the application of green roofs shows an increase of concentrations (reaching 60% during specific time periods). Overall the results shows that a strategic placement of vegetation in cities has the potential to make an important contribution to the improvement of air quality and sustainability of urban environments.

Keywords: Air quality, CFD modelling, Resilience measures, Road traffic emissions

6.1. INTRODUCTION

Air pollution in urban environments with dense population has become an important research issue in the past two decades, with several studies of the airflow and dispersion patterns in cities (e.g., Borrego et al., 2003; Buccolieri et al., 2011; Amorim et al., 2013; Salmon et al., 2013). In Europe, emissions of many atmospheric pollutants have decreased substantially over the last years, resulting in an improved air quality across the region. However, air pollutants concentrations are still too high (exceedances of air quality standards still occur), and air quality problems persist, especially in cities where the majority of population live (EEA, 2016a). More recently, the interaction between climate change, air pollutant emissions and atmospheric concentrations has been considered a crucial research field. As Markakis et al., (2014) denotes, the impact of climate change on air quality at the local scale is still a current research challenge, since much has still to be explored in order to understand and accurately predict the changes in pollutant levels under future climatic conditions and at different spatial scales.

It is well known that road traffic emissions are one of the major problems of life quality in urban areas (EEA, 2016a, Jeanjean et al., 2016). The economic recession of 2008 resulted in lower transport demand and, consequently, in a reduction of both greenhouse gas emissions (GHG) and air pollutants emission (i.e. particulate matter [PM], carbon monoxide [CO], nitrogen dioxide [NO_2], among other) from the sector in the following years. Despite this slow down period, the European's overall transport emissions in 2014 were 20% higher than their 1990 levels. In 2014, about a quarter of the European's total GHG emissions came from road traffic. According to preliminary data, passenger cars contributed to 44% of transport sector emissions, and heavy-duty vehicles and bus a further 18% (EEA, 2016b).

Changes in climate are firmly expected over the 21st century (IPCC, 2013). Climate change will result in an impact on the general weather patterns, in particular, wind climatology, temperature, sunshine hours and rainfall patterns. This in turn may result in a change to the processes that govern chemical transformations in the atmosphere, which will cause air quality changes. In this sense, despite the European legislation imposes a transition to cleaner alternative fuels to reduce emissions, it is crucial that cities are able to absorb the impacts related to climate change and poor air quality. The inclusion of green infrastructures (i.e. green roofs, urban green areas, green walls) have been pointed as low-cost and easily applicable strategies to deal with extreme weather events (Carvalho et al., 2017). This type of resilience measures increases the evapotranspiration process and available surface moisture in cities, redirecting the energy partitioning to the form of latent heat flux rather than the sensible heat (as discussed in Chapter 4). Through reducing sensible heat flux between the atmosphere and the built-up surfaces (i.e. roads and sidewalks surfaces, walls and roofs of buildings), the urban temperature is reduced. Additionally, beyond the economic and social benefits related to the inclusion of vegetated areas in cities (EC, 2015), some works have also showed an ability of these infrastructures to improve air quality and mitigate air pollution (EEA, 2011). Many studies have concluded that the aerodynamic (dispersion and deposition) effects of trees are more important than the chemical effects (i.e. uptake) (Nowak et al., 2006) and of those, that dispersion appears to be more important than deposition (Jeanjean et al., 2016). Modelling studies have shown a modest

impact of vegetation on air pollutants deposition with less than a few percent reduction (Nowak et al., 2006; Tallis et al., 2011; Selmi et al., 2016).

With the continuous increase of hardware capabilities and the optimisation of numerical methods, Computational Fluid Dynamics (CFD) models have become common tools to simulate airflow and air pollutant dispersion patterns at street level (Amorim et al., 2013; Zheng et al., 2015). CFD is a branch of fluid mechanics which aims at solving numerically a system of partial differential equations that describes the motion of fluids by Navier-Stokes equations. CFD models can be classified into three categories according to the technique to numerically solve the Navier–Stokes equations: i) Reynolds-Averaged Navier-Stokes (RANS) approach; ii) Large-Eddy Simulation (LES); iii) Direct numerical simulation (DNS) approach. The choice among these three methods is a balance between the cost and the goal. Several studies have been using CFD models with boundary conditions given by mesoscale models to perform air flow and dispersion analyses in city areas. Tewari et al. (2010) and Miao et al. (2013) demonstrated that by using outputs from the Weather Research and Forecast (WRF) model as the initial and boundary conditions, the prediction ability of a CFD model applied over an urban area can be improved.

In this study a set of numerical simulations, at street canyon level, have been performed to assess the aerodynamic effect of different resilience measures, based on green infrastructures, in the flow (wind velocity) and dispersion (air pollutant concentrations) processes within a built-up area of Portugal in the city of Porto. A modelling system composed by the WRF-CFD models was used. An urban canopy parameterization scheme was used in the WRF simulation to better simulate urban meteorological conditions. The work is focused in the most critical air pollutants of the study area (with frequent exceedances of the annual limit value for NO_2 and the daily limit value for PM10 [Monteiro et al., 2007; Borrego et al., 2012; Miranda et al., 2016]), which are also the main pollutants emitted by the road traffic sector: nitrogen oxides (NO_X), particulate matter with an aerodynamic diameter less than 10 µm (PM10), and carbon monoxide (CO). Additionally, carbon dioxide (CO_2) is also assessed due to its importance as greenhouse gas and due to the most recent outcomes that shows the harmful effects of CO_2 for human health, and so, it should be treated as an air pollutant. This work provides a holistic approach to deal with air quality problems, by adapting the concept of resilience to air pollution and evaluating the ability of a city to tackle air pollution issues through green urban planning. This paper is presented as follows: Section 6.2 describes the modelling setup methodology including a brief description of the applied models and their configuration for the simulations. Also in Section 6.2 the case study is characterized and the green resilience scenarios are defined. A comparative analysis between the different scenarios, as well as a model validation, are presented in Section 6.3. Summary and conclusions follow in Section 6.4.

6.2. DATA AND METHODS

6.2.1. Model setup

Mesoscale model

The WRF model, version 3.7.1, was set up with four domains (Figure 6-1). The outer domain (D1), covering Europe and North of Africa, has 173x142 horizontal grid cells with horizontal resolution of 27 km; the nested domain D2 covers the Iberian Peninsula and has a 175×166 horizontal grid cells with a horizontal resolution of 9 km; and D3 covers the Northwest of Portugal and has 121×109 horizontal grid cells with a horizontal resolution of 3 km. The inner domain (D4) has 34×34 horizontal grid cells with horizontal resolution of 1 km, covering the Porto urban area. The vertical grid was composed by 30 vertical layers up to the top of the computational domain (50 hPa). The two-way nesting technique (Skamarock et al., 2008) was applied for the simulations.

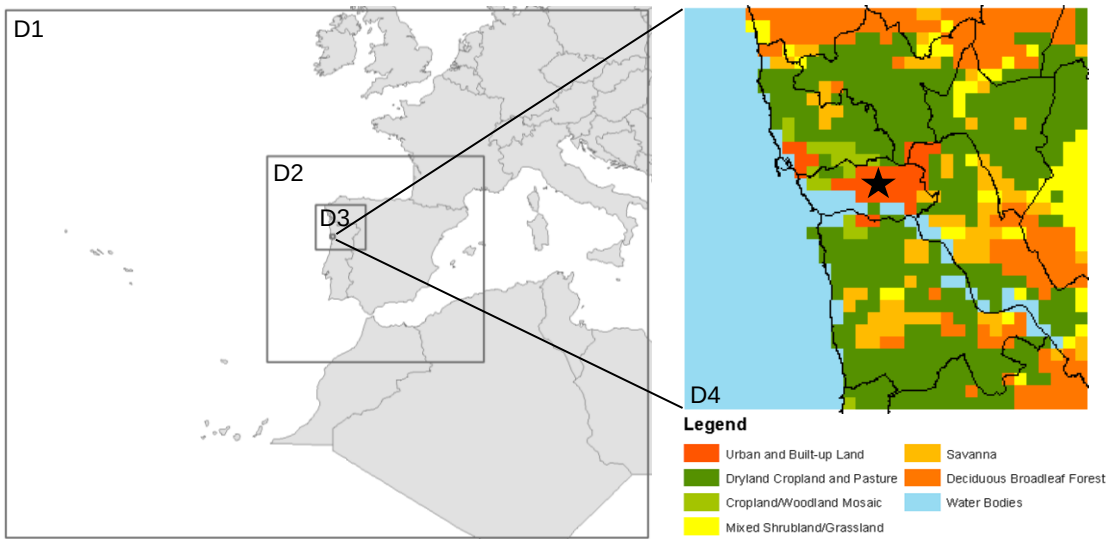

Figure 6-1. Configuration of the WRF model domains. Horizontal resolution of the coarse domain is 27 km with 173x142 horizontal grid cells (D1). The inner domain has a horizontal resolution of 1 km with 34x34 horizontal grid cells (D4). The black star shows the location of the study area (classified as Urban or Built-up Land, according to the United States Geological Survey (USGS) 24 land use categories).

The meteorological initial and boundary conditions were initialized with ERA-Interim data from the European Centre for Medium-Range Weather Forecasts (ECMWF) global analysis (horizontal resolution of 1º x 1º) with a temporal resolution of 6-h intervals. The sea surface temperatures and the soil moisture were also initialized using the ECMWF data. Information regarding the land use/land cover was taken from the Corine land cover project (Büttner et al., 2006) 2006 version (CLC2006), with a 3 arc-seconds horizontal resolution, remapped to the United States Geological Survey (USGS) 24 land use categories, following the methodology proposed by Pineda et al. (2004). The physics parameterizations were selected based on recommendations included in Wang et al. (2014), as well as on validation and sensitivity studies previously performed over Portugal (Carvalho et al., 2006; Monteiro et al. 2015, 2016). The physical options for the inner domain included: the Dudhia shortwave

radiation scheme (Dudhia, 1989) and the RRTM (Rapid Radiative Transfer Model) longwave radiation scheme (Mlawer et al., 1997); the Yonsei University (YSU) Planetary Boundary Layer scheme (Hong et al., 2006), and the WRF single moment 5-class scheme (Hong et al., 2004).

In order to better represent the physical processes involved in an urban environment (exchange of heat, momentum and water vapour) the Noah land surface scheme with a single layer urban canopy model (UCM) was also used. The UCM has a simplified urban geometry. Some of its features include, shadowing from buildings, reflection of short and longwave radiation, wind profile in the canopy layer and multi-layer heat transfer equation for roof, wall and road surfaces (Kusaka et al., 2001; Kusaka and Kimura, 2004). A full description of the WRF simulations and of the physical parameterizations used can be found in Chapter 5.

The WRF model was used to provide the initial and boundary conditions (velocity components) to the CFD model to recalculate flow fields for the area of interest. A grid cell nearest to the location of CFD domains (at north-northwest, according to the predominant wind direction) was selected and used to this purpose.

CFD model

The Computational Fluid Dynamics (CFD) model, VADIS (pollutant dispersion in the atmosphere under variable wind conditions) was applied to a densely built-up neighbourhood (Figure 6-2) within the Porto urban area (D4). VADIS was developed as a tool to estimate the dispersion of pollutants in the atmosphere and it was prepared to deal with unfavourable dispersion conditions, low wind speeds (<2 $m \cdot s^{-1}$). This model was also adapted to urban street canyon air pollution calculation due to the traffic road emissions and to the estimation of local hot-spots (Borrego et al., 2003). Currently, VADIS has the capability to support multi-obstacle (buildings and trees) and multi-source description as well as, time varying flow fields and time varying emissions, allowing the evaluation of maximum short-term local concentrations in urban geometries (Amorim et al., 2013).

The VADIS structure is based on two modules. The FLOW module uses the numerical solution of the three-dimensional (3D) Reynolds Averaged Navier-Stokes equations and the 1st order $k - \varepsilon$ turbulence model to calculate the wind, turbulent viscosity, pressure, turbulence kinetic energy and temperature 3D fields. In this module two different grids are used: the wind and the cartographic grids. The information related to the obstacles (buildings and vegetation) and to the emission sources position (e.g. roads) and dimension is defined on the cartographic grid. The wind field is calculated over a Eulerian grid, which is overlaid to the cartographic one and rotates according to the wind direction. The grids dimension and number of cells in each axis must be defined as a compromise between the required resolution and accuracy, and the computational demand. The DISPER module applies the Lagrangian approach to the computation of the 3D pollutant concentration field using the wind field previously estimated by FLOW. This approach assumes that the spatial and temporal dispersion of the mass of pollutant emitted is represented by a large number of numerical particles arbitrarily released

in the flow. In each time step, each particle displacement is calculated by the sum of a deterministic component obtained from the velocity field, the stochastic component related with the local turbulence translated by the Langevin stochastic theory and the influence of the fluctuation forces, represent by the Langevin equation (Lee and Naesslund, 1998). Initially, the wind field is calculated considering the stationary conditions (FLOW module) and then the model calculated the displacement of these numerical particles over the cartographic grid (DISPER module). The output provided by VADIS includes the three wind velocity components, the turbulent viscosity, the turbulent kinetic energy, the turbulent dissipation, the temperature and the pollutant concentration in each grid cell for the entire cartographic grid.

The VADIS model includes the Urban Vegetation (URVE) module, which accounts for the aerodynamic effects of trees over the 3D wind field, to better understanding the flow and dispersion of air pollutants in urban environments. The main concept behind the simulation of the aerodynamic effect of urban vegetation is the extension of the standard mean flow and turbulence equations with additional source terms for momentum, turbulent kinetic energy and its dissipation that mathematically represent the aerodynamics behind the interaction of leaves and branches with the 3D wind flow. Consequently, the dispersion of the emitted air pollutants is conditioned by vegetation trough this disturbed wind flow. The magnitude of this perturbation depends most of all on the characteristics of the vegetation itself (e.g., location, size) and of the incoming air flow (e.g., velocity, direction, turbulence). A more complete description of VADIS can be found on Borrego et al. (2003, 2004) and Amorim et al. (2013).

VADIS performance has been improved through the years. The simulation results were validated with wind tunnel measurements performed at the Department of Environment and Planning of the University of Aveiro (Richards et al., 2006) as well as through comparison with measured data from air quality stations (Borrego et al., 2003, 2004; Amorim et al., 2013). The model performance was also evaluated through comparison with other numerical models (i.e. the FLUENT model [Vardoulakis et al., 2011; Amorim et al., 2013]).

6.2.2. Model application

6.2.2.1. Case study description

The study area is located at approximately 3 km north (N) of the Porto city centre (Portugal), and is a typical built-up neighbourhood in the city. The area consists in a residential, commercial and recreational area with a few sparse green areas; the majority of the area is covered by impervious surfaces (90%). In the vicinity of the site, both residential and commercial areas are characterized by high buildings (around 6 floors). The area comprises important traffic thoroughfares bounded by the presence of a complex array of buildings (Figure 6-2). The existence of a meteorological station located inside the study area allows the evaluation of wind velocity simulations.

The numerical simulations were performed following the best practice guidelines proposed by the COST Action 732 (Frank et al., 2007). In this sense, for the simulation of urban flows with multiple buildings, the vertical, horizontal and downwind extensions of the computational domain were defined with a minimum of $5H_{max}$, where H_{max} represents the height of the tallest building. The complexity of the urban objects (buildings and trees) present in both domains was reduced by assembling adjacent individual volumes with similar characteristics. Specifically, in the case of trees, the grouped elements were defined as parallelepipeds positioned at a given distance above ground, representing the average trunk height. The generation of the urban objects (3D buildings, trees and roads) have been virtually defined in VADIS using the geometry pre-processors developed, based on the coordinates of the objects (Figure 6-2). A brief description of the study area (baseline scenario) is given in Table 6-1.

Regarding boundary conditions, at ground and buildings surfaces no-slip conditions were imposed. The standard wall functions proposed by Launder and Spalding (1974) were used. In the near-wall region the logarithmic law-of-the-wall for the mean velocity was applied. Wall roughness effects were modelled applying the law-of-the-wall modified for roughness. The assembled tree volumes were defined in the model as porous elements, in which transport equations were solved. A key parameter to describe the vegetated canopy characteristic is the Leaf Angle Distribution (LAD), which varies according the species, site fertility, time of the day and the year, weather conditions and even within stands (Amorim et al., 2013). However, due to the difficulty and complexity inherent to the measurement of the vertical distribution of forest canopy elements, few data are available. In this sense, and according to the work of Lalic and Mihailovic's (2004) work, an average LAD of 1 $m^2 \cdot m^{-3}$ was considered. The emission sources (roads) were defined as line sources, and created as fluid zones.

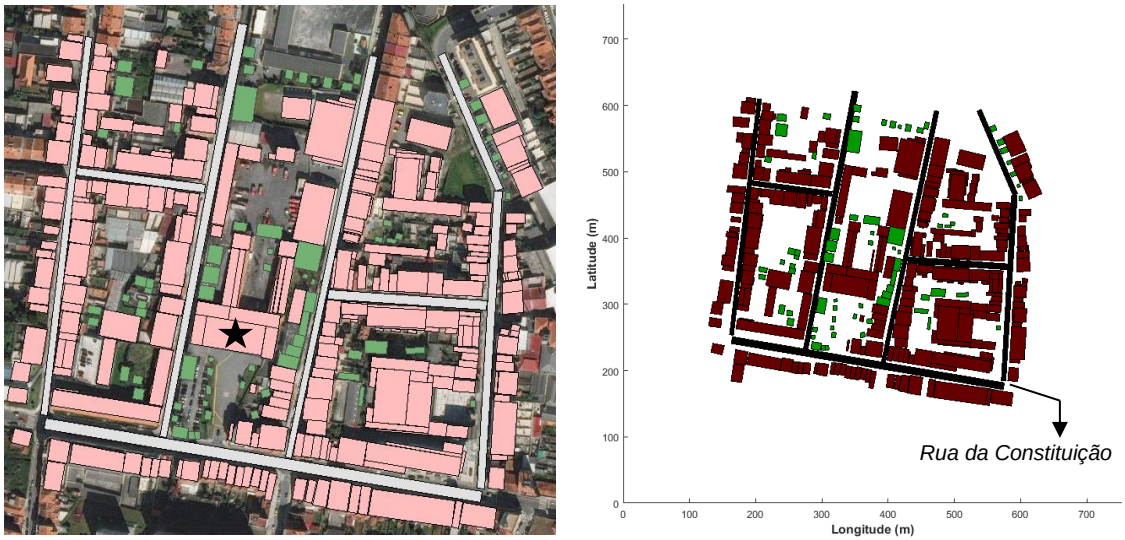

Figure 6-2. 2D computational domain generated by the VADIS model for the set of buildings (in dark red), trees (in green) and roads (in black) (image on the right). The computational domain was developed based on satellite images of the study area (image on the left). The black star indicates the location of a meteorological station (wind velocity).

Table 6-1. General description of the computational domain (baseline scenario) (Ld and Wd represent the total length and width of the domain, including the open belt around the built-up area. Letter N indicates number).

Domain		**Mesh**		**Buildings**			**Trees**		**Roads**
Ld x Wd (m)	Type (-)	Resolution (m)	N cells (-)	N sets (-)	Height range (m)	N sets (-)	Crown height (m)	Total height (m)	N sets (-)
753 x 753	Regular	3	251 x 251	298	3.0 -25.0	72	1.0 – 6.0	2.0 - 9.0	8

Inflow boundary conditions for the wind velocity components were provided by the WRF model at 10 m high. Richards and Howey's (1993) vertical profile equations were used to specify the variation of velocity (U), k and ε with height at the inlet boundaries assuming neutral stability conditions. A typical surface roughness length value, defined as 1.5, for an urban area with medium height was considered (Grimmond and Oke, 1999). A week and weekend day were selected to characterize distinct emission dispersion behaviours. The selected periods correspond to neutral stability conditions, in agreement with the numerical approach adopted in this study. Figure 6-3 shows the wind rose for the study periods. The data show that wind direction was predominantly from Northwest (more than 30%) for both days. The wind velocity oscillates between the days and the hours; the week day shows an average wind velocity of 3 $m \cdot s^{-1}$, reaching a maximum value of 6.6 $m \cdot s^{-1}$ (at 3 p.m.). At the weekend day the average wind velocity was of 2.2 $m \cdot s^{-1}$, reaching 3.8 $m \cdot s^{-1}$ (at 2 p.m.).

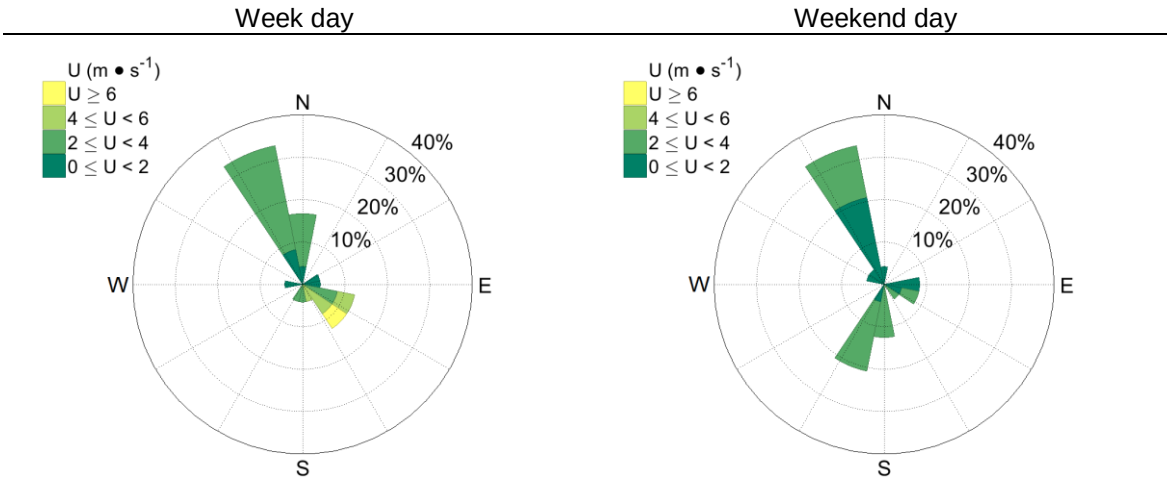

Figure 6-3. Wind roses at the inlet boundaries of the study area, for the week and weekend day periods.

The main road in the study domain is the *Rua da Constituição* with a total of two traffic lanes. Seven other streets perpendicular to the main road were also considered. Traffic flow data, for both study periods, were acquired using automatic devices in the study area. For the roads in which no data were available, empirical rates expressing the relation with the traffic in the surroundings roads were applied. Figure 6-4 shows the daily fluctuation of traffic volumes. The traffic flow data show a well-defined traffic dynamic and distinguished for the week and weekend days. At the week day, the peak periods occur at the early morning, between 7-9 a.m. (the daily traffic is reached at 8 a.m.), and at the beginning of the night between 7-8 p.m. (around 74% of the daily traffic). The off-peaks periods mostly occur at the night between 10 p.m. and 6 a.m. (daily traffic less than 25%). This is a typical behaviour of the traffic flow for a large city downtown. At the weekend day, the peak periods occur later; at 12 a.m. and 1 p.m. during the morning and between 11 p.m. and 3 a.m. during the night. On average, the daily traffic at the weekend is around 15% less than the registered at the week day. For both days, and even during off-peaks periods, a low volume ratio is maintained for all the domain.

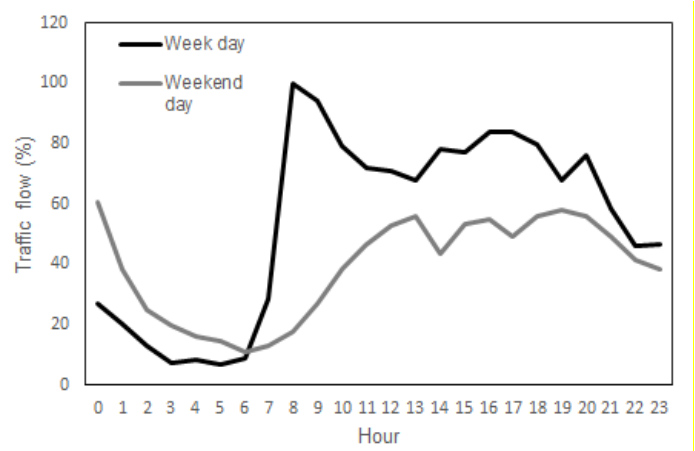

Figure 6-4. Typical daily traffic volume profile for both study periods (in percentage).

Hourly averaged air pollutant emissions were defined for each road applying the Transport Emission Model for Line Sources (TREM), based on vehicles counting data and according to the model cascade methodology validated by Borrego et al. (2003). TREM is based on the MEET/COST methodology. Emission factors are derived from the average speed (approximately 50 km h^{-1} in the considered roads), which is an approach with good results when the influence of driving dynamics can be neglected (Amorim et al., 2013). Beyond the traffic flows and vehicle speed for each road segment, the emission is estimated taking into account the aggregation of vehicles in the following categories: passenger cars, light duty vehicles, heavy duty vehicles and urban buses. For each vehicle category, different classes were considered that distinguish engine age, type and capacity, vehicle weight, fuel type (petrol, diesel and LPG), and emission reduction technology (emission standards implementation associated to vehicle age). Simulations were performed in an hourly temporal frame for NO_X, PM10, CO and CO_2.

6.2.2.2. Resilience scenarios

The concept of resilience has been widely used in the most recent research to denote the need of cities to increase the capability to tolerate or absorb the impacts related to climate change (i.e. heat waves). However, most of the resilience measures focused on the implementation of green infrastructures can also improve the quality of urban environment. In this sense, two resilience measures were selected based on consistently reported benefits and multifunctionality: green areas and green roofs. To assess the influence of these measures on wind flow and air pollutants dispersion four scenarios were defined, comprising: i) a baseline scenario, with the current characteristics, both in terms of wind flow and air pollutants concentration, of the case study; ii) an urban green area scenario, which consists in the implementation of a urban green area in the center of the domain (by replacing the current buildings); iii) a green roof scenario, which consists in the application of green roofs in a specific area of the domain; the area was selected to allow a direct comparison between the urban green area and green roofs implementation; iv) a "grey" scenario, which consists in the removal of the current vegetation; this scenario was defined to assess the importance of the vegetation in the atmospheric dispersion and air quality.

The domain dimension, the mesh resolution, the boundary conditions and the air pollutant emissions were kept constant for all the scenarios. Table 6-2 shows the general characteristics of the computational domains for each scenario. The computational domains for the grey and the green scenarios are displayed in Figure 6-5.

Table 6-2. General description of the computational domains used to simulate the different resilience scenarios.

		"Grey" scenario	**Urban Green Area**	**Green roofs**
Buildings	N sets	298	278	298
	Height range (m)	3.0 – 25.0	3.0 – 25.0	3.0 – 25.0
Trees	N sets	0	92	92
	Crown height (m)	0	1.0 – 6.0	1.0 – 6.0
	Total height (m)	0	2.0 – 20.0	1.0 (height of green roofs) – 9.0 (maximum height of trees)
Roads	N sets	8	8	8

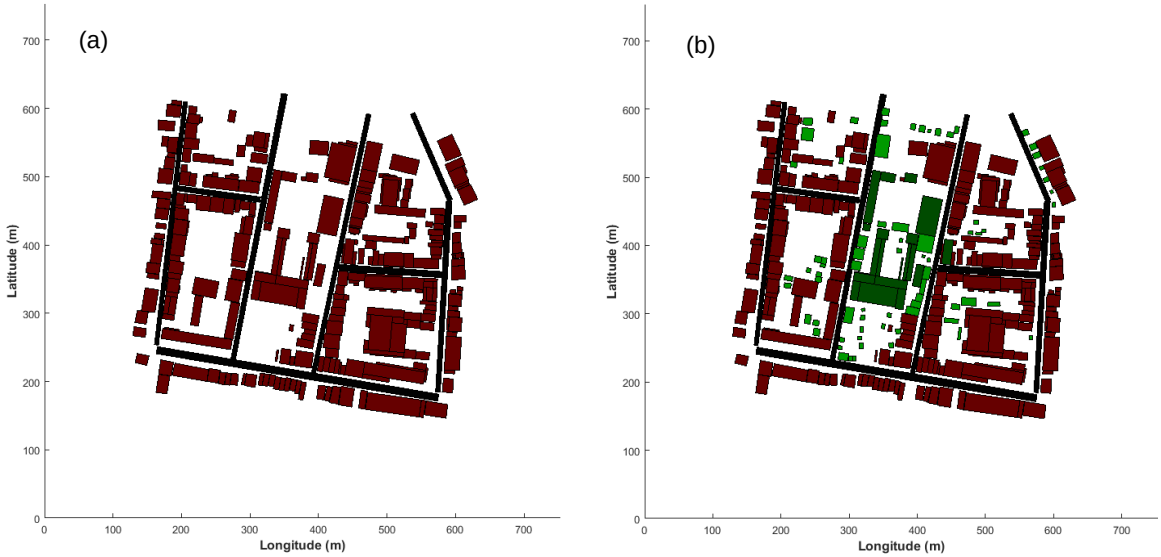

Figure 6-5. 2D computational domains generated by the VADIS model for the resilience scenarios: (a) "grey" scenario (without trees) and (b) both urban green area and green roofs scenarios. The dark red shows the set of buildings, the light green shows the trees, the black shows the roads, and the dark green shows the intervention area for the implementation of both green roofs and urban green area.

6.3. RESULTS AND DISCUSSION

Given the described methodology (section 6.2), the capability of VADIS to simulate the wind flow was evaluated (section 6.3.1), since most of the resilience measures under study will influence the flow pattern. Then, the influence of resilience measures on air pollutants concentration was assessed in terms of behaviour and magnitude (section 6.3.2).

6.3.1. Flow validation and baseline characterization

The performance and accuracy of the model was evaluated in terms of wind flow through the application of the BOOT software (Chang and Hanna, 2005). The following parameters were calculated: average bias (MB), normalised mean square error (NMSE), Pearson correlation coefficient (r), and factor of two (FAC2). Results are shown in Table 6-3. Additionally, time series for both week and weekend day were analysed to assess the ability of VADIS to represent the daily wind velocity variability (Figure 6-6). The measured data were provided by the meteorological station located inside the domain (see section 6.2).

Table 6-3. Statistical parameters for the assessment of modelling performance relative to the measurements. A total of 48 values (hours) were used to perform this analysis.

	Statistical Parameters			
Model acceptance criteria	MB ($m \cdot s^{-1}$)	NMSE (-)	r (-)	FAC2 (-)
	-	<1.5	-	>0.5
Wind velocity simulation	-0.34	0.10	0.767	0.917

The temporal variation of the mean hourly values of measured/modelled wind velocity shows, for both study periods, a good agreement. The statistical parameters also indicate a good performance of VADIS, with a correlation between the measured and modelled data of 0.77 and a NMSE lower (0.10) than the maximum of 1.5 defined by the acceptance criteria of Chang and Hanna (2005). FAC2 also shows a value that is in accordance with the acceptance criteria (higher than 0.5). Overall the model exhibits a tendency to underestimate the wind velocity, with a negative MBE of 0.34 $m \cdot s^{-1}$. These results are in accordance with the data obtained in previous works (Borrego et al., 2003, 2004, Amorim et al., 2013) and gives the confidence to apply the model for the different resilience scenarios.

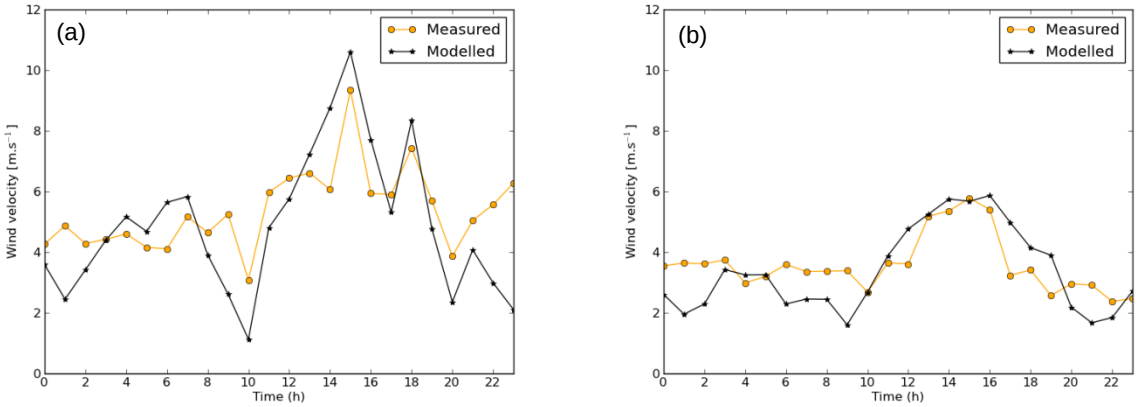

Figure 6-6. Time evolution of the hourly values of wind velocity ($m \cdot s^{-1}$) measured in the meteorological station and simulated for the same location, for both study periods: (a) week day; (b) weekend day.

Since to distinguish periods, in terms of both emissions and meteorological conditions, was considered, a comparison of the influence of these factors on air pollutants concentration is provided (Figure 6-7). This analysis was done in an hourly base and considering a spatial average of the domain. The results reveal that both pollutants have a similar profile. The concentration profiles follow the behaviour of the traffic flow, as expected, with the higher concentrations obtained at the week day and for the peak periods of road traffic (maximum concentrations are obtained at 10 a.m. with values of around 445, 149, 10 and 40 $\mu g \cdot m^{-3}$ for CO, CO_2, PM10 and NO_X, respectively, which is a result of a combined effect of low wind velocity and higher emissions). At the off-peak periods the concentrations are very similar for both days, despite the differences in the traffic flow (as previously mentioned, at the weekend the traffic flow is 15% less than the observed at the week day). This behaviour is related to the low wind velocity registered in this period at the weekend day (around 2.2 $m \cdot s^{-1}$, which compared with the week day correspond to a reduction of the wind velocity in the range of 14-51%) that does not promote the air pollutants dispersion. A low dispersion implies that air pollutants are retaining near the emitting source, increasing the levels of air pollutants concentration. Values of around 119, 31, 3 and 2 $\mu g \cdot m^{-3}$, are obtained for CO, CO_2, PM10 and NO_X, respectively, for the off-peak period (22 p.m. – 7 a.m. and 12 a.m. – 18 p.m.).

The modelled concentrations are considerably lower than the limit values of the European legislation, namely, the limit hourly value for CO (40 000 $\mu g \cdot m^{-3}$) the limit hourly value for NO_2 (200 $\mu g \cdot m^{-3}$), the limit daily value for PM10 (50 $\mu g \cdot m^{-3}$). These results are in accordance with the average values measured in an air quality monitoring station (classified as traffic station according the dominant emission source) located near of the study domain. The averaged measured values, in an hourly base, were the following: 389.3 $\mu g \cdot m^{-3}$ of CO, 18.5 $\mu g \cdot m^{-3}$ of PM10 and 64.2 $\mu g \cdot m^{-3}$ of NO_X. For CO_2, no measurements are available.

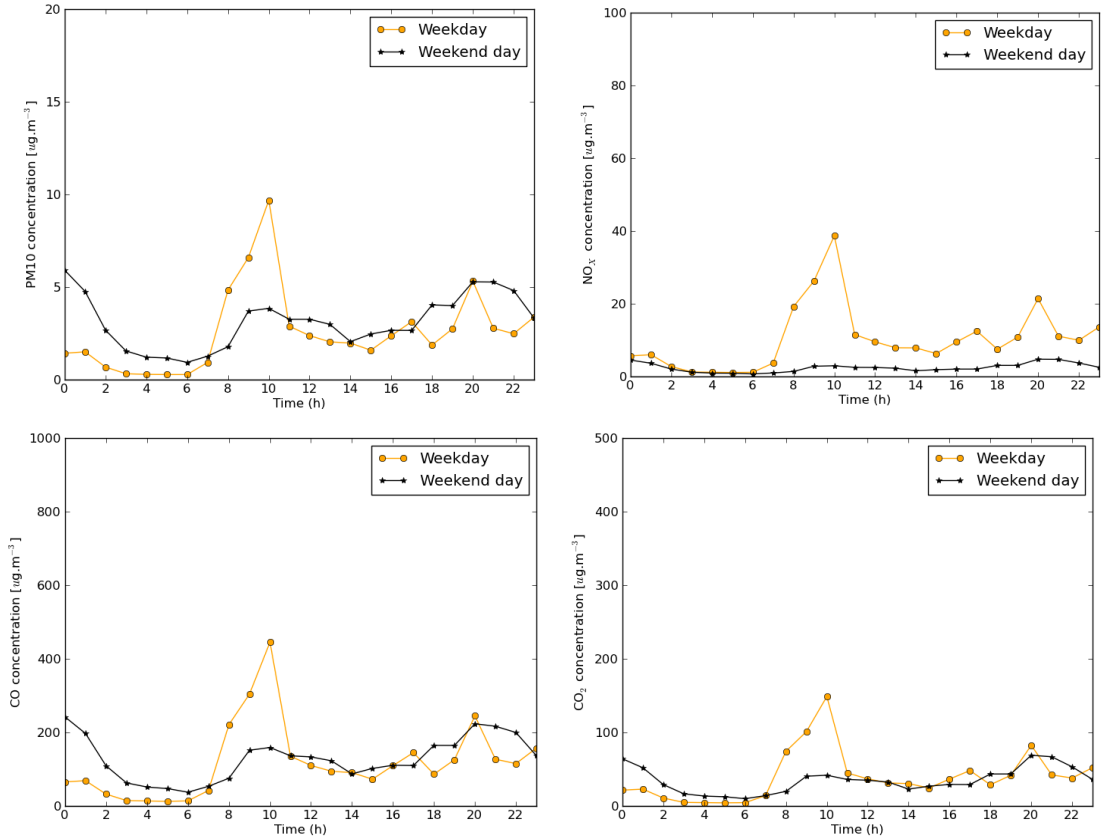

Figure 6-7. Time evolution of the mean hourly modelled values of PM10, NO_X, CO and CO_2 concentrations ($\mu g \cdot m^{-3}$), spatially averaged for the entire domain (baseline) for the week and weekend days.

6.3.2. Resilience scenarios analysis

The effects of the resilience measures on the air pollutants dispersion were investigated considering as reference the baseline domain. Two different approaches were used to provide this analysis: i) mapping of the hourly concentrations for each air pollutants and for each scenario (Figures 6-8 to 6-11) to understand the spatial variability of the air pollutants concentration according to the configuration of the urban elements (buildings and vegetation); for this analysis two different periods of the week day were selected (9 a.m. and 8 p.m.) based on the higher emissions and the different wind conditions; ii) time evolution of the hourly mean for both pollutants, based on a spatial average of the domain, to quantitatively assess the influence of resilience measures.

For all the pollutants, at the baseline scenario, the higher concentration values occur in *Rua da Constituição* and in the adjacent pedestrian area, as a result of the conjoint influence of higher road traffic emissions and the wind flow direction (winds blow from northwest at 9 a.m. and from northeast at 8 p.m.). It can be observed that when the wind blows from northwest (i.e. 9 a.m.) the air pollutants are retained in leeward side of the street canyon (buildings on the lower left side of the domain – west side of *Rua da Constituição*) increasing the air pollutants concentration in this area; this is a result of the influence of the 3D configuration of buildings over the wind flow. This behaviour is originated by the oblique roof-level incoming winds that induce a counter-clockwise swirling flow along the canyon (Amorim et al., 2013). As a result, this vertical airflow transports the pollutant emitted near the ground level by traffic towards the leeward of the street canyon, where the pollutants are trapped by the decreased vertical exchange rate of air with the above roof-level atmosphere. It is also clear that this behaviour does not occur in east side of the *Rua da Constituição* since the dispersion of air pollutants is channelled through the existent open space between buildings.

Additionally, it was observed, for the great majority of the hourly simulations, that the effects induced by the vegetated canopy on the wind flow lead to the formation of hot-spots around trees, in specific areas, with an increase of air pollutants concentration. The magnitude of these effects is mostly dependent on the orientation of the incoming wind in relation to the positioning of the emission sources, buildings and trees. Thereby, can be inferred that the effect of trees on air quality is extremely spatially dependent, mostly because the heterogeneous positioning of trees that induces complex wind flow patterns. These results are in accordance with the findings of previous studies which have shown that the aerodynamic effect of trees would end up trapping road emissions (Gromke et al., 2008; Buccolieri et al., 2011; Wania et al., 2012). Other studies have found that the alignment of trees with the incoming wind enhance the ventilation, promoting air pollutants dispersion (Amorim et al., 2013; Abhijith and Gokhale, 2015). In fact, this can be seen in the results obtained by 8 p.m., which show a reduction of both number and magnitude of hot-spots around trees when compared with the data for 9 a.m. (reduction of around 50%). This is only a result of wind orientation since the wind velocity is the same for both time periods (1.6 $m \cdot s^{-1}$). It can be concluded that the street canyon trees have the ability to be beneficial for air quality, depending on the prevailing wind direction, wind speed, street canyon and surrounding buildings geometry.

When the set of buildings in the central part of the domain are replaced by a green urban area, the results show a reduction of the air pollutants concentration of around 16% (compared with the baseline scenario), in the overall domain and for all the analysed pollutants. The decrease of air pollutants concentration is due to an increase in the turbulence production (Jeanjean et al., 2016) related to the increase of wind velocity (around +1 $m \cdot s^{-1}$, on average, when compared with the baseline; maximum difference of +2 $m \cdot s^{-1}$ is obtained at 3 p.m.). It can also be seen that despite the general improvement of air quality (decreasing of air pollutants concentration), the implementation of an urban green area lead to the formation of additional hot-spots due to the rearrangement of vertical flow structures. Therefore, the higher concentrations within the green urban area are a consequence of: i) air recirculation induced by the building's walls and trees; and ii) the decrease of wind velocity at

these spots (reduction of around 40%, when compared with the baseline; a maximum difference of -60% is obtained at 10 a.m.), which then decreases the dispersion. Additionally, it was concluded that for a wind speed equal or lesser than 1 $m \cdot s^{-1}$, no turbulent dispersion occurs under laminar conditions and the trees in the green urban area are shown to increase air pollutants concentrations in this area. Overall, the implementation of green urban areas promotes the improvement of air quality in their surroundings for several pollutants and thus, reduces the related effects on human health. A suggestion of this work is that, in general, for cities with average wind speeds greater than 1.5 $m \cdot s^{-1}$ a high vegetation cover improves air pollutants dispersion in an urban environment (great number of trees, better benefits). However, the cover management of trees (vegetation design), the species used and related LAD (tree species with high LAD are the best to enhance the aerodynamic dispersion [Jeanjean et al., 2016]) should be taken into account by urban planners.

Regarding the green roof scenario, the results does not show an improvement of air quality. This is mostly due to the fact that horizontal flow is weaker with green roofs (around 40% less when compared with baseline scenario). Overall, for most of the hourly simulations, the air pollutants concentration in terms of dispersion pattern is the same than the obtained for the baseline scenario (at 3 m above the ground). However, the magnitude of the air pollutants concentration is higher in specific areas when compared with the baseline scenario. Despite these findings, some studies have found a positive effect of green roofs on pollutant dispersion near roads (Berardi et al., 2014, Speak et al., 2012). Speak et al. (2012) found that while not as effective as street trees, due to lower surface roughness lengths and increased distance from sources, green roofs can be considered to reduce urban air pollution because their construction does not require major upheaval of the urban built environment, as tree-planting schemes often do. Another possible way to consider the benefits of green roofs on air quality improvement is by taking into account their capability to enhance buildings energy saving and to decrease the Urban Heat Island (UHI). As UHI increases radiant temperature and cooling loads of buildings, the effectiveness of green roofs in reducing the heat island will indirectly result in reducing energy consumption (Santamouris, 2014). Many studies mention that the decrease of energy consumption through green roofs would indirectly reduce the level of pollution (e.g., Sarrat et al., 2006; Stathopoulou et al., 2008). Should also be noted that, since the green roofs change the local temperature, they will influence the thermal stability of the atmosphere, and so, the magnitude and behaviour of air pollutants dispersion changes according to the stability conditions of the atmosphere (neutral, stable or unstable conditions).

The air pollutants concentration patterns in the “grey” scenario (without trees), highlights the importance of traffic flow, prevailing wind velocities and street geometry in determining pollutant concentrations within street canyons. The obtained results show that in the leeward side (of the *Rua da Constituição*) the concentrations are 7% [CO], 5% [CO_2], 10% [NO_X] and 9% [PM10] higher when compared with the baseline. Comparing the leeward and windward sides for these conditions, the results indicate that concentrations are 1.4 times higher in the leeward side, for both pollutants; a maximum difference of 2.6 times higher is obtained at 10 a.m. for CO, PM10 and NO_X, while for CO_2 the difference is of 2.2 times higher, at the same hour. These findings are in accordance with

modelling and field's studies that consistently reported that on the leeward side, pollutants concentrations are 2-3 or more times higher than those on the windward side of the street canyon (Vardoulakis et al., 2002, 2003; Salmond and McKendry, 2009; Xie et al., 2009). It can also be seen that the hot-spots observed in the baseline around the trees does not occur in the "grey scenario", confirming that these hot-spots are a result of the influence of vegetation canopy in wind flow. Overall, the results here obtained indicate that the absence of vegetation does not benefit the urban air quality.

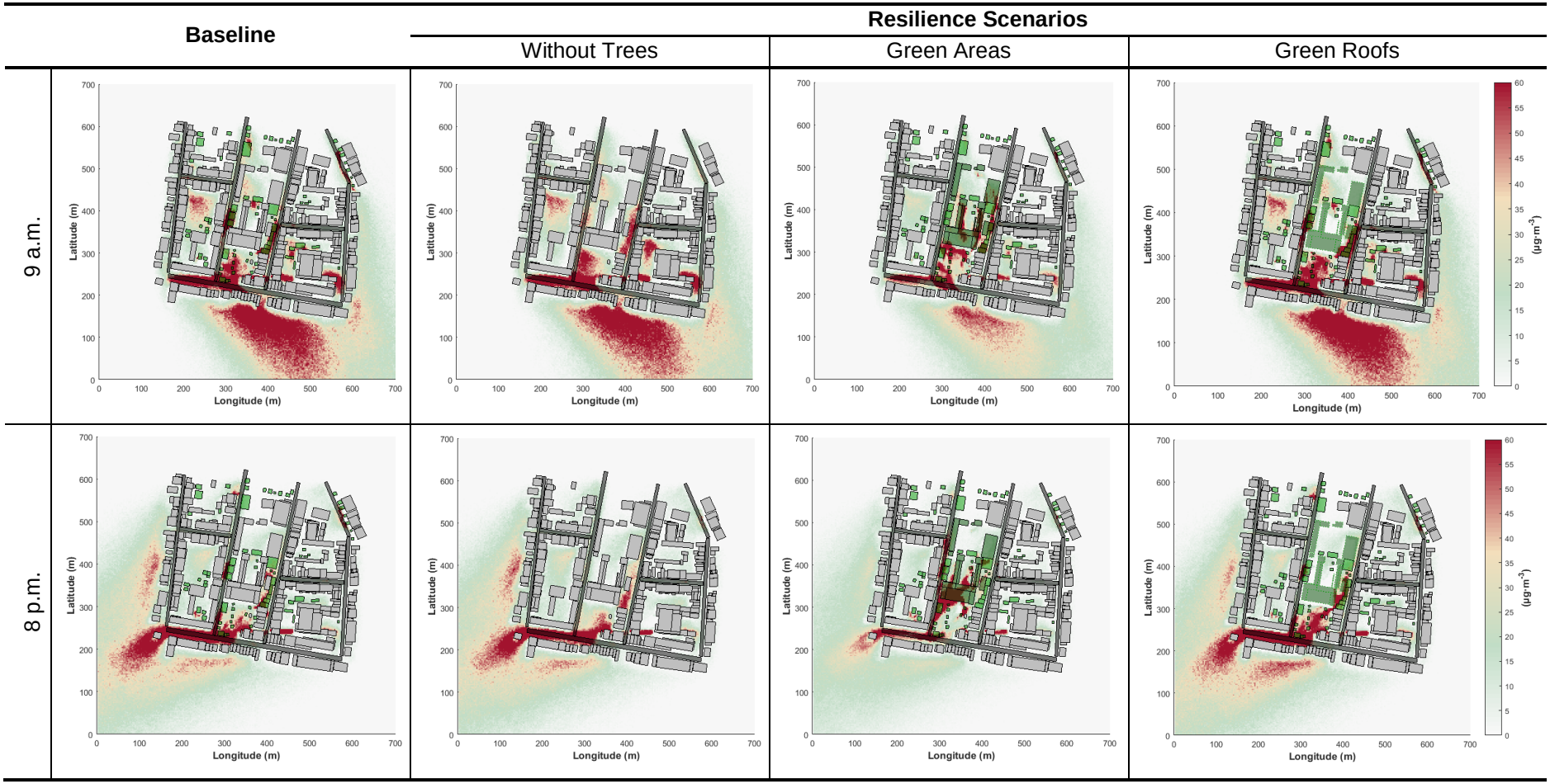

Figure 6-8. PM10 concentration field for the scenarios under study for 3 m high horizontal streamlines. Contours refer to the period of 9 a.m. (with a wind velocity of 1.6 $m \cdot s^{-1}$ and a wind direction of 330º) and 8 p.m. (with a wind velocity of 1.6 $m \cdot s^{-1}$ and a wind direction of 57º) for the week day.

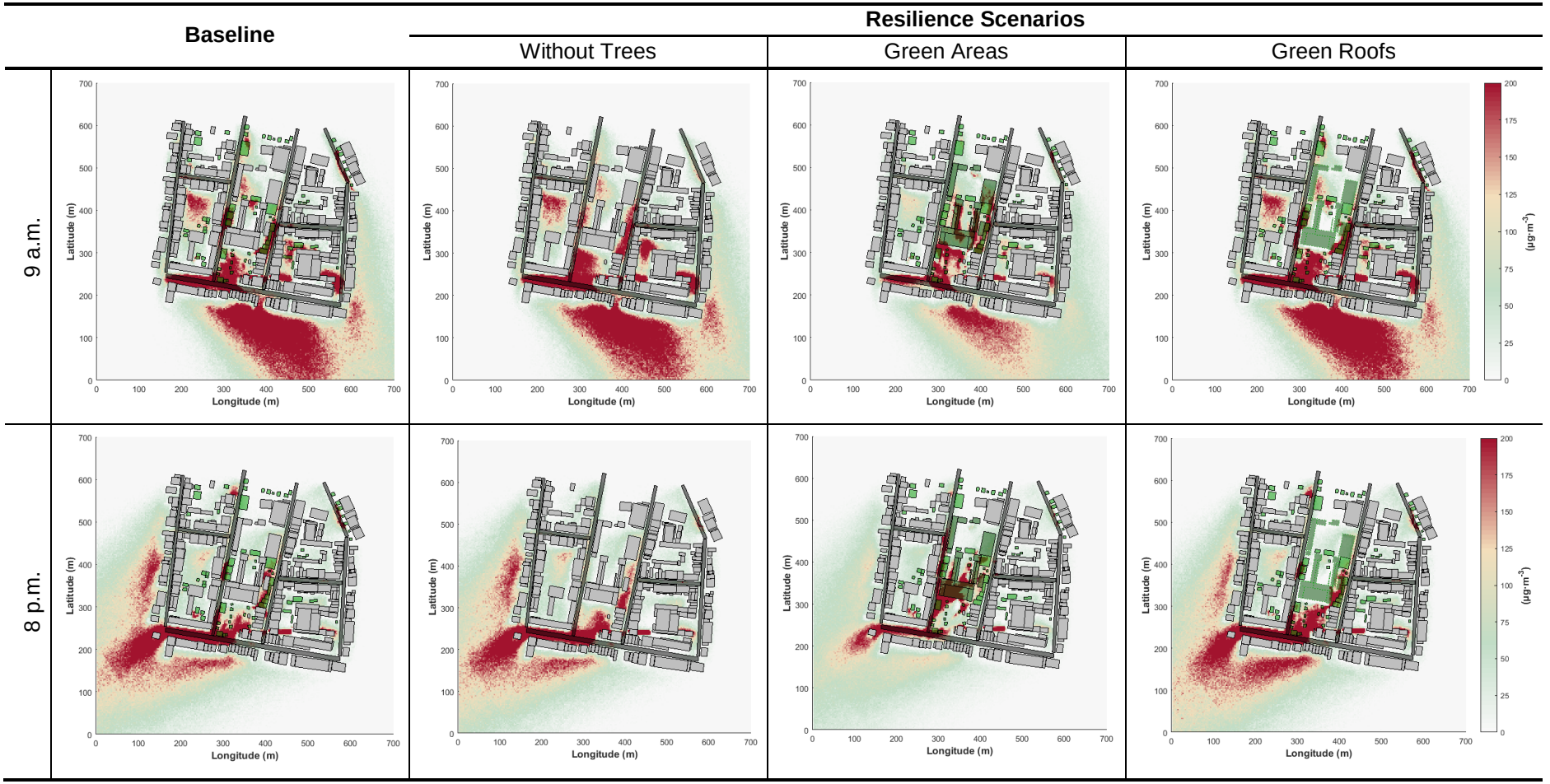

Figure 6-9. NO_X concentration field for the scenarios under study for 3 m high horizontal streamlines. Contours refer to the period of 9 a.m. (with a wind velocity of 1.6 $m \cdot s^{-1}$ and a wind direction of 330º) and 8 p.m. (with a wind velocity of 1.6 $m \cdot s^{-1}$ and a wind direction of 57º) for the week day.

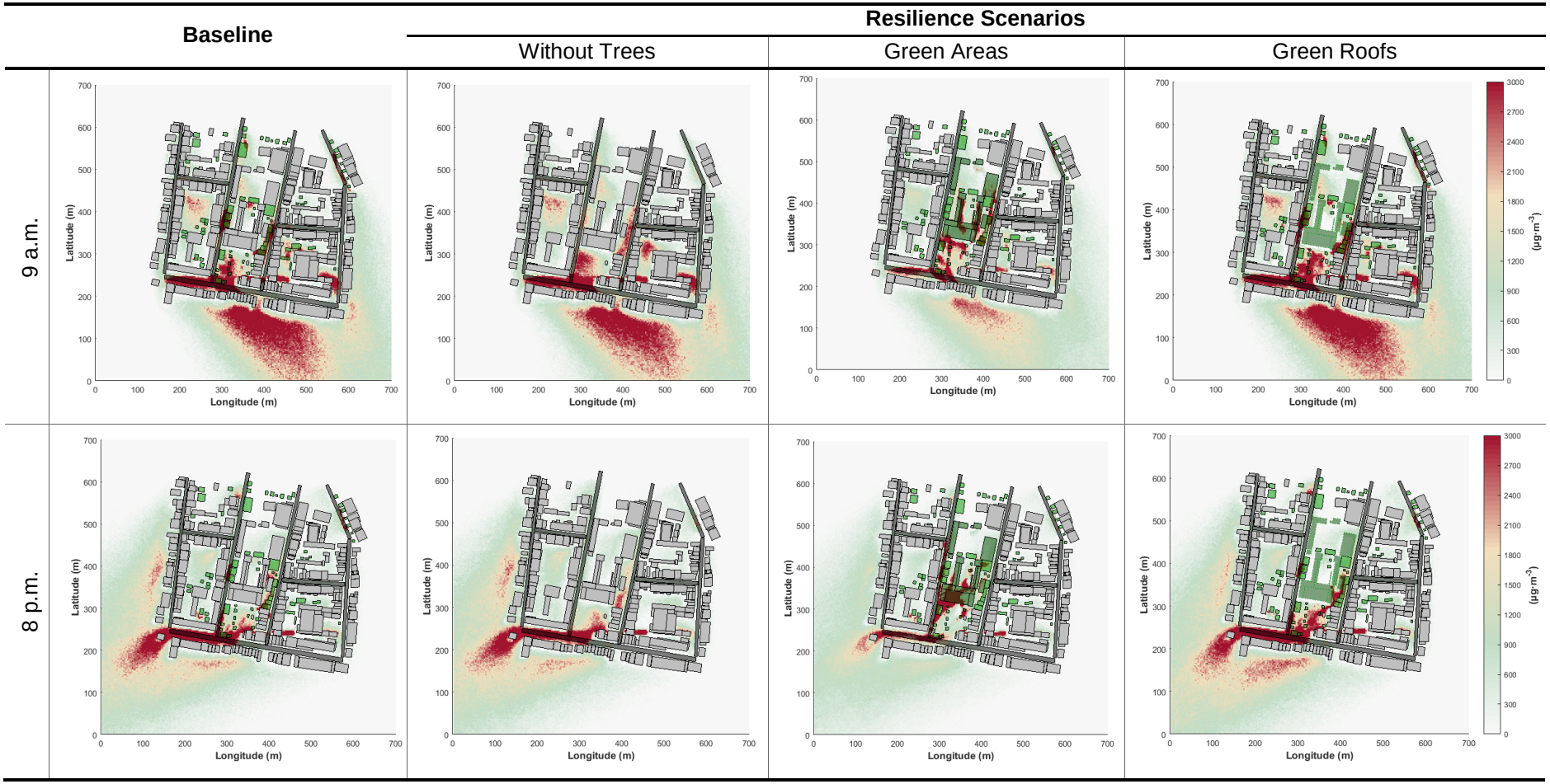

Figure 6-10. CO concentration field for the scenarios under study for 3 m high horizontal streamlines. Contours refer to the period of 9 a.m. (with a wind velocity of 1.6 $m \cdot s^{-1}$ and a wind direction of 330º) and 8 p.m. (with a wind velocity of 1.6 $m \cdot s^{-1}$ and a wind direction of 57º) for the week day.

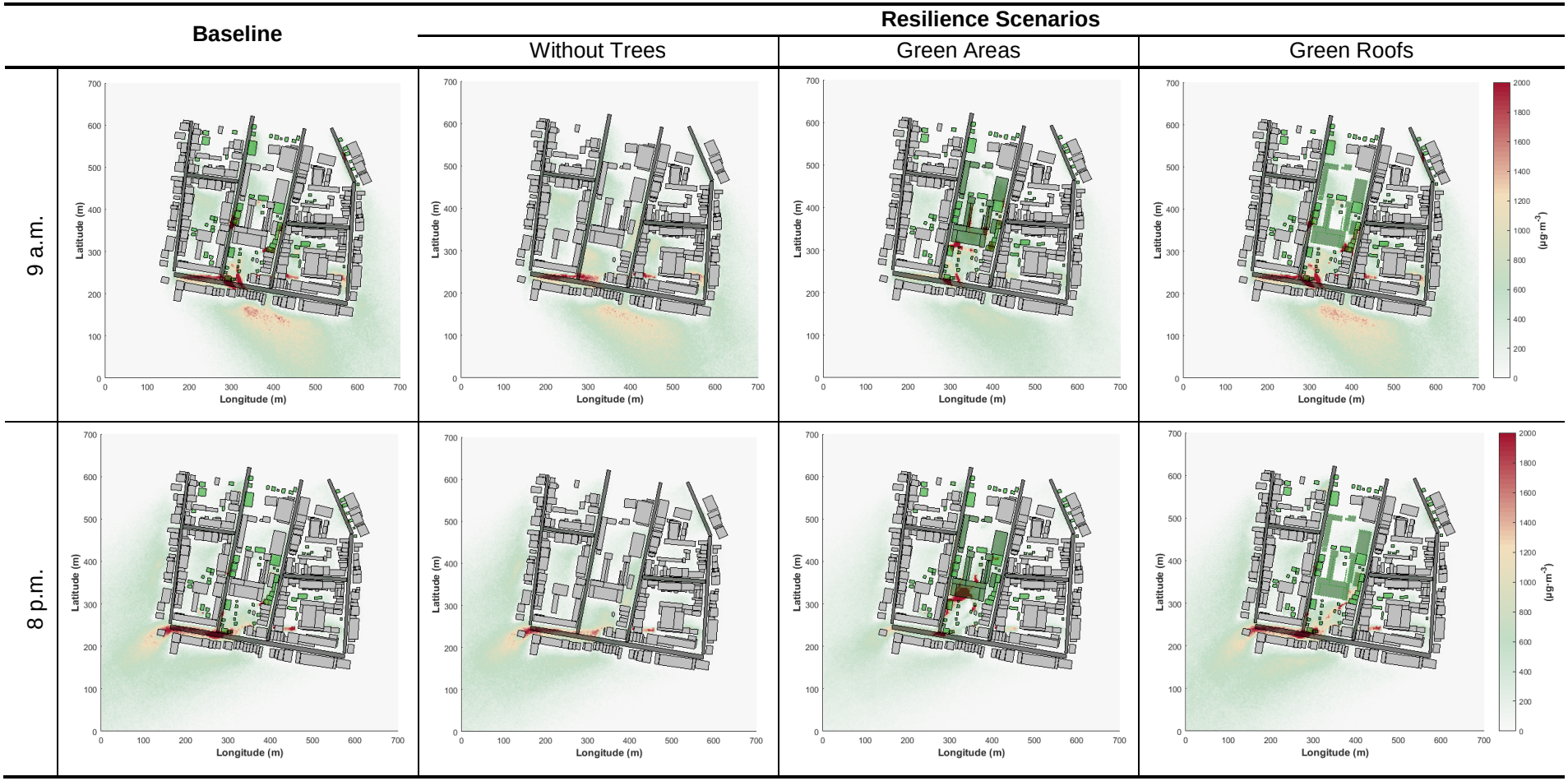

Figure 6-11. CO_2 concentration field for the scenarios under study for 3 m high horizontal streamlines. Contours refer to the period of 9 a.m. (with a wind velocity of 1.6 $m \cdot s^{-1}$ and a wind direction of 330º) and 8 p.m. (with a wind velocity of 1.6 $m \cdot s^{-1}$ and a wind direction of 57º) for the week day.

Figure 6-12 shows the time evolution of the mean hourly values for the different pollutants under study and for the set of the modelled scenarios. This analysis allows a quantitative comparison of the effects of the resilience scenarios in the air pollutants concentration values and was performed based on the average concentration values for all the cells of the domain. Therefore, the results represent the average behaviour of the study area, giving an idea of how resilience measures might influence the air quality of this region as a whole.

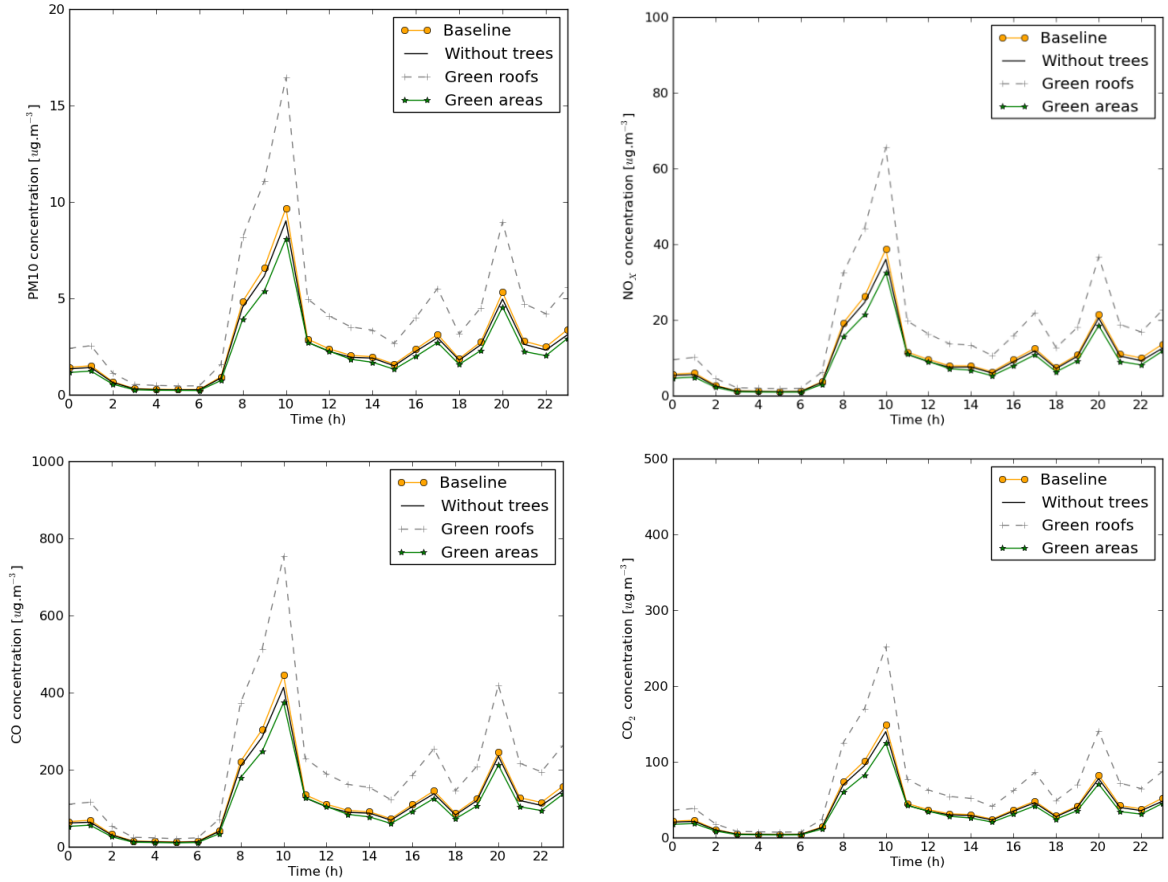

Figure 6-12. Comparative analysis of the time evolution of the mean hourly modelled values of PM10, NO_X, CO and CO_2 concentrations ($\mu g \cdot m^{-3}$) for the scenarios under study and for the week day, in a spatial average of the domain.

It is observed that the implementation of green roofs is the worst scenario in terms of concentration values for all the analysed air pollutants. In fact, for the majority of the simulation period, in particularly at 10 a.m., 5 p.m. and 20 p.m. green roofs result in 60% increase of pollutants concentration in relation to the baseline scenario (related to peaks of road traffic and wind flow). The CO_2 is the pollutant whose concentration most increases with the implementation of this type of resilience measures. As previously mentioned, this is mainly due to the changes promoted by the presence of vegetation in the wind flow, namely the influence in the vertical exchange rates of polluted air with the above roof-level atmosphere. It is interesting to realise that, despite the vegetation are implemented in a high level (building roof), it has a great influence at the pedestrian height (3 m in this case) for both wind flow and pollutants dispersion.

The inclusion of an urban green area is the scenario showing more benefits for air quality, with a general reduction of pollutants concentrations. The greater benefits (a reduction of air pollutants concentration of around 20%) are obtained along the periods 7-8 a.m. and 8-9 p.m. This is quite important since the identified periods correspond to road traffic peaks where the people are most exposed to air pollution (whether people are driving, walking on the street or at home). These benefits on air quality are also important under a climate change scenario, because NO_X and PM10 concentrations (annual means) will increase in the study region, even if emissions remain at current levels (Sá et al., 2016). CO is the pollutant that shows a higher reduction of its concentration, followed by PM10, CO_2 and NO_X. Beyond the air quality benefits, vegetation provides a set of ecosystem services namely: i) environmental, mostly related to its ability to abate the effects of climate change; ii) economic, for example, through the creation of local job opportunities; and iii) social, since having areas where the people can socialize and be in liaison with nature improves health and well-being.

The “grey” scenario shows a slight reduction (around 5%) for both pollutants concentration, mostly related with the dissipation of the hot-spots promoted by trees, which are characterized by higher air pollutants concentration. These results should be carefully analysed because of the potential fake notion of air quality improvement in the absence of vegetation. As previously mentioned, in the “grey” scenario an increase of the air pollutants concentration is observed near the emitting source, especially in the leeward side of the street canyon.

Overall, results reinforce the conclusions previously made with the analysis of the spatial distribution of air pollutants concentration, showing the benefits in terms of air quality improvement, of increasing the vegetation rates at the city level, when the city morphology and wind conditions are taken into consideration.

6.4. CONCLUSIONS

Nowadays, air quality problems still persist, especially in cities, where most of the European population lives. To make a city resilient to air pollution is a growing need, particularly in the current context of climate change. It is crucial the implementation of options that go further than the typical technological measures. This work aimed to assess the influence of different resilience measures, based on green infrastructures, in the flow and dispersion of air pollutants (CO, CO_2, NO_X, PM10) in a typical built-up area in Portugal. The WRF-CFD modelling setup was applied to quantitatively evaluate how the urban morphology and the green infrastructures affect the wind field and the pollutant distribution within the study area. Two distinguished periods were analysed and a set of scenarios were developed for this purpose.

The model performance (wind flow) was assessed for the current conditions (baseline scenario), showing a good capability of the CFD to simulate the wind patterns, with a Pearson correlation factor of 0.77 and a NMSE of 1.0, which is substantially lower than the threshold of 1.5 defined by modelling acceptance criteria. The analysis of resilience scenarios showed that green infrastructures have a role to play at city scale.

The results showed that the implementation of a green urban area leaded to an overall improvement of air quality, with a general decrease of both air pollutants concentration values of around 16%, mostly related to an enhanced ventilation and dispersion capacity of the street canyon. However, at some hot-spots, the air pollutants concentration increased due to lower wind velocities and the formation of additional recirculation areas. The implementation of green roofs showed an increase pollutants concentration, at specific areas, due to a decrease of the horizontal flow. This increment promoted an overall degradation of air quality in the study area, compared with the baseline scenario. The “grey” scenario (absence of vegetation) showed that local air quality is strongly dependent on the linkages between the traffic flow, meteorological conditions, the 3D configuration of the street canyon, and the presence of trees. Overall, the results indicate that, the absence of vegetation does not benefit the urban air quality. For all scenarios, the results showed that the change of the wind direction can strongly affect the dispersion patterns of pollutants (and concentrations), which was a more sensitive factor than the wind speed.

For the set of the analysed scenarios, the implementation of a green urban area is the best option for air quality improvement. Notwithstanding the overall benefits, it should be noted that in many city areas, space constrains mean that there are only limited opportunities for increasing vegetation density (especially tree density) within the existing urban fabric. This fact combined with the formation of hot-spots within the trees, shows the importance of using CFD tools in urban planning with the goal of optimising the role of green infrastructures on human comfort and health. Further works are required to investigate whether the findings in this study holds for other building configurations (such as a finitely long street canyon configuration and an array of cubical buildings) and other real urban morphologies, as well as, to other climate conditions.

6.5. REFERENCES

Abhijith K., Gokhale S. (2015). Passive control potentials of trees and on-street parked cars in reduction of air pollution exposure in urban street canyons. Environmental Pollution 204, 99-108.

Amorim J.H., Rodrigues V., Tavares R., Valente C., Borrego C. (2013). CFD modelling of the aerodynamic effect of trees on urban air pollution dispersion. Science of the Total Environment 461-462, 541-551.

Berardi U., GhaffarianHoseini A., GhaffarianHoseini A. (2014). State-of-the-art analysis of the environmental benefits of green roofs. Applied Energy 115, 411 – 428.

Borrego C., Tchepel O., Salmim L., Amorim J.H., Costa A.M., Janko J. (2004). Integrated modelling of road traffic emissions: application to Lisbon air quality management. Cybernetics And Systems: An International Journal 35, 535-548.

Borrego C., Sá E., Carvalho A., Sousa S., Miranda A.I. (2012). Plans and Programmes to improve air quality over Portugal: a numerical modelling approach. International Journal of Environment And Pollution 48, 60-68.

Borrego C., Tchepel O, Costa A.M, Amorim J.H. Miranda A.I. (2003). Emission and dispersion modelling of Lisbon air quality at local scale. Atmospheric Environment 37, 5197-5205.

Buccolieri R., Salim S.M., Leo L.S., Di Sabatino S., Chan A., Lelpo P., et al. (2011). Analysis of local scale trees atmosphere interaction on pollutant concentration in idealized street canyons and application to a real urban junction. Atmospheric Environment 45, 1702-1713.

Büttner G. Feranec G. Jaffrain G. (2006). Corine land cover nomenclature illustrated guide (Addendum 2006). http://eea.eionet.europa.eu/Members/irc/eionetcircle/spatial/library?l=/clc2005_update/clc2006_technical/draft/nomenclaturedoc/_EN_1.0_&a=d.

Carvalho A.C., Carvalho A., Gelpi I., Barreiro M., Borrego C., Miranda A.I., Perez–Munuzuri V. (2006) Influence of topography and land use on pollutants dispersion in the Atlantic coast of Iberian Peninsula. Atmospheric Environment 40, 3969–3982.

Carvalho D., Martins H., Marta-Almeida M., Rocha A., Borrego C. (2017). Urban resilience to future urban heat waves under a climate change scenario: A case study for Porto urban area (Portugal). Urban Climate 19, 1-27.

Chang J.C., Hanna S.R. (2005). Technical descriptions and user's guide for the BOOT statistical model evaluation software package, version 2.0. p. 62.

Dudhia J. (1989). Numerical study of convection observed during the winter monsoon experiment using a mesoscale two-dimensional model. Journal of the Atmospheric Sciences 46, 3077-3107.

European Commission, EC. (2015). Towards an EU Research and Innovation policy agenda for Nature-Based Solutions & Re-Naturing Cities.Final Report of the Horizon 2020 Expert Group on 'Nature-Based Solutions and Re-Naturing Cities'.Luxembourg: Publications Office of the European Union. ISBN 978-92-79-46051-7.

European Environment Agency, EEA. (2011). Green infrastructure and territorial cohesion: The concept of green infrastructure and its integration into policies using monitoring systems. Luxembourg: Publications Office of the European Union. ISBN 978-92-9213-242-2.

European Environment Agency, EEA. (2016a). Air quality in Europe — 2016 report. Luxembourg: Publications Office of the European Union. ISBN 978-92-9213-847-9.

European Environment Agency, EEA. (2016b). Transport in Europe: key facts and trends. Article, Signals - Towards clean and smart mobility. [Available in: https://www.eea.europa.eu/signals/signals-2016/articles/transport-in-europe-key-facts-trends].

Franke J., Hellsten A., Schlünzen H., Carissimo B. (2007). Best practice guideline for the CFD simulation of flows in the urban environment COST Action 732, quality assurance and improvement of microscale meteorological models, COST Office, p. 51.

Grimmond C.S.B., Oke T.R. (1999). Heat storage in urban areas: observations and evaluation of a simple model. Journal of Applied Meteorology and Climatology 38, 922–940.

Gromke C., Buccolieri R., Di Sabatino S., Ruck B. (2008). Dispersion study in a street canyon with tree planting by means of wind tunnel and numerical investigations — evaluation of CFD data with experimental data. Atmospheric Environment 42, 8640-8650.

Hong S.-Y., Dudhia J., Chen, S.-H. (2004). A revised approach to ice microphysical processes for the bulk parameterization of clouds and precipitation. Monthly Weather Review 132, 103–119.

Hong S.-Y., Noh Y., Dudhia J. (2006). A new vertical diffusion package with an explicit treatment of entrainment processes. Monthly Weather Review 134, 2318-2341.

Intergovernmental Panel on Climate Change, IPCC. (2013). Summary for Policymakers. In: Climate Change 2013: The Physical Science Basis. Contribution of Working Group I to the Fifth Assessment Report of the Intergovernmental Panel on Climate Change [Stocker, T.F., D. Qin,G.-K. Plattner, M. Tignor, S.K. Allen, J. Boschung, A. Nauels, Y. Xia, V. Bex and P.M. Midgley (eds.)]. Cambridge University Press, Cambridge, United Kingdom and New York, NY, USA.

Jeanjean A.P.R., Monks P.S., Leigh R.J. (2016). Modelling the effectiveness of urban trees and grass on PM2.5 reduction via dispersion and deposition at a city level. Atmospheric Environment 147, 1-10.

Kusaka H., Kondo H., Kikegawa Y., Kimura F. (2001). A simple single layer urban canopy model for atmospheric models: comparison with multi-layer and slab models. Boundary Layer Meteorology 101, 329-358.

Kusaka H., Kimura F. (2004). Coupling a single-layer urban canopy model with a simple atmospheric model: impact on urban heat island simulation for an idealized case. Journal of the Meteorological Society of Japan 82, 67-80.

Lalic B., Mihailovic D.T. (2004). An empirical relation describing leaf-area density inside the forest for environmental modelling. Journal of Applied Meteorology and Climatology 7, 641-645.

Launder B.E., Spalding D.B. (1974). The numerical computation of turbulent flows. Computer Methods in Applied Mechanics and Engineering 3, 269-289.

Lee R., Naesslund E. (1998). Lagrangian stochastic particle model simulations of turbulent dispersion around buildings. Atmospheric Environment 32, 665-672.

Markakis K., Valari, A. Colette, O. Sanchez, O. Perrussel, C. Honore, R. Vautard, Z. Kilmont, S. Rao. (2014). Air quality in the mid-21st century for the city of Paris under two climate scenarios; from the regional to local scale. Atmospheric Chemistry and Physics 14, 7323-7340.

Miao Y., Liu S., Chen B., Zhang B., Wang S., Li S. (2013). Simulating urban flow and dispersion in Beijing by coupling a CFD model with the WRF model," Advances in Atmospheric Sciences 30, 1663–1678.

Miranda A.I., Ferreira J., Silveira C., Relvas H., Duque L., Roebeling P., Lopes M., Costa S., Monteiro A., Gama C., Sa E., Borrego C., Teixeira J.P. (2016). A cost-efficiency and health benefit approach to improve urban air quality. Science of The Total Environment 569, 342-351.

Mlawer E.J., Taubman S.J., Brown P.D., Iacono M.J., Clough S.A. (1997). Radiative transfer for inhomogeneous atmospheres: RRTM, a validated correlated-k model for the longwave. Journal of Geophysical Research 102D, 16663-16682.

Monteiro A., Miranda A.I., Borrego C., Vautard R. (2007) Air quality assessment for Portugal. Science of Total Environment 373, 22-31.

Monteiro A., Ferreira J., Ribeiro I., Fernandes A.I., Martins H., Gama C., Miranda A.I. (2015). Air quality over Portugal in 2020. Atmospheric Pollution Research 6, 788-796.

Monteiro A., Gouveia S., Scotto M.G., Lopes J., Gama C., Feliciano M., Miranda A.I. (2016) Investigating ozone episodes in Portugal: a wavelet-based approach. Air Quality Atmosphere and Health 9, 775-783.

Nowak D., Crane D., Stevens J. (2006). Air pollution removal by urban trees and shrubs in the United States. Urban Forestry & Urban Greening 4, 115 – 123.

Pineda N., Jorba O., Jorge J., Baldasano J.M. (2004). Using NOAA AVHRR and SPOT VGT data to estimate surface parameters: application to a mesocale meteorological model, Int. J. Remote Sensing 25, 129-143.

Richards K., Schatzmann M., Leitl B. (2006). A wind tunnel investigation of thermal effects within the vicinity of a single block building with leeward wall heating. Journal of Wind Engineering and Industrial Aerodynamics 94, 621 – 636.

Richards P.J., Hoxey R. (1993). Appropriate boundary conditions for computational wind engineering models using the k-ε turbulence model. Journal of Wind Engineering and Industrial Aerodynamics 46–47, 145-153.

Sá E., Martins H., Ferreira J., Marta-Almeida M., Rocha A., Carvalho A., Freitas S., Borrego C. (2016). Climate change and pollutant emissions impacts on air quality in 2050 over Portugal. Atmospheric Environment 131, 209-224.

Salmond A., Mckendry I.G. (2009). Influences of meteorology on air pollution concentrations and processes in urban areas. R.E. Hester, R.M. Harrison (Eds.), Issues in environmental science & technology 28 air quality in urban environments, The Royal Society of Chemistry, London, pp. 23-41.

Salmon J.A., Williams D.E., Laing G., Kingham S., Dirks K., Longley I., Henshaw G.S. (2013). The influence of vegetation on the horizontal and vertical distribution of pollutants in a street canyon. Science of the total Environment 443, 287-298.

Santamouris M. (2014). Cooling the cities – a review of reflective and green roof mitigation technologies to fight heat island and improve comfort in urban environments. Solar Energy 103, 682-703.

Sarrat C., Lemonsu A., Masson V., Guedalia D. (2006). Impact of urban heat island on regional atmospheric pollution. Atmospheric Environment 40, 1743-1758.

Selmi W., Weber C., Rivière E., Blond N., Mehdi L., Nowak D. (2016). Air pollution removal by trees in public green spaces in Strasbourg city, France. Urban Forestry and Urban Greening 17, 192-201.

Skamarock, W.C., Klemp, J.B., Dudhia, J., Gill, D.O., Barker, D.M., Huang, X.Y., Wang, W., Powers, J.G. (2008). A Description of the Advanced Research WRF Version 3. NCAR/TN-475+STR, pp.113.

Speak A.F. Rothwell J.J., Lindley S.J., Smith C.L. (2012). Urban particulate pollution reduction by four species of green roof vegetation in a UK city. Atmospheric Environment 61, 283 – 293.

Stathopoulou E., Mihalakakou G., Santamouris M., Bagiorgas H.S. (2008). Impact of temperature on tropospheric ozone concentration levels in urban environments. Journal of Earth System Science 117, 227-236.

Tallis M., Taylor G., Sinnett D., Freer-Smith P. (2011). Estimating the removal of atmospheric particulate pollution by the urban tree canopy of London, under current and future environments. Landscape and Urban Planning 103, 129-138.

Tewari M., Kusaka H., Chen F. et al. (2010). Impact of coupling a microscale computational fluid dynamics model with a mesoscale model on urban scale contaminant transport and dispersion. Atmospheric Research 96, 656–664.

Vardoulakis S., Gonzalez-Flesca N., Fisher B. (2002). Assessment of traffic-related air pollution in two street canyons in Paris: implications for exposure studies. Atmospheric Environment 36, 1025-1039.

Vardoulakis S., Fisher B.E.A., Pericleous K., Gonzalez-Flesca N. (2003). Modelling air quality in street canyons: a review. Atmospheric Environment 37, 155-182.

Vardoulakis S., Dimitrova R., Richards K., Hamlyn D., Camilleri G., Weeks M., Sini J-F., Britter R., Borrego C., Schatzmann M., Moussiopoulos N. (2011). Numerical Model Inter-comparison for Wind Flow and Turbulence Around Single-Block Buildings. Environmental Modelling and Assessment 16, 169–181.

Wang W., et al. (2014), User's guide for advanced research WRF (ARW) modeling system version 3.6, Tech. Rep., Mesoscale and Microscale Meteorology Division–National Center for Atmospheric Research (MMM-NCAR).

Wania A., Bruse M., Blond N., Weber C. (2012). Analysing the influence of different street vegetation on traffic-induced particle dispersion using microscale simulations. Journal of Environmental Management 94, 91-101.

Xie X-M., Wang J-S., Huang Z. (2009). Traffic emission transportation in street canyons. Journal of Hydrodynamics 21, 108-117.

Zheng Y., Miao Y., Liu S., Chen B., Zheng H., Wang S. (2015). Simulating Flow and Dispersion by Using WRF-CFD Coupled Model in a Built-Up Area of Shenyang, China. Advances in Meteorology 2015, 15 pp.

CHAPTER 7

7. General Conclusions

The main purpose of the research presented in this thesis was to provide an integrated assessment of the interaction between resilience measures and climate change effects, and its influence on the urban air quality, based on the application of a modelling system tool. This research, performed through a series of spatial analysis and modelling approaches, intends to contribute to improve the knowledge regarding the accuracy of the atmospheric processes at the urban/local scale in numerical weather and air quality models, as well as a comprehensive understanding of the linkages between climate change, air quality and surface energy balance. The main achievements are presented and organized in seven chapters starting with the overall introduction to the particular topics, current status of air quality and surface energy balance, and their relationships, available modelling approaches, and an overview of the challenges related to climate change in cities, namely their vulnerability and opportunities to increase their resilience. Although detailed discussions of the results and conclusions have been included in the individual Chapters (from 2 to 6), the present section summarizes the most important findings of those discussions and their implication.

7.1. SUMMARY OF RESEARCH AND FINDINGS

As was understood, surface energy balance plays an important role to urban microclimate. Understanding how energy in the form of radiation and heat influences the urban climate, and how, in turn, urban microclimate impacts the surface energy balance, is recognized as crucial to improve the accuracy of numerical weather and air quality models, as well as, to address the challenges of urban planning and increase cities resilience to climate change effects. The surface energy balance is strongly dependent on the prevailing regional and local climate and its built-up structure. In this sense, the first step comprised the application and validation of WRF-SUEWS modelling setup to assess the influence of distinct land use characteristics of Portugal (high intensity residential – urban area; and low intensity residential – suburban area) on all the components of the surface energy balance (Chapter 2). Additionally, it was also analysed the relative importance of each variable of the surface energy balance to the energy partitioning. It was concluded that the turbulent sensible and latent heat fluxes are modelled relatively well by SUEWS, with a correlation factor of around 0.7 and a NMSE of 3. The model simulates the diurnal behaviour of the fluxes, but a consistent overestimation of the Q_H was observed (MBE of 14.7 and 51.4 $W \cdot m^{-2}$ for suburban and urban areas, respectively). The latent

heat flux was underestimated in the urban area (negative MBE, -12 $W \cdot m^{-2}$) and overestimated (26.8 $W \cdot m^{-2}$) in the suburban area. Overall, SUEWS does not fully replicate the observed fluxes; however, due to its relatively undemanding input requirements and its simplicity, is able to be applied for emerging applications: i) assessment of how climate change influences the behaviour and magnitude of the energy fluxes at the urban level and how the changes in the energy fluxes in turn impact the urban climate; ii) to explore options for urban planning and local/regional climate change mitigation and adaptation. Additionally, the model is able to quantify the role of surface cover fraction on the surface energy balance, having been concluded that:

- the fraction of the vegetated surface, exerts an important control on Q_E; in low intensity residential area represented 49% of the daytime available energy, while in the high intensity residential area, due to the high impervious nature of the surface, a reduced Q_E (7.9% of the daytime available energy) was found;
- Q_H and ΔQ_S were the most important fluxes in the urban surface energy balance (50% and 43% of the daytime energy balance, respectively), due to the higher man-made materials, and their related heat capacity, as well as due to the increased surface area;
- Q_F is higher in the high intensity residential area when compared with the low intensity residential area; however, for both areas a few percentage of the energy goes to Q_F (a maximum of 3% of the daytime available energy).

Since the surface energy balance results from the combination of land use characteristics and local microclimate, the significance of the meteorological input data to the variability of each component of the surface energy balance was also investigated. For that the stepwise regression method was applied. The conclusion allows understanding that surface energy balance will be affected by climate change. From the obtained results, can be concluded that Q_F were not weather-dependent (in a directly way). The analysis showed that ΔQ_S and Q_H has a statistically significant relationship to incoming shortwave radiation and air temperature, for both study areas. For Q_E, different significant relationship was obtained depending on the analysed area. The greatest influence on the variability of Q_E is precipitation for the urban area and incoming shortwave radiation for the suburban area (followed by precipitation), indicating that the water availability is a limiting factor for the development of the latent heat flux.

The quantified contribution of meteorological variables to the surface energy balance, strengthen the need to assess the impacts of climate change on the surface energy balance, especially in high urbanised areas as it is the case of Porto urban area. In this sense, the WRF-SUEWS modelling system (driven by the MPI-ESM-LR model) was applied to evaluate the behaviour and magnitude of the surface energy balance in Greater Porto area under the IPCC RCP8.5 scenario (Chapter 3). One reference year of the past period (reference scenario) and one future year of the medium-term future period (future scenario), statistically representative of each period of 20 years, were simulated. To enable the comparison between the two scenarios (reference and future), all the SUEWS inputs were kept constant, varying the meteorological conditions.

The results revealed that the changes in the meteorological variables (a temperature increase and a reduction of precipitation, relative humidity and wind velocity) changed the partitioning of the energy fluxes. Analysing a region as a whole (through the weighted average of the energy fluxes, based on the land use proportions that exists in the domain), the future modelled scenario (compared with the reference scenario) predicted that the sensible heat flux and the net storage heat flux will increase around 40% and 35% respectively, related to the increase of the global solar radiation (around 10%). In contrast, the latent heat flux will decrease by around 20%, mostly related to the decreasing of precipitation levels. The changes in the magnitude of the different fluxes result in an increase of around 15% of the net all-wave radiation. Regarding the anthropogenic heat flux, the results revealed an indirect relation between its behaviour/magnitude and the changes in the meteorological variables.

To a more accurate analysis, the changes in the surface energy balance was assessed in terms of land use type: urban (considering the grid cells classified as *Urban and Built-Up area*) and non-urbanized (considering a weight spatial average, excluding the grid cells classified as *Urban and Built-Up area* and *Water Bodies*). This analysis allowed the assessment of urban feedback to the changing climate, as well as, the evaluation of how non-urbanized areas will respond to climate change. Despite the differences in the magnitude of the urban fluxes, between scenarios, the results showed that the behaviour of the partitioning of the available energy was maintained between the reference and the future scenarios. Urban areas (by comparison with non-urbanized areas) showed higher values of sensible heat flux due to the combination between the higher fraction of man-made materials the reduced fraction of vegetative land cover (which implies a smaller latent heat flux); the urban surfaces have also higher heat capacity which leads to a non-negligible storage heat flux.

Due to the complexity of the atmosphere-surface system and their exchanges, can be predicted the implications of the changes in the energy balance in the urban climate of the Greater Porto area. The increase in the sensible heat flux and reduction of the latent heat flux, will result in higher surface temperature and a reduction of the precipitation. These results are particularly critical for the study area, since the obtained changes in the surface energy balance will enhance the magnitude and the severity of the extreme weather events, namely heat waves and heat island phenomenon, effects that are directly related with temperature increase. These results highlighted the need to investigate resilience measures (e.g., green and blue infrastructures solutions) and its effectiveness to mitigate the changes promoted by climate change.

As a result, the influence of a set of resilience measures in the energy fluxes was assessed (Chapter 4). To perform this analysis, the WRF-SUEWS modelling system was applied to the Porto urban area, with a high horizontal resolution (200x200 m). Based on the revised literature, two resilience measures were selected according their recognized benefits in terms of reduce heat waves effects: green areas and white roofs. The analysis was performed in a future climate, have being selected five heat waves (an extreme weather event). Four scenarios were developed to assess the effectiveness of the resilience scenarios: i) baseline scenario (without the implementation of resilience measures; ii) white roofs scenario, which comprised the introduction of white roofs in areas with high residential density; ii) green scenario, which consisted in the duplication of the existing green areas; iii) combined scenario,

which included a combination of the two previously measures (duplication of the existing green areas plus the introduction of white roofs in areas with high residential density).

Results showed that the inclusion of green urban areas increases the evaporation and the available surface moisture, redirecting the energy to the form of latent heat flux rather than sensible heat (a maximum Q_E increase of +200 $W \cdot m^{-2}$ and a maximum Q_H decrease up to -170 $W \cdot m^{-2}$). The shading effect of vegetation and the absorption of solar radiation also promote a reduction of storage heat flux (a maximum reduction of -46 $W \cdot m^{-2}$). The application of white roofs (increases the solar radiation reflection, due to the higher albedo effect) reduces both sensible and storage heat flux (maximum reduction of -62.8 and -35 $W \cdot m^{-2}$, respectively). For all the analysed scenarios, the influence in the energy balance components is restricted to the area where the measures were applied. The conjugation of the individual benefits related to each resilience scenario makes the combined scenario the most effective resilience scenario, producing a clear reduction in the average Q_H and ΔQ_S field and an increase of Q_E. According to these results it is expected that the introduction of these resilience measures will improve the urban population thermal comfort due to the reduction of both mean and maximum temperature.

The application of WRF-SUEWS modelling system represented an important attempt to quantitatively assess the surface energy balance at urban scale in Portugal, at distinct fields: i) clearly distinguish the influence of land use to the daytime energy partitioning; ii) increase the knowledge related to the atmosphere-surface exchanges and its linkages to the current urban climate and, mainly, evaluate the implications for the future climate; iii) a full understanding of the role of urban planning, associated with the implementation of adaptation strategies to deal with climate change effects, to urban climate. The mains advantages of WRF-SUEWS modelling system, which are directly linked to the innovation of the performed work, can be summarized in three main features:

- Allowed a complete spatial coverage of the surface energy balance, which represent a step forward regarding the majority of the works developed in this research field, since most of studies have been developed through flux measurements, and so, with a delimited footprint area;
- Allowed a complete assessment of the surface energy balance, since all the components of this balance were analysed; most of the studies were focused in the turbulent fluxes (sensible and latent heat) or in the storage heat flux, and, more recently, in the anthropogenic heat flux;
- Allowed a prognostic analysis, which implies different test runs, in a short time-consuming period, which is highly advantageous for policy makers and stakeholders' decision making.

Having evaluated the role of the surface energy balance (through the assessment of each individual component) to the urban climate, the next step consisted in evaluating if the inclusion of surface energy balance in mesoscale meteorological models, as urban simulation schemes combined with urban parameters customized for individual urban areas, could increase the accuracy of modelling urban climate.

In this sense, the performance of three different urban parameterizations, with different levels of complexity, on modelling local energy fluxes were assessed. An analysis of how these urban parameterizations influence the accuracy of meteorological modelling were also made (Chapter 5). The bulk urban parameterization (LSM) and the single-layer urban canopy model (UCM) were evaluated as well as an individual/independent urban energy balance model, the Surface Urban Energy and Water Balance Scheme (SUEWS). The two first models are available as a WRF model module, whereas SUEWS is an individual model. To a more complete analysis different levels of urbanization were considered in the analysis.

Comparison between modelled and measured data showed that UCM simulation compares better with the near-surface air temperatures, being able to a more realist representation of the air temperatures differences related to different land covers (in particular, different levels of urbanization). Model performance for both UCM and LSM in modelling local wind speeds was similar in terms of statistic metrics. However, the results showed that the UCM has the potential to more accurately simulate the observed wind speeds in terms of the daytime profile related to the surface land use. The UCM performance in modelling the urban microclimate was attributed to a good capability in simulate turbulent (sensible and latent heat fluxes) energy partitioning over urban covers. The higher suppression of urban vegetation effects in the LSM significantly overestimated the sensible heat and underestimated the latent heat fluxes, over both low and high intensity residential areas, resulting in systematic positive biases in near-surface air temperatures. This assessment highlighted the importance of choose a suitable model according to the study focus, not only regarding the model physics but also regarding the surface parameters used in the model runs. For example, it was found that irrigation and oasis effect of urban green areas, evaporation of urban impervious surfaces, and anthropogenic latent and sensible heat release, improved the ability of the UCM to simulate latent and sensible heat flux.

As have been discussed, air pollution is a result of the combined effect of emissions and meteorological conditions. Increase the accuracy of the tools that estimate these features is crucial to realistic evaluate the air quality at city level, as well as to developed appropriated adaptation strategies. If the models are not capable to model current conditions and/or to respond appropriately to parameters changes, then simulations for future scenarios and different interventions could be very misleading. In this thesis, a focus was made in the accuracy of urban microclimate modelling. Using the WRF-UCM model as a tool to initialize the CFD model VADIS, the aerodynamic effect of different resilience measures, based on green infrastructures (green urban areas and green roofs), in the flow and dispersion processes in a typical built-up neighbourhood of city of Porto was evaluated (Chapter 6). A set of numerical simulations (in an hourly base), at street canyon level (3 m of horizontal and vertical resolution), were performed to achieve this goal, and four air pollutants were analysed: CO, CO_2, NO_X, PM10. A typical (both in terms of meteorological conditions and emissions) week and weekend day were evaluated.

The analysis of resilience scenarios showed that the green infrastructures has a role to play at a city scale. The implementation of a green urban area leaded to an overall improvement of air quality, with

a general decrease of all the air pollutants concentration of around 16%, mostly related to an enhanced ventilation and dispersion capacity of the street canyon. However, at some hot-spots within the trees, the air pollutants concentration increased due to lower wind velocities and the formation of additional recirculation areas. This fact shows the importance of use CFD tools in urban planning with the goal of optimizing the role of trees in air quality. The implementation of green roofs showed an increase of all the air pollutants concentration, for a pedestrian height and at specific areas, due to a decreasing of horizontal flow. This increment promoted an overall degradation of air quality in the study area, compared with the baseline scenario. The “grey” scenario (absence of vegetation) showed that local air quality is strongly dependent on the linkages between the traffic flow, meteorological conditions, the 3D configuration of the street canyon, and the presence of trees. Overall, the results showed that there is no benefit to urban air quality with the absence of vegetation. For all the scenarios, the results showed that the change on the wind direction can significantly affect the dispersion patterns of pollutants (and its concentration), which was a more sensitive factor than the wind speed. In this sense, the implementation of a green urban area showed to be the best option for air quality improvement, and so, to improve human comfort and human health.

To summarize, the developed work showed that changes in the urban planning/urban morphology can influence the magnitude of the surface energy balance, which can directly affect the urban microclimate and the urban air quality. It was concluded that the implementation of the studied resilience measures would increase Porto city resilience to climate change effects, in particularly to high temperatures and heat waves, as well as, to improve air quality. These findings are highly advantageous for policy makers and stakeholders’ decision making, especially due to the current air quality problems and the urban heat island effect felt in Porto urban area, issues that future projections already have showed that will increase in the future.

7.2. EMERGING AREAS AND FUTURE CHALLENGES

Since surface energy balance magnitude and air quality levels are highly dependent of local climate and land use characteristics, further works are required to investigate whether the findings in this study holds for other urban morphologies and other climate conditions. If it is expected some similarities in terms of the behaviour, the magnitude of the influence of climate change on the surface energy balance and in air quality, as well the effectiveness of resilience measures, will change according the sites.

Beyond that, both research fields have their own challenges. In terms of the surface energy balance, a more accuracy of the modelled energy fluxes would be obtained if a better representation of ΔQ_S was included in the models, since its underestimation increases the bias of Q_H and consequently the energy partitioning (Q_H/Q_E). This is mostly related to the current difficulty in directly measuring ΔQ_S, future developments of the measurement techniques are crucial; an understanding of the physical formulation underling ΔQ_S will allow the increase of models’ performance. Additionally, a more

accurate representation of the anthropogenic heat flux for the study sites could also improve the models' performance. Inaccurate estimation of Q_F can result in poor simulation of the other heat fluxes, particularly in areas of high population density where a large Q_F is observed. To be able to define guidelines for policy makers at national level, a complementary analysis between measurement and modelling approaches should be made in more Portuguese cities.

The current projections of urban population, in particularly its continuous growth, determine the fact that air quality, and their linkage to climate change, will be a challenge of the future research. The development of resilience measures, from urban to districts and street level, according to each city characteristics (geography, dimension, environmental problems, among others), will be crucial; thereby the air quality models will play an important role. A constant increase the accuracy of urban features in air quality models is needed. At street level, this accuracy should imply that CFD models takes into account both physical and chemical processes. In terms of physical processes, the physical equations incorporated in CFD models should be able to consider both dispersion and deposition effects of particulate matter with an equivalent aerdodynamic diameter of less than 1 μm, due to its relation to human health effects. This development should be followed by model evaluation.

The European policy in terms of increase cities resilience to climate change (at different sectors) is being driven through the investment on the so-called nature based solutions. These nature-based solutions provide sustainable, cost-effective, multi-purpose and flexible alternatives for various objectives. As a result, chemical processes in CFD models should be incorporated to quantify the pollutants uptake, allowing to establish a methodology able to assess the air pollution reduction capability from different green infrastructures. If the ability of green infrastructures to remove different air pollutants are quantified, it is possible determine the most effective green species in reducing air pollution. Additionally, if a balance between the capability of green infrastrucutres to remove air pollutants and the pollutants emitted by them in its activity (e.g. VOCs) is known, it is possible perform a cost-benefit analysis and so, promote an adequate urban planning.

In terms of the characterization of surface energy balance and air quality, and the effectiveness of resilience measures under climate change scenarios, the application of the modelling tools to more than one climatic scenario is recommended, to a better characterization of the range of possible changes that can be detected in future. An ensemble of results from the set of scenarios may give important information about the uncertainty analysis and promote a better evaluation of future air quality, surface energy balance and their linkages.

APPENDICES

APPENDIX A

APPENDIX A: Spectral Plots Analysis

Figures A-1 to A-3 shows a spectral plots analysis, as a monthly ensemble, for w'T', w'H_2O' and w'CO_2' co-spectra, and for u, w, T spectra, as three half hours binned, used to guarantee the good performance of EC methodology at the urban site.

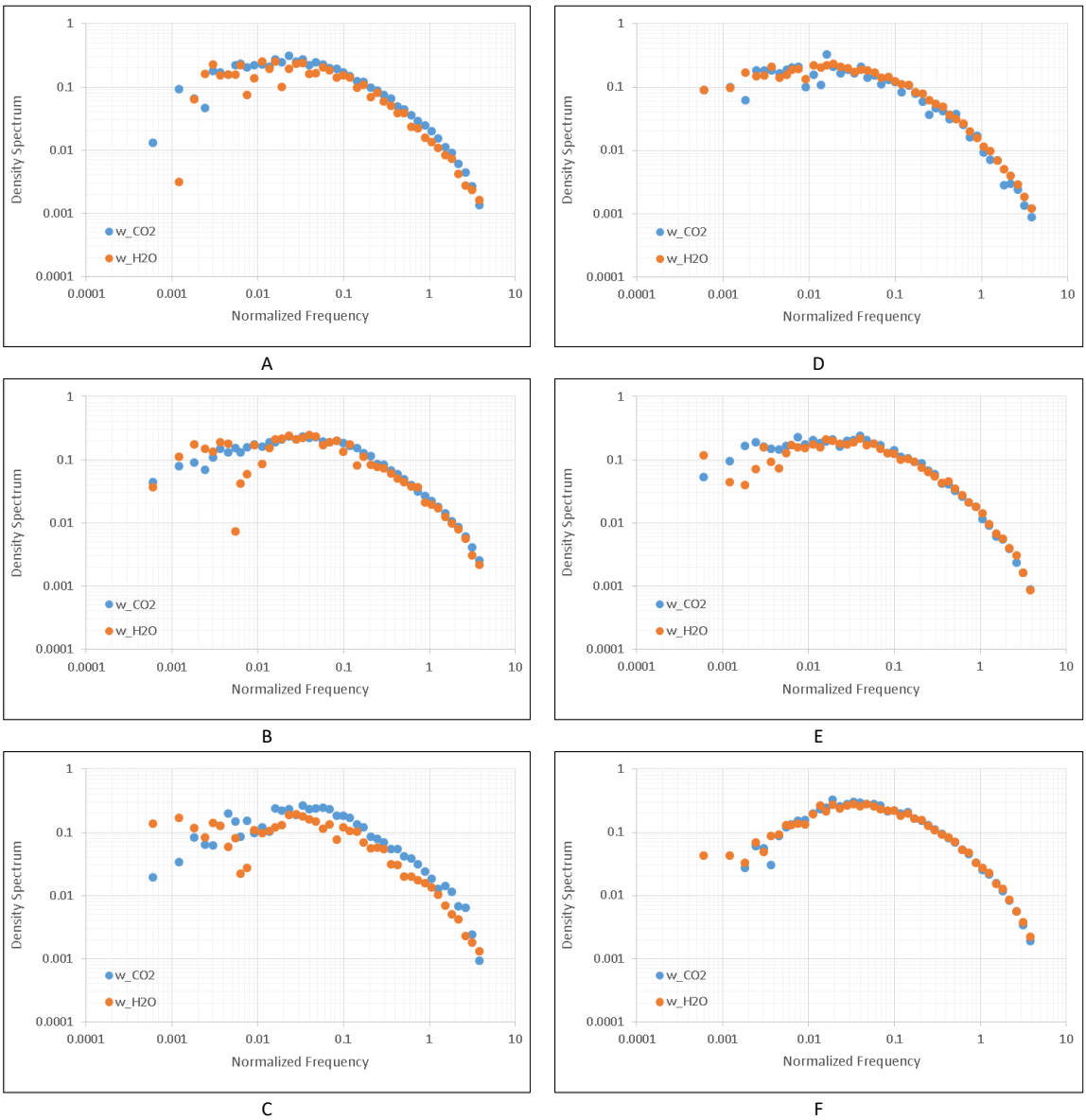

Figure A-1. Ensemble cospectra for Porto (A, B, C - August 12a.m. – 3p.m., 3p.m. – 6p.m., 6p.m. – 9p.m.; D, E, F - December 12a.m. – 3p.m., 3p.m. – 6p.m., 6p.m. – 9p.m).

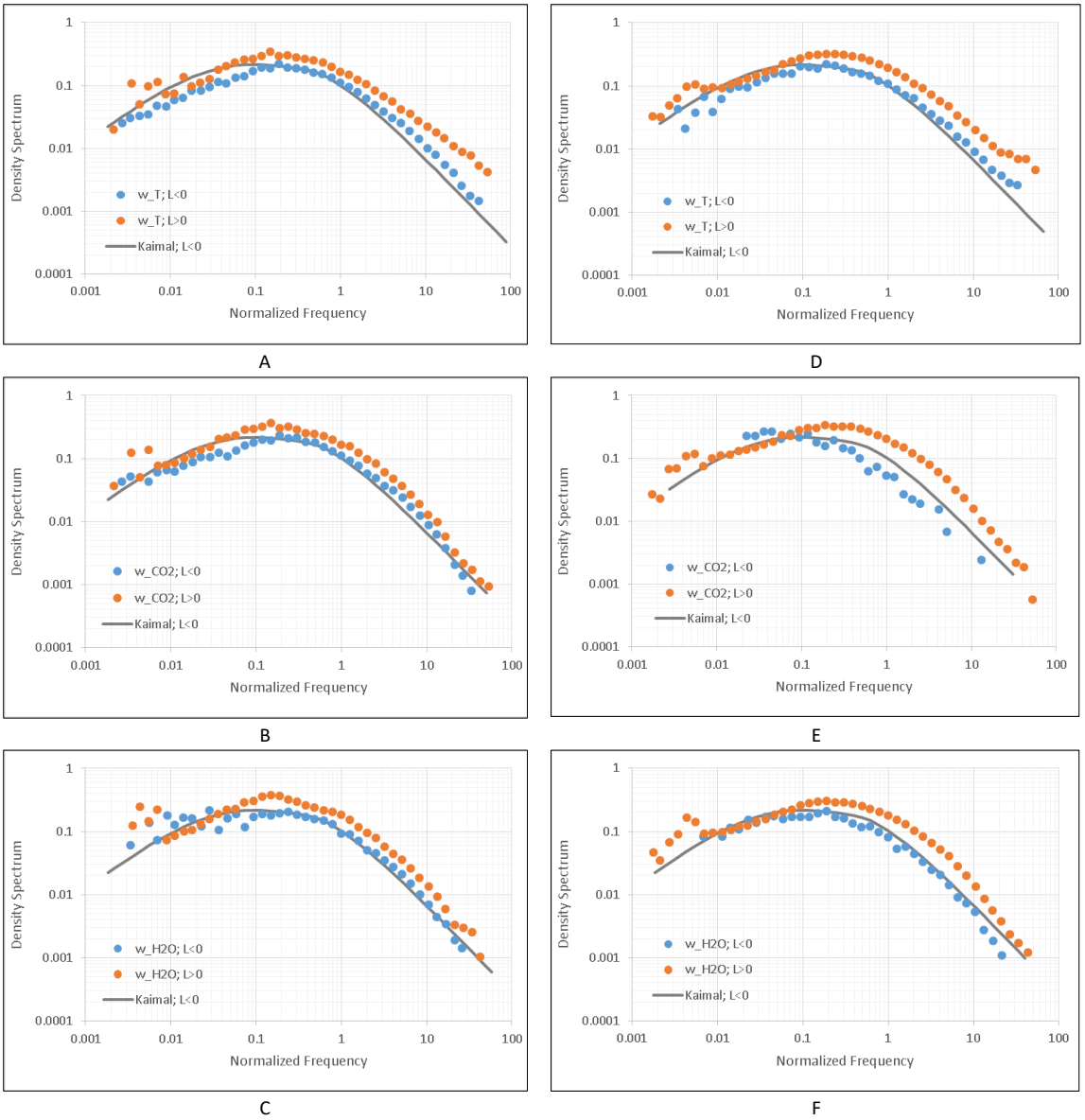

Figure A-2. Ensemble and model cospectra for Porto under unstable and stable conditions (A, B, C - August - w'T', w'CO_2', w'H_2O'; D, E, F - December - w'T', w'CO_2', w'H_2O').

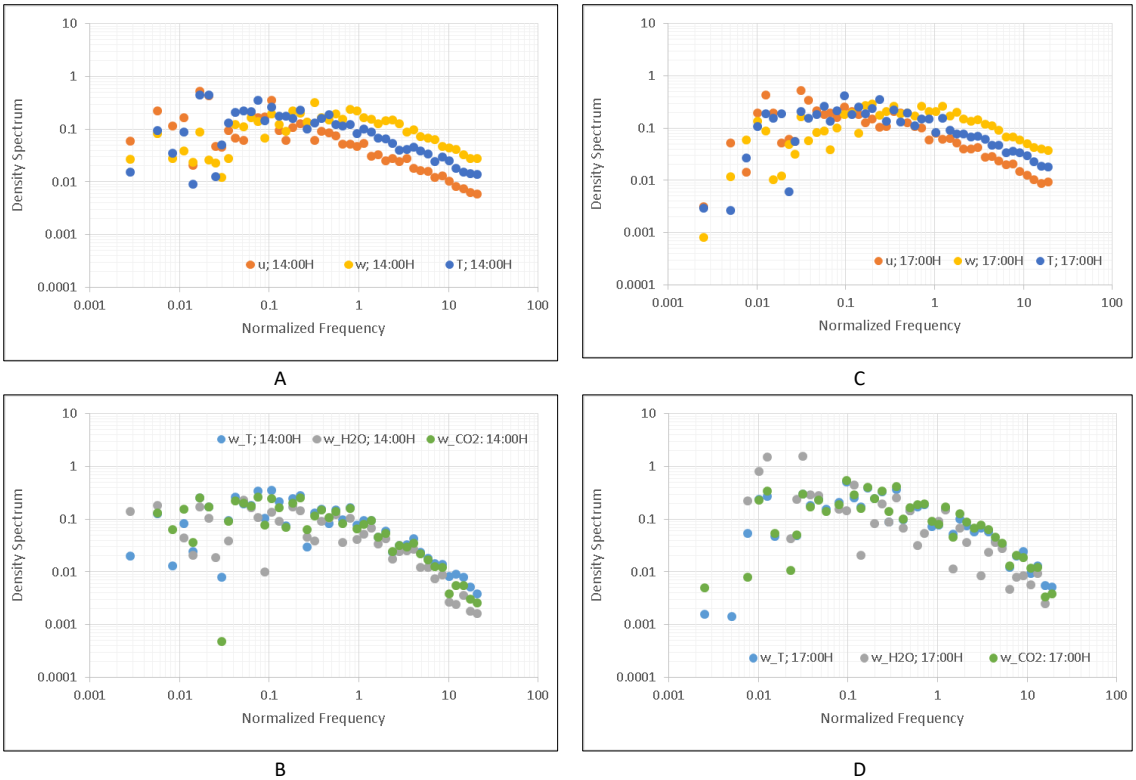

Figure A-3. Binned spectra and cospectra for Porto, at 3/8/2014 (A, B - u', w', T' ,w'T', w'H_2O' at 2 p.m.; C, D - u', w', T', w'T', w'H_2O' at 5 p.m.).

APPENDIX B

APPENDIX B: Statistical analysis of the meteorological variables used to force SUEWS model

Figures B-1 and B-2 present time-series and scatter plots to qualitatively compare the modelled results (meteorological variables) with the measurements.

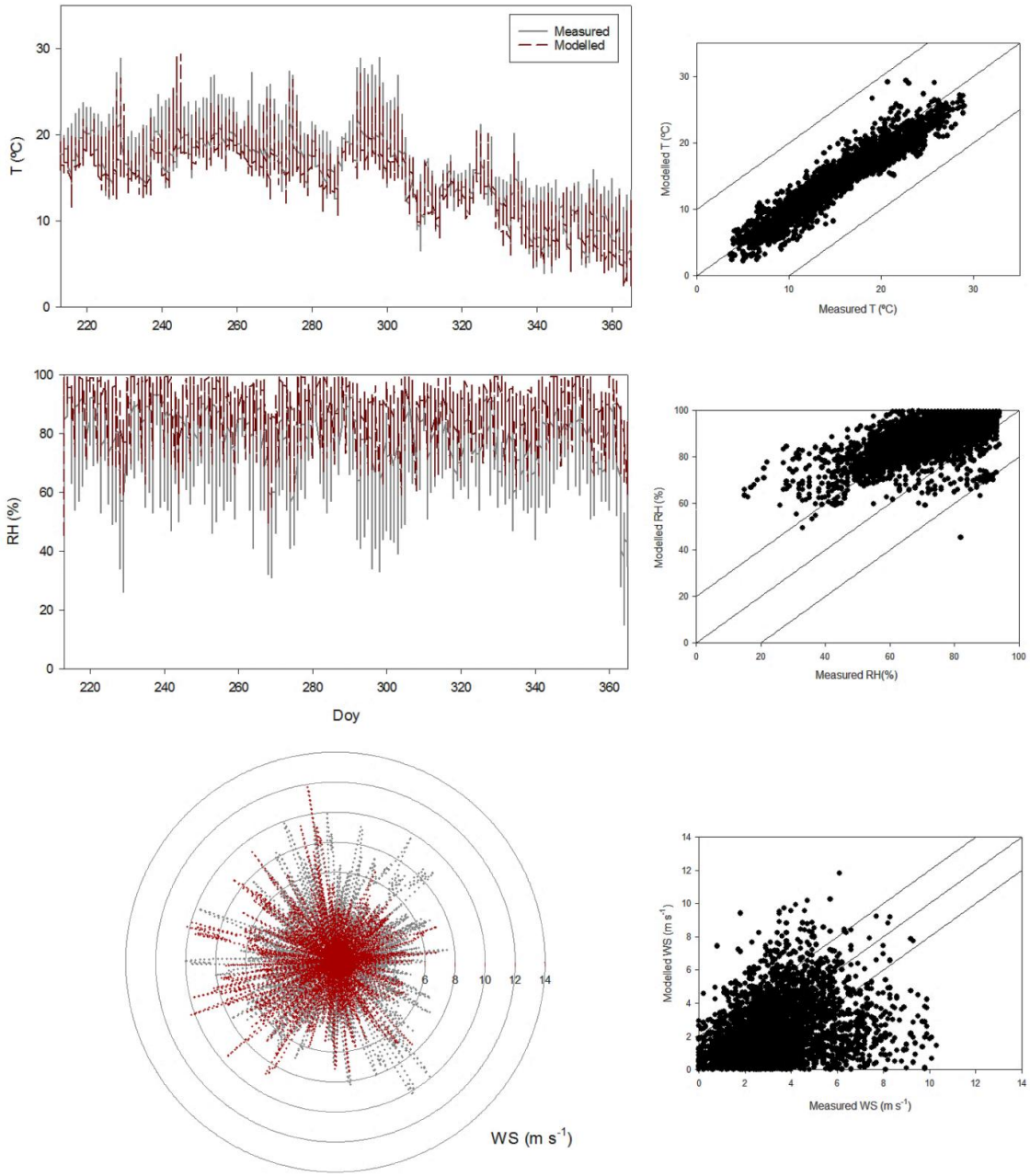

Figure B-1. Evaluation of WRF model performance for urban site based on a 5-month simulation: time series of temperature (T), relative humidity (RH) and wind speed (WS) (on left); and its respective scatter plots (on right).

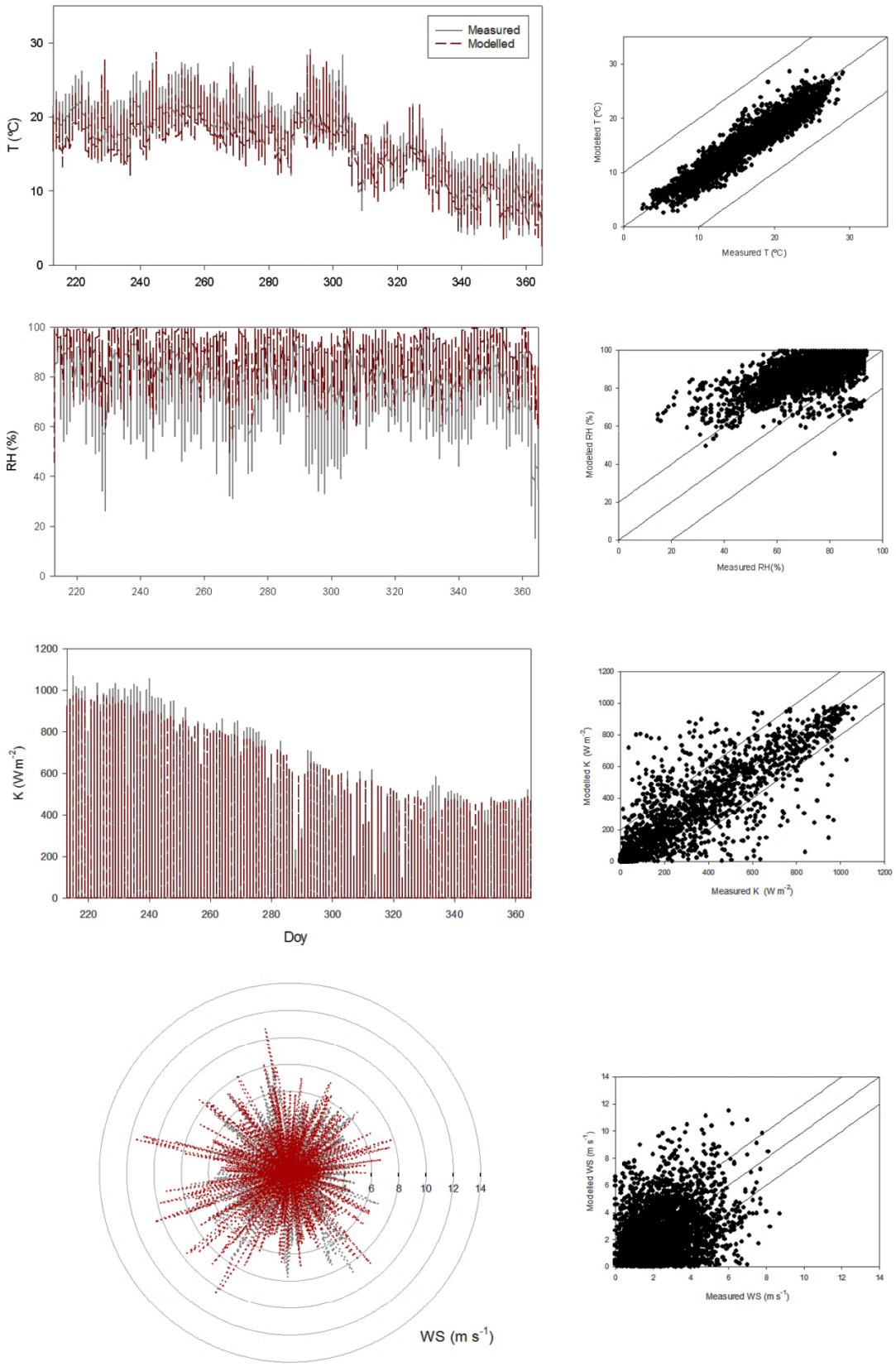

Figure B-2. Evaluation of WRF model performance for suburban site based on 5-month simulation: time series of temperature (T), relative humidity (RH) and wind speed (WS) (on left); and its respective scatter plots (on right).